

Monday Morning, October 29, 2012

Actinides and Rare Earths Focus Topic
Room: 6 - Session AC+MI+SS+TF-MoM

Electronic Structure and Spectroscopy of Actinides

Moderator: A.J. Nelson, Lawrence Livermore National Laboratory

9:00am **AC+MI+SS+TF-MoM3 Strong Correlations and the Electronic Structure of the Actinide Dioxides, R.L. Martin**, Los Alamos National Laboratory **INVITED**

The series of actinide dioxides (AnO_2 , $An=Pa, \dots Cm$) are difficult challenges for electronic structure theory. The early members of the series are Mott insulators, the band gap corresponding to f_7^2 transitions, while the later members, beginning with PuO_2 , are $O2p \rightarrow An5f$ charge transfer insulators. I will review recent experimental results (X-ray absorption, photoemission and optical band gaps) which now allow us to distinguish among several many-body approximations to their electronic structure, including the SIC, DFT+U, DMFT+U and hybrid DFT (HSE) approaches.

9:40am **AC+MI+SS+TF-MoM5 Synchrotron Radiation Studies of Actinide Compounds, S.M. Butorin**, Uppsala University, Sweden **INVITED**

Core-to-core resonant inelastic x-ray scattering (RIXS) and valence-to-core RIXS techniques are two complimentary ways for probing the electronic structure in actinide systems. Specific cuts of the core-to-core RIXS maps around $M\beta$ and L lines of actinides represent remarkably improved high-resolution x-ray absorption spectra of actinide $3d$ and $2p$ edges, respectively, as a result of limited lifetime broadening of core holes present in shallower levels in the final state of the spectroscopic process. That allows for more detailed studies of unoccupied states and better oxidation states assignments. In turn, the valence-to-core RIXS spectra are only limited by the instrumental resolution and provide information about actinide chemical bonding and interactions between valence electrons.

A comparison of experimental data with results of model calculations shows that the resonant spectra of actinide systems recorded at the actinide $M(3d)$ and $O(5d)$ thresholds which probe the $5f$ states can be interpreted using the many-body theory, such as the Anderson impurity model, while the data obtained at the $L3$ threshold and representing the $6d$ states of actinides can be described within a single-particle approach, such as LDA+ U (local density approximation with supplemented Coulomb interaction U) framework.

In course of discussion of the above statements, we present the RIXS data for a number of actinide systems with emphasis on the results contributing to understanding of the U-O and Pu-O phase diagrams, in particular data for UO_{2+x} , U_4O_9 , U_3O_8 and PuO_{2+x} . The influence of the Coulomb interaction between $5f$ electrons on the electronic structure of actinides is also discussed.

10:40am **AC+MI+SS+TF-MoM8 Quasiparticle Dynamics in Uranium Systems from Ultrafast Spectroscopies, T. Durakiewicz**, Los Alamos National Laboratory

Every time we add a new dimension to an experimental method, we open a window to novel, unexpected and fascinating phenomena. Here we show the results of our focused effort of adding time-domain to the powerful experimental techniques of Angle Resolved Photoelectron Spectroscopy (ARPES) and reflectivity. The novel tools are applied to actinides and help us understand the details of the electronic structure of the correlated f -electron materials.

In the hidden order system URu_2Si_2 we investigate the massive renormalization of the Fermi surface at specific k values. The application of time-resolved ARPES allowed a direct measurement of the momentum-resolved quasiparticle lifetime which was shown to increase by an order of magnitude at the hidden order transition. Time-resolved ARPES together with the ultrafast reflectivity results provided evidence for forming a multiple gap structure, including the hybridization gap, pseudogap and HO gap [1, 2].

Another actinide system of interest is a Mott insulator UO_2 , where we have investigated the complex dynamics of the Hubbard excitons. We have found that the dynamics can be divided into four distinct processes: instantaneous hop, picosecond lattice deformation, phonon emission and relaxation, and the slow relaxation related to the propagation of Hubbard excitons [3]. We

have also obtained the first direct measurement of Hubbard gap in $5f$ system [4].

The novel femtosecond pump-probe methods provide unique information about the dynamics of $5f$ quasiparticles, and open novel possibilities in addressing the long-standing questions about the role of near-Fermi level band renormalization in establishing the physical properties of correlated materials.

References

- [1] Physical Review B 84, 161101(Rapid Comm.) (2011)
- [2] Physical Review B 84, 161103(Rapid Comm.) (2011)
- [3] Physical Review Letters 106, 207402 (2011)
- [4] manuscript in preparation

11:00am **AC+MI+SS+TF-MoM9 Comparison of Spectroscopic Data with Cluster Calculations of Plutonium, Plutonium Dioxide and Uranium Dioxide, J.G. Tobin, S.W. Yu, B.W. Chung**, Lawrence Livermore National Laboratory, *M.V. Ryzhkov*, Russian Academy of Science-Ekaterinburg, *A. Mirmelstein*, Russian Federation Nuclear Center-Snezhinsk

Using spectroscopic data produced in the experimental investigations of bulk systems, including X-Ray Absorption Spectroscopy (XAS), Photoelectron Spectroscopy (PES) and Bremstrahlung Isochromat Spectroscopy (BIS) [1-5], the theoretical results within for UO_2 [6], PuO_2 [6] and Pu [7] clusters have been evaluated. The calculations of the electronic structure of the clusters have been performed within the framework of the Relativistic Discrete-Variational Method (RDV). [6,7] The comparisons between the LLNL experimental data and the Russian calculations are quite favorable. The cluster calculations may represent a new and useful avenue to address unresolved questions within the field of actinide electron structure, particularly that of Pu . Observation of the changes in the Pu electronic structure as a function of size suggests interesting implications for bulk Pu electronic structure.

Acknowledgements

Lawrence Livermore National Laboratory is operated by Lawrence Livermore National Security, LLC, for the U.S. Department of Energy, National Nuclear Security Administration under Contract No. DE-AC52-07NA27344. JGT and SWY were supported by the DOE Office of Science, Office of Basic Energy Science, Division of Materials Science and Engineering. Work at the RAS and VNIITF was supported in part by Contract B590089 between LLNL and VNIITF. The Advanced Light Source (ALS) in Berkeley and the Stanford Synchrotron Radiation Laboratory are supported by the DOE Office of Science, Office of Basic Energy Science.

References

1. J.G. Tobin and S.-W. Yu, Phys. Rev. Lett, **107**, 167406 (2011).
2. S.-W. Yu, J. G. Tobin, J. C. Crowhurst, S. Sharma, J. K. Dewhurst, P. Olalde-Velasco, W. L. Yang, and W. J. Siekhaus, Phys. Rev. B **83**, 165102 (2011).
3. J.G. Tobin, B.W. Chung, R. K. Schulze, J. Terry, J. D. Farr, D. K. Shuh, K. Heinzelman, E. Rotenberg, G.D. Waddill, and G. Van der Laan, Phys. Rev. B **68**, 155109 (2003).
4. J.G. Tobin, P. Söderlind, A. Landa, K.T. Moore, A.J. Schwartz, B.W. Chung, M.A. Wall, J.M. Wills, R.G. Haire, and A.L. Kutepov, J. Phys. Cond. Matter **20**, 125204 (2008).
5. S.-W. Yu, J. G. Tobin, P. Olalde-Velasco, W. L. Yang, and W. J. Siekhaus, J. Vac. Sci. Tech. A. **30**, 011402 (2012).
6. M.V. Ryzhkov and A.Ya. Kupryazhkin, J. Nucl. Materials **384**, 226 (2009).
7. M.V. Ryzhkov, A. Mirmelstein, S.-W. Yu and J.G. Tobin, "Probing Actinide Electronic Structure through Pu Cluster Calculations," submitted to Phys. Rev. B, Feb 2012.

Spectroscopic Ellipsometry Focus Topic

Room: 19 - Session EL+TF+AS+EM+SS+PS+EN+NM-MoM

Spectroscopic Ellipsometry for Photovoltaics and Semiconductor Manufacturing

Moderator: M. Creatore, Eindhoven University of Technology, the Netherlands, H. Wormeester, MESA+ Institute for Nanotechnology, University of Twente, Enschede, The Netherlands

8:20am **EL+TF+AS+EM+SS+PS+EN+NM-MoM1 Multichannel Spectroscopic Ellipsometry: Applications in I-III-VI₂ Thin Film Photovoltaics**, *R.W. Collins, D. Attygalle, P. Aryal, P. Pradhan, N.J. Podraza*, University of Toledo, *V. Ranjan, S. Marsillac*, Old Dominion University **INVITED**

Multichannel spectroscopic ellipsometry (SE) has been applied successfully as an in situ, real time tool for optimizing, monitoring, and controlling multi-stage deposition processes in various thin film photovoltaics (PV) technologies. A particularly challenging process optimization problem involves the thermal co-evaporation of individual elements of Cu, In, Ga, and Se in a three-stage process, which has proven to produce high quality Cu(In_{1-x}Ga_x)Se₂ (CIGS) materials and high performance PV devices. This three-stage process provides a high level of flexibility in determining the phase, composition, and microstructure of the film, but also generates greater challenges in run-to-run reproducibility of the optimized process. Information extracted from real time SE measurements includes the evolution of the bulk layer and one or more surface layer thicknesses, as well as layer dielectric functions. The layer dielectric functions can be analyzed further to extract the phase and alloy compositions and the defect density or grain size, which can assist in understanding the fabrication process, in optimizing solar cells, and ultimately in monitoring and controlling the optimized process for improved reproducibility. In this study, the focus is on analysis of ellipsometric (ψ , Δ) spectra acquired by real time SE in order to characterize (i) the structural and compositional evolution in (In,Ga)₂Se₃ film growth from In, Ga, and Se fluxes in the first stage, (ii) the transition from Cu-poor to Cu-rich CIGS at the end of the second stage, which occurs under Cu and Se fluxes, and (iii) the transition from Cu-rich to the desired Cu-poor CIGS, which defines the end of the third and final stage, and occurs under a second application of In, Ga, and Se fluxes. After the transition from Cu-poor to Cu-rich material in the second stage, a Cu_{2-x}Se phase near the surface of the bulk layer is tracked. In the Cu-rich to Cu-poor transition, this Cu_{2-x}Se phase has fully reacted with In, Ga, and Se to form CIGS. Studies using a standard Mo substrate and 2 μ m thick CIGS for solar cells have also revealed features in the (ψ , Δ) spectra characteristic of the anticipated changes in the near surface phase composition as established by detailed modeling on thinner and smoother films. Although careful analysis of real time SE is expected to provide quantitative information on the surface properties and their evolution in this case of solar cells, control of the deposition has been successful simply by monitoring real time changes in the ellipsometric (ψ , Δ) spectra.

9:00am **EL+TF+AS+EM+SS+PS+EN+NM-MoM3 Contribution of Plasma Generated Nanoparticles to the Growth of Microcrystalline Silicon Deposited from SiF₄/H₂/Argon Gas Mixtures**, *J.-C. Dornstetter, S. Kasouit, J.-F. Besnier*, Total S.a, France, *P. Roca i Cabarrocas*, LPICM-CNRS, Ecole Polytechnique, France

Despite the low fabrication cost of thin film silicon solar modules, this type of technology remains non competitive in main stream markets because of the high BOS costs, due to the low energy conversion efficiency of this type of modules (~10%). We have recently shown that microcrystalline silicon films deposited using SiF₄/H₂/Argon RF capacitive plasmas have excellent structural and transport properties, compared to films deposited using conventional SiH₄/H₂ mixtures, allowing for a very good carrier collection, even for thick cells, and Voc values of 0.55 V, without device optimization, thus opening up the path for the realization of high performance solar cells. However, little is known so far about the growth mechanism of this type of materials and the reason for such interesting properties. Studies of silicon thin films deposition from SiF₄/H₂ mixes, under conditions different from ours, suggested that the growth is due to the deposition of SiF₂ radicals, followed by the abstraction of fluorine by hydrogen. Previous work within our group has also shown that deposition occurs only when particles are present in the plasma, and that growth starts from crystallites without any amorphous phase. We present here a systematic study of the growth of microcrystalline films, together with the composition of nanoparticles attracted by thermophoresis to cold traps located both on the walls of the plasma chamber and in the fore line as a function of deposition conditions.

The composition of the deposit on the traps is found to be amorphous at low power/ low hydrogen conditions and becomes crystalline when either of them increases. This correlates well with an increase in atomic hydrogen concentration in the plasma, as estimated by actinometry. The crystalline fraction of the deposited film was measured using in-situ ellipsometry and was found to correlate with the composition of the deposit on the cold traps. Deposition rate is drastically reduced when a water cooled trap is installed on the walls of the plasma chamber, and switches off at high H₂ flow rates. Under these conditions, TEM and AFM images, show that at the initial stages of the growth the film is constituted of sparse, hexagonal crystalline particles, having sizes on the order of few tens of nanometers. We interpret the data above as a result of plasma-generated nanocrystals being a significant contribution to the deposited film. This may explain the excellent electronic properties of the films, as the particles are formed in the bulk of the plasma region, free from energetic ions bombardment. We will correlate the structural properties and the film growth mechanisms to the properties of solar cells.

9:20am **EL+TF+AS+EM+SS+PS+EN+NM-MoM4 Multichannel Spectroscopic Ellipsometry for CdTe Photovoltaics: from Materials and Interfaces to Full-Scale Modules**, *P. Koirala, J. Chen, X. Tan, N.J. Podraza*, The University of Toledo, *S. Marsillac*, Old Dominion University, *R.W. Collins*, The University of Toledo

Real time spectroscopic ellipsometry (RTSE) has been implemented in studies of the evolution of the semiconductor structural and optical properties during sputter deposition of thin film polycrystalline CdS/CdTe solar cells on transparent conducting oxide (TCO) coated glass substrates. Analysis of the real time optical spectra collected during CdS/CdTe deposition requires an optical property database as a function of measurement temperature for all substrate components. These include not only soda lime glass, but also an SiO₂ layer and three different SnO₂ layers. We report optical functions parameterized versus temperature for the glass substrate and its overlayers starting from room temperature and ending at elevated temperature above which the semiconductor layers are deposited. In fact, such a database has additional applications for on-line, through-the-glass monitoring applications of coated glass at elevated temperature. In the RTSE studies, knowledge of the temperature dependent optical functions of the substrate components enables an accurate substrate temperature determination before the onset of deposition and is critical for accurate extraction of the semiconductor layer optical properties. We implement RTSE to study the filling process of the surface roughness modulations on the top-most SnO₂ substrate layer and modification of the optical properties of this layer. This modification is further studied post-deposition by infrared spectroscopic ellipsometry. In addition to providing information on interface formation to the substrate during film growth, RTSE also provides information on the bulk layer CdS growth, its surface roughness evolution, as well as overlying CdTe interface formation and bulk layer growth. Information from RTSE at a single point during solar cell stack deposition assists in the development of a model that can be used for mapping the completed cell stack properties, which can then be correlated with device performance. Independent non-uniformities in the layers over the full area of the cell stack enable optimization of cell performance combinatorially.

9:40am **EL+TF+AS+EM+SS+PS+EN+NM-MoM5 Determination of Electronic Band Gaps from Optical Spectra**, *R.A. Synowicki*, J.A. Woollam Co., Inc.

The band gap of a material E_g is defined theoretically as the lowest energy for electronic transition from the valence to conduction bands in a solid. For an ideal material free of defects this is the photon energy or wavelength where the optical properties change from transparent to absorbing. However, real materials contain defects which cause absorption to begin below the band gap (i.e. the Urbach Tail) making determination of the true band gap position difficult. For example, in a solar cell the measured absorption edge represents the onset of transitions first due to defects, then from band to band. Empirical methods used to determine the band gap in real materials with defects include the Tauc plot and the Mott-Davis plot. More theoretical mathematical dispersion models such as the Tauc-Lorentz, Cody-Lorentz, and Herzinger-Johs models have been developed which include an adjustable band gap parameter. The various plots and dispersion model methods will be discussed and applied to different materials measured optically via spectroscopic ellipsometry, intensity transmission, reflection, absorption, or a combination of these methods.

10:00am **EL+TF+AS+EM+SS+PS+EN+NM-MoM6 Optical Modeling of Plasma-Deposited ZnO: Extended Drude and its Physical Interpretation**, *H.C.M. Knoops, M.V. Ponomarev, J.W. Weber, N. Leick, B.W.H. van de Loo, Y.G. Melese, W.M.M. Kessels, M. Creatore*, Eindhoven University of Technology, the Netherlands

High-quality transparent conductive oxides such as ZnO are important due to their electrical and optical properties. To improve these properties the

responsible physical processes have to be understood. Traditionally, charge-carrier-scattering processes are investigated by combining morphology data and Hall measurements. This contribution discusses the extensive optical modeling of plasma-deposited ZnO and how its interpretation directly provides insight into the relevant charge-carrier-scattering processes at different length scales. The interpretation is generalized to the concept of frequency-dependent resistivity, which is used to explain the applicability of different Drude models.

Thin films (50-1000 nm) of Al-doped and undoped ZnO were deposited using an expanding thermal plasma MOCVD process.¹ Conditions of high pressure and high diethyl zinc flow allowed for dense films with low electrical resistivities (e.g., $4 \times 10^{-4} \Omega \text{ cm}$ at 300 nm). The films were analyzed with variable-angle spectroscopic ellipsometry (SE) (0.75 – 5.0 eV), FTIR reflection spectroscopy (0.04 – 0.86 eV), Four-point-probe (FPP), and Hall measurements.

The SE and FTIR data were combined and fitted with classical and extended Drude² models. The high intensity of the Drude in the FTIR range resulted in a high sensitivity with which the carrier concentration and mobility could even be determined for thin (~40 nm) undoped ZnO films. An extended Drude model was needed to correctly model the SE energy range, which was explained by the dominance of ionized impurity scattering and a reduction of this scattering for higher photon energies. The grain-boundary-scattering mobility could be determined by the difference between optical and Hall mobilities.³ When combined with FPP results, the effective mobility can be determined from these optical techniques without the use of Hall measurements. The optical response above the band gap was modeled by a PSEMI or Tauc-Lorentz oscillator model, where a broadening and shift of the transition was seen for increasing carrier concentration.⁴

These insights and a generalized view of electron scattering in ZnO at different length scales will be presented.

1. Ponomarev et al., *J. Appl. Phys.* **Submitted** (2012)
2. Ehrmann and Reineke-Koch, *Thin Solid Films* **519**, 1475 (2010)
3. Steinhauser et al., *Appl. Phys. Lett.* **90**, 142107 (2007)
4. Fujiwara and Kondo, *Phys. Rev. B* **71**, 075109 (2005)

10:40am **EL+TF+AS+EM+SS+PS+EN+NM-MoM8 The Ellipsometric Response of Single-Crystal Silicon to Doping**, *H.G. Tompkins*, Consultant

The current wisdom is that for ellipsometry in the UV-vis-NIR spectral range, doping of single-crystal silicon can be ignored. We study the ellipsometric response of silicon doped with arsenic at various levels. We also studied the response after implant (before activation) and after the activation (anneal). We find that for samples implanted with $1E18$ atoms/cm³, the single-crystal silicon was not amorphized. Implants of $2E19$ atoms/cm³ and higher left an amorphous layer on the surface of the wafer the thickness of which was about the depth of the implant. Activation of the sample implanted with $2E19$ atoms/cm³ returned the sample to single-crystal silicon and the ellipsometric response in the UV-vis-near IR is essentially that of undoped silicon. However, the response in the mid-IR is that the extinction coefficient is no longer zero. For samples implanted with $2.5E20$ atoms/cm³ and greater, annealing did not return the UV-vis-near IR ellipsometric response to that of single-crystal silicon. Although this amount of other material (arsenic) is still less than about one tenth of one percent, our conjecture is that the microstructure simply could not be returned to that of a single crystal. As with the lower doped sample, the mid-IR spectral region showed significant increase in the extinction coefficient.

11:00am **EL+TF+AS+EM+SS+PS+EN+NM-MoM9 The Effect of Stress on the Optical Properties Semiconductor Films**, *A.C. Diebold, G.R. Muthinti, M. Medikonda, T.N. Adam*, College of Nanoscale Science and Engineering, University at Albany, *A. Reznicek, B. Doris*, IBM Research at Albany Nanotech

Here we review the impact of stress on the complex dielectric function of semiconductor films measured using spectroscopic ellipsometry. Two relevant examples of stressed semiconductor layers are pseudomorphic epitaxial layers fabricated during semiconductor manufacturing and strained silicon on insulator (sSOI) wafers. Stress is known to shift the energies of direct gap critical point transitions in semiconductors. The biaxial stress in pseudomorphic films grown on silicon wafers can be as high as that used during opto-elastic studies of bulk semiconductors. The amount of stress in un-relaxed, pseudomorphic films of $Si_{1-x}Ge_x$ on Si (100) reaches 1 GPa for alloys with 20% Ge and is more than 3 GPa for films with > 50% Ge. The bi-axial stress in sSOI is typically ~1 GPa. An elastic theory approach for the effect of strain on the k*p determined band structure and optical transition energy is well known. Both low shear stress and high shear stress approximations can apply to the shift in transition energy depending on the magnitude of the spin orbit splitting energy vs the magnitude of the shear

stress. Until recently it was difficult to obtain sets of samples that test both approximations. Here we discuss results from our recent study of pseudomorphic films of $Si_{1-x}Ge_x$ on Si (100) from $x=0.05$ to 0.75 which covers both low and high shear regimes. We also present our recent study of the dielectric function of thinned sSOI which illustrates the impact of stress on the optical transitions for the Si layer on sSOI. All of these samples are examples of new materials being used in semiconductor research. The results of this study are directly transferred into cleanroom spectroscopic ellipsometry systems used for process control during manufacturing.

11:20am **EL+TF+AS+EM+SS+PS+EN+NM-MoM10 Numerical Ellipsometry: Spectroscopic n-k Plane Analysis of Thin Films Growing on Unknown Layered Substrates**, *F.K. Urban, D. Barton*, Florida International University

Spectroscopic ellipsometry measurements on thin films commonly make use of prior knowledge of the structure and optical properties of the underlying substrate. However, imprecision in substrate statistics propagates into the solution for the film of interest. Thus it is more accurate to have a method for solving for film properties which simultaneously obtains whatever is needed about the substrate. And it makes solutions possible whether or not book data or previous substrate solutions are available. In this work we apply Complex Analysis in the n-k plane to achieve solutions employing the well-know reflection equations. The method is carried out at each measured wavelength and does not necessitate an *a-priori* assumption of optical property dependencies on wavelength. The mean square error has been improved by many orders of magnitude, a selected limit of 10^{-14} as opposed to 1 to 30 or so for least squares. Thus the full accuracy of the ellipsometer is now available for more accurate measurements of film thickness and optical properties. The method requires six measurements during growth. The first is used to determine the relationship between R_p and R_s at the film-substrate interface. The following four are used to uniquely determine the values of R_p , R_s , and film n , k , and d . The final measurement confirms the unique solution. Suitability of the model is tested by comparing measurements at two of more wavelengths for self consistency. Results for n and k of the growing film are examined across the measurement spectrum in comparison with parameterizations in common use.

Graphene and Related Materials Focus Topic
Room: 13 - Session GR+EM+NS+PS+SS+TF-MoM

Graphene Growth
Moderator: M. Spencer, Cornell University, V.D. Wheeler, U.S. Naval Research Laboratory

8:20am **GR+EM+NS+PS+SS+TF-MoM1 Synthesis Ingredients Enabling Low Noise Epitaxial Graphene Applications**, *D.K. Gaskill, L.O. Nyakiti, V.D. Wheeler*, U.S. Naval Research Lab, *A. Nath*, George Mason Univ., *V.K. Nagareddy*, Newcastle University, UK, *R.L. Myers-Ward, N.Y. Garces, S.C. Hernández, S.G. Walton*, U.S. Naval Research Lab, *M.V. Rao*, George Mason Univ., *A.B. Horsfall*, Newcastle Univ., UK, *C.R. Eddy, Jr.*, U.S. Naval Research Lab, *J.S. Moon*, HRL Labs LLC

Sensors made from graphene flakes have demonstrated single molecule detection [Schedin *et al.*, *Nat Mat* **6**, 652 (2007)]; this ultra-sensitivity is likely due to the high crystalline quality of the graphene and the associated relative lack of defects that give rise to noise. The low noise nature of high quality graphene should also facilitate other applications, e.g., low-noise amplifiers. Combined with the unique ambipolar property of graphene field effect transistors (FETs), the low noise character of graphene would significantly advance the performance of frequency multipliers, mixers and high-speed radiometers. To exploit these applications, high quality, reproducible wafer-scale epitaxial graphene (EG) with minimal thickness variations and defects are essential requirements. Here, crucial graphene synthesis elements required to achieve the wafer-scale quality goal are described. Understanding the effect of substrate misorientation as well as hydrogen etch and Si sublimation conditions for graphene synthesis on the (0001) SiC surface is essential to achieve improved and reproducible wafer-scale graphene quality. For example, the impact of processing factors such as temperature control, laminar gas flow and substrate rotation on large area EG uniformity are described using examples created in an Aixtron SiC epitaxy reactor. In addition, managing SiC step formation on the nominal (0001) orientation is significant for achieving uniform EG thickness on terraces and to minimize additional growth at the step edges; this is illustrated using data from atomic force microscopy and scanning electron microscopy images in combination with Raman spectroscopy maps and x-ray photoelectron spectroscopy analysis. Managing step formation combined with optimal growth leads to the suppression of the Raman defect

"D" band confirming minimal grain boundaries and defects, which are additional sources of electronic noise. Lastly, contactless Leighton resistivity maps of 75 mm wafers are used to illustrate the overall uniformity of optimally synthesized graphene as well as to show the resistance state-of-the-art, with individual wafers exhibiting about a $\pm 3\%$ relative variation. Examples of the impact of this synthesis approach on chemical sensors devices and FETs will be shown, each exhibiting 1/f noise behavior down to 1 Hz and possessing noise spectral densities similar to reports from exfoliated graphene. Hence, careful control of EG formation across the wafer results in improved quality which subsequently leads to the reduction or elimination of additional noise sources from graphene defects that would then adversely affect device performance.

8:40am **GR+EM+NS+PS+SS+TF-MoM2 Growth of Graphene by Catalytic Decomposition of Ethylene on Cu(100) and Cu(111) With and Without Oxygen Predosing, Z.R. Robinson, P. Tyagi, T. Mowll, C.A. Ventrice, Jr., University at Albany- SUNY, K. Clark, A.-P. Li, Oak Ridge National Laboratory**

Graphene growth on Cu substrates has become one of the most promising techniques for the mass production of graphene, and therefore significant effort has been put into developing growth conditions that lead to large area, defect and grain boundary free graphene films. One key consideration is the influence that the underlying copper substrate has on the growth of the graphene. In order to study this, graphene growth on Cu(100) and Cu(111) was carried out in a UHV system. The samples were heated using an oxygen series button heater. The hydrocarbon pressure was measured using a capacitive manometer instead of an ion gauge, which could cause dissociation of the hydrocarbon molecules. Initially, it was found that annealing the crystals to 900 °C resulted in impurity segregation at the surface. Several cycles of sputtering at 600 °C were required to remove all bulk impurities so that the surface remained clean even after annealing to 900 °C. Initial attempts to grow graphene by annealing each crystal to temperatures as high as 900 °C in UHV, followed by backfilling the chamber with up to 5×10^{-3} torr of C_2H_4 did not result in graphene formation. It was found that by first backfilling the chamber with C_2H_4 and then raising the temperature from 25 °C to 800 °C, graphene growth could be achieved. A four-domain epitaxial overlayer is observed for the Cu(100) surface. Pre-dosing the Cu(100) with oxygen at 300 °C, which forms a saturation coverage of chemisorbed oxygen, was found to result in a 2-domain graphene overlayer using similar growth conditions. A study of the effect of oxygen pre-dosing on the growth of graphene on Cu(111) has been initiated.

9:00am **GR+EM+NS+PS+SS+TF-MoM3 Impact of Growth Parameters on Uniformity of Epitaxial Graphene, L.O. Nyakiti, V.D. Wheeler, R.L. Myers-Ward, J.C. Culbertson, U.S. Naval Research Laboratory, A. Nath, George Mason University, N.Y. Garcés, U.S. Naval Research Laboratory, J. Howe, Oak Ridge National Laboratory, C.R. Eddy, Jr., D.K. Gaskill, U.S. Naval Research Laboratory**

Epitaxial graphene (EG) offers a facile method for attaining large area graphene for device applications. Since wafer uniformity and thickness control is vital, a systematic study of the parameters affecting the EG growth process was performed and the optimal conditions for obtaining uniform morphology and high electronic quality were determined. EG was synthesized in a low pressure Ar flowing ambient on $8 \times 8 \text{ mm}^2$ 6H-SiC(0001) substrates that were offset 0.8° from the basal plane, using an Aixtron VP508 reactor. The samples were placed on a rotating ~ 100 mm diameter susceptor and excellent EG layer uniformity and run-to-run reproducibility were obtained. The investigation focused upon the critical synthesis parameters of temperature (T) (1520-1660°C) and time (t) (15-60 min), an *in-situ* H_2 etch conditions (1520-1600°C for 10-30min). Morphology, layer thickness, chemical analysis, and strain variations across the samples were characterized using electron microscopy, AFM, XPS and μ -Raman spectroscopy. Large-area van der Pauw Hall effect was performed to quantify the graphene mobility (μ), and carrier density. Results show that growth T and t had the most significant impact on EG electronic and morphological properties. For example, synthesis at 1660°C for 30min resulted in 4-8 monolayers (ML) and a step-bunched morphology with high concentration of wrinkles originating from the step-edge and pinned at the nearest terrace edge. Other morphological features were pits primarily located at the step edges having a depth ~ 20 nm and density $6.4 \times 10^6 \text{ cm}^{-2}$. In contrast, EG synthesis at 1520°C for 30min results in uniform ML coverage along the terrace width that is devoid of pits and wrinkles. Mobility was found to have a drastic dependence on graphene thickness. Under optimal conditions, 1-2 ML were obtained and μ as high as $1240 \text{ cm}^2 \text{ V}^{-1} \text{ s}^{-1}$ was achieved; in contrast, for EG with >2 ML $\mu \sim 550 \text{ cm}^2 \text{ V}^{-1} \text{ s}^{-1}$, presumably due to interlayer interaction and electronic screening. XPS C1s and Raman 2D spectra of EG grown on substrates after undergoing *in-situ* H_2 etch at different times did not show shifts in peak position/intensity suggesting lack of etch time dependence on EG electronic or structural quality. Yet etch

conditions affect the final morphology, as EG synthesis performed after an *in-situ* H_2 etch at 1600°C resulted in step-bunched morphology with step heights 5-10nm, whereas, substrates etched at 1520°C had EG with step-heights 10-15nm. In addition other growth parameters investigated were found to be of secondary importance, including: Ar pressure, flow rates, and sample cool down conditions.

9:20am **GR+EM+NS+PS+SS+TF-MoM4 Uniform Epitaxial Growth of Charge Neutral Quasi-Free-Standing Monolayer Graphene on a 6H-SiC(0001) Surface by Combination of Metal Silicidation and Intercalation, H. Shin, I. Song, C.-Y. Park, J.R. Ahn, Sungkyunkwan University, Republic of Korea**

Intrinsic high mobility of graphene are much reduced in graphene devices by various factors. Two critical factors degrading mobility are uniformity in an atomic structure such as number of a layer and an interaction with a substrate. Recently Shuai-Hua Ji *et al.* reported quantitatively that conductivity is much reduced by one sixth when electrons pass through a boundary between monolayer and bilayer graphene at a step edge in comparison to conductivity of monolayer graphene. This suggests that uniformity of number of graphene layer is a more crucial factor than expected. In particular, in epitaxial graphene on SiC, the uniformity of number of layer is an intrinsic and serious problem because Si is more rapidly sublimated near a step edge in the formation of epitaxial graphene by thermal evaporation of Si and, subsequently, epitaxial graphene with different layers coexists intrinsically on a terrace. Another factor degrading mobility is an interaction between graphene and a substrate. In epitaxial graphene, the interaction was reduced by intercalation of metal or molecule such as H, F, and Au between graphene and a substrate, which results in quasi freestanding graphene. Various charge neutral quasi freestanding graphene has been reported, but the charge neutrality was found at an optimal coverage of an intercalated element and annealing temperature. This makes it difficult to achieve spatially homogeneous charge neutrality of quasi freestanding graphene, and a method with a broad range of coverage and temperature is demanded. We demonstrate that charge neutral quasi freestanding monolayer graphene can be grown uniformly without coexistence of a buffer layer and a bilayer graphene which limit mobility of epitaxial monolayer graphene. Because coexistence of two different phases is inevitable on a SiC surface, uniform monolayer graphene was produced based on two different phases, a Si-rich phase and a C-rich phase called a buffer. Pd was deposited on both the Si-rich and C-rich phases and annealed up to 900°C. The Si-rich phase produced Pd silicide and charge neutral quasi freestanding monolayer graphene was produced on the Pd silicide while, on the C-rich phase, Pd was intercalated between the buffer layer and SiC resulting in charge neutral quasi freestanding monolayer graphene, where the quasi freestanding monolayer graphene on two different regions was connected atomically. The combination of Si silicidation and intercalation result in uniform charge neutral quasi freestanding uniform monolayer on a SiC surface, where the electronic and atomic structures were observed using angle-resolved photoemission spectroscopy and scanning tunneling microscopy.

9:40am **GR+EM+NS+PS+SS+TF-MoM5 Epitaxial Graphene on Ir(111) - A Playground for the Fabrication of Graphene Hybrid Materials, T.W. Michely, Universität zu Köln, Germany INVITED**

Carefully optimizing the growth of graphene on Ir(111) yields a virtually defect free, weakly bound epitaxial monolayer ranging from quantum dot sizes to macroscopic extension. In the talk I will show how this system can be used to construct new types of graphene based materials. Specifically, patterned adsorption of transition metals results in dense cluster arrays with exciting magnetic and catalytic properties. Intercalation underneath the graphene allows one to manipulate the properties of graphene itself, e.g. its ability to adsorb atoms and molecules as well as its magnetism.

10:40am **GR+EM+NS+PS+SS+TF-MoM8 Graphene Growth Studied with LEEM, PEEM, EELS, ARPES, MEIS, and STM, R.M. Tromp, J.B. Hannon, M.W. Copel, S.-H. Ji, F.M. Ross, IBM T.J. Watson Research Center INVITED**

We have studied the growth of graphene on a variety of substrates, including SiC (both Si and C terminated), polycrystalline Cu and Ni foils, as well as single-crystal Ni foils. Low Energy Electron Microscopy (LEEM) and Photo Electron Emission Microscopy (PEEM) offer the unique opportunity to follow the growth in real time, as it proceeds at high temperature, and in the presence of processing gases such as disilane (for growth on SiC) or ethylene (for growth on the metal substrates). Low Energy Electron Diffraction (LEED) allows us to determine crystallographic orientations as well as atomic structure of areas well below a micrometer in extent. Information on electronic structure can be obtained from the plasmon loss features using Electron Energy Loss Spectroscopy (EELS), or from Angle Resolved Photo Electron Spectroscopy (ARPES). These spectroscopic experiments are carried out in the LEEM/PEEM

microscope using an in-line energy filter with which energy and angle resolved analysis of the electrons can be performed on selected areas. Finally, to obtain information on the layer-by-layer evolution of the graphene films, particularly on SiC, we have used isotope sensitive Medium Energy Ion Scattering (MEIS), to follow the growth by thermal decomposition of ^{12}C vs ^{13}C graphene monolayers from a three-bilayer thick Si^{13}C homoepitaxial film grown on a SiC substrate. Taken together, these results provide a comprehensive view of the growth of graphene films. In this talk, we will review the most salient results of these studies, and their relevance to the use of graphene films for electronic applications. To address the latter, we will discuss the results of three-probe STM experiments in which we measured the excess resistivity of a graphene sheet as it crosses an atomic step of the underlying substrate.

11:20am **GR+EM+NS+PS+SS+TF-MoM10 Spatial Confinement of Epitaxy of Graphene on Microfabricated SiC to Suppress Thickness Variation, H. Fukidome, T. Ide, H. Handa, RIEC, Tohoku Univ., Japan, Y. Kawai, Tohoku Univ., Japan, F. Fromm, Univ. Erlange-Nürnberg, Germany, M. Kotsugi, T. Ohkouchi, JASRI/SPring-8, Japan, H. Miyashita, Tohoku Univ., Japan, Y. Enta, Hirosaki Univ., Japan, T. Kinoshita, JASRI/SPring-8, Japan, Th. Seyller, Univ. Erlange-Nürnberg, Germany, M. Suemitsu, RIEC, Tohoku Univ., Japan**

Epitaxial graphene on SiC (EG) is promising owing to a capability to produce high-quality film on a wafer scale [1]. One of the remaining issues is microscopic thickness variation of EG near surface steps, which induces variations in its electronic properties and device characteristics. To suppress the variation, spatial confinement of surface reactions is effective. The spatial confinement using substrate microfabrication, for instance homoepitaxy and sublimation on microfabricated Si substrates, can induce self-ordering of steps, and even produce step-free surfaces [2]. The spatial confinement is therefore anticipated effective to obtain EG without the thickness variation.

We have for this reason applied the spatial confinement to the epitaxy of graphene on 6H-SiC(0001). For the spatial confinement, 6H-SiC(0001) substrates were microfabricated by using electron beam lithography and fast atomic beam etching using sulfur hexafluoride [3, 4]. Epitaxial graphene on the microfabricated 6H-SiC(0001) substrates was obtained by annealing at 1923 K in Ar ambience [2]. It is verified by using low energy electron microscopy (LEEM) and photoemission electron microscopy (PEEM) that step-free SiC surface and EG without thickness variation can be formed on smaller patterns [4]. This result clearly demonstrate that the spatial confinement is effective for the epitaxy of graphene on SiC. Furthermore, Raman spectroscopy and LEEM reveals that the spatial confinement can suppress the fluctuations of the electronic properties, e.g. (unintentional) doping in EG [4].

In conclusion, we have demonstrated that the spatial confinement of EG is effective to control both structural and electronic properties. This novel technique can boost the development of electronic devices based on EG.

[References]

- [1] K. V. Emstev et al., Nature Mater. 8 (2009) 203.
- [2] Y. Homma et al., Jpn. J. Appl. Phys. 35 (1996) L241.
- [3] T. Ide et al., accepted for the publication in Jpn. J. Appl. Phys.
- [4] H. Fukidome et al., submitted.

11:40am **GR+EM+NS+PS+SS+TF-MoM11 Three-Dimensional Graphene Architecture Growth and Its Facile Transfer to Three-Dimensional Substrates, J.-H. Park, Sungkyunkwan University, Republic of Korea, H.-J. Shin, J.Y. Choi, Samsung Advanced Institute of Technology, Republic of Korea, J.R. Ahn, Sungkyunkwan University, Republic of Korea**

Recent development of large area graphene synthesis on metal layer by chemical vapor deposition (CVD) or epitaxial growth on silicon carbide (SiC) opened the possibility for applications such as transparent electrodes for ITO replacement. For instance, graphene has been demonstrated for use in a liquid crystal display (LCD) and/or organic light emitting diode (OLED) test cell as a bottom electrode. However, the actual device, e.g., an active-matrix (AM) LCD, operates by switching individual elements of a display, using a thin-film transistor (TFT) for each pixel. Here, the pixel electrode of a display should extend down to the transistor's source or drain, thereby making contact with a via hole, which demands that a three-dimensional (3D) architecture electrode be deposited on a flat surface as well as its side walls. Although large-area graphene growth can be applied for a wide range of applications, 3D graphene architecture growth has not been realized for actual devices due to the original limitation of planar graphene growth. Herein, we demonstrate for the first time 3D graphene architecture growth and its facile transfer to a planar and/or 3D substrate. To prevent agglomeration of nano-scale metal catalyst by the CVD process, we chose a SiC system. Graphene, a few layers thick, was epitaxially grown

on a pre-patterned SiC substrate with nano-size thickness which was produced by photolithography and dry etching. Graphene on a vertical facet of the SiC pattern with a few-hundred nanometers in height was perfectly prepared using this approach, contrary to the CVD method. Furthermore, we suggest the use of a facile transfer method of graphene on SiC to a SiO₂ substrate using thermal release tape after hydrogen intercalation. In spite of the troublesome transfer issue of SiC, the geometry of the 3D graphene was perfectly transferred onto the planar SiO₂ as well as the 3D SiO₂ structure. In other words, the 3D graphene architecture was maintained as a floating cap structure on planar SiO₂ and the vertical facet of the 3D SiO₂ structure was well covered. Moreover, the graphene bottom layer without a 3D cap and the inverted bowl structure in the 3D graphene architecture were selectively transferred by controlling intercalation and pressure. These approaches could provide a beneficial method for preparing a 3D graphene architecture as well as for modifying the ordered structure to be utilized in real devices.

Surface Science

Room: 21 - Session SS-MoM

Nonequilibrium and Nonlinear Processes

Moderator: D. Diesing, University of Duisburg-Essen, Germany, E. Karpov, University of Illinois at Chicago

8:20am **SS-MoM1 Hot Electron Flow Generated by Photon Absorption Probed with Metal-Semiconductor Nanodiodes, J.Y. Park, Y.K. Lee, KAIST, Republic of Korea**

A continuous flow of hot electrons that are not at thermal equilibrium with the surrounding metal atoms is generated by the deposit of energy from the external source to the surface through nonadiabatic electronic excitation. Here we show that hot electron flow generated on a gold thin film by photon absorption (or internal photoemission) is amplified by localized surface plasmon resonance. This was achieved by direct measurement of photocurrent on a chemically modified gold thin film of metal-semiconductor (TiO₂) Schottky diodes. Photons coupled into the modified gold thin film excite surface plasmon resonance, which enhances hot electron flows going over Schottky barrier between the gold film and TiO₂. The short-circuit photocurrent obtained with low-energy photons is consistent with Fowler's law, confirming the presence of hot electron flows. The morphology of the metal thin film was modified to a connected gold island structure after heating such that it exhibits surface plasmon. Photocurrent and optical measurements on the connected island structures revealed the presence of a localized surface plasmon at 550 ± 20 nm. The results indicate an intrinsic correlation between the hot electron flows generated by internal photoemission and localized surface plasmon resonance. We discuss the effect of dye molecules or metal nanowires on gold film in the efficiency of internal photoemission.

8:40am **SS-MoM2 The Nature of Charge Transfer at Metal-Liquid Interface: Equilibrium vs. Non Equilibrium Processes, D. Bürstel, M. Scheele, I. Nedrygailov, D. Diesing, University of Duisburg-Essen, Germany**

The hydrogen evolution reaction is one of the key reactions in catalysis whereby protons from a liquid phase discharge at a metal surface and form atomic hydrogen. A correlation between the reaction rate and the chemisorption energy of the metal-hydrogen species (so called Volcano plot) was motivated for decades by an exponentially increasing reaction rate originated from a stronger chemisorption energy by arguments from the equilibrium thermochemistry. Progress in the study of metal-gas phase interactions points to electronically excited states, when atoms adsorb on a metal or chemical reactions with molecules occur. Up to now metal-liquid interfaces are not in the focus of research activities considering non equilibrium processes in the course of interfacial chemical reactions. We show experimental concepts how reactions on metal-liquid interfaces can be reviewed with respect to the existence of chemically induced electronic excitations. In a theoretical model we show that even small deviations from the electronic equilibrium may change the rate of the discharge reaction of protons on metal surfaces.

9:00am **SS-MoM3 Probing Surface Chemical Reactions with Metal Nanofilm - Semiconductor Schottky Diodes, I. Nedrygailov, E. Hasselbrink, D. Diesing, University of Duisburg-Essen, Germany**

Most catalytic chemical reactions are complex processes, which include a variety of steps such as molecular and dissociative adsorption on a solid surface, interactions between intermediates, and desorption of products from the surface to the gas phase. Considerable effort has been made to achieve a detailed microscopic understanding of the dynamics of these

processes using different experimental and theoretical methods, nevertheless still little is known about the routes of energy transfer accompanying the gas-surface interactions. As shown by McFarland, Nienhaus and coworkers, dissipation of chemical energy, released in catalytic reactions on metals, may proceed non-adiabatically by transferring a part of the energy into electronic degrees of freedom. This process is caused by a nonequilibrium state of the adsorbate surface complex and leads to the excitation of highly energetic (hot) electrons and holes in the metal surface. Detection of the excited charge carriers in metals is rather challenging because they relax within some 10 fs due to scattering processes (including electron and phonon pathways). A loophole is the use of metal nanofilm - semiconductor Schottky diodes. A ballistic transport of the excited charge carriers from the metal surface, where the excitation takes place, into the underlying semiconductor is possible in such diodes allowing for the direct detection of the hot electrons and holes as a chemicurrent. Detailed studies of chemicurrents can further our knowledge about the role of electronic and nuclear degrees of freedom in the dissipation of the chemical energy and thereby can give us a key for understanding of surface dynamics. In this contribution, we report on our methodology of nanofilm Pt-SiO₂-Si Schottky diodes manufacturing and their application as detectors for chemically induced currents. We show experimental results with currents of up to several μ A detected in the Pt-SiO₂-Si diodes while the Pt top electrode is exposed to molecular hydrogen, oxygen or their mixtures with different molar ratios and a pressure in the range of 1 – 10 mbar. Thermal effects and electronic excitations in the Pt top electrode of Pt-SiO₂-Si diodes, caused by the water formation reaction, are considered as possible sources of the observed currents.

9:20am **SS-MoM4 Non-adiabatic Electronic Effects in Multiquanta Energy Transfer and Reactions at Metal Surfaces: Do We Need to Go Beyond the Electronic Friction Picture?**, *D.J. Auerbach*, University of California, Santa Barbara, *K. Golibruch*, University of Göttingen, Germany, *A. Kandratsenka*, Max Planck Institute for Biophysical Chemistry, Germany, *R. Cooper*, *C. Bartels*, University of Göttingen, Germany, *I. Rahinov*, The Open University of Israel, *A.M. Wodtke*, University of Göttingen, Germany

Interactions of molecules at metal surfaces can result in nonadiabatic electronic energy exchange with the metal. This complicates theoretical strategies designed to simulate surface reactivity, most of which today are based on the assumption that the electronic motion can be treated adiabatically, i.e. within the Born-Oppenheimer approximation. One widely applied electronically nonadiabatic theory that makes the leap beyond the Born-Oppenheimer approximation is “electronic friction”. In this method coupling of adsorbate motion to metal electrons is treated as a weak perturbation involving frictional forces modifying the molecular dynamics in a systematic and simple way.

Recent experiments on multiquantum vibrational excitation at metal surfaces suggest that at least for certain systems, multi quantum transitions involve energy transfer between the molecule and a single electron hole pair of the solid. These processes might better be described as an electron transfer reaction than as friction. These results suggest that theoretical approaches that go beyond electron weak coupling and electronic friction will be needed to properly treat electronically nonadiabatic effects in surface chemistry.

9:40am **SS-MoM5 Experimental Evidence of Non-adiabatic Effects in Gas-Surface Interactions**, *H. Nienhaus*, University of Duisburg-Essen, Germany **INVITED**

The perturbation of the electronic system during gas-metal interactions can cause significant electronic excitations with lifetimes on the femtosecond timescale [1]. Such non-adiabatic processes occur when electronic states are injected below the Fermi level such rapidly that the occupation of the states by resonant charge transfer is delayed. According to Zener’s criterion [2] this happens more likely in cases of fast nuclear motion and of low coupling between gas particle and metal states. Experimental evidence of chemically induced electronic excitations is gained by detecting exoelectron emission into the vacuum, surface chemiluminescence and internal hot hole or hot electron chemicurrents. The latter method uses thin-film electronic devices with internal potential barriers as high-pass energy filters. Metal-semiconductor (Schottky) diodes are the most prominent examples for sensitive detectors of both, hot charge carriers and chemiluminescence photons. Independent measurements of the phenomena uncover the various excitation mechanisms. An empty state below the Fermi level may inject a hot hole into the band of occupied electronic metal states or can be filled after Auger relaxation leading to an excited electron in the metal surface. For the oxidation of metals these two fundamental processes can be experimentally distinguished. In addition, it is shown that rapid state injection does not necessarily imply the dissociation of the oxygen molecule as peroxide formation also leads to a significant excitation of the electronic system. The non-adiabatic energy transfer can be associated with a rapid

intermolecular motion of the oxygen atoms during the reactive collision. The interaction of chlorine with potassium will be discussed as an example for a strong chemiluminescence reaction. By use of K/Ag/Si-multilayer Schottky diodes the coupling between emitted photons and Ag surface plasmons leads to an enhanced photocurrent in the device at a typical Ag film thickness of around 50 nm. Competing effects in the devices due to adiabatic energy dissipation, e.g., local heating of the system, are discussed. In the experiments such can be either certainly excluded or clearly separated from the non-adiabatic signatures.

[1] B.I. Lundqvist et al. in : Handbook of Surface Science, Vol. 3, Eds.: E. Hasselbrink and B.I. Lundqvist (North-Holland, Amsterdam, 2008), pp. 430-524.

[2] C. Zener, Proc. R. Soc. Lond. A 137 (1932) 696.

11:20am **SS-MoM10 Analysis of Chemicurrent Components Induced by Hydrogen Oxidation on Pt/n-GaP and Pt/n-SiC Planar Schottky Nanostructures**, *S. Dasari*, *M. Hashemian*, *E. Karpov*, University of Illinois at Chicago

Studies of chemically induced hot electron flow over Schottky barriers in planar metal-semiconductor nanostructures provides interesting possibilities for electrolyte-free conversion of chemical energy into electricity in solid-state devices and ultra-fast sensor applications. A method is described here to separate the hot electron current contribution to the total generated current based on in-situ resistive heating of cathode nanolayer of the Schottky structure. The total current is comprised of the hot electron and thermal components. The method preserves usability under application-relevant conditions requiring lower sample temperatures and higher pressures of a reactive gas mixture. Analysis of the current induced during oxidation to water of molecular hydrogen in 60-150 Torr mixtures on Pt/n-GaP nanostructure surface at 341-433 K is performed. Hot electron contribution to the total current has a nonmonotonic dependence on temperature, and its fraction reaches 25% at 341 K and 32% at 433 K. We also found that adsorption of molecular hydrogen and nitrogen gases on Pt/SiC planar nanostructure at normal atmospheric conditions leads to generation of a detectable chemicurrent only in the case of hydrogen. Nitrogen admission conditions were tuned to imitative an equal or greater thermal effect of adsorption as observed during admission of hydrogen gas; therefore the recorded chemicurrent cannot be thermally driven. Adsorptive chemicurrents can occur from admission of hydrogen to samples not only at pre-vacuum conditions, as in earlier studies, but also in reactive and inert gas mixtures at normal atmospheric pressure.

11:40am **SS-MoM11 Enhanced Chemicurrent Effect of H₂ Oxidation on Porous MIM Nanostructures**, *E. Karpov*, *M. Hashemian*, *S. Dasari*, University of Illinois at Chicago

Understanding of the basic charge transfer processes at solid interfaces with reactive gas mixtures is a pathway toward advanced sensing, novel catalyst and energy conversion applications. In particular, currents induced in surface reactions on catalytic nanofilms forming Schottky or MOS type contact with a semiconductor substrate have received considerable attention during the last decade. Physical nature of these currents is intriguing, since the Schottky nanofilm device contains no explicit ion conductive layer, and it resembles a photovoltaic cell much closer than an electrochemical device. In this presentation we report on observation stationary chemicurrents in the 0.1 mA/cm² range induced by molecular hydrogen oxidation on surface of porous Pt/TiO₂/Ti nanostructures with a potential barrier at room temperature conditions. Possible physical and chemical mechanisms of the current production are discussed.

Monday Afternoon, October 29, 2012

Actinides and Rare Earths Focus Topic
Room: 6 - Session AC+TF+SS+MI-MoA

Actinides and Rare Earths: Thin Films and Surface Science

Moderator: R.K. Schulze, Los Alamos National Laboratory

2:00pm **AC+TF+SS+MI-MoA1 Rare Earth 4f Hybridization in Gallium Nitride**, *J.W. McClory, S.R. McHale*, Air Force Institute of Technology, *L. Wang, W.N. Mei*, University of Nebraska-Lincoln, *J.C. Petrosky*, Air Force Institute of Technology, *J. Wu, R. Palai*, University of Puerto Rico – San Juan, *Ya.B. Losovyj*, Louisiana State University, *P.A. Dowben*, University of Nebraska-Lincoln **INVITED**

The location of the Gd, Er and Yb 4f states within the GaN valence band has been explored both experimentally and theoretically. The 4d – 4f photoemission resonances for various rare earth doped GaN thin films (RE = Gd, Er, Yb) provide an accurate depiction of the occupied 4f state placement within the GaN valence band. The resonant photoemission show that the major Er and Gd rare earth 4f weight is at about 5-6 eV below the valence band maximum, similar to the 4f weights in the valence band of many other rare earth doped semiconductors. For Yb, there is very little resonant enhancement of the valence band of Yb doped GaN, consistent with a largely 4f^{14-d} occupancy. The placement of the rare earth 4f levels is in qualitative agreement with theoretical expectations.

2:40pm **AC+TF+SS+MI-MoA3 Revisiting the Yb Electronic Structure with Low-Energy Photoemission Spectroscopy**, *F. Offi*, CNISM and Univ. Roma Tre, Italy, *P. Vilmercati, L. Petaccia, S. Gorovikov*, ELETTRA Sincrotrone Trieste, Italy, *A. Ruocco*, CNISM and Univ. Roma Tre, Italy, *M.I. Trioni*, CNR-ISTM, Milano, Italy, *A. Rizzo*, CNISM and Univ. Roma Tre, Italy, *A. Goldoni*, ELETTRA Sincrotrone Trieste, Italy, *G. Stefani*, CNISM and Univ. Roma Tre, Italy, *G. Panaccione*, CNR-IOM, Basovizza-Trieste, Italy, *S. Iacobucci*, CNI-IFN, Rome, Italy

The peculiar electronic structure of rare-earth elements and compounds is mostly defined by the partially filled 4f band. Of particular interest is the investigation of the valence states, which is linked to the degree of hybridization of f electrons with delocalized s-d bands. In the simple case of Yb, the 4f states are fully occupied with a Fermi level of 6s character and a 2+ valency. However, the occupation of the Yb valence band has been the subject of several investigations over the years, intended in particular to separate the contribution of 5d states. Early experimental photoelectron emission (PES) spectra at very low excitation energy ($h\nu < 10$ eV) have reported a spectral modulation in the region close to the Fermi level that was attributed to the emission from a 5d band. The poor energy resolution did not allow however a detailed investigation of such spectral features. In recent years this low energy photoemission spectroscopy (LEPES) encountered a renewed interest, under the stimulus of the extremely high energy resolution obtainable with laser excited LEPES and given the expectation of a large increase of the bulk sensitivity at these low energies. We monitored the 4f spectral intensity in polycrystalline Yb films in the LEPES regime (between 5.5 and 21 eV photon energy, with experiments at the BaDELPH beamline of the ELETTRA synchrotron radiation facility), observing a moderate increase of the electron attenuation length and, thus, a moderate increase of the information depth when we reach the lowest energies. By lowering the photon energy below about 11 eV a prominent peak at the Fermi level is observed. The analysis of its intensity variation versus photon energy and the comparison of the experimental spectra with *ab initio* density of states (DOS) calculations allow to attribute this structure to a p band crossing the Fermi level, enhanced at selected photon energies due to the influence of the empty DOS, probably amplified by a photoionization cross section effect and by the general increase of the photoelectron yield at low photon energy. In this respect LEPES may thus be considered as a probe of the joint DOS.

3:00pm **AC+TF+SS+MI-MoA4 Erbium Rare Earth Thin Film Hydride Stress Studies as a Function of Processing Techniques**, *J.L. Provo*, J.L. Provo Consulting

An important part of understanding the behavior of rare earth, Group 3A and 4A thin film hydrides is the determination of indirect effects such as stress in the film lattice which can lead to film flaking. In this study, special vacuum sample containers were prepared to observe and record basal-plane film stress levels, and film flaking (optical observations).

The special vacuum sample containers contained erbium deuteride (ErD₂) and erbium tritide (ErT₂) films on AT and BT quartz resonator substrates with chromium underlays in pairs prepared by air-exposure, (in-situ)

evaporate-load and reactive evaporation hydriding techniques. The erbium deuteride samples were prepared as controls for aging studies. All samples were processed with PVD Electron Beam deposition techniques, hydriding techniques mentioned above and a 450°C temperature bakeout and exhaust in consideration of the $\alpha \rightarrow \beta$ crystal phase transformation in crystalline quartz at 573°C.

Samples for the measurement of initial film deposition stress as a function of hydride processing and for the determination of stress produced in ErT₂ films due to the generation of helium-3 with time (i.e., tritium decay) were designed to utilize the double-resonator technique developed by EerNisse(1). Measurements of mass change and induced film stress were determined by frequency measurement changes obtained with a precision frequency counter, data being taken from the output of a one transistor Colpitts type driving oscillator circuit in which the crystal is an integral part.

A summary of initial film deposition stress (tensile) and film aging accumulative stress (compressive) for the erbium films from the different deposition and hydriding techniques is given. Reactively evaporated erbium occluder films were seen to have an initial film deposition tensile stress approximately 5 times less than (in-situ) evaporate-load films and 11 times less than air-exposed loaded films. Accumulative aging compressive stress for erbium occluder films were shown to be more variable but data indicate that reactively evaporated film aging stress is less than that of (in-situ) evaporate-load and air-exposed tritided films.

(1)-J. Appl. Phys. 43, 1330 (1972)

3:40pm **AC+TF+SS+MI-MoA6 Splat Cooling Technique Contributing to Understanding of Uranium Systems**, *L. Havela*, Charles University, Czech Republic, *A. Gonçalves, J.-C. Waerenbogh, L. Pereira*, ITN Sacavém, Portugal, *I. Tkach*, Charles University, Czech Republic, *N.-T. Kim-Ngan*, Pedagogical University Cracow, Poland, *T.B. Scott*, University of Bristol, UK

The splat cooling technique is one of the methods of ultrafast cooling of a melt, particularly suitable for small amounts of material. In particular cases it can help to overcome constraints imposed by thermodynamics. One of them was the issue of magnetic properties of non-stoichiometric Laves phase UFe₂. This compound has a ferromagnetic ground state (with both U and Fe magnetic moments). An excess of U, achieved by quenching, led to the decrease of T_C from 162 K for pure compound to 112 K for UFe_{1.7} [1]. Quenching was, however, unable to provide Fe-rich material, with expected increase of T_C. Using splat cooling of a series of materials with various off-stoichiometry from UFe₂ to UFe₆ we found that the cubic Laves phase structure (with sum-micron grains) can absorb excessive Fe up to the stoichiometry UFe_{2.3}. Additional excess leads to the segregation of α -Fe [2]. The increase of T_C up to 230-240 K was the impact on magnetic properties. The spontaneous magnetization also increases from 1.0 μ_B /f.u. in UFe₂ to 1.9 μ_B /f.u. in UFe_{2.3}. ⁵⁷Fe Mössbauer spectroscopy reveals that the excessive Fe atoms enter the U sublattice and develop higher magnetic moments (approx. 1.0 μ_B /Fe).

Applying the splat cooling technique on pure and doped U metal had the aim to stabilize the high temperature bcc phase (γ -U) to low temperatures, to be able to establish its basic electronic properties. In particular, changes in magnetic characteristics and electronic specific heat can be expected due to the modest volume expansion comparing to orthorhombic α -U. We found that splat cooling reduces the necessary concentration of dopants and U with 12 at.% Mo has no traces of α -U. The Sommerfeld coefficient $\gamma = 19$ mJ/mol K² estimated for pure γ -U is enhanced comparing to 11 mJ/mol K² for pure U splat, which is close to values given in literature [3] for the U metal. The splats exhibit a superconducting ground state with T_c ranging from 1.24 K for pure U to 2.11 K for 15 % Mo. The γ -U superconductivity is characterized by a large critical field exceeding 6 T and a sharp λ -type anomaly in specific heat C_p(T) with the size corresponding to the BCS theory. The superconductivity of a pure U splat, which contains only traces of γ -U, has much lower critical field (0.33 T) and the weak anomaly in C_p(T) does not convince about the bulk character of superconductivity.

This work was supported by Grant Agency of the Czech Republic under the grant No. P204/10/0330.

[1] A.T. Aldred, J.Magn.Magn.Mater. 10, 42 (1979).

[2] L. Havela et al., Intermetallics 19, 113 (2011).

[3] J.C. Lashley et al., Phys. Rev. B 63, 224510 (2001).

4:00pm **AC+TF+SS+MI-MoA7 Investigation of Rare Earth Doped Lithium Tetraborate Glasses with XAFS and Emission and Excitation Spectroscopy.** *T.D. Kelly, J.W. McClory, D.A. Buchanan, A.T. Brant, J.C. Petrosky*, Air Force Institute of Technology, *Ya.B. Losovyj*, Louisiana State University, *V.T. Adamiv, Ya.V. Burak*, Institute of Physical Optics, *P.A. Dowben*, University of Nebraska-Lincoln

The local structure of rare earth doped lithium tetraborate ($\text{Li}_2\text{B}_4\text{O}_7$) glasses has been studied by extended x ray absorption fine structure (EXAFS) at the rare earth L shells and by optical emission and excitation spectroscopies. The samples investigated were 1% rare earth doped by weight with Gd and Nd. The EXAFS signal was recorded in fluorescence mode with the energies calibrated for Nd L1 and L3 edges and Gd L3 edge. X rays were applied to the samples to activate emission and excitation centers in the glasses. The spectra were analyzed to determine rare earth occupation sites in the lithium tetraborate crystal structure and the emission and excitation lines due to rare earth doping.

4:40pm **AC+TF+SS+MI-MoA9 Eu-implanted p-type GaN: Charge-Driven Luminescence Hysteresis and Identification of a Possible Charge-State-Alternation Resonance of the Mg Acceptor.** *K.P. O'Donnell, P.R. Edwards, R.W. Martin*, Strathclyde University, Scotland, UK, *K. Lorenz, E. Alves, V. Darakchieva*, ITN Sacavém, Portugal, *M. Bockowski*, Unipress, Poland

Europium-doped p-type GaN shows *spectral switching* and *luminescence hysteresis* when samples are temperature-cycled between room temperature and 20 K (*K.P. O'Donnell et al, Late News paper at ICPS2012, Zurich*). An explanation of this unusual behaviour may be found in the charge-state dependence of the local structure of the Mg acceptor in GaN, recently modelled by J.L. Lyons et al., (*Phys. Rev. Lett.* 108, 156403 (2012)). Eu ions, sensitive to their local environment, may act as 'spectators' of the charge-induced local distortions. The dominant impurity-induced luminescence spectrum at RT (hereafter, Eu0) *switches completely* to another spectrum (Eu1) when samples are cooled below 25 K. Upon subsequent warming of the sample, Eu1 fades with increasing temperature, as expected, but Eu0 *does not reappear* until the temperature exceeds 150 K; its recovery is complete only above 210 K. The noted temperature extremes correspond to hole localisation (carrier freeze-out) and delocalisation, respectively. Here, we extend Lyons' model to consider the possibility of observing the resonance in which the acceptor alternates rapidly between neutral and negative charge states, leading to a spatial oscillation of the associated defect between Eu0 and Eu1 forms, and describe the possible spectral identification of this resonance.

Spectroscopic Ellipsometry Focus Topic

Room: 19 - Session EL+TF+BI+AS+EM+SS-MoA

Spectroscopic Ellipsometry: From Organic and Biological Systems to Inorganic Thin Films

Moderator: M.S. Wagner, The Procter & Gamble Company

2:00pm **EL+TF+BI+AS+EM+SS-MoA1 Biochemical Optical Sensors Based on Highly-Ordered Slanted Columnar Thin Films.** *D. Schmidt, K.B. Rodenhausen*, University of Nebraska-Lincoln, *J. VanDerslice, T.E. Tiwald, J.A. Woollam Co., Inc., E. Schubert, M. Schubert*, University of Nebraska-Lincoln

Highly-ordered three-dimensional nanostructure thin films offer substantially increased surface area for attachment of organic layers, and in addition, new detection principles due to the physical properties of the nanostructures. For example, upon material attachment the optical birefringence of the nanostructures changes due to screening of polarization charges. Because of these advantages, highly-ordered three-dimensional nanostructure thin films lend themselves as suitable candidates for studying of organic attachments as well as for low-cost humidity sensing, for example.

We utilize glancing angle electron-beam deposition for fabrication of highly spatially coherent metal slanted columnar thin films. Subsequently, the nanostructures may be further functionalized with thin conformal coatings by means of atomic layer deposition. The ellipsometry model analysis and resulting anisotropic optical properties of hybrid metal slanted columnar thin films determined by generalized spectroscopic ellipsometry in the visible and near-infrared spectral region will be discussed. We will be reviewing research in this area and report in particular on in-situ monitoring of organic attachments using ellipsometry combined with quartz crystal microbalance with dissipation. Exemplarily, we discuss studies of fibronectin protein adsorption, octanethiol chemisorption (self-assembled monolayer growth) on platinum coated titanium slanted columnar thin films as well as relative humidity sensing.

2:20pm **EL+TF+BI+AS+EM+SS-MoA2 Studies of Optical Properties of Hybrid J-aggregates and Nanocrystal Quantum Dots Layers for Photonic Applications.** *K. Roodenko, H.M. Nguyen, L. Caillard, A. Radja, O. Seitz, Yu.N. Gartstein, A.V. Malko, Y.J. Chabal*, The University of Texas at Dallas

The integration of organic materials and inorganic nanocrystal quantum dots (NQDs) on the nanoscale offers the possibility of developing new photonic devices that utilize the concept of resonant energy transfer between an organic material and NQDs. Electromagnetic coupling that takes place between excitons—bound electron-hole pairs—at the interfaces of the hybrid composite can be utilized for light-emitting, photovoltaic and sensor applications.

As the key ingredients for the nanocomposite material system reported in this work are the J-aggregates (JA, dye self-assembled molecules) that have exceptional optical absorption due to their strong oscillator strength. NQDs on the other hand combine a variety of important properties, such as high quantum yields, excellent photo- and chemical stability, and size dependent, tunable absorption and emission. Excitation energy transfer in NQDs / J-aggregate hybrids is characterized by their strong excitonic transitions at room temperature with spectrally well-defined absorption and emission.

In order to understand the energy transfer mechanisms in such complex systems, optical properties of JA and NQDs/JA hybrid systems were characterized by means of spectroscopic ellipsometry and polarized IR spectroscopy.

Spectroscopic ellipsometry in 0.6-5 eV spectral range was employed to study optical properties of J-aggregates drop-casted on silicon surfaces. Thin JA films were found to exhibit strong optical anisotropy due to the specific molecular orientation of thin layers on Si substrates. Variation of optical properties due to the deposition of nanocrystal quantum dots (NQDs) was systematically studied for applications in new photonic devices that utilize excitonic energy transfer from NQDs to JA layer. Ellipsometric results were cross-referenced with atomic force microscopy (AFM) data to derive a quantitative understanding of the distribution of NQDs upon deposition on JA layer. Integration of hybrid colloidal NQD/JA structures could be potentially attractive for a range of optoelectronic applications.

2:40pm **EL+TF+BI+AS+EM+SS-MoA3 Love and Death, the Story of Most Proteins and Most Surfaces as Told by Spectroscopic Ellipsometry.** *T. Benavidez, K. Chumbuni-Torres, J.L. Felhofer, C.D. Garcia*, The University of Texas at San Antonio **INVITED**

Biosensors are analytical platforms that integrate a biological recognition element with a signal transducer. Because they have the potential to provide rapid, real-time, and accurate results, biosensors have become powerful tools in clinical and biochemical settings. Our group is particularly interested in the development of electrochemical biosensors based on enzymes adsorbed to nanomaterials. When integrated to microfluidic devices, these sensors offer sensitivity, portability, low cost, and the possibility of analyzing turbid samples. Adsorption was selected to immobilize the biorecognition element because it is one of the simplest and most benign methods, avoiding cross-linking reactions or additional components (such as entrapping polymers). Most importantly, as adsorption is a required (and sometimes limiting) step for any immobilization mechanism, the identification of key variables influencing this process can be applied to a variety of strategies. Although several techniques have been used to study the adsorption of proteins to nanomaterials,¹ only a few of them provide information about the kinetics of the process in real time. This is a critical aspect, as most of the post-adsorption conformational changes occur within a few minutes after the interaction.² Among those, reflectometry was used by our group to perform the first kinetic study related to the interaction of proteins with carbon nanotubes.³ These kinetic studies have been recently extended to the interaction of enzymes (D-amino acid oxidase,⁴ catalase,⁵ and glucose oxidase⁶) by variable angle spectroscopic ellipsometry, which enabled a more thorough analysis of the interaction process with a much more versatile experimental design.^{7,8} The use of VASE demonstrated that a number of variables, (being the amount of enzyme only one of them) can influence the biological activity of proteins adsorbed to the substrate. Furthermore, our results indicate that the activity of enzymes adsorbed to nanomaterials can be directly related to the kinetics of the adsorption process (dG/dt).⁵

Please see supplemental document for figures and footnotes.

3:40pm **EL+TF+BI+AS+EM+SS-MoA6 Detailed Photoresist and Photoresist Processing Studies using Spectroscopic Ellipsometry.** *C. Henderson*, Georgia Institute of Technology **INVITED**

Spectroscopic ellipsometry has become an invaluable tool for the study of a wide variety of thin film systems. In particular, it has become extremely valuable in the development and study of advanced photoresists and of lithographic processes used in the production of integrated circuits and other related semiconductor devices. In our work, we have used

spectroscopic ellipsometry to study a variety of problems related to photoresists including swelling phenomena, exposure induced refractive index changes, and ultra-fast dissolution phenomena. We have combined spectroscopic ellipsometry with quartz crystal microbalance techniques to simultaneously study thin film optical properties, thickness, film mass, and film modulus. Such techniques have been particularly useful in understanding the dissolution properties of polymeric photoresists developed for 193 nm lithography. This talk will review some of the applications for spectroscopic ellipsometry in this field and in particular will highlight some of the results of our work made possible using spectroscopic ellipsometry.

4:20pm **EL+TF+BI+AS+EM+SS-MoA8 Ellipsometric Characterization of a Thin Titaniumoxide Nanosheets Layer.** *H. Wormeester, G. Maidecchi, S. Kumar, A. Kumar, A. ten Elshof, H.J.W. Zandvliet*, MESA+ Institute for Nanotechnology, University of Twente, The Netherlands

The photochemical properties of titaniumoxide make this a widely studied material. Of special interest is a thin nanostructured layer of such a material. A variety of a nanostructured material is the single sheet titaniumoxide that can be obtained by delaminating a layered titanate, with stoichiometry $Ti_{1-x}O_{2-4x}$ ($x=0.0875$). The slight titanium deficiency leads to a negatively charged nanosheet that can be used as a building block in a layer by layer assembled composite film [1]. In this work we used Langmuir Blodgett to deposit successive thin layers of nanosheets. The electronic properties of these layers were investigated with ellipsometry and Scanning Tunneling Microscopy (STM). The optical spectra show the well known absorption peak at 4.6 eV for titaniumoxide nanosheets. The optical spectra can be well modeled with a Cody-Lorentz dielectric function profile providing a bandgap of ... eV, a value also found from STM IV spectroscopy. The Cody-Lorentz profile also indicates a slight below band gap light absorption by the nanosheet material.

[1] T. Sasaki, Y. Ebina, T. Tanaka, M. Harada, M. Watanabe and G. Decher, Chem. Mater. 2001, 13, 4661

4:40pm **EL+TF+BI+AS+EM+SS-MoA9 Preparation of Abrupt LaAlO₃ Surfaces Monitored by Spectroscopic Ellipsometry.** *C.M. Nelson, M. Spies, L.S. Abdallah, S. Zollner, Y. Xu, H. Luo*, New Mexico State University

LaAlO₃ is a polar perovskite oxide, used as a single-crystal substrate in oxide epitaxy. It has created much interest for novel electronic applications, because a two-dimensional electron gas is formed at LaAlO₃/SrTiO₃ heterostructures. The purpose of our work is twofold: First, we are interested in an accurate determination of the complex refractive index of LaAlO₃ at room temperature. Second, we studied the impact of various cleaning methods on the abruptness of the LaAlO₃ surface.

We obtained a commercial single-side polished LaAlO₃ substrate with 2-inch diameter and a (100) pseudo-cubic surface orientation. The surface was polished with an rms roughness below 0.8 nm. We determined the ellipsometric angles ψ and Δ for LaAlO₃ at 300 K from 0.7 to 6.5 eV. For a bulk insulator with a clean smooth surface, the phase change Δ should be zero or π below the band gap. In practice, this never happens, because surfaces are covered with overlayers (adsorbed organic or water vapors). Surface roughness has a similar effect on the ellipsometric spectra as a surface overlayer. Even for an abrupt bulk/air interface, there is a thin (~0.5nm) transition region where the electron wave functions leak from the crystal into the ambient. For the as-received sample, the data were described with a Tauc-Lorentz model for LaAlO₃, plus 2.1 nm of surface layer thickness (described as an effective medium with 50% density of the bulk). After ultrasonic cleaning in acetone, the overlayer thickness decreased to 1.8nm. Next, we mounted the wafer in a UHV cryostat, pumped down to below 10⁻⁸Torr, and acquired an ellipsometric spectrum at 70°. The surface layer thickness was reduced to 1.2 nm, presumably because a part of the adsorbed surface layer (especially water) desorbed under vacuum.

So far, everything worked as expected, but here it gets interesting: We heated the sample to 700 K for about an hour to desorb the remaining surface overlayer. After cooling down to 300 K, we measured the ellipsometric angles again at 70° angle of incidence from 0.7 to 6.5 eV. The ellipsometric angle Δ at 2 eV was reduced to below 0.2°, consistent with a surface layer thickness of less than 1 Å, much less than the surface roughness specified by the supplier (8 Å).

In conclusion, a macroscopically smooth and clean LaAlO₃ surface was prepared by ultrasonic cleaning of the wafer in acetone, followed by heating in UHV to 700 K. The resulting surface layer thickness was below 1 Å, as measured by spectroscopic ellipsometry. We will report Tauc Lorentz parameters. We will also describe the temperature dependence of the LaAlO₃ dielectric function from 77 to 700 K. This work was supported by NSF (DMR-11104934).

5:00pm **EL+TF+BI+AS+EM+SS-MoA10 Determination of the Refractive Index of a Gold-Oxide Thin Film Using X-Ray Photoelectron Spectroscopy and Spectroscopic Ellipsometry.** *K. Cook, G.S. Ferguson*, Lehigh University

A two-step procedure will be presented for measuring the complex refractive index of an electrochemically produced oxide film on a gold surface. In the first step, the composition and the thickness of the oxide film were determined using angle-resolved X-ray photoelectron spectroscopy. The experimental composition defined the system, thereby avoiding assumptions about the film stoichiometry that would otherwise be required. The value of thickness derived from these measurements was then used to calculate n and k from ellipsometric data collected across the visible spectrum (350 - 800 nm).

Oxide Heterostructures-Interface Form & Function Focus Topic

Room: 7 - Session OX+SS+TF+MI-MoA

Chemistry of Oxide Surfaces and Interfaces

Moderator: M. Engelhard, EMSL, Environmental Molecular Sciences Laboratory

2:00pm **OX+SS+TF+MI-MoA1 Investigation of Al₂O₃ Nanostructure Surfaces Using Charge Optimized Many Body Potentials.** *D.E. Yilmaz, T. Liang, S.B. Sinnott, S.R. Phillpot*, University of Florida

Aluminum oxide nanostructures have drawn attention due to their interesting physical and optical properties. In particular, photoluminescence peaks for these systems are attributed to oxygen vacancies and surface effects. Here, we apply third-generation Charge Optimized Many Body (COMB) potentials for the Al-A1₂O₃ system to investigate the properties of Al₂O₃ nanoparticle surfaces. In particular, the elastic properties and local atomistic strain distribution of nanoparticles with a range of sizes are determined, and the corresponding vibrational spectra are determined. The effect of oxygen vacancies and adsorbed surface atoms on the local strain and vibrational spectra are also determined. This work is supported by the National Science Foundation (DMR-1005779).

2:20pm **OX+SS+TF+MI-MoA2 Manipulating Ferroelectric Surfaces for Direct NO_x Decomposition.** *M.W. Herdich, A. Kakekhan, S. Ismail-Beigi, E.I. Altman*, Yale University

Current technology for removing nitrogen oxides from engine exhausts relies on nearly stoichiometric air to fuel ratios. Under these conditions, the concentrations of CO and unburned hydrocarbons in the exhaust stream are high enough to efficiently remove adsorbed oxygen from the platinum based catalysts in catalytic converters, ensuring that the catalysts do not become saturated with adsorbed oxygen. Direct catalytic decomposition of NO_x to N₂ and O₂ in the presence of excess O₂ would eliminate the need for reducing species in automobile engine exhaust streams, allowing these engines to be run more efficiently. We have been investigating the potential of ferroelectric supports to modify the behavior of supported layers to enable direct NO_x decomposition. Our approach involves first principles density functional theory and surface science techniques. Using both approaches we have investigated the interactions of N, O, and NO with bare ferroelectric lead titanate surfaces and surfaces modified to expose catalytic layers, in particular Ru oxides. Theory indicates that the behavior of the PbTiO₃ surface towards these species is sensitive to the polarization direction and termination of the ferroelectric and that stable RuO₂-terminated surfaces can be created by manipulating the termination of the substrate. Experiments take advantage of plasma sources that allow the behavior of O and N atoms to be studied individually and epitaxial growth to manipulate the termination of the ferroelectric support. Favored reaction pathways are assessed using theory and temperature programmed desorption and related mass spectrometry methods.

2:40pm **OX+SS+TF+MI-MoA3 Catalyst Synthesis by Atomic Layer Deposition.** *P.C. Stair*, Northwestern University & Argonne National Laboratory

INVITED
Atomic Layer Deposition (ALD) has enormous potential for the synthesis of advanced heterogeneous catalysts with control of composition and structure at the atomic scale. The ability of ALD to produce conformal oxide coatings on porous, high-surface area materials can provide completely new types of catalyst supports. At the same time ALD can achieve highly uniform catalytically active metal and oxide phases with (sub-) nanometer dimensions.

Vanadium oxide species supported on high surface area oxides are among the most important catalytic materials for the selective, oxidative

conversion of hydrocarbons to useful chemicals. In our laboratory ALD has been used to synthesize both the catalytic vanadium oxide and the supporting oxide on both high surface powders and anodic aluminum oxide (AAO) nanoliths. These materials have been characterized by SEM, XRF, ICP, UV-Vis absorption spectroscopy, Raman spectroscopy and evaluated for the oxidative dehydrogenation (ODH) of cyclohexane.

More recently we have studied the synthesis of supported metal particles and developed what we call "ABC-type" ALD in which metal nanoparticles and support materials are grown sequentially in each ALD cycle. This method makes possible the synthesis exceptionally small particles, ca. 0.5 nm. Using additional ALD support layers at the conclusion of the growth, the metal particles can be stabilized against sintering while still remaining active at high temperatures and reaction conditions. Moreover, the catalysts resist coke formation which is a leading cause of catalyst deactivation. These properties are imparted as a result of anchoring step and edge atom sites while leaving facet sites open for catalysis.

3:40pm OX+SS+TF+MI-MoA6 Energy Alignment at Organic/Oxide Interfaces: The Influence of Adsorption Geometry and Chemical Bond on Interface Dipole, S. Rangan, C. Ruggieri, S. Coh, R.A. Bartynski, K. Chitre, E. Galoppini, Rutgers University

The lack of control of the energy alignment at the interface between an organic layer and an oxide substrate remains a limitation to the performance of promising technologies such as dye sensitized solar cells, organic light emitting diodes or organic thin film transistors. The energy alignment depends not only on the choice of the starting materials, but also on more subtle parameters such as oxide surface termination or defects, and molecular layer preparation mode.

In an effort to disentangle the different aspect of the interface of an organic/oxide system, we have studied simultaneously the adsorption geometry and the energy alignment of the Zn(II) tetraphenylporphyrin (ZnTPP) molecule on the TiO₂(110) and ZnO(11-20) surfaces. Two approaches have been pursued: 1) in-situ evaporation of the ZnTPP on a clean oxide surface prepared in ultra-high vacuum resulting in weakly bound multilayers or monolayers 2) ex-situ sensitization in a solution of ZnTPP derivative, modified with COOH anchoring group for chemisorption at the oxide surface.

Scanning tunnel microscopy has been used to characterize the clean oxides and the ZnTPP adsorption modes. X-ray photoemission, ultra-violet photoemission and inverse photoemission spectroscopies have allowed the exploration of both occupied and unoccupied states of the electronic structure, resulting in the full characterization of the energy alignment at the surface as a function of the molecular overlayer thickness. The electronic transport gap, obtained from the latter experimental techniques has also been compared to the optical gap obtained from reflection electron loss spectroscopy, thus allowing the characterization of bound excitonic states.

The effect of the ZnTPP/oxide interface preparation, as well as the effect of the oxide substrate on the energy alignment will be presented. The discussion will be extended to metallic substrates such as Ag(100) and Au(111) surfaces

4:00pm OX+SS+TF+MI-MoA7 Energy-Level Alignment at Organic/Oxide Interfaces, M.T. Greiner, Z.-H. Lu, University of Toronto, Canada

INVITED

Oxide/organic interfaces play an important role in many organic electronic device designs. Oxides are frequently used as buffer layers to tune the energy-level alignment between electrodes and organic semiconducting layers, and thus allow for efficient hole/electron injection. As per the 'integer charge-transfer' (ICT) model, energy-level alignment at electrode/organic interfaces is governed by the electrode's Fermi level and the organic molecule's oxidation/reduction potential. While the ICT model was originally proposed for organic/organic interfaces, it also applies to a broad range of transition metal oxides. In this presentation we will discuss the energy-level alignment (ELA) of several organic semiconductors with transition-metal oxides. We will show that ELA is primarily governed by an oxide's work function, and that ELA is relatively insensitive to oxide electronic structure. As transition metal oxides can exhibit a wide range of work functions (~ 2 - 7 eV), and can possess a wide range of electronic properties (p-type to n-type) they are very versatile materials for use in organic electronics. We will their properties—such as work function and electronic structure—can best be utilized for use as buffer layers in organic light-emitting diodes and organic photovoltaics.

4:40pm OX+SS+TF+MI-MoA9 Variable Kinetic Energy XPS of the Buried P3HT/ITO Interface, M.T. Brumbach, Sandia National Laboratories, J.C. Woicik, National Institute of Standards and Technology

The characterization of buried interfaces is difficult and often has to be performed by post-processing methods where the interface is revealed, disturbed, and possibly altered by environmental exposure. Variable kinetic energy X-ray photoelectron spectroscopy (VKE-XPS) offers the ability to tune the depth of analysis while the use of hard X-rays allows for a deeper analysis. The combination of variable energy hard X-rays for XPS (HAXPES) allows for systematic evaluation through a buried interfacial region. An important inorganic/organic interface for use in organic photovoltaic devices is the poly(3-hexylthiophene) (P3HT) interface with indium tin oxide (ITO). In this work P3HT/ITO buried interfaces were examined using X-ray energies from 2.2-3.9 keV. The ITO surface was additionally prepared using different pretreatment conditions. The P3HT film protected the ITO surface from adventitious adsorbents and allowed for sensitivity to the buried ITO surface. Robust peak fitting parameters were obtained to model the O 1s and In 3d lineshapes. The deconvolution of these lineshapes allowed for the clear identification of a surface layer on the ITO which is oxidized to a greater extent than the underlying bulk ITO. The surface oxide layer, composed of indium oxide and indium hydroxide, is deficient of oxygen vacancies and would therefore be expected to act as an insulating barrier on the ITO surface. Peak fitting conditions allowed for an estimation of the thickness of this insulating layer. Sandia National Laboratories is a multi-program laboratory managed and operated by Sandia Corporation, a wholly owned subsidiary of Lockheed Martin Corporation, for the U.S. Department of Energy's National Nuclear Security Administration under contract DE-AC04-94AL85000.

5:00pm OX+SS+TF+MI-MoA10 Organic Molecules Adsorbed on the ZnO(10-10) Surface: An Infrared Reflection Absorption Spectroscopy Study, M. Buchholz, Karlsruhe Institute of Technology, Germany, H. Noei, Y. Wang, Ruhr University Bochum, Germany, A. Nefedov, Ch. Wöll, Karlsruhe Institute of Technology, Germany

Except for gold, every metal forms an oxide on its surface when exposed to the ambient atmosphere. The understanding of chemical processes taking place on metal oxide surfaces are thus of crucial importance. One of the most important oxides is ZnO. As a result of its semiconducting and optical properties, this material is used in many applications such as gas sensors, thin film solar cells, as well as in photocatalysis and photooxidation[1]. The important surfaces of ZnO are the polar Zn- or O-terminated ZnO(0001) and ZnO(000-1) as well as the mixed-terminated ZnO(10-10) surface. The latter is the dominating surface for ZnO powder particles and energetically most favorable.

Here we report on the adsorption of formic acid and maleic anhydride (MA) molecules on the mixed-terminated ZnO(10-10) surface. Formic acid is a good model molecule for understanding the anchoring of carboxylic dye molecules in dye-sensitized solar cells. The choice of MA is motivated by the importance of the industrial process where MA is hydrogenated using Cu/ZnO catalysts. The identification of the reaction mechanism requires the identification of intermediates using IR-spectroscopy[2].

In last decades numerous IR investigations of oxide powders have been reported. An unambiguous assignment of the features present in the complex powder IR spectra, however, is only possible on the basis of reference data recorded for well-defined systems, e.g. surfaces of single crystals with defined orientation. Unfortunately, Infrared Reflection Absorption Spectroscopy (IRRAS) studies of molecular adsorbates on oxide single crystals, and, in particular on ZnO, are extremely scarce due to the fact that the sensitivity of IRRAS to adsorbate vibrations is two orders of magnitude lower for oxides than for metals. Whereas in case of TiO₂ recently with improved experimental setups adsorbate vibrations have been observed for a number of cases[3], to our knowledge molecular vibrations on clean ZnO single crystal surfaces have not yet been reported. With our novel UHV-IRRAS setup[4] high-quality IR spectra of different molecular adsorbates on ZnO(10-10) could be recorded in a routine fashion. In this presentation the obtained results will be presented and discussed.

M. Buchholz gratefully acknowledges the financial support from the Helmholtz Research School "Energy-Related Catalysis".

[1] C. Wöll, Prog. in Surf. Sci. **2007**, 82, 55-120.

[2] S. G. Girol, T. Strunskus, M. Muhler, C. Wöll, *J. Phys. Chem. B* **2004**, 108, 13736-13745.

[3] M. C. Xu, H. Noei, M. Buchholz, M. Muhler, C. Wöll, Y. M. Wang, *Catal. Today* **2012**, 182, 12-15.

[4] Y. Wang, A. Glenz, M. Muhler, C. Wöll, *Rev. Sci. Instrum.* **2009**, 80, 113108-113106.

5:20pm **OX+SS+TF+MI-MoA11 In Situ Interface Analysis of Self-Assembled Monolayers on Metal Surfaces at High Water Activities by Means of a PM-IRRAS/QCM-Setup, I. Giner, M. Maxisch, G. Grundmeier**, University of Paderborn, Germany

Aluminum and its alloys are widely used as engineering material and in a wide range of applications ranging from the aviation industry to the automotive and construction industries. As almost all engineering metals, aluminum under ambient conditions is covered by a native oxide film which alters significantly its surface physical and chemical properties. For corrosion protection and adhesion promotion, oxide covered aluminum surfaces are coated with organic films. Ultra-thin films or even monomolecular layers of organic acids like self-assembled monolayers (SAMs) of organophosphonic and organocarboxylic acids have been investigated as new advanced interfacial layers for aluminum alloys.¹ However, the stability of the self-assembled monolayers under environmental conditions is an aspect for technical applications. Different studies concerning to the stability and structure of the self-assembly monolayers under high humidity's conditions have been performed.² These studies revealed that the organic film decreased the amount of interfacial water layer but cannot prevent the water diffusion through the monolayer.³ The aim of the present work is to establish an in-situ setup combining quartz crystal microbalance (QCM) and PM-IRRAS to study the chemistry of passive films and adsorbed organic monolayers at high humidity. The metal coated quartz was used as the reflecting substrate for the PM-IRRAS measurement. Thereby, the structure of the monolayer, the amount of adsorbed water and the chemical state of the surface layer in the presence of an adsorbed water layer could be analysed in-situ. The surface hydroxyl density prior to organic molecule adsorption was adjusted by means of low temperature Ar- and H₂O- plasma treatments. Adsorption studies of H₂O on nonadecanoic carboxylic acid (NDA) monolayer modified surfaces in comparison to bare oxide covered aluminum surfaces showed, that the NDA monolayer leads to a reduced amount of adsorbed water based on the inability of water to form hydrogen bonds to the low energy aliphatic surface chemistry. Moreover the kinetics of chemisorption of water indicated by the oxyhydroxide peak growth at SAM/metal interfaces could be significantly inhibited. Furthermore, it is noticeable that interfacial carboxylate group coordinatively bound the oxide as well as the orientation of the NDA monolayer is not affected by the adsorption of several monolayers water. *Bibliography* 1. Thissen, P et al. *Langmuir* **2010**, *26*, (1), 156-164 2. Thissen, P et al. *Surface & Coatings Technology* **2010**, *204* (21-22), 3578-3584. 3. Maxisch, M et al. *Langmuir* **2011**, *27* (10), 6042-6048

Surface Science

Room: 21 - Session SS-MoA

Surface Dynamics

Moderator: D.J. Auerbach, University of California, Santa Barbara

2:00pm **SS-MoA1 Creation and Reaction of Solvated Electrons at the Vacuum-Liquid Interface, W.A. Alexander**, Montana State University, *J.P. Wiens*, University of Wisconsin-Madison, *T.K. Minton*, Montana State University, *G.M. Nathanson*, University of Wisconsin-Madison **INVITED** Over the last 70 years, thousands of reactions between solvated electrons and dissolved species have been investigated in water and other protic solvents. Electrons born at the surface of the solvent, however, may react differently than those created within it. In this talk, I will describe gas-liquid scattering experiments using an impinging beam of sodium atoms that ionize upon contact and create electrons at the surface of liquid glycerol. We find that these electrons produce hydrogen atoms and hydrogen molecules, hydroxide ions and water, and glycerol radicals. Remarkably, nearly half the hydrogen atoms created near the surface escape into vacuum before reacting with the solvent.

2:40pm **SS-MoA3 Liquid-Crystal to Solid-Crystal Phase Transition in Flexible Aryl-Triazole Oligomer Adsorbates at the Liquid / HOPG Interface, B. Hirsch, K. McDonald, A. Flood, S.L. Tait**, Indiana University - Bloomington

Supramolecular self-assembly at the liquid / solid interface is a powerful strategy for the bottom-up fabrication of complex and well-ordered structures. In order to achieve greater functionality, molecules with functional groups that possess symmetries other than those of the substrate must be included. Here, we explored this idea by integrating the pseudo-C5 triazole moiety into an oligomer through facile synthesis using well-known click chemistry. The molecules initially adsorbed without direct commensuration with HOPG (high oriented pyrolytic graphite) in a lamellar-like liquid-crystalline phase. Subsequent molecular conformational

changes are believed to enable a spontaneous phase transition to a more condensed crystalline phase. The crystalline phase forms a dynamic bilayer, in which ripening of the second layer domains was observed. We will present scanning tunneling microscopy (STM) snapshots of this evolution and discuss the dynamics associated with these phase transitions and bilayer formation. Packing models and phase dependence on experimental conditions will be presented. This work lays the foundation for extending the library of self-assembling molecules to develop higher functionality at surfaces.

3:00pm **SS-MoA4 State-Resolved Studies of Methane Activation: Mechanistic Insights into Gas-Surface Reactivity, A.L. Utz**, Tufts University

Gas-surface reactivity measurements performed with vibrational and rotational state selected reagents provide precise energetic resolution that can be exploited to uncover important aspects of gas-surface reactivity. This talk will focus on two examples. In the first, we explore the surface temperature dependent reactivity of methane (CH₄) molecules prepared in the ν_3 C-H stretching state. We find that at low incident kinetic energy, thermal excitation of the Ni(111) surface can increase reaction probability by nearly three orders of magnitude. Calculations from the Jackson group provide insight into the origin of this effect. As a second example, we will describe recent experiments that compare the reactivity of the symmetric (ν_1) and antisymmetric (ν_6) C-H stretching states in di-deutero methane, CH₂D₂, on Ni(111). That work explores how the vibrational symmetry of the reactant molecule may influence the rate and pathway of rapid intramolecular vibrational energy redistribution (IVR) that occurs just prior to reaction, and it tests whether vibrationally adiabatic models for methane activation in the gas phase are also applicable to methane reactivity on a metal surface.

Taken together, the work highlights how general patterns of energy flow within the gas-surface reaction complex can influence reactivity patterns, and how the kinetics of energy redistribution might be used to control or enhance the rate or selectivity of reactions on surfaces.

3:40pm **SS-MoA6 Autocatalytic Decomposition Mechanism of Aspartic Acid on Cu(110) Surfaces, B.S. Mhatre, A.J. Gellman**, Carnegie Mellon University

Surface explosions are surface reaction mechanisms wherein an autocatalytic increase in the reaction rate results in the reaction proceeding to completion over a very narrow temperature range during heating. While several substrate-adsorbate systems exhibiting decomposition via surface explosion mechanism have been identified, a detailed understanding of the mechanism remains unclear. We have successfully identified aspartic acid as a suitable probe for studying surface explosion mechanism on Cu(110) surface. Because a wide range of isotopically labeled varieties of aspartic acid are commercially available, we have been able to conduct a detailed investigation of its autocatalytic reaction mechanism. Using specifically labeled aspartic acid molecules, we have identified the reaction products and identified the origins of atoms in the decomposing aspartic acid molecules. The explosive nature of the reaction mechanism has enabled us to study its kinetics using isothermal methods by heating the Cu(110) surface to a constant temperature and then monitoring the product desorption as a function of time. We observe a significant lag time during which nucleation of the reaction is occurring without observable desorption of products. Once the reaction begins, it proceeds to completion over a relatively short time period. Our preliminary studies on chiral Cu(643)^{R&S} surfaces indicate that aspartic acid exhibits enantiospecific surface decomposition kinetics. The ultimate objective of this work is to be able to identify the mechanism and in particular, the steps in the mechanism which are responsible for the enantiospecificity.

4:00pm **SS-MoA7 Quantum Tunneling Driven Assembly and Diffusion of Hydrogen and Deuterium on Cu(111), A.D. Jewell***, Tufts University, *G. Peng*, University of Wisconsin Madison, *G. Kyriakou*, Tufts University, *M. Mavrikakis*, University of Wisconsin Madison, *C.H. Sykes*, Tufts University

Hydrogenation reactions are central to the petrochemical, fine chemical, pharmaceutical, and food industries and are of increasing interest in energy production and storage technologies. The processes of molecular adsorption, dissociation, diffusion, association, and desorption are important surface phenomena in heterogeneous catalysis. Typical heterogeneous catalysts often employ alloys based on platinum, palladium, rhodium and ruthenium. While these metals are active at modest temperature and pressure, they are not always 100% selective and are expensive.

* Morton S. Traum Award Finalist

Given that molecular hydrogen (H₂) dissociation is often the rate limiting step, one strategy is to engineer the minimal catalytic ensemble that will activate H₂ but leave the other reactants untouched. We describe a system which offers low dissociation barriers at one location on the surface and weaker binding in other regions. The Pd/Cu surface alloy was prepared in the dilute limit in which 1% Pd resides as individual, isolated substitutional atoms in a 99% Cu(111) surface. In terms of adsorption, these Pd atoms significantly lower the barrier to H₂ dissociation and allow the spillover of H atoms onto the Cu surface.[1]

This system also offers the opportunity to study the diffusion, association, and assembly of large quantities of H and D on the Cu(111) surface. Through careful low-temperature scanning tunneling microscopy (STM) tracking experiments we show that quantum tunneling effects dominate the diffusion properties of H and D on the Cu surface.[2] With this direct visualization and quantification of quantum tunneling effects in adatom diffusion, we reveal two types of weak interactions between H adatoms, which lead to assembly into small clusters and larger assemblies of small clusters. We show that the self-assembly of H into large islands is, in fact, a tunneling effect resulting from inter-atom energy being much smaller than the diffusion barrier. We further demonstrate that these latter effects are not at play for D. Density Functional Theory (DFT) calculations provide estimates for both diffusion and interaction energies. Theory also provides quantum tunneling probabilities that agree well with experiment.[2]

References:

- [1] G. Kyriakou, M.B. Boucher, A.D. Jewell, E.A. Lewis, T.J. Lawton, A.E. Baber, H.L. Tierney, M. Flytzani-Stephanopoulos, and E.C.H. Sykes, *Science* **335**, 1209 (2012).
- [2] A.D. Jewell, G. Peng, G. Kyriakou, M. Mavrikakis, E.C.H. Sykes, in preparation.

4:20pm SS-MoA8 H Absorption Depth Profiling Measurement at Ultra-thin Pd(111) Film by Thermal Desorption Spectroscopy, Y. Aoki, S. Nakajima, H. Hirayama, Tokyo Institute of Technology, Japan

Palladium is a peculiar metal with non-activated dissociation and bulk incorporation of hydrogen. Previous studies of H thermal desorption spectroscopy (TDS) at Pd(111) indicated that large H₂ exposures at ~100K induce a non-saturating desorption signal which is so called as α peak at 180 K [1]. The absorption origin of the α peak was inferred as the hydrogen located in subsurface sites just below the top surface Pd atoms layer, where it is stabilized at low temperatures by an energy barrier with respect to bulk sites. However, a hydrogen depth profiling measurement by nuclear reaction analysis (NRA) at the Pd(001) surface indicated that the α_1 peak (which regards as α peak at the Pd(111)) has to be assigned to the deeper located H in the 0-50 monolayer [ML] subsurface region [2]. The actual H depth distribution however was difficult to assess precisely with NRA, since the beam induced local heating was suspected to cause a partial escape of H from detection by diffusion into the bulk. To investigate the α -H origin without any heating ambiguity, TDS has been observed at well-defined ultra-thin Pd(111) films. Controlling the Pd film thickness enables us to seek the α -H depth profiling.

Pd film was deposited at the 50 ML of Ag(111) coated Si(111) surface by a Knudsen cell at room temperature. The Pd surface structure was characterized by a reflection high-energy electron diffraction (RHEED) and an atomic force microscopy (AFM). Pd(111) film grew layer-by-layer at the Ag(111) surface when grown at room temperature without any interdiffusion. The lattice constant mismatch between Pd and Ag of 4.9 % expanded the Pd lattice constant when the Pd thickness (θ_{Pd}) was below 80 ML. It recovered the bulk lattice constant at $\theta_{Pd} > 80$ ML. H₂ was exposed to the Pd(111) surface at 102 K with an exposure pressure of 1×10^{-4} Pa. By integrating α -TDS signal, α -H absorption amount of H₂ exposure dependence ($< 4 \times 10^4$ L) and of θ_{Pd} dependence (< 560 ML) were observed.

H absorption on the Pd film ($\theta_{Pd}=420$ ML) saturated as ~8 ML at the maximum exposure of 4×10^4 L. The averaged α -H concentration corresponded to 1.9 %. The θ_{Pd} dependence of α -H at the exposure of 4050 L showed that the α -H absorption increased with θ_{Pd} (maximum θ_{Pd} was 560 ML). H concentration at $\theta_{Pd}=80$ ML was 1.8 % which was close to the saturated concentration, it decreased to 1.2 % at $\theta_{Pd}=560$ ML. Our result indicated that the α -H absorption progress from near the surface region, but it possibly to absorb at the deeper bulk region than that of the previous NRA measurement at the high exposures.

References;

- [1]. G. E. Gdowski *et al.* Surf. Sci. 181, L147 (1987).
- [2]. M. Wilde *et al.* Surf. Sci. 482, 346 (2001).

4:40pm SS-MoA9 Novel Insight Into the Formation Mechanism of Subsurface Hydrogen at Pd(110) Surfaces, S. Ohno, M. Wilde, K. Fukutani, The University of Tokyo, Japan

The present study investigates the microscopic hydrogen (H) absorption mechanism at palladium (Pd) (110) single crystal surfaces. The unique properties of H-Pd interactions such as non-activated H₂ dissociation and facile bulk absorption are well known, yet an accurate atomic-level understanding of the H transportation across the surface, i.e., penetration into the Pd interior and hydride formation during absorption as well as the H release into the gas phase has not been achieved. We apply ¹H(¹⁵N, α)¹²C resonant nuclear reaction analysis (NRA) for nondestructive H depth profiling in combination with thermal desorption spectroscopy (TDS) to quantitatively reveal the H-concentration-depth distribution and to unambiguously assign characteristic TDS features to surface-adsorbed and subsurface-absorbed H-species. To obtain additional insight into the release mechanism during thermal desorption of the H states absorbed in the Pd interior, the internal state distribution of desorbing H₂ molecules is characterized with a rovibrational state selective resonance-enhanced multiphoton ionization (REMPI) technique.

TDS experiments using isotope labeling for the surface-adsorbed and subsurface-absorbed H states reveal that two parallel absorption routes exist that lead to two distinctly different depth distributions of Pd hydride in the near-surface region which give rise to separate TDS signatures (α_1 at T=160 K and α_3 at T>190 K), respectively. The first absorption pathway involves only a few (~4%) minority sites (presumably defects) at which penetration is highly efficient and leads to in-plane localized nucleation of hydride that remains concentrated within a few nanometers below the surface (α_1 state). The second absorption route proceeds on regular terraces with a significantly slower penetration rate per site so that subsurface H diffusion leads to a more extended hydride depth distribution (α_3 state, several tens of nm below the surface). A clear difference between the two H absorption states (α_1 , α_3) is also seen in the REMPI internal-state populations of desorbing H₂. Both absorption pathways critically require gas phase H₂, replace surface-adsorbed H atoms with the gas phase isotope, and have activation energies (< 100 meV) much smaller than expected for the isolated subsurface migration of chemisorbed H. The results are accounted for by a concerted mechanism, in which pre-adsorbed H transits into the subsurface while its vacated adsorption site is simultaneously refilled by a nearby 'nascent' H atom in a state of high potential energy, which is supplied through gas phase H₂ dissociation at vacancies in the chemisorption layer.

5:00pm SS-MoA10 Glide-Plane-Specific Selectivity of HREELS Demonstrated in H:Si(110)-(1x1) Phonon Dispersion, T. Yamada, RIKEN, Japan, S.Y. Matsushita, Tohoku University, Japan, H. Kato, Science University of Tokyo, Japan, A. Kasuya, S. Suto, Tohoku University, Japan

We observed the consequence of surface glide-plane symmetry over the phonon vibration on a typical, well-defined silicon wafer. We recorded surface phonon dispersion curves on hydrogen-terminated Si(110)-(1x1) by means of high-resolution electron energy loss spectroscopy (HREELS). This surface, H:Si(110)-(1x1), was prepared by etching a Si(110) wafer in 40% aqueous solution of NH₄F. H:Si(110)-(1x1) structure involves a glide-plane symmetry, denoted as *p2mg*, along the short segment of the rectangular unit cell, containing two H-Si bonds. This glide-plane symmetry is also lucid in the extinction rule observed in the pattern of low energy electron diffraction (LEED). The normal vibrational modes are doubled into the in-phase and anti-phase modes. However, for the phonons propagating along the glide plane, ones of those pairs are excluded according to the wave vector. The H-Si symmetric stretching, anti-phase out-of-plane bending, and anti-phase in-plane bending exist only for the wave vectors in the 1st Brillouin zone, and the others exist only in the 2nd Brillouin zone. The impact scattering selection rule furthermore limits the normal modes visible to HREELS. We have verified this special case of phonon dispersion by recording angular-resolved vibrational spectra. The surface phonon dispersion curves were recorded over the 1st and 2nd Brillouin zones, by adjusting the angular configuration as well as the incident electron energy. The experimental dispersion curves are in a fair agreement with the theoretical prediction [2]. However, along Γ -X direction, the H-Si stretching mode (~ 2080 cm⁻¹) just composes a single branch as a concatenation of the symmetric mode in the 1st Brillouin zone, and the asymmetric mode in the 2nd Brillouin zone. Similarly, the out-of-plane bending (~ 680 cm⁻¹) curve is also single. This is due to the glide-plane symmetry. The in-plane bending modes are all cancelled by the EELS impact selection rule. As for the propagating direction vertical to the glide plane (Γ -X' direction), the pairs of stretching and out-of-plane bending appear simultaneously. The sub-surface phonon modes (< 600 cm⁻¹) also follow the same rule. This is a special case for the glide-plane symmetry, reflected over the reciprocal unit cell as the property of phonon waves propagating along the surface.[1] M.

Eremtchenko et al., Surf. Sci. 582 (2005) 159.[2] V. Gräschus et al., Phys. Rev. B 56 (1997) 6482.

Tuesday Morning, October 30, 2012

Biomaterial Interfaces

Room: 23 - Session BI+SS+AS-TuM

Biomolecules at Interfaces

Moderator: P. Kingshott, Swinburne University of Technology, Australia

8:20am **BI+SS+AS-TuM2 Computer Simulation of Water-Mediated Adhesion between Organic Surfaces**, A.J. Pertsin, M.H. Grunze, University of Heidelberg, Germany

The adhesive forces operating between various surfaces in aqueous media are of interest in many areas ranging from biology to electronics. This refers, in particular, to surfaces formed by self-assembled monolayers (SAMs) on solid substrates to modify the surface-sensitive properties of the latter. Another important example is provided by supported lipid bilayers, where the water-mediated bilayer-substrate adhesion determines the stability of the system. The present study is concerned with surfaces formed by a hydrophobic methyl-terminated SAM (C-SAM), a hydrophilic carboxyl-terminated SAM (hereafter, O-SAM), and a phosphatidylethanolamine (PE) bilayer. The surface-water-surface system was treated as an open one using the grand canonical Monte Carlo technique. The free energies of adhesion were evaluated by integration of simulated pressure-distance relations. For SAMs, both symmetric and asymmetric confinements were considered, as formed by like and unlike SAMs, respectively. As the confinement was increased, water confined by the C-SAMs experienced capillary evaporation. As a consequence, the adhesion energy was mainly determined by the direct interaction between bare C-SAMs. In the asymmetric SAM system, an incomplete capillary evaporation was observed, with the number of water molecules dropped by more than an order of magnitude. The remaining water molecules were all adsorbed on the O-SAM, while the C-SAM was separated from the rest of the system by a thin vapor layer. The calculated free energies of adhesion were in acceptable agreement with available experimental data. Unlike the SAM systems involving the hydrophobic C-SAM, the PE/water/C-SAM system did not experience capillary evaporation up to the highest confinements tried. A likely reason is a high molecular-level "roughness" of the PE/water interface due to a deep penetration of water in the PE bilayer. The pressure-distance dependence showed a slightly repulsive region with a depth comparable with the statistical uncertainty in pressure. By contrast, the pressure-distance curve of the PE/water/O-SAM system showed a well-defined minimum with a depth of about 0.7 kbar. The integration of this curve resulted in an adhesion free energy of 19 ± 3 mJ/m², close to the value obtained for the O-SAM/water/O-SAM and O-SAM/water/C-SAM systems (~ 25 mJ/m²).

8:40am **BI+SS+AS-TuM3 Adsorption from Saliva - Properties of Adsorbed Layers and Comparison with Other Systems**, T. Arnebrant, L. Lindh, J. Sotres, Malmö University, Sweden **INVITED**

Adsorbed salivary protein layers will cover soft and hard surfaces in the oral cavity, where they fulfill a protective function influencing adhesion and wear, and also surfaces of devices exposed to saliva. Properties of salivary films will depend on the characteristics of the surface on which they are formed as well as solution conditions (salt, pH) and will affect surface properties such as wettability and charge. Moreover, normal and lateral forces between surfaces bearing salivary films will be distinctly different than for bare surfaces. Such changes in surface properties and interactions may be relevant not only for events at oral interfaces but also for the operation of monitoring or sampling devices immersed in or exposed to saliva. Here, we show how a combined characterisation of these systems through different surface techniques provides important information on the role of this body fluid which is not available through more common chemical or biochemical approaches. The presentation will describe adsorption characteristics of salivary proteins from the total secretion as well as for purified fractions including single protein preparations. Influence by surface properties and ambient (solution) conditions will be outlined. Data on structure of salivary films as obtained by *in situ* ellipsometry, QCM-D and neutron reflectivity will be reported. Furthermore, SFA and AFM measurements of DLVO, steric, adhesive and frictional forces between surfaces bearing salivary films will be discussed. A new method for estimating the strength of salivary films based on simultaneous recording of roughness and friction data from AFM will also be described.

References: Protein Adsorption in the Oral Environment, Arnebrant T, In Biopolymers at Interfaces 2nd ed. (M. Malmsten Ed.) Marcel Dekker, 2003, pp 811-856

Friction force spectroscopy as a Tool to Study the Strength and Structure of Salivary Films. Sotres J., Liselott L., Arnebrant T. 2011. *Langmuir*, 27 (2011), 13692-13700.

9:20am **BI+SS+AS-TuM5 An Atomic Force Microscopy Based Method for the Determination of Protein Stability**, O. Croad, University of Nottingham, UK, S. Rigby-Singleton, Molecular Profiles Ltd., UK, C.J. Roberts, D.J. Scott, P.M. Williams, S. Allen, University of Nottingham, UK

A method for the early detection of instability and aggregation propensity of proteins and other biological macromolecules would be valuable for the rapid development of novel biopharmaceutical formulations. The aim of this study was to investigate the potential of atomic force microscopy (AFM) based adhesion force measurements to meet this need. We report the first key step in demonstrating this approach; a clear relationship between how frequently an AFM probe adheres to a protein coated surface and the fraction of unfolded proteins on that surface. Instability and subsequently protein denaturation are commonly linked with protein aggregation, and hence formulation failure. It was found that for the protein bovine serum albumin (BSA), the adhesion between AFM tips and protein-coated samples occurred much more frequently as either the concentration of a denaturant or temperature was gradually increased. We compared this behaviour with fluorescence based studies of the BSA unfolding in solution. Both methods provided us with almost identical ΔG values of stability and 50% unfolding ($[D]^{50\%}$) values. The data demonstrates for the first time, an AFM based method for protein stability determination. Interestingly, the method also appears to be a good reporter of the protein solution behaviour. With further development this approach could be utilized to screen for instability and aggregation propensity of a given protein therapeutic, in a range of conditions. The ultimate aim is to create a robust technique that can be performed rapidly and routinely.

9:40am **BI+SS+AS-TuM6 Von Willebrand Factor A1 Domain Structure and Function Changes on Surfaces**, E. Tronic, W. Thomas, D.G. Castner, University of Washington

The clotting protein von Willebrand Factor (VWF) binds to platelet receptor glycoprotein 1ba (GPIba) when VWF is activated, such as when VWF is exposed to a surface or is under high shear. However, the mechanism of surface activation is not known. This study characterizes function and adsorption behavior of the VWF A1 domain, which contains the GPIba binding site. Surfaces tested are glass, polystyrene, and tissue culture polystyrene. Highest VWF A1- GPIba binding is observed when A1 is adsorbed onto polystyrene, as measured by platelet rolling velocity in a parallel plate flow chamber assay. X-ray photoelectron spectroscopy (XPS) showed comparable A1 amounts are present on each surface, suggesting functional differences were not explained by differences in surface coverage. A1 surface structure was investigated using ELISA, time-of-flight secondary ion mass spectrometry (ToF-SIMS) and near-edge x-ray absorption fine structure (NEXAFS). Using monoclonal antibodies binding to a nonlinear epitope within A1, ELISA showed lower antibody binding for A1 adsorbed to polystyrene than to glass or tissue culture polystyrene. ToF-SIMS was used to identify differences in amino acid exposure, and NEXAFS showed different amide backbone ordering on the three surfaces. These studies demonstrate that the surface dependence of A1 function is likely due to differences in adsorbed surface orientation and/or conformation. This is an important consideration in *in vitro* models, where A1 is typically immobilized onto synthetic surfaces, and is also of interest for blood-contacting biomaterials. Additional studies have been done on A1 and two A1 mutants adsorbed on collagen coated tissue culture polystyrene. One mutant exhibits similar ELISA and ToF-SIMS results to the wild type A1, while the other mutant exhibits differences. This indicates that mutations in A1 can affect the conformation/orientation changes that result from A1 adsorption onto collagen.

10:40am **BI+SS+AS-TuM9 Combining Catalysis and Self-Assembly: Towards Evolvable Soft Matter**, R. Ulijn, University of Strathclyde, UK **INVITED**

Molecular networks are key to the adaptiveness of biological systems and it would be very useful if this concept could be introduced into simple man-made functional materials, which could adapt to changing environments. In biology, adaptiveness (as a consequence of evolution) is achieved through a combination of catalysis, self-assembly, molecular recognition and compartmentalisation. These individual molecular processes are closely linked, a situation which may be achieved in laboratory based systems by sharing of building blocks between these individual processes, thereby giving rise to networked systems that are highly responsive and adaptive to changing external conditions. We have made the first steps towards developing evolvable materials, and will present progress in (i)

structure/function relationships in peptide self-assembly, (ii) development of catalytic peptides, (iii) self-selecting peptide libraries achieved by combining fully reversible amino acid exchange in self-assembling peptide systems. The overall aim of this area is to produce laboratory made molecular materials that incorporate the above features and are able to adapt and change their properties in response to external environmental changes. Potential applications in biomaterials science will be discussed.

11:20am **BI+SS+AS-TuM11 Bio/Nano Interfaces of De Novo Design: Small Proteins with Large Potential**, M.G. Ryadnov, National Physical Laboratory, UK

Our ability to manipulate function at interfaces in native and near-native environments is critical for the fabrication of nanostructured materials and devices. Biomolecular self-assembly lends itself to robust bio-nano systems. However, exact construction strategies to enable desired applications stumble upon the lack of control over self-assembly processes. De novo peptide design provides a saving solution to this.[1] Small proteins can be designed to deliver functions that are otherwise accessible only to macromolecular subcellular complexes. Examples include gene delivery systems,[2] fibrillar microscopic structures for tissue repair[3] and responsive antimicrobial agents[4]. A key factor in all such designs is their structural and functional relevance to native self-assembling structures, be these viruses, extracellular matrices or host defence systems. Thus, this is our ability to construct such materials at will that advances the development of efficient bio/nano-interface technologies.[5] **References** 1. Ryadnov, M. G. (2012) Prescriptive peptide design. In *Amino acids, peptide and proteins*. (Farkas, E. & Ryadnov, M. G., eds.) SPR, RSC Publishing (2012), v.37. 2. Lamarre, B., Ravi, J. & Ryadnov, M. G. (2011) GeT peptides: a single-domain approach to gene delivery. *Chem. Commun.*, 47, 9045-9047. 3. Bella, A., Ray, S., Shaw, M. & Ryadnov, M. G. (2012) Arbitrary self-assembly of peptide extracellular microscopic matrices. *Angew. Chem. Int. Ed.*, 51, 428-431. 4. Ryadnov, M. G., Mukamolova, G. V., Hawrani, A. S., Spencer, J. & Platt, R. (2009) RE-coil: an antimicrobial peptide regulator. *Angew. Chem. Int. Ed.* 48, 9676-9679. 5. Ryadnov, M. G. (2009) *Bionanodesign: Following the Nature's touch*. RSC Publishing, 250 pp.

11:40am **BI+SS+AS-TuM12 Application of CD and SRCD Techniques to the Study of Protein/Nanoparticle Complexes**, G. Ceccone, S. Laera, L. Calzolari, D. Gilliland, EC-JRC-IHCP, Italy, R. Hussein, G. Siligardi, Diamond Light Source, UK, F. Rossi, EC-JRC-IHCP, Italy

Nanotechnology is having a large impact in very different scientific fields and the use of nanotechnology-based materials is not just limited to research laboratories, but has already been applied in several industrial sectors and into real products as disparate as medical diagnostic tools, drug delivery systems, cosmetics, and consumer products.

In particular, engineered nanoparticles (ENPs) are used in different applications such as cosmetics, food and medicine and currently more than 600 products containing nanomaterials are already on the market[1,2,3]. At the same time there is a growing public concern about the safety of ENPs since it has been demonstrated that those intended for industrial and medical applications could cause adverse effects in mammals or aquatic organisms by specific mechanisms depending on their physical chemical properties[4]. However, the interaction of nanomaterials with complex matrices is far to be understood. In fact, although it is now increasingly accepted that the surface of nanoparticles in a biological environment is modified by the so called "protein corona"[5,6], the importance of the detailed structure of the adsorbed protein-solution interfaces is still not much addressed in the nanotoxicology literature[7].

In this work, we report the use of Circular Dichroism (CD) and Synchrotron Radiation Circular Dichroism (SRCD) to detect changes in the secondary structure and stability of different classes of proteins interacting with nanoparticles. In particular, we show that by using the SRCD we can detect structural changes of proteins in the nanomolar concentration range when they form protein-nanoparticle complexes[8]. Furthermore, the adsorption of protein on NP modifies their melting point in a composition and size dependent manner, indicating once more that the protein corona formation is strongly depending on the nanoparticles physico-chemical properties. For instance, while the presence of Au NPs do not influence the thermal unfolding process of human serum albumin (HSA), a significant decrease of the HSA melting temperature (about 6°C) is observed in presence of Ag NPs.

-
- [1] R.A. Petros, J. M. DeSimone, *Nature Rev.*, **9**, (2010), 616.
[2] G.J. Noynek et al., *Crit. Rev. Toxicol.*, **37**, (2007), 251.
[3] N. Sozer, J.L. Kokini, *Trends in Biotechnol.*, **27(2)**, (2009), 82.
[4] G. Obersdorter et al., *Env. Health Persp.* **113**, (2005), 823
[5] I. Lynch, K. A. Dawson, *Nanotoday*, **3(1-2)**, (2008), 40

- [6] M.P. Monopoli et al., *J. Am. Chem Soc.*, **133**, (2011), 2525
[7] P. Sabatino et al., *J. Coll Interface Sci.*, **314**, (2007), 389
[8] S. Laera et al., *Nano Lett.*, **11**, (2011), 4480.

In Situ Microscopy and Spectroscopy Focus Topic Room: 7 - Session IS+AS+SS+EN-TuM

In Situ Spectroscopic Studies of Catalysis and Gas-Solid Reactions

Moderator: B. Roldan Cuenya, University of Central Florida

8:00am **IS+AS+SS+EN-TuM1 Ambient Pressure XPS for Alternative Energy Research and Environmental Science**, H. Bluhm, Lawrence Berkeley National Laboratory **INVITED**

Solid/vapor and liquid/vapor interfaces play a major role in many processes in the environment and technology. Examples include heterogeneous catalysis, fuel cell technology, aerosol chemistry, and weathering of minerals and rocks. The measurement of these interfaces under realistic conditions of gas pressure and temperature has gained increasing importance over the last decades. Ambient pressure photoelectron spectroscopy (APXPS) is a promising technique for the investigation of liquid and solid surfaces in the presence of gases at pressures in the Torr range. The heart of an APXPS instrument is a differentially pumped electrostatic lens system that separates the sample, which is in a gas atmosphere at pressures of up to 5 Torr, from the electron spectrometer, which is kept in vacuum. This talk will discuss the history and basics of APXPS and show examples of the application of APXPS to the study of aqueous solution, metal oxides, soot, and fuel cell electrodes under reaction conditions.

8:40am **IS+AS+SS+EN-TuM3 In Situ Soft X-ray Photon-in/Photon-out Spectroscopy of Photo-electrochemical Reactions of Hematite in Water Splitting**, J.H. Guo, Lawrence Berkeley National Laboratory, A. Braun, Empa, Swiss Federal Laboratories for Materials Science and Technology, K. Sivula, Ecole Polytechnique Fédérale de Lausanne (EPFL), Switzerland, D. Bora, Lawrence Berkeley National Laboratory, J.F. Zhu, L. Zhang, University of Science and Technology of China, M. Grätzel, Ecole Polytechnique Fédérale de Lausanne (EPFL), Switzerland, E.C. Constable, University of Basel, Switzerland

Hydrogen fuel generation by solar water splitting in photoelectrochemical cells (PEC) is one of the first steps in artificial photosynthesis and an essential part of the holy grail of solar energy conversion. Iron oxide, literally "rust", is an interesting PEC photoanode material because of its affordability, good stability, good spectral match of the solar spectrum, and yet controversial because of its poor electronic structure. At present, iron oxide is taking center stage as prospective PEC anode material.

PEC electrodes are typically semiconducting metal oxides to form electron-hole pairs when struck by light. In the photoanodes such as hematite, the generated holes must diffuse to the iron oxide surface where they can oxidize water to oxygen. However, the electronic structure of iron oxide is such that the photogenerated holes tend to recombine and annihilate with the electrons before reaching the surface and performing the required chemical work on water splitting. Currently, researchers worldwide try to understand the peculiarities of iron oxide so as to invent strategies to improve this material.

The Advanced Light Source produces soft X-rays which are optimally suited to study the electronic structure of electrode materials and which can detect electron holes. But the holes needed for solar water splitting by iron oxide require an anodic electric bias plus the illumination. Moreover, the holes are transitional and quite elusive. Also, soft X-rays cannot easily peek into a PEC cell. The unique design of the in-situ cell at the ALS has overcome the burden [1-3]. Recently the experiment has been performed for studying, under in-situ and operando conditions, the hole generation in a specifically designed photoelectrochemical cell. The oxygen valence band signature was recorded while tuning the PEC relevant parameters, two different types of holes in the valence band near the Fermi energy are discovered [4].

References:

- [1] "X-ray Emission Spectroscopy of Hydrogen Bonding and Electronic Structure of Liquid Water", J.-H. Guo et al., *Phys. Rev. Lett.* **89**, 137402 (2002).
[2] "Electronic Structure of Cobalt Nanocrystals Suspended in Liquid", H. Liu et al., *Nano Lett.* **7**, 1919 (2007).

[3] "In situ soft X-ray absorption spectroscopy investigation of electrochemical corrosion of copper in aqueous NaHCO₃ solution", P. Jiang et al., *Electrochem. Comm.* **12**, 820 (2010).

[4] "Direct Observation of Two Electron Holes in a Hematite Photoanode during Photoelectrochemical Water Splitting", A. Braun et al., *J. Phys. Chem. C* **116**, 16870 (2012).

9:00am **IS+AS+SS+EN-TuM4 XANES and Ambient Pressure XPS (APXPS) Study: Investigations of the Local Structure and Final-State Effect in Partially Reduced SnOx Nanoislands on Pt(111)**, S. Axnanda, Z. Liu, B. Mao, Lawrence Berkeley National Laboratory

Heterogeneous catalysts consisting of small particles having a high concentration of structural defects and under-coordinated sites make up the majority of the catalytic processes in industrial chemistry. One important recent example of interest shows that the interface-confined coordinatively unsaturated ferrous (CUF) sites together with the metal supports (FeO_x/Pt(111)) are active for dioxygen activation which causes the ensemble to be highly efficient for CO oxidation at low temperature under typical operating conditions of a proton-exchange membrane fuel cell.[1-2] In this work, we report another spectroscopic evidence to further confirm an enhanced reactivity at the edges of small catalyst particles. The system in interest is partially oxidized SnO_x (Sn²⁺) nanoislands supported on Pt(111) for ethanol oxidation reaction (EOR), an electrode material in a direct alcohol fuel cell (DAFC). Our findings suggested that SnO_x/Pt(111) inverse catalysts have improved activity for EOR in acidic media as compared to a bare Pt(111) surface.[3] We also found that the most active surface had a small coverage of SnO_x (0.3- 0.4 ML). Water activation at low potentials is currently attributed to be the promoting effect of SnO_x nanoparticles, since this enhances the oxidation of chemisorbed CO formed on Pt sites during the EOR.[4] To better understand this increased activity, we performed study with the goal to indicate the actual state of Sn in SnO_x nanoislands before and after the SnO_x /Pt(111) is used in EOR showing the increased activity: purely oxide Sn or mixed Sn alloy and Sn oxide, using a combination of APXPS and XANES techniques. BE shift in the XPS core-line spectra of Sn and O, soft X-ray XANES spectra (Sn M4,5-edge, O K-edge) will be collected and compared to the corresponding XPS spectra (Sn 3d, O 1s) to explain the actual state of Sn before and after the SnO_x/Pt(111) is used in the EOR.

1. Fu, Q., et al., Interface-Confined Ferrous Centers for Catalytic Oxidation. *Science*, 2010. 328: p. 1141.

2. Deng, X., et al., Reactivity Differences of Nanocrystals and Continuous Films of α -Fe₂O₃ on Au(111) Studied with In Situ X-ray Photoelectron Spectroscopy. *J. Phys. Chem. C*, 2010. 114: p. 22619.

3. Zhou, W.P., et al., Enhancement in Ethanol Electro-Oxidation by SnOx Nanoislands Grown on Pt(111): Effect of Metal Oxide-Metal Interface Sites. *Journal of Physical Chemistry C*, 2011. 115: p. 16247.

4. Axnanda, S., W.P. Zhou, and M.G. White, CO Oxidation on Nanostructured SnO_x/Pt(111) surfaces: Unique Properties of Reduced SnO_x. *Phys. Chem. Chem. Phys.*, 2012. Submitted.

9:20am **IS+AS+SS+EN-TuM5 Epitaxial Strontium Substituted Lanthanum Cobalt Oxides Investigated using In Situ Ambient Pressure X-ray Photoelectron Spectroscopy Near Operating Conditions Under Applied Potentials**, E. Crumlin, E. Mutoro, Massachusetts Institute of Tech., Z. Liu, Lawrence Berkeley National Lab, M.D. Biegalski, Oak Ridge National Lab, W.T. Hong, Massachusetts Institute of Tech., H.M. Christen, Oak Ridge National Lab, H. Bluhm, Lawrence Berkeley National Lab, Y. Shao-Horn, Massachusetts Institute of Tech.

Operating conditions for solid oxide fuel cell (SOFC) are typically at high temperatures (~500 – 1000 °C) and ambient pressures (~1 atm). We have to understand how the physical and chemical properties of SOFC materials, particularly the cathode which is responsible for a majority of the fuel cells area specific resistance, change under operating conditions. Such data can provide insights into the mechanism of the oxygen reduction reaction (ORR) which may lead to material development strategies to improve the cathode performance. However, these operating conditions are far away from conventional characterization techniques that are often applied at room temperature or even in ultrahigh vacuum (UHV). Our recent work using *in situ* ambient pressure X-ray photoelectron spectroscopy (APXPS) has shown that (001) oriented epitaxial films of La_{0.8}Sr_{0.2}CoO_{3- δ} (LSC₁₁₃) can exhibit Sr enrichment in the near-surface perovskite lattice structure ("lattice") as temperatures were raised from 220 °C to 520 °C in a p(O₂) of 1×10⁻³ atm. In contrast under the same conditions, a bulk pellet of LSC demonstrated no changes in Sr content within the "lattice" region. The Sr enrichment is believed to play a key role in the observed one order of magnitude enhancement in ORR activity (as measured by the surface exchange coefficient, k^s) of the (001) epitaxial films relative to bulk LSC₁₁₃. In this work, we continue the previous investigations of the chemical properties of (001) epitaxial LSC₁₁₃ as a function of temperature cycling

between 220 °C and 520 °C at a p(O₂) of 1×10⁻³ atm. Additionally, the comparison of LSC₁₁₃, (La_{0.5}Sr_{0.5})₂CoO_{4+ δ} (LSC₂₁₄), and LSC₂₁₄-decorated LSC₁₁₃ (LSC_{113/214}) at p(O₂) of 1×10⁻³ atm as a function of temperature and under applied cathodic potentials will be presented in order to provide insights into the physical origin responsible for the observed ~3 orders of magnitude ORR activity enhancement of LSC_{113/214} relative to (001) epitaxial LSC₁₁₃.

9:40am **IS+AS+SS+EN-TuM6 Probing Nitrogen and Metal Speciation in Non-Platinum Electrocatalysts by Ambient Pressure X-ray Photoelectron Spectroscopies and DFT Calculations**, K. Artyushkova, B. Halevi, A. Serov, The University of New Mexico, B. Kiefer, New Mexico State University, P. Atanassov, The University of New Mexico

X-ray Photoelectron Spectroscopy (XPS) has been the main surface analysis method for determining the chemical environment and coordination of nitrogen and transition metal (TM) in the non-precious group metal oxygen reduction reaction (ORR) electrocatalysts. Even though there is an agreement that Me-N_x serve as one of the possible active sites in ORR, the distribution of Me-N₂ vs Me-N₄ centers and their specific role still remains unresolved. XPS which heavily relies on use of reference spectra in accurate identification of species cannot address this issue directly as no reference compounds with Me-N₂ moieties are available. The assignment of peaks and nitrogen coordination is not straightforward due to overlapping peaks that appear within a narrow energy window of 2.5-eV and the full width half maximum (fwhm) for individual species is on the order of 1.2-1.5-eV. Being able to calculate binding energy shifts based on molecular structure can be very important tool for assisting in this task. We will report on BE shifts that have been calculated at the DFT level and their comparison to experimentally obtained values for metal-less and metal-containing porphyrins. Information obtained from the DFT calculations will be used as input into curve-fitting XPS spectra for various model N-Me containing compounds as well as from electrocatalyst. We will compare chemical information derived from conventional XPS as well as in-situ ambient-pressure XPS using variable energy synchrotron source.

10:40am **IS+AS+SS+EN-TuM9 Resolving Growth of Palladium Nanocatalysts Using In Situ FT-IR, XAS and PDF under Practical Atomic Layer Deposition Conditions**, Y. Lei, J. Lu, B. Liu, H. Zhao, J. Greeley, P. Chupas, J. Miller, J.W. Elam, Argonne National Laboratory

Nanostructured Pd catalysts prepared by ALD have been demonstrated highly active for alkene hydrogenation, methanol decomposition reaction, and alcohol oxidation for fuel cells. Development of supported Pd nanoparticles with Controlled size/structure relies on the fundamental understanding of the two half reactions with high precision during Pd ALD. However, evolution of Pd surface species, as well as the subsequent nucleation and growth of palladium nanoparticles during Pd ALD is still not clear.

Mechanism of assembly of highly dispersed Pd nanoparticles on TiO₂ surfaces from palladium hexafluoroacetate (Pd(hfac)₂) were investigated by means of *in situ* Infrared (IR) spectroscopy, X-ray absorption spectroscopy (XAS) and pair distribution function (PDF) under practical atomic layer deposition condition simultaneously. Density function theory simulation was applied to understanding the reaction mechanism. On chlorine-containing TiO₂ surface, Pd(hfac)₂ primarily adsorbed on TiO₂ surface as Pd(hfac)Cl₂* species, confirmed by both XAS and DFT calculations. *In-situ* FT-IR results reveal that deligation of Pd(hfac)Cl₂* species began at as low as 100 °C with the present of formalin. Further on, *in-situ* XAS results indicated that cleavage of Pd-O bond occurred first, followed by cleavage of Pd-Cl bond. Sequentially, Pd atoms started to gain mobility and agglomerate to small nanoparticles. The hfac ligands spilled to TiO₂ surface as site blockers for ALD. The surface poisons were eventually removed at 225 °C. Nano-size palladium-carbon phase was also found after long exposure of formalin. Atomic resolution aberration-corrected STEM image showed one nanometer size crystalline Pd particles were synthesized using ALD. The catalytic performance of these Pd nanocatalysts was further demonstrated in several applications.

In summary, dynamic growth of Pd nanocatalysts was obtained utilizing a combination of *in-situ* techniques.

11:00am **IS+AS+SS+EN-TuM10 Catalyst Characterization using In Situ XAS and XPS: From Nanoparticles Synthesis to Evolution of Structural/Electronic Properties under Reaction Conditions**, A.M. Karim, Pacific Northwest National Laboratory **INVITED**

Catalysts are used to facilitate the important industrial chemical processes, leading to products valued in the trillions of dollars annually just in the U.S and most catalysts used in large-scale processes are solids. To maximize the number of sites available for reaction, catalysts are typically comprised of metallic/metal oxide nanoparticles dispersed on high surface area supports.

The activity and selectivity of metallic nanoparticles strongly depend on their size, shape and composition [1-8]. In order to design more active and selective catalysts, it is essential to identify the catalytically active sites and understanding their geometric and electronic properties which requires: (1) synthesis of well-defined catalyst structures and (2) the ability to correlate individual reaction pathway(s) with the type of active site(s) available on the catalyst surface under reaction conditions.

This talk is going to cover our work on *in situ* characterization of nanoparticles from the synthesis stage to the evolution of their structural/electronic properties under reaction conditions using X-ray photoelectron and X-ray absorption spectroscopies. The catalyst systems that will be covered include:

Pd nanoparticles synthesis in solution: Understanding the nucleation and growth mechanisms.

Supported Pt, PtRe and PtNi nanoparticles under aqueous phase reaction condition: Correlating the structural and electronic properties with the catalytic activity and selectivity.

References:

- [1] Boudart, M. *Adv. Catal.* 1969, 20, 153.
- [2] Boudart, M. *Journal of Molecular Catalysis* 1985, 30, 27.
- [3] Ichikawa, S.; Poppa, H.; Boudart, M. *Journal of Catalysis* 1985, 91, 1.
- [4] Somorjai, G. A.; Carrazza, J. *Industrial & Engineering Chemistry Fundamentals* 1986, 25, 63 [5] Liu, Z.; Hu, J. E.; Wang, Q.; Gaskell, K.; Frenkel, A. I.; Jackson, G. S.; Eichhorn, B. *Journal of the American Chemical Society* 2009, 131, 6924.
- [6] Alayoglu, S.; Nilekar, A. U.; Mavrikakis, M.; Eichhorn, B. *Nature Materials* 2008, 7, 333.
- [7] Sinfelt, J. H. *Journal of Catalysis* 1973, 29, 308.
- [8] Sinfelt, J. H. *Accounts of Chemical Research* 1977, 10, 15.

11:40am **IS+AS+SS+EN-TuM12 *In Situ* Study of the Oxidation of CO over Ir(111)**, J. Knudsen, Lund University, Sweden, Y. Monya, Keio University, Japan, J. Schnadt, M.A. Arman, E. Grånäs, Lund University, Sweden, H. Kondoh, Keio University, Japan, J.N. Andersen, Lund University, Sweden

The platinum group metals are known to be excellent catalysts for the oxidation of carbon monoxide, and the reaction mechanisms over the surfaces of these metals have been studied for a long time. Nevertheless, only during recent years a new picture has emerged which suggests that the catalytically active phase often is formed first under reaction conditions – which implies realistic pressures rather than ultrahigh vacuum (UHV) – and that it is different from the adsorption structures known from UHV experiments. In the case of the Pt(111) surface a very oxygen-rich chemisorbed phase has been suggested as the catalytically active phase [1], whereas a surface oxide have been suggested for the Ru(0001) surface [2]. Thus, for each different surface different phases and mechanisms might be at play, and, moreover, the phase might depend quite strongly on the conditions (pressure and temperature) used.

With this in mind we have studied the CO oxidation reaction over the Ir(111) surface and the related adsorption systems of CO and oxygen on Ir(111) using a combination of *in situ* Ambient pressure x-ray photoelectron spectroscopy (APXPS) – carried out at the new APXPS instrument at the Swedish synchrotron radiation facility MAX IV Laboratory – and *ex situ* Scanning tunnelling microscopy (STM) and x-ray photoelectron spectroscopy (XPS) measurements performed in UHV.

A recent surface x-ray diffraction study reports different oxygen phases for the Ir(111) surface at oxygen pressures from 10^{-6} to 100 mbar – chemisorbed oxygen, a trilayer, a multilayer oxide, and a bulklike oxide [3]. Concentrating on pressures at around 1 mbar, we find a variety of oxygen-rich structures. The corresponding CO adsorption phase formed at 1 mbar CO pressure is an assembly of separated CO_{16} clusters with the CO molecules sitting in on-top sites [4].

The reactivity at 1 mbar total pressure ($\text{O}_2:\text{CO}$ ratio 9:1) and at different temperatures was studied by APXPS and simultaneous monitoring of the gas composition. We find that the phase with the highest activity for the oxidation of CO is a surface phase which contains both CO and oxygen. By comparing with the measured adsorption structures of oxygen we find that the oxygen structure is quite similar to the $p(2\times 1)\text{-O}$ structure formed on Ir(111) under UHV conditions. This contrasts with what is found for other platinum group metals such as the Pt(111) surface [2], for which CO oxidation is favoured over oxygen rich phases.

- [1] A. L. Gerrard, J. F. Weaver, *J. Chem. Phys.* **123** (2005) 224703.
- [2] H. Over et al., *Science* **287** (2000) 1474.
- [3] Y. B. He et al., *J. Phys. Chem.* **112** (2008) 11946.
- [4] L.-M. Yang, S.-L. Yau, *J. Phys. Chem. B.* **104** (2000) 1769.

Surface Science

Room: 21 - Session SS-TuM

Surface Reactivity of Oxides

Moderator: A.L. Utz, Tufts University

8:00am **SS-TuM1 Preparation, Characterization and Catalytic Activity of Model WO_3 Catalysts**, Z. Dohnalek, Pacific Northwest National Laboratory **INVITED**

Supported early transition metal oxides have important applications in numerous catalytic reactions. In our studies, conversion of small aliphatic alcohols to alkenes, aldehydes/ketones, and ethers is employed to probe the structure-activity relationships on model WO_3 catalysts. To understand how the structure and binding of WO_3 species affect catalytic properties we prepared a number of well-characterized systems. Direct sublimation of WO_3 solid was used to generate cyclic gas-phase (WO_3)₃ clusters. As shown in our matrix isolation experiments, sublimation leads to pure (WO_3)₃ clusters. The (WO_3)₃ clusters were embedded in alcohol matrices and their support-free chemistry was explored in subsequent temperature programmed reaction experiments. Model supported catalysts were created by depositing (WO_3)₃ clusters on $\text{TiO}_2(110)$ and $\text{FeO}(111)$ and subsequently characterized using scanning tunneling microscopy and surface sensitive spectroscopies. In other studies, epitaxial and nanoporous thin WO_3 films were prepared on Pt(111). The catalytic chemistry of all the systems is compared and contrasted with that observed on unsupported (WO_3)₃ clusters. Calculations employing Density Functional Theory provide molecular-level mechanistic insight into the role structure and binding of (WO_3)₃ clusters to the support plays in determining their catalytic properties.

This work was supported by the US Department of Energy, Office of Basic Energy Sciences, Division of Chemical Sciences, Geosciences & Biosciences and performed in Environmental Molecular Sciences Laboratory (EMSL), a national scientific user facility sponsored by the Department of Energy's Office of Biological and Environmental Research and located at Pacific Northwest National Laboratory (PNNL). PNNL is a multiprogram national laboratory operated for DOE by Battelle.

8:40am **SS-TuM3 EUV Photon Enhanced Oxidation of Carbonaceous Layer at a TiO_2 Film Surface**, N.S. Faradzhev, J.T. Yates, Jr., University of Virginia, S.B. Hill, T.B. Lucatorto, National Institute of Standards and Technology

We report the photo oxidation of a carbonaceous layer originally grown by 92 eV radiation-induced chemistry. The C film is supported on a surface of a nm thick amorphous TiO_2 film. Photo oxidation is achieved using various oxygen-containing molecules. The TiO_2 film mimics one of the possible protective layers of EUV Lithography optics, and the C film mimics optics contamination produced by 92 eV photons in a EUVL stepper apparatus. The C layer (~4 nm) is deposited by photodecomposition of the linear hydrocarbon molecule, *n*-tetradecane, using the NIST synchrotron ultraviolet facility (SURF III) in an UHV cell. The kinetics of C growth and C removal are monitored in real time using *in situ* single wavelength ellipsometric measurements. After each set of experiments, *ex-situ* XPS is used to detect the residual thickness of the carbonaceous film and the changes in its chemical state. We found that exposure to a vapor beam of several O-containing molecules has little or no effect on the C film in the dark. In the presence of EUV photons, the ability of these molecules to volatilize carbon as either CO or CO_2 increases significantly. The carbon removal rate increases with the partial pressure of the oxidizer. The substrate temperature has little effect on the carbon removal rate and this is in contrast to the rate of radiation-induced C growth that exhibits a very strong temperature dependence. The rate of removal of C depends upon the EUV irradiation and does not occur appreciably in the dark.

Although the studies are not finished yet, our results indicate that processes of C growth and C removal may proceed via different routes. In an earlier study, we found that during C growth, the hydrocarbon molecule arrives at the surface in its ground state and forms a weak bond to the bare or C-covered TiO_2 surface. The molecule is not trapped permanently and will thermally desorb within a characteristic time. It can also be either photo-desorbed or photo-decomposed to produce the carbonaceous film via direct (photo excitation) or indirect (secondary electron excitation, e.g. DEA) processes. For photo oxidation, the first step requires the formation of a strong bond of the oxidizer molecule to the surface. An oxidizer molecule will either arrive at the surface in an electronically excited molecular state or arrive in its ground state and find an EUV-activated long-lived electronically excited state at the surface. In both cases, the oxidizer molecule will stay on the surface for a sufficiently long time to decompose and react to produce a volatile product (e.g. CO).

This study is being performed as a part of EUVL Contamination cooperative research at NIST and UVA.

9:00am **SS-TuM4 Reactions of Water with Vacuum Fracture Surfaces of Sodium-Aluminosilicate Glass: Effects of Composition on Reactivity, K. Adib, J.E. Dickinson,** Corning Incorporated

We have synthesized different ternary $\text{SiO}_2:\text{Al}_2\text{O}_3:\text{Na}_2\text{O}$ glasses containing bridging oxygens and non-bridging oxygens (NBO) and fractured them in ultrahigh vacuum to produce pristine surfaces. X-ray photoelectron spectroscopy of oxygen core levels and valence band were used to determine the fraction of non-bridging oxygens (SiONa) to bridging oxygens (SiOSi and SiOAl) on the vacuum fractured surfaces. For those glasses where the NBO fractions of the total oxygen were held constant, a 0.2 eV variance was observed in the binding energies of the NBO O1s core levels consistent with substantial changes, as a function of composition, in the ionicity of the bond between the NBO and sodium. The fracture surfaces were then exposed to partial pressures of H_2O at ambient temperature. It was observed that water reacts primarily with the NBO's to produce SiOH in place of SiONa. Non-bridging oxygens from glass compositions that contained less alumina had lower electron binding energy and were more likely to react with water. Molecular dynamics simulations were used to elucidate the role of H_3O^+ in the reaction of water with the non-bridging oxygens.

9:20am **SS-TuM5 Reactivity of Highly-hydroxylated $\text{TiO}_2(110)$ Surface Prepared via Carboxylic Acid Adsorption and Photolysis, I. Lyubnitsky, Y.G. Du, N.G. Petrik,** Pacific Northwest National Laboratory, N.A. Deskins, Worcester Polytechnic Institute, Z.-T. Wang, M.A. Henderson, G.A. Kimmel, Pacific Northwest National Laboratory

We present a novel, photochemical approach to prepare a highly-hydroxylated $\text{TiO}_2(110)$ and discuss the reactivity of the resulting surface. $\text{TiO}_2(110)$ surfaces with an OH_b coverages up to 0.5 ML have been obtained upon trimethyl acetic acid (TMAA) dissociative adsorption and subsequent photolysis at 300 K. The formation and chemistry of such surface have been examined at the atomic level by a combination of scanning tunneling microscopy, temperature-programmed desorption, photo stimulated desorption, and density functional theory methods. Deprotonation of TMAA molecules upon adsorption produces both surface bridging hydroxyls (OH_b) and bidentate trimethyl acetate (TMA) species with saturation coverage of near 0.5 ML. The TMA species can be selectively removed by ultra-violet light irradiation while OH_b 's survive photolysis. At high coverages, the OH_b species typically occupy second-nearest neighbor sites along the bridging oxygen row locally forming linear (2×1) structures of different lengths, although the surface is less ordered on a long scale. The annealing of the highly-hydroxylated surface leads to hydroxyl recombination and H_2O desorption with $\sim 100\%$ yield, thus ruling out the diffusion of H into the bulk. In agreement with experimental data, theoretical results show that the recombinative H_2O desorption is preferred over both H bulk diffusion and H_2 desorption processes.

9:40am **SS-TuM6 Infrared Spectroscopy of CO_2 Adsorbed on $\text{TiO}_2(110)$, N.G. Petrik, G.A. Kimmel,** Pacific Northwest National Laboratory

We have studied the adsorption of CO_2 on $\text{TiO}_2(110)$ using reflection-absorption infrared spectroscopy (RAIRS) and temperature programmed desorption (TPD). Infrared spectra were obtained for s- and p-polarized light with the plane of incidence parallel and perpendicular to the [001] azimuth of $\text{TiO}_2(110)$. As a result, the RAIRS provide detailed information on the adsorption geometry for the CO_2 versus coverage. Initially, CO_2 adsorbs in vacancies in the bridge-bonded oxygen (BBO) rows with the peak for the asymmetric stretch seen at 2346.5 cm^{-1} for both s- and p-polarized light. Hydroxylation or oxidation of the vacancies suppresses this feature. After filling the vacancies, CO_2 adsorbs on Ti_{5c} sites ($\text{CO}_2(\text{Ti})$). The asymmetric stretch for $\text{CO}_2(\text{Ti})$ starts at $\sim 2342 \text{ cm}^{-1}$ and then red-shifts to 2332 cm^{-1} at 1 ML. CO_2 TPD spectra show that the shift in the RAIRS spectra correlates with a decrease in the CO_2 binding energy from ~ 47 to $\sim 34 \text{ kJ/mol}$ as the coverage increases from 0 to 1 ML. For $\text{CO}_2(\text{Ti})$, the absorbances for the s-polarized spectra are similar for both azimuths indicating that the ensemble-average of the adsorbed CO_2 has approximately equal components along both azimuths. The p-polarized RAIRS spectra show that $\text{CO}_2(\text{Ti})$ also adsorbs with a component normal to the surface. Between 1 and 1.5 ML, CO_2 adsorbs on BBO sites. These CO_2 absorb only s-polarized light with its plane of incidence parallel to the BBO rows indicating that the molecules are oriented parallel to the surface and perpendicular to the BBO rows. The CO_2 RAIRS spectra are compared with STM results and DFT theory to provide detailed insight into its molecular orientation and coverage-dependent mobility.

10:40am **SS-TuM9 Low-temperature Dissociation of CO_2 on Ni/CeO₂/Ru(0001) Model Catalyst, D.D. Kong,** University of Science and Technology of China, K.-H. Ernst, EMPA, Switzerland, J.F. Zhu, University of Science and Technology of China

Model Ni/CeO₂(111) catalysts were prepared by depositing nickel atoms onto well-ordered cerium oxide films grown on Ru(0001) and were investigated using photoelectron spectroscopy (XPS) and reflection absorption infrared spectroscopy (RAIRS). It is found that the fully oxidized CeO₂ thin films are slightly reduced to CeO_{1.97} after 0.2 ML Ni deposition. When CO_2 is exposed to the surface of clean CeO₂(111) film at 97 K, the physisorbed linear molecular CO_2 and carboxylate species are observed. However, on the CeO₂(111) surface covered with 0.6 ML Ni, CO_2 immediately dissociates upon adsorption at 97 K, leading to the formation of Ni-CO adsorbates and partial oxidation of Ni nanoparticles. This dissociation activation of CO_2 is inhibited when Ni nanoparticles on CeO₂ are pre-oxidized. In contrast to the results reported for CO_2 adsorption on Ni single-crystals where the dissociation temperature was found to be higher than 240 K, the much lower dissociation temperature ($\sim 97 \text{ K}$) for CO_2 on Ni nanoparticles supported on CeO₂(111) suggests that the Ni/CeO₂ catalyst exhibits high activity toward CO_2 activation.

11:00am **SS-TuM10 Adsorption and Diffusion of Acetone on Rutile $\text{TiO}_2(110)$, B. Zhang, Y. Xia,** Baylor University, J. Ye, Q. Ge, Southern Illinois University Carbondale, Z. Zhang, Baylor University

Understanding the surface reaction processes of acetone on metal oxide surfaces is important for photo-oxidation of toxic organic molecules. We have studied the adsorption and the diffusion of acetone on reduced rutile $\text{TiO}_2(110)$ surfaces using variable temperature scanning tunneling microscopy (STM). At room temperature (RT) acetone molecules prefer to adsorb on bridging-bonded oxygen vacancy sites. The sequential isothermal STM images show that acetone molecules are mobile at RT. They hop between unoccupied vacancy sites via both apparent along-row diffusion and apparent cross-row diffusion processes. Images obtained at temperatures below RT show that there are two barriers involved in these diffusion processes: (1) the diffusion barrier along the Ti row, and (2) the barrier from the vacancy site to the neighboring Ti row. The latter is the rate limiting step. DFT calculations agree with experimental results.

11:20am **SS-TuM11 Variations in Reactivity for Acetaldehyde and Acetic Acid with the Crystallographic Orientation of Cerium Oxide Thin Films, P.M. Albrecht, D.R. Mullins,** Oak Ridge National Laboratory

Cerium oxide is a vital component in many heterogeneous catalytic processes. The various crystallographic faces of ceria present significantly different surface structures and compositions, which may result in an orientation-dependent catalytic reactivity. The structure and composition determine the availability of adsorption sites, the spacing between those adsorption sites, and the ability of surface O to participate in a reaction. The adsorption and reaction of various oxygenated hydrocarbons on cerium oxide surfaces are of interest from the standpoint of understanding the catalytic properties of the material. Studies on the interactions of alcohols, aldehydes, ketones, and carboxylic acids on well-defined CeO₂ surfaces have been motivated predominantly by the rich chemistry produced by the variation in the Ce oxidation state and the associated O vacancies. Alcohols, carbonyls, and carboxylic acids vary significantly in their strength of interaction with the surface and consequently in their reaction products. Here, we report a study of the adsorption and dissociation of acetaldehyde (CH_3CHO) on CeO₂(100). CeO₂(100) films were grown by pulsed laser deposition on Nb-doped SrTiO₃(100). In addition to the fully oxidized CeO₂(100) surface, experiments were conducted on reduced surfaces containing $\sim 60\%$ Ce³⁺ (CeO_{1.7}) prepared by methanol exposure at 660 K. Reaction products were monitored by temperature programmed desorption (TPD), and surface intermediates were determined by soft x-ray photoelectron spectroscopy (sXPS) and near-edge x-ray absorption fine structure (NEXAFS). The key result is that acetaldehyde reacts with oxidized CeO₂(100), whereas it does not react with oxidized CeO₂(111). The most intense products are CO, CO₂, and water, with trace amounts of crotonaldehyde and acetylene. On reduced CeO_{1.7}(100), the oxygenated products are largely eliminated and ethylene and H₂ are produced. Residual C is also left on the surface. Recent results indicate that the chemistry of acetic acid (CH_3COOH) is also significantly different on CeO₂(100) compared to CeO₂(111). Acetone is a major product on CeO₂(100) whereas only a trace amount of ketonization occurs on CeO₂(111). Research sponsored by the Division of Chemical Sciences, Geosciences, and Biosciences, Office of Basic Energy Sciences, US Department of Energy, under contract DE-AC05-00OR22725 with Oak Ridge National Laboratory, managed and operated by UT-Battelle, LLC. Use of the National Synchrotron Light Source, Brookhaven National Laboratory, was supported by the US Department of Energy, Office of Science, Office of Basic Energy Sciences, under Contract No. DE-AC02-98CH10886.

11:40am **SS-TuM12 The Entropies of Adsorbed Molecules**, *C.T. Campbell, J.R.V. Sellers*, University of Washington

Adsorbed molecules are involved in many reactions on solid surface that are of great technological importance. As such, there has been tremendous effort worldwide to learn how to predict reaction rates and equilibrium constants for reactions involving adsorbed molecules. Theoretical calculation of both the rate constant and equilibrium constant for such reactions require knowing the standard entropy and enthalpy of the adsorbed molecule. While much effort has been devoted to measuring and calculating the enthalpies of well-defined adsorbates, few measurements of the entropies of adsorbates have been reported. We present here a new way to determine the standard entropies of adsorbed molecules (S_{ad}^0) on single crystal surfaces from temperature programmed desorption data, prove its accuracy by comparison to entropies directly measured using equilibrium adsorption isotherms on MgO(100), and apply it to published data to extract new entropies. Most importantly, when combined with reported entropies, we find that at high coverage they linearly track the entropy of the gas-phase molecule at the same temperature (T) as:

$$S_{ad}^0(T) = 0.70 S_{gas}^0(T) - 3.29R,$$

with a standard deviation of only 2R from 0 to 60R, where R is the gas constant. These entropies, which are $\sim 2/3$ of that for the gas, are huge compared to most theoretical predictions (e.g. the harmonic approximation commonly employed in combination with DFT estimates of reaction barriers). This relationship applies at temperatures where desorption rates are fast enough to perform EAI and TPD measurements ($\sim 10^{-3}$ to 100 monolayers/s). It provides an important tool to aid in estimating equilibrium constants and rate constants for reactions where these adsorbates are involved, as proven here for prefactors in the Arrhenius rate constant for desorption. The prefactor can be estimated as :

$$v = (k_B T/h) \exp\{0.30 S_{gas}^0(T)/R + 3.29 - 9.31 \ln[(m/m_{Ar})(T/298K)]\},$$

where m/m_{Ar} is the mass of the adsorbate relative to Ar. For longer adsorbed molecules where $S_{gas}^0(T)$ exceeds 60 K (e.g. linear alkanes with >11 carbons), their entropies remain a constant 20.7R below gas entropies, and $\sim 10.4R$ below Trouton's Rule for liquid entropies.

Work supported by NSF under CHE-1010287.

Tuesday Afternoon, October 30, 2012

Graphene and Related Materials Focus Topic
Room: 13 - Session GR+AS+NS+SP+SS-TuA

Graphene Characterization Including Microscopy and Spectroscopy

Moderator: J.C. Hone, Columbia University

2:00pm **GR+AS+NS+SP+SS-TuA1 High Resolution Real and Reciprocal Space Photoelectron Emission Microscopy on Heterogeneous Graphene/SiC(000-1)**, *K. Winkler, B. Kroemker*, 10micron NanoTechnology, Germany, *N. Barrett*, IRAMIS, Saclay, France, *E. Conrad*, GeorgiaTech

We present energy filtered electron emission spectromicroscopy with high spatial and wave-vector resolution on few-layer epitaxial graphene on SiC(000-1) grown by furnace annealing.

Conventional electron spectroscopy methods are limited in providing simultaneous real and reciprocal or k-space information from small areas under laboratory conditions. Therefore, the characterization of materials with only micron scale sample homogeneity such as epitaxially grown graphene requires new instrumentation. Recent improvements in aberration compensated energy-filtered photoelectron emission microscopy (PEEM) can overcome the known limitations in both synchrotron and laboratory environments. Here we report 2D maps of the k-parallel π - π^* band dispersion in micron-scale regions and correlate them with spatially resolved chemical information on the same regions. Only the combination of high lateral, high energy, high k-resolution and controlled switching between real space and k-space allows detailed understanding of micron size sample sites with 1-3 layers graphene. The experiments underline the importance of simultaneous lateral, wave vector and spectroscopic resolution on the scale of future electronic devices in order to precisely characterize the transport properties and band alignments.

2:20pm **GR+AS+NS+SP+SS-TuA2 Evidence of Nanocrystalline Semiconducting Graphene Monoxide during Thermal Reduction of Graphene Oxide in Vacuum**, *C. Hirschmugl, E. Mattson, H. Pu, S. Cui, M. Schofield, S. Rhim, G. Lu, M. Nasse*, University of Wisconsin Milwaukee, *R.S. Ruoff*, University of Texas at Austin, *M. Weinert, M. Gajdardziska-Josifovska, J. Chen*, University of Wisconsin Milwaukee

As silicon-based electronics are reaching the nanosize limits of the semiconductor roadmap, carbon-based nanoelectronics has become a rapidly growing field, with great interest in tuning the properties of carbon-based materials. Chemical functionalization is a proposed route, but syntheses of graphene oxide (G-O) produce disordered, nonstoichiometric materials with poor electronic properties. We report synthesis of an ordered, stoichiometric, solid-state carbon oxide that has never been observed in nature and coexists with graphene. Formation of this material, graphene monoxide (GMO)[1], is achieved by annealing multilayered G-O. A combination of transmission electron microscopy and infrared microspectroscopy have provided critical experimental evidence to identify the novel structure. These results indicate that the resulting thermally reduced G-O (TRG-O) consists of a two-dimensional nanocrystalline phase segregation: unoxidized graphitic regions are separated from highly oxidized regions of GMO. GMO has a quasi-hexagonal unit cell, an unusually high 1:1 O:C ratio, and a calculated direct band gap of approximately 0.9 eV.

This work was supported by the NSF (CMMI-0856753 and CMMI-0900509). This work is based upon experiments performed at the Synchrotron Radiation Center. The SRC is funded by the University of Wisconsin-Madison and the University of Wisconsin-Milwaukee. Work performed at the SRC IRENI beamline been done with support from an NSF Major Research Instrumentation grant (DMR-0619759). The authors thank Bruker Technologies for the Grazing Angle Objective used for this work.

[1] Mattson, E.C. et al., ACSNano (2011) 5 (2011) 9710-9717.

2:40pm **GR+AS+NS+SP+SS-TuA3 Scanning Tunneling Spectroscopy of Epitaxial Graphene: Local Band Mapping and Wavefunction Engineering**, *P.N. First*, Georgia Tech **INVITED**

Because the crystalline orientation is determined prior to growth, epitaxial graphene (EG) on silicon carbide is an excellent material to consider for 2D wavefunction engineering, where device properties are designed through wavefunction confinement and material strain. In pursuit of this goal, we use scanning tunneling microscopy (STM) and spectroscopy (STS) to characterize the local structural and electronic properties of EG and a

simple EG nanostructure. With some care, STS can be used to measure the full energy-momentum dispersion of both filled and empty states, on length scales determined by the coherence of the graphene wavefunctions. Applying a magnetic field introduces a field-tunable comb of discrete Landau level energies that we use to obtain high momentum resolution, to characterize the tip-induced surface potential, and to detect subtle interlayer interactions in a multilayer graphene stack. * Work performed in collaboration with NIST Center for Nanoscale Science and Technology ** Funded in part by NSF and by NRI-INDEX.

4:00pm **GR+AS+NS+SP+SS-TuA7 Intercalation of O₂ an CO Controlled by the Mesoscopic Structure of Graphene**, *E. Grånäs, J. Knudsen*, Lund University, Sweden, *U. Schröder, T. Gerber, C. Busse*, Universität zu Köln, Germany, *M.A. Arman, K. Schulte, J.N. Andersen*, Lund University, Sweden, *T.W. Michely*, Universität zu Köln, Germany

Intercalation of gases between epitaxial graphene and its substrate has become a topic of interest for studies due to, for example, the unique opportunities to modify the graphene-substrate interaction and the possibilities to perform chemistry under the graphene layer. Further, a profound knowledge about graphenes stability in gases at elevated temperatures and pressures is essential for, among other things, the correct interpretation of gas adsorption studies on graphene supported metal cluster arrays.

We have studied intercalation and etching of Ir(111) supported graphene upon gas exposure to common gasses such as O₂ and CO in the entire pressure interval from 10⁻⁸ to 0.1 mbar. Comparing perfect graphene layers without holes with graphene films, that only covers a fraction of the Ir(111) surface, we reveal that the holes - or more specific the graphene edges - are essential for intercalation.

For oxygen exposed graphene we develop a coherent picture of temperature dependent oxygen etching and intercalation. Using X-ray photoemission spectroscopy (XPS) and scanning tunnelling microscopy (STM) we show that a perfect graphene layer is stable against etching and intercalation up to 700 K, whereas at higher temperatures etching, but no intercalation, takes place. In contrast, a partial graphene coverage on Ir(111) enables dissociative oxygen adsorption on the bare Ir and subsequent intercalation underneath graphene flakes at 355 K and above. Intercalated oxygen remains stable up to a temperature of 600 K, above this temperature it desorbs in the form of CO or CO₂. We have determined XPS and STM fingerprints for the intercalated oxygen structure and we unambiguously assign it to a p(2x1)-O structure similar to the one observed on clean Ir(111). The decoupling of the intercalated graphene film from the metal substrate is directly visualized through the inability to form well-ordered Pt cluster arrays on the O-intercalated areas of graphene on Ir(111). Further, we have identified the rate limiting step for oxygen intercalation to be unlocking of the graphene edge and propose that this takes place through bond breaking between graphene edge bonds and the Ir substrate.

Using a combination of high pressure X-ray photoemission spectroscopy (HP-XPS) and STM we also show that CO intercalation takes place at room temperature and pressures in the 1 mbar range. The adsorption structure of intercalated CO is determined to be (3√3 × 3√3)R30°, identical to the structure observed on clean Ir(111) upon high pressure CO exposure.

4:20pm **GR+AS+NS+SP+SS-TuA8 Long-range Atomic Ordering and Variable Interlayer Interactions in Two Overlapping Graphene Lattices with Stacking Misorientations**, *T. Ohta, T.E. Beechem*, Sandia National Laboratories, *J.T. Robinson*, Naval Research Laboratory, *G.L. Kellogg*, Sandia National Laboratories

We report a method to examine the effect of stacking misorientation in bilayer graphene by transferring chemical vapor deposited (CVD) graphene onto monolithic graphene epitaxially grown on silicon carbide (SiC) (0001). The resulting hybrid bilayer graphene displays long-range Moiré diffraction patterns having various misorientations even as it exhibits electron reflectivity spectra nearly identical to epitaxial bilayer graphene grown directly on SiC. These varying twist angles affect the 2D (G')-band shape of the Raman spectrum indicating regions of both a monolayer-like single π state and Bernal-like split π states brought about by the differing interlayer interactions. This hybrid bilayer graphene fabricated via a transfer process therefore offers a means to systematically study the electronic properties of bilayer graphene films as a function of stacking misorientation angle.

The work at Sandia National Laboratories was supported by LDRD and by the US DOE Office of Basic Energy Sciences, Division of Materials Science and Engineering. Sandia National Laboratories is a multi-program laboratory managed and operated by Sandia Corporation, a wholly owned subsidiary of Lockheed Martin Corporation, for the U.S. Department of Energy's National Nuclear Security Administration under contract DE-

AC04-94AL85000. The work at NRL was funded by the Office of Naval Research.

4:40pm **GR+AS+NS+SP+SS-TuA9 Chemically-resolved Interface Structure of Epitaxial Graphene on SiC(0001)**, *J.D. Emery*, Northwestern Univ., *B. Detslefs*, European Synchrotron Radiation Fac., France, *H.J. Karmel*, Northwestern Univ., *V.D. Wheeler*, U.S. Naval Research Lab, *J.M.P. Alaboson*, Northwestern Univ., *L.O. Nyakiti*, *R.L. Myers-Ward*, *C.R. Eddy, Jr.*, *D.K. Gaskill*, U.S. Naval Research Lab, *M.C. Hersam*, Northwestern Univ., *J. Zegenhagen*, European Synchrotron Radiation Fac., France, *M.J. Bedzyk*, Northwestern Univ.

The implementation of graphene into next-generation electronics will require production high-quality graphene at the wafer scale. One promising route for the production of wafer-scale graphene is to grow epitaxial graphene (EG) via thermal decomposition of Si-terminated SiC (SiC(0001)). This method produces high-quality EG, but is accompanied by the formation of the so-called "buffer layer" at the interface, which is known to affect the electronic properties of the graphene. Despite numerous efforts to determine the nature of the buffer layer, debate persists concerning its atomic and chemical structure. Here, we use the X-ray Standing Wave (XSW) technique to create a precise chemically-sensitive description of the distributions of Si and C at the interface. This technique, which combines X-ray scattering and X-ray Photoelectron Spectroscopy (XPS), is capable of locating coherent distributions of chemically distinct species above a single crystal surface. This allows for a more detailed description of the interface than those afforded by scattering or XPS alone. Our analysis shows that the buffer layer, which is present in both UHV and furnace-grown EG/SiC(0001), contains no substantial non-bulk or oxide silicon component, and is thus purely carbon. We identify two chemically distinct carbon species within the interface layer, each with a distinct location above the Si-terminated surface, and report their positions and distributions with sub-angstrom precision. These results help to clarify long-standing uncertainties about the interfacial structure of graphene/SiC(0001). Further, we also highlight the potential for XSW with XPS as a valuable tool in the structural determination of complex interfaces, such as functionalized, doped, or intercalated epitaxial graphene.

5:00pm **GR+AS+NS+SP+SS-TuA10 Formation of Graphene on SiC(000-1) in Disilane and Neon Environments**, *G. He*, *N. Srivastava*, *R. Feenstra*, Carnegie Mellon University

We have prepared graphene on the SiC(000-1) surface (the so-called *C-face* of the {0001} surfaces), by heating the SiC in a Si-rich environment produced either by using disilane ($\approx 10^{-4}$ Torr) or cryogenically-purified neon (1 atm). With the Si-rich environments, we obtain considerably better uniformity in the thickness for thin, \approx ML-thick graphene on the C-face compared to that observed in samples prepared in vacuum or in an argon environment. We also find that different interface structures occur in these environments. In particular, we find a graphene-like buffer layer forming at the interface, analogous to the well known behavior of the SiC(0001) surface (the Si-face).

Studies are performed using atomic force microscopy (AFM), low-energy electron diffraction (LEED), and low-energy electron microscopy (LEEM). For graphene prepared in vacuum, LEED patterns show a characteristic 3×3 pattern together with graphene streaks. In contrast, for the graphene produced in either the disilane environment ($\approx 10^{-4}$ Torr) or 1 atm of neon, LEED patterns reveals a complex $\sqrt{43} \times \sqrt{43} - R \pm 7.6^\circ$ arrangement along with graphene spots. This structure is somewhat similar to the well known $\sqrt{3} \times \sqrt{3} - R30^\circ$ "buffer layer" of the Si-face, with satellite spots surrounding the primary Si spots, and is interpreted as arising from a C-rich buffer layer on the SiC. Selected area diffraction on those surface areas reveals a wavevector magnitude precisely equal to that of graphene, thus proving that the buffer layer does indeed have structure very close to that of graphene (the pattern is interpreted as a distortion of the buffer-layer graphene due to bonding to the underlying SiC). Using LEEM, measurements from the buffer layer of the reflected intensity of the electrons as a function of their energy reveal a new characteristic reflectivity curve, not seen for vacuum-prepared graphene.

After oxidation of the samples, the $\sqrt{43} \times \sqrt{43} - R \pm 7.6^\circ$ spots disappear and $\sqrt{3} \times \sqrt{3} - R30^\circ$ spots appear on the surface. This latter behavior is interpreted as oxidation of the SiC surface beneath the buffer layer. Selected area diffraction on portions of the surface that were previously identified as buffer layer still reveal a wavevector magnitude precisely equal to that of graphene. However, LEEM reflectivity curves on those areas reveal a completely new spectrum, indicative of a "decoupling" of the buffer from the SiC. This decoupling is consistent with our interpretation of this new interface structure as being a graphene buffer layer on C-face SiC.

This work is supported by NSF.

5:20pm **GR+AS+NS+SP+SS-TuA11 Characterization of Few Layer Graphene Films Grown on Cu-Ni and SiC Substrates**, *P. Tyagi*, *J.D. McNeilan*, *J. Abel*, *F.J. Nelson*, *Z.R. Robinson*, *R. Moore*, *A.C. Diebold*, *V.P. LaBella*, *C.A. Ventrice, Jr.*, University at Albany - SUNY, *A.A. Sandin*, *D.B. Dougherty*, *J.E. Rowe*, North Carolina State Univ., *C. Dimitrakopoulos*, *A. Grill*, *C.Y. Sung*, IBM T.J. Watson Res. Center, *S. Chen*, *A. Munson*, *Y. Hao*, *C.W. Magnuson*, *R.S. Ruoff*, Univ. of Texas at Austin

The electronic structure of graphene depends on the number of graphene layers and the stacking sequence between the layers. Therefore, it is important to have a non-destructive technique for analyzing the overlayer coverage of graphene directly on the growth substrate. We have developed a technique using angle-resolved XPS to determine the average graphene thickness directly on metal foil substrates and SiC substrates. Since monolayer graphene films can be grown on Cu substrates, these samples are used as a standard reference for a monolayer of graphene. HOPG is used as a standard reference for bulk graphite. The electron mean free path of the C-1s photoelectron is determined by analyzing the areas under the C-1s peaks of monolayer graphene/Cu and bulk graphite and results in a value of 12.3 ± 0.8 Å. With this electron mean free path, the graphene coverage of a film of arbitrary thickness can be determined from the areas under the C-1s peaks of the sample of interest, the monolayer graphene/Cu, and HOPG samples. Analysis of graphene coverages for graphene films grown on Cu-Ni substrates shows that a uniform monolayer is first formed before the growth of a second layer. The thickness of both the graphene overlayer and intermediate buffer layer has been determined on 6H-SiC substrates. Raman spectroscopy data have also been taken on these samples and compared to the overlayer coverages determined with XPS. This research was supported in part by the National Science Foundation (grant no. 1006350/1006411).

5:40pm **GR+AS+NS+SP+SS-TuA12 Thickness-related Electronic Properties of Single-layer and Few-layer Graphene Revealed by Single-pass Kelvin Force Microscopy and dC/dZ Measurements**, *J. Yu*, *S. Wu*, Agilent Technologies, Inc.

Graphene has attracted much attention recently due to their exotic electronic properties. Potential applications of graphene sheets as ultrathin transistors, sensors and other nanoelectronic devices require them supported on an insulating substrate. Therefore, a quantitative understanding of charge exchange at the interface and spatial distribution of the charge carriers is critical for the device design. Here, we demonstrate that atomic force microscopy (AFM)-based technique Kelvin force microscopy (KFM) can be applied as an experimental means to quantitatively investigate the local electrical properties of both single-layer and few-layer graphene films on silicon dioxide. Our measurements indicate that the surface potential of single-layer graphene is 60 mV higher than that of the silica interfacial layer. The effect of film thickness on the surface potential of few-layer graphene is observed. For example, a 66 mV increase in the surface potential is detected for an eleven-layered film with respect to a nine-layer film. Furthermore, with the introduction of multiple lock-in amplifiers (LIAs) in the electronics for scanning probe microscopes, single-pass kelvin force microscopy and probing of the other electric property such as local dielectric permittivity via the capacitance gradient dC/dZ measurements are allowed by the simultaneous use of the probe flexural resonance frequency ω_{mech} in the first LIA targeting the mechanical tip-sample interactions for surface profiling, and a much lower frequency ω_{elec} (both in the second LIA and its second harmonic in the third LIA) for sample surface potential and dC/dZ measurements, respectively. In contrast to surface potentials, the dC/dZ measurements show that local dielectric permittivity of few-layer graphene films maintain at the same level regardless of the film thickness. Such simultaneous monitoring of multiple electronic properties that exhibit different behaviors in response to the graphene layers provides us a way to achieve both a comprehensive characterization and a better understanding of graphene materials.

Reactivity of Size and Shape Selected Nanoparticles**Moderator:** C.T. Campbell, University of Washington

2:00pm **SS+NS-TuA1 2012 AVS Gaede-Langmuir Award Lecture: Surface Photochemistry on Compact Crystals and on Metal Nanoparticles, D. Menzel***, Fritz-Haber Institut, and Techn. Univ. Muenchen, Germany

INVITED

Adsorbing a molecule on a substrate changes its photochemistry. I shall briefly review characteristics of surface photochemistry, established mechanisms, and effects such as whether the substrate acts mainly as source or sink of electronic excitations of adsorbates, how long the latter survive, and how effects which influence their localization and delocalization influence the success rate of excitations. For laser excitation, linear and nonlinear response to excitations can occur.

Use of nanoparticles (MNPs) instead of bulk metals further changes surface photochemistry, mainly by changing the substrate optical excitations (e.g. the Mie plasmon of MNPs), and excitation lifetimes and efficiency (by confinement). This will be illustrated by data obtained in the past years in Berlin on NO dimers adsorbed on Ag NPs with varied size (2 to 10 nm) supported on thin alumina films on NiAl single crystals, laser-excited with 2 to 5 eV, with *in situ* comparison with Ag(111). The main channel is photodesorption of NO; conversion to N₂O + O, and to NO(ad) stabilized by O also occur. Adsorption energies were characterized by TPD, cross sections (PCS) by photo-depletion, and desorbate energy distributions (translation, rotation, vibration) by TOF and REMPI analysis. Linear and nonlinear fluence dependencies of desorption signals have been found with *ns* and *fs* laser pulses, respectively. The main changes in NO photodesorption are found in the PCS which are strongly enhanced by plasmon excitation and more weakly by excitation confinement, and show clear size dependences interpreted by counteracting influences. The branching into the minor photoreaction channels is also changed at Ag NPs compared to Ag(111) which is due to varying PCS enhancement factors. The photochemical mechanism, however, as evidenced by state-resolved analysis of the desorbing NO molecules, remains the same – formation of transient negative ions by hot electrons in the substrate – for most of the investigated range (with an exception for high energy and small particles). With *fs* laser pulses further drastic PCS increases are found even at low fluences at the NPs but not at Ag(111). This nonlinear effect is explained by re-excitation of hot electrons confined in the NPs within a single laser pulse. But even here the individual dynamics stay the same. This action of NPs on the success probability of excitations with essentially unchanged dynamics appears to be the typical behavior for photochemistry on MNPs. Only in an unusual case (Xe/Ag NPs) we have seen a direct influence of plasmon excitation on desorption.

These findings may help in the understanding of photocatalysis on MNPs.

2:40pm **SS+NS-TuA3 Photocatalytic Deposition of Au onto Ordered Linear Arrays of TiO₂ Nanoparticles, J. Taing, A. Margarella, Y. Liu, J.C. Hemminger**, University of California Irvine

TiO₂ nanoparticles were decorated onto the step edges of highly oriented pyrolytic graphite (HOPG) via physical vapor deposition. Gold shells and nanoparticles were then grown on the TiO₂ nanoparticles using a photoelectrochemical cell whereupon a photocatalytic reduction mechanism is verified by photocurrent measurements. Samples of TiO₂ nanoparticles on HOPG, acting as a photoelectrode, were placed in a half-cell and immersed in either an electrolyte solution of 1.0 M NaCl or 1.0 M NaNO₃. Bare HOPG, acting as a counter electrode, was placed in a second half-cell and immersed in the same electrolyte solution. The two half-cells were connected by a salt bridge and the electrodes by a picoammeter. Upon irradiation of the TiO₂ nanoparticles by 365 nm UV light from a 200 W Hg lamp, photogenerated electrons produced a photocurrent. Subsequent to introducing 1 mL of 15 μM HAuCl₄ into the cell containing the TiO₂ nanoparticles, the photocurrent decreased as a result of the reduction of Au³⁺ to Au on TiO₂. Scanning electron microscopy (SEM), transmission electron microscopy (TEM), x-ray dispersive spectroscopy (EDS), and x-ray photoelectron spectroscopy (XPS) were used to characterize the morphology, crystal structure, and chemical identity of the nanoparticles. Images of TiO₂ nanoparticles encapsulated in Au are included in the supplement.

* Gaede Langmuir Award Winner

3:00pm **SS+NS-TuA4 Catalytic Activity of Gold-supported TiO₂ Nanocrystals Towards Simple Alcohols, D.V. Potapenko, Z. Li, Y. Lou, R.M. Osgood**, Columbia University

Titanium oxide is a versatile photocatalytic material and it has been the subject of much research throughout the last two decades. Nanostructuring is one approach for tailoring the properties of a catalyst. Previously we have developed a method of preparation of structurally homogenous TiO₂ nanocrystals on Au(111) substrate through oxidation of Ti-Au surface alloy. In this work we explore catalytic properties of the nanocrystals through a series of temperature programmed desorption (TPD) studies with simple alcohols: ethanol and 2-propanol. Similarly to the single crystal TiO₂ rutile(110) surface, TiO₂ nanocrystals on Au(111) catalyze dehydrogenation of ethanol and 2-propanol into ethylene and propene. Dehydrogenation was observed in a wide range of temperatures from 400 to 550 K, which is lower than the temperature of the corresponding reaction on rutile(110). More interestingly, we have observed formation of acetone from 2-propanol on our TiO₂/Au(111) surface at around 450 K; this reaction was not observed on rutile(110). The reactivity patterns of TiO₂/Au(111) show strong dependence on geometry and structure of the nanocrystals.

4:00pm **SS+NS-TuA7 Structure, Chemical State, and Reactivity Investigations of Size- and Shape-Selected Nanocatalysts under Operando Conditions, B. Roldan Cuenya**, University of Central Florida

INVITED

The rational design of the next-generation of catalysts requires detailed knowledge of the correlation between structure, chemical composition, and reactivity. Even though Pt and Pd are among the most industrially relevant and widely investigated nanocatalysts, their complex interaction with common reactants such as oxygen still provides many challenges to the scientific community. In this work, the relation between the structure and reactivity of nanocatalysts “at work” was obtained via X-ray absorption fine-structure spectroscopy, X-ray photoelectron spectroscopy, and mass spectrometry. Homogeneous size- and shape-selected metal nanoparticles (NPs) have been synthesized by means of diblock copolymer encapsulation.

The influence of the nanoparticle *shape* on the reactivity of Pt nanocatalysts on γ-Al₂O₃ will be described. Nanoparticles with similar size distributions (~0.8-1 nm) but with different shapes were found to display distinct reactivities for the oxidation of 2-propanol. A correlation between the number of undercoordinated atoms at the NP surface and the onset reaction temperature was observed. Furthermore, platinum oxides were found to be the active species for the partial oxidation of 2-propanol, while the complete oxidation was catalyzed by oxygen-covered metallic Pt NPs.

The evolution of the structure and oxidation state of ZrO₂-supported Pd nanocatalysts during the *in situ* reduction of NO with H₂ will also be discussed. Prior to the onset of the reaction, NO-induced redispersion of the Pd NPs over the ZrO₂ support was observed, and Pd^{δ+} species detected. This process parallels the high production of N₂O observed at the onset of the reaction (>120°C), while at higher temperatures (≥ 150°C) the selectivity shifts toward N₂. Interestingly, concomitant with the onset of N₂ production, the Pd atoms re-aggregate into large metallic Pd NPs, which were found to constitute the active phase for the H₂-reduction of NO. The evolution of the oxidation state of Pd and Pt NPs during the oxidation of NO and the role of the NP size will also be presented.

Our findings highlight the decisive role of the nanoparticle structure and chemical state in catalytic reactions and the importance of *in situ* reactivity studies to unravel the microscopic processes governing catalytic reactivity.

4:40pm **SS+NS-TuA9 Particle Size, Support and Alloying Effects in Electrocatalysis: Relationships with Heterogeneous Catalysis, B.E. Hayden**, University of Southampton, UK

INVITED

High-Throughput Physical Vapour Deposition (HT-PVD) based on Molecular Beam Epitaxy methods¹ has been used to synthesize libraries of catalysts which have subsequently been screened for their electrochemical activity and stability. A screening method is briefly described² which has been applied to measurements on model supported metal nano-particle HT-PVD catalyst libraries.

Considerable effort has been made to find alternative supports for platinum based catalysts in order to improve the particle stability and improve the three-phase boundary in fuel cell applications. HT-PVD model catalyst methodology has been applied to the study of support and particle size effects in electrocatalysis.³ Experiments have demonstrated the potential for using a support such as titania to induce CO oxidation electro-catalytic activity in gold particles,⁴ with an optimum particle size observed at ca. 3nm (Figure). No induced activity is observed for carbon supports. The similarities with the low temperature oxidations exhibited by supported Au in heterogeneous catalytic are highlighted. Extending this methodology to supported platinum based catalysts, the effect of particle size is

demonstrated in the reduction of oxygen for the model carbon supported platinum catalysts, highlighting the limitations of catalyst dispersion. Supporting platinum on titania can result in a strong poisoning of the oxygen reduction catalysis.⁵

The combination of ab-initio theory and electrocatalyst screening also provides a powerful combination in the search for precious metal alloy and non noble metal alloy catalysts. Examples are given for anode hydrogen oxidation (HOR) catalysts such as Pd based,⁶ and tungsten copper⁷ alloys.

References

1. S. Guerin and B. E. Hayden; *J. Comb. Chem.* 8 (2006) 66-73.
2. S. Guerin, B.E. Hayden, et.al.; *J. Comb. Chem.* 6 (2004) 149 - 158.
3. S. Guerin, B.E. Hayden, D. Pletcher, et.al.; *J. Comb. Chem.* 8 (2006) 791-798.
4. B.E. Hayden, D. Pletcher and J.-P. Suchsland; *Angewandte Chemie Int. Ed.* 46 (2007) 3530-3532.
5. B.E. Hayden, D. Pletcher, J.-P. Suchsland et.al.; *Phys. Chem. Chem. Phys.* 11 (2009) 1564-1570. *ibid*: *Phys. Chem. Chem. Phys.*, 2009, 11, 9141–9148.
6. F. A. Al-Odail, A. Anastasopoulos, and B. E. Hayden; *Phys. Chem. Chem. Phys.* 12 (2010) 11398-11406. *Ibid*; *Topics in Catalysis* 54 (2011) 77-82.
7. A. Anastasopoulos, J. Blake, John and B.E. Hayden; *J. Phys. Chem. C*, 115 (2011) 19226-19230.

5:20pm **SS+NS-TuA11 The Growth and Structures of Metal Nanoparticles on Ordered ZrO₂(111) Surfaces**, *Y. Han, S.W. Hu, Y.H. Pan, J.B. Hou, H.B. Pan, J.F. Zhu*, University of Science and Technology of China

Metal nanoparticles supported on zirconia have attracted much attention in recent years owing to their variety of technological applications such as heterogeneous catalysis and gas sensor operation. In particular, as catalysts, the interface properties of metal/ZrO₂ referring to the morphology, charge transfer, thermal stability and reactivity play crucial roles in determining their real applications. In this presentation, we report our recent studies on the growth, electronic structures and thermal stabilities of metal nanoparticles (Cu, Ag and Au) on well-defined ZrO₂ thin films by synchrotron radiation photoemission spectroscopy (SRPES) together with scanning tunneling microscopy (STM) and low electron energy diffraction (LEED). The well-defined ZrO₂(111) oxide thin films were epitaxially grown on Pt(111). It was found that the growth behavior of metals on ZrO₂(111) strongly depends on the morphologies of oxide surfaces and the interfacial interactions between the metal deposits and the ZrO₂(111) films. The binding energies of all three metal core-level peaks shift monotonically toward higher binding energy with decreasing the metal particle sizes. The contributions of initial and final state effects to the core level binding energy shifts are differentiated using the Auger parameters. At very low coverages, most likely Au forms Au^{δ+}, while Ag remains the metallic state and Cu forms Cu⁺ on ZrO₂(111).

5:40pm **SS+NS-TuA12 Structure and Electronic Properties of Ni Nanoparticles Supported on Reducible CeO₂(111) Thin Films**, *Y.H. Zhou*, Xiamen University, Republic of China, *J. Zhou*, University of Wyoming

Ceria-supported Ni nanoparticles have been of great interest as ethanol and methane reforming catalysts for hydrogen production in fuel cell applications. Recent studies have indicated that the catalytic reactivity of these ceria-supported Ni nanoparticles can be influenced by the redox properties of ceria as well as the synergistic effect between the two. To elucidate the nature of their activity, we studied Ni particles deposited on fully oxidized CeO₂(111) and reduced CeO_{1.88}(111) thin films using scanning tunneling microscopy and x-ray photoelectron spectroscopy at the fundamental level. Ceria thin films were grown in situ on Ru(0001) under ultrahigh vacuum conditions. Ni was vapor-deposited onto ceria thin films. At 300 K, metallic Ni is the only species present on the reduced ceria. However, a small amount of Ni is oxidized to Ni²⁺ on CeO₂. Oxidation of Ni on CeO₂ can be facilitated by annealing as well as by depositing Ni at 500 K. Scanning tunneling microscopy studies show that Ni forms two-dimensional particles on ceria at room temperature, which suggests a strong Ni-ceria interaction. The particles can agglomerate into large three-dimensional structures with further heating. The structure and electronic properties of Ni metal particles on ceria were further compared to those of bimetallic Ni-Au and Ni-Rh particles.

Tuesday Afternoon Poster Sessions

Spectroscopic Ellipsometry Focus Topic

Room: Central Hall - Session EL+TF+AS+EM+SS-TuP

Spectroscopic Ellipsometry Poster Session

EL+TF+AS+EM+SS-TuP1 Ellipsometric Characterization of Iron Pyrite (FeS₂) and Samarium Sesquisulfide (Sm₂S₃) Thin Films. A. Sarkar, N.J. Ianno, University of Nebraska-Lincoln, J.R. Brewer, Rare Earth Solar

Iron pyrite (FeS₂) and samarium sesquisulfide (Sm₂S₃) are transition metal chalcogenides characterized as absorbing semiconductors with bandgaps of 0.95 eV and 1.8 eV respectively. Synthesis of both *n*-type and *p*-type samples have been reported in the form of single crystals and thin films for both materials. As a result of these properties they have received considerable interest as photovoltaic absorber materials. We present the characterization of FeS₂ and Sm₂S₃ thin films using spectroscopic ellipsometry. FeS₂ thin films were synthesized by sulfurizing DC magnetron sputtered iron films and reactive ion sputtered iron (III) oxide films in H₂S / Ar atmosphere. Sm₂S₃ thin films were synthesized by reactive ion sputtering of Sm in an H₂S / Ar atmosphere. This analysis gives the optical properties of chalcogenide films from near-UV (300 nm) to the mid-IR (20 μm). This can then be correlated to the structural and electronic properties as well. The analysis is corroborated with results obtained from Raman spectroscopy, scanning electron microscopy, profilometry, X-ray diffraction (XRD), and Van der Pauw measurements. The ellipsometric results can be used to access different processing methods for synthesizing FeS₂ and Sm₂S₃, to determine the presence of different phases and intermediate products. This work will lay the foundation for employing *in situ* ellipsometry as a process monitor and quality control tool during manufacture of earth abundant chalcogenide thin films.

EL+TF+AS+EM+SS-TuP2 Temperature Dependence of the Dielectric Function of Germanium by Spectroscopic Ellipsometry. A.A. Medina, L.S. Abdallah, S. Zollner, New Mexico State University

Germanium has important applications in photovoltaics as a substrate for III/V triple-junction solar cells, especially in space vehicles and for terrestrial concentrator-based applications. Unfortunately, the optical properties of germanium (complex refractive index and absorption coefficient) and their temperature dependence (important to consider the effects of the space environment or the radiation-induced heating in concentrators) are not as well known as for silicon, which limits the accuracy of modeling for solar cells and Ge-based optical interconnects. In this work, we report precision measurements of the complex refractive index of germanium from 0.5 to 6.6 eV at room temperature using variable-angle spectroscopic ellipsometry. To improve accuracy, especially at photon energies below 2 eV, we used a Berek waveplate compensator. By cleaning a commercial Ge wafer in isopropanol followed by deionized water, we were able to reduce the native oxide thickness to 1.3 nm. Heating the wafer in UHV at 700 K did not reduce the oxide thickness further. (The oxide thickness can be determined with precision measurements of Δ below the band gap on a single-side polished wafer.) From the ellipsometric angles of the Ge wafer measured at three angles of incidence (65, 70, and 75°), we calculated the dielectric function from 0.5 to 6.6 eV, by correcting for the effects of a native oxide.

Mounting our wafer in a compact UHV cryostat allowed temperature-dependent measurements from 80 to 700 K at 70° angle of incidence. Using similar methods as described above, we determined the dielectric function at different temperatures. We also determined the critical-point parameters (amplitude, energy, phase angle, and broadening) of the E₀, E₁, E₁+Δ₁, E₀' , and E₂ critical points as a function of temperature. To separate the non-resonant contributions from the critical-point line shapes, we calculated the second derivative of the dielectric function with respect to photon energy and fitted the result to analytical line shapes with two-dimensional critical points. In general, our results are in good agreement with those of Viña *et al.* However, our results cover a wider spectral range and are more accurate because of the use of a compensator. Work is in progress to form thermal oxides on Ge wafers by annealing in oxygen, which will allow a multi-wafer analysis for Ge similar to work on Si by Herzinger *et al.*

This work was supported by NSF (HRD-0803171 and DMR-11104934) and the New Mexico Louis Stokes Alliance for Minority Participation.

Reference: L. Viña, S. Logothetidis, M. Cardona Phys. Rev. B **30**, 1979 (1984).

Surface Science

Room: Central Hall - Session SS-TuP

Surface Science Poster Session

SS-TuP1 MORTON S. TRAUM AWARD FINALIST: Quantum Tunneling Driven Assembly and Diffusion of Hydrogen and Deuterium on Cu(111). A.D. Jewell*, Tufts University, G. Peng, University of Wisconsin Madison, G. Kyriakou, Tufts University, M. Mavrikakis, University of Wisconsin Madison, C.H. Sykes, Tufts University

Hydrogenation reactions are central to the petrochemical, fine chemical, pharmaceutical, and food industries and are of increasing interest in energy production and storage technologies. The processes of molecular adsorption, dissociation, diffusion, association, and desorption are important surface phenomena in heterogeneous catalysis. Typical heterogeneous catalysts often employ alloys based on platinum, palladium, rhodium and ruthenium. While these metals are active at modest temperature and pressure, they are not always 100% selective and are expensive. Given that molecular hydrogen (H₂) dissociation is often the rate limiting step, one strategy is to engineer the minimal catalytic ensemble that will activate H₂ but leave the other reactants untouched. We describe a system which offers low dissociation barriers at one location on the surface and weaker binding in other regions. The Pd/Cu surface alloy was prepared in the dilute limit in which 1% Pd resides as individual, isolated substitutional atoms in a 99% Cu(111) surface. In terms of adsorption, these Pd atoms significantly lower the barrier to H₂ dissociation and allow the spillover of H atoms onto the Cu surface.[1] This system also offers the opportunity to study the diffusion, association, and assembly of large quantities of H and D on the Cu(111) surface. Through careful low-temperature scanning tunneling microscopy (STM) tracking experiments we show that quantum tunneling effects dominate the diffusion properties of H and D on the Cu surface.[2] With this direct visualization and quantification of quantum tunneling effects in adatom diffusion, we reveal two types of weak interactions between H adatoms, which lead to assembly into small clusters and larger assemblies of small clusters. We show that the self-assembly of H into large islands is, in fact, a tunneling effect resulting from inter-atom energy being much smaller than the diffusion barrier. We further demonstrate that these latter effects are not at play for D. Density Functional Theory (DFT) calculations provide estimates for both diffusion and interaction energies. Theory also provides quantum tunneling probabilities that agree well with experiment.[2] References: [1] G. Kyriakou, M.B. Boucher, A.D. Jewell, E.A. Lewis, T.J. Lawton, A.E. Baber, H.L. Tierney, M. Flytzani-Stephanopoulos, and E.C.H. Sykes, Science **335**, 1209 (2012). [2] A.D. Jewell, G. Peng, G. Kyriakou, M. Mavrikakis, E.C.H. Sykes, in preparation.

SS-TuP2 MORTON S. TRAUM AWARD FINALIST: Coverage-Dependent Interfacial Electronic Structures of Thiophenol and p-Fluorothiophenol on Cu(111). S.-Y. Hong*, P.-C. Yeh, J. Dadap, R.M. Osgood, Columbia University

Femtosecond two-photon photoemission spectroscopy is used to investigate and compare the interfacial electronic structures of thiophenol and p-fluorothiophenol films on Cu(111) as a function of molecular coverage. A new state is found to emerge as the coverage is increased; simultaneously, the Cu(111) Shockley surface state disappears for both molecular species. This similarity in behavior is shown to originate from spatial lateral confinement of the surface electron. In addition, the change in the workfunction vs. coverage shows that the two thiophenols exhibit almost identical behavior until an inflection point at ~1/3 ML coverage but then subsequently diverge. This divergent behavior is attributed to the changing orientation of the phenyl group with coverage. At a full monolayer, the net change in the workfunction for the two molecules have opposite signs, which can be explained using a quantitative model based on a surface and molecular dipole moments.

SS-TuP3 MORTON S. TRAUM AWARD FINALIST: Understanding Molecular Adsorption on Graphene-based Hybrid Nanostructures by In Situ Infrared Microspectroscopy. E. Mattson*, S. Cui, K. Pande, H. Pu, M. Schofield, G. Lu, M. Weinert, M. Gajdardziska-Josifovska, J. Chen, C. Hirschmugl, University of Wisconsin Milwaukee

Graphene is an emerging platform for many applications, and being a strictly two-dimensional material, is particularly sensitive to atomic and

* Morton S. Traum Award Finalist

molecular adsorption. These characteristics have made graphene-based materials a rising candidate for sensing applications targeting harmful chemicals which pollute our living environment. While under ideal ultra high vacuum (UHV) conditions, graphene monolayers have demonstrated single molecule detection sensitivity, such performance is not feasible under realistic operating conditions. To further improve sensitivity of graphene towards gas detection, we have performed controlled functionalization of graphene with oxygen and decoration with nanoparticles (NPs), where the graphene films act as a sensitive conduction channel, while oxygen functional groups, defects and NPs provide active adsorption sites. While these materials yield impressive performance, little is known about the chemical nature of the substrate/adsorbate interactions. To this end, we have performed *in situ* synchrotron-based infrared microspectroscopy (IRMS) on these atomically thin, micrometer-scale hybrid graphene materials during exposure to the environmentally significant gases NO₂ and NH₃ under *normal working conditions* (e.g., atmospheric pressure at low concentrations of target gases). Under such conditions, native functional groups are naturally present on the hybrid surfaces and may in fact contribute to the sensing processes. We have investigated hybrid sensing materials consisting of both chemically and thermally reduced graphene oxide (RGO) and chemically RGO decorated with tin dioxide NPs using transmission electron microscopy (TEM) and synchrotron-based IRMS. Experiments were performed at the synchrotron radiation center (SRC) in Stoughton, WI using the recently commissioned infrared environmental imaging (IRENI) beamline. Our studies of the as-produced materials have identified the native functional groups at the hybrid surfaces which are present under normal working conditions. As-produced chemically reduced GO contains functional groups due to residual carbonyl and epoxide species, while SnO₂-decorated RGO contains surface hydroxyl groups, adsorbed water and surface carbonyl groups. We then performed *in situ* IRMS upon exposure to gases to identify the chemical nature of the adsorbates and the resulting changes in the surface composition and electronic properties of the substrate materials. *In situ* IRMS results for NH₃ and NO₂ adsorption on RGO and SnO₂-decorated RGO will be presented.

SS-TuP4 MORTON S. TRAUM AWARD FINALIST: Layer-by-Layer Assembly of Organic Molecular Donor-Acceptor Heterojunctions on Vicinal Gold Surfaces, J. Wang*, J.-M. Tang, G.P. Miller, K. Pohl, University of New Hampshire

Molecular co-self-assembly of technological-relevant organic electron-donor and electron-acceptor molecules into ordered heterostructures on surfaces provides a fundamental molecular-level insight into how these two kinds of molecules would interact in a model organic photovoltaic cell with appropriate electrodes. I will present a study of the self-assembly of functionalized pentacenes (electron donors) and fullerenes (electron acceptors) into a layer-by-layer heterojunction on stepped gold surfaces by scanning tunneling microscopy (STM) characterization and density functional theory (DFT) calculations. The pentacene derivative -- 6,13-dichloropentacene (DCP) -- forms a striking long-range ordered brick-wall self-assembled monolayer (SAM) on a stepped Au(788) vicinal surface, with the long-axis parallel to the step edges [1]. Subsequently deposited fullerene (C₆₀) molecules form parallel triple, double, and single long molecular chains on top of the intact DCP SAM on Au(788) [2]. The novel organic-metal and organic-organic interfacial interactions, as well as the adsorption geometry, have been explored by DFT. The adsorbed C₆₀'s form parallel commensurate (3:2) molecular chains on top of the DCP lattice -- three fullerenes line up with two DCP molecules along the long axis. The initial C₆₀ chains grow along the upper step edges of the DCP/gold terraces. The observed adsorption position for the second C₆₀ chain is the trough between two DCP molecular rows in accordance with the DFT calculations. The calculated C₆₀-chain spacing of 1.1 nm agrees well with the experimental result. This subtle chain formation is attributed to the delicate balance of intermolecular interactions, interfacial dipolar interactions, and stepped-substrate interactions. The electronic properties for this model 3-component organic/metallic system, such as charge transfer between donors and acceptors, between the gold substrate and the molecular layers, will be discussed.

[1] J. Wang, I. Kaur, B. Diaconescu, J.-M. Tang, G. P. Miller, and K. Pohl, *ACS Nano* 5 (2011) 1792.

[2] J. Wang, J.-M. Tang, G. P. Miller, and K. Pohl, in preparation, (2012).

SS-TuP5 MORTON S. TRAUM AWARD FINALIST: Synthesis and Characterization of Yttrium Aluminum Garnet and Lanthanum Zirconate Particles, R.R. Hart§, S.L. Gollub, G. Walker, B.R. Rogers, Vanderbilt University

Rare-earth doped yttrium aluminum garnet (YAG) and lanthanum zirconate (LZO) are luminescent ceramics that have been used in TV's, LED's, metal oxide transistors, and as laser sources. These materials are thermally and chemically stable. Recent work at Vanderbilt by the Walker and Rogers research groups has shown that the emitted spectrum of proton irradiated LZO particles differs from that of non-irradiated particles, suggesting these materials may be used as passive radiation exposure indicators.

We will discuss the combustion synthesis and characterization of YAG and LZO particles. Combustion synthesis involves heating a mixture of metal nitrates and a fuel until the mixture ignites. If the proper conditions are used, the energy released by the combustion is sufficient to form polycrystalline material. The type and amount of fuel used in the synthesis affect the amount of gaseous by-products produced and flame temperature achieved during a reaction, both of which affect the crystallite size formed. The organic fuels included in this study are urea and glycine with adiabatic flame temperatures 1780°C and 1210°C, respectively. Urea's higher flame temperature makes this fuel attractive for combustion syntheses. However, urea shows signs of degradation beginning around 120 °C, well below its ignition temperature. Glycine does not appear to degrade until approximately 230°C much closer to its ignition temperature. The trade-off between degradation and adiabatic flame temperature suggests the temperature ramp rate used will significantly affect the performance of combustion syntheses carried out with these fuels.

We will present results of detailed thermogravimetric analysis and differential scanning calorimetry (TGA/DSC) experiments used to study the effects of heating rate on the combustion process and on the characteristics of the material formed. TGA/DSC-determined heats of combustion and heat capacities of the reactants and products will also be presented.

Characterization results of powders made using conditions determined by the TGA/DSC experiments will also be presented. X-ray photoelectron spectroscopy (XPS) was used to determine chemical bonding information. Rutherford backscattering spectroscopy (RBS) was used to provide quantitative elemental composition of the material. X-ray diffraction (XRD) was used to determine the crystallinity of the material and to estimate crystallite sizes. Photoluminescence spectroscopy (PL) was used to characterize the materials' emission spectra.

SS-TuP6 The Influence of the Magnetic Field on the Photo-Functional Property of TiO₂/Ni/TiO₂ Thin Films Prepared by Sputtering, A. Toyoda, I. Takano, Kogakuin University, Japan

Since the photoinduced decomposition of water on TiO₂ electrodes were discovered, various characteristics based on photocatalyst have attracted extensive interest. TiO₂ is anticipated as one of materials which are alternative for an existing solar cell based on silicon. TiO₂ shows relatively high reactivity and chemical stability under UV light whose energy exceeds a band gap of 3.2 eV in the anatase crystalline phase. The sun can provide an abundant source of photons, however, UV light accounts for the only small fraction (5 %) of the sun's energy compared to the visible region (45 %). Many techniques have been examined to achieve this purpose.

In this study, the glass (Corning#1737) was used as the substrate. After the TiO₂ layer was prepared by reactive magnetron sputtering using a Ti target in an Ar/O₂ gas mixture, the Ni layer was deposited by using DC sputtering. Finally the TiO₂ layer was coated on the Ni layer. The TiO₂/Ni/TiO₂ multi-layer films were constituted with the first TiO₂ layer of 100 - 200 nm, second Ni layer of 25 nm and the third TiO₂ surface layer of 0 - 100 nm. Composition and microstructure of these films were investigated by X-ray photoelectron spectroscopy and X-ray diffraction, respectively. Chromatic change of a methylene blue solution was applied to photocatalytic evaluation. Light irradiation to TiO₂ films in a methylene blue solution was carried out using a commercial sterilizing lamp as ultraviolet light and an artificial sun lamp as visible light. Transmittance of a methylene blue solution was measured by a spectrophotometer. In this experiment the relationship between the photocatalytic effect and the magnetic field was investigated. Magnets with magnetic field intensity of 0.15 - 0.23 T were placed on the outside of a methylene blue cell. We anticipated that the magnetic field affected separation of an electron and a hole.

The XRD patterns of TiO₂ prepared by reactive magnetron sputtering showed anatase (101) and rutile (110) of TiO₂. The anatase content for the crystal structure of the TiO₂ was 82 %. When the magnetic field was applied in the parallel direction to the substrate surface, the TiO₂/Ni/TiO₂ thin film with the thinner TiO₂ surface layer, i.e. the third layer of 50 nm, showed the higher photocatalytic property. It was clear that the magnetic field affected a photocatalytic property.

* Morton S. Traum Award Finalist

SS-TuP7 Photo-function Property of TiO₂/Cu₂O Thin Films by Reactive Magnetron Sputtering. T. Nakajima, I. Takano, S. Arahara, Kogakuin University, Japan

Characteristics based on photo-inducement of TiO₂ have attracted various interests in many fields. One of those characteristics is a photocatalytic effect. The photocatalytic effect shows antifouling or antimicrobial activity and also has the ability to decompose environmental pollutants. The most important characteristic as a photocatalyst of TiO₂ is well known that photo-excited state is very stable and does not cause self-decomposition. Therefore, the electrolysis of water is performed under ultraviolet irradiation to TiO₂. However the light reaction region of TiO₂ is limited at ultraviolet region corresponded with only about 3 % of sunlight.

In this study, to improve the photo-function property of TiO₂ the double layer films were fabricated by the constitution of the TiO₂ layer with 3.0 - 3.2 eV and the Cu₂O layer with 2.2 eV in a band gap energy. Each constitution of the film with TiO₂/Cu₂O and Cu₂O/TiO₂ was also investigated about optical permeability. Furthermore, to prevent diffusion of Cu from the Cu₂O layer to the TiO₂ layer, the TiN layer was inserted between the TiO₂ layer and the Cu₂O layer. TiN has a high melting point, stability and the suitable electric property as a barrier layer. Those TiO₂/Cu₂O and TiN were fabricated by reactive magnetron sputtering. Composition and microstructure of these films were investigated by X-ray photoelectron spectroscopy and X-ray diffraction, respectively. Chromatic change of a methylene blue solution was applied for the photocatalytic evaluation. Light irradiation to the sample in a methylene blue solution was carried out using a commercial sterilizing lamp as ultraviolet light and an artificial sun lamp as visible light. Transmittance of a methylene blue solution was measured by a spectrophotometer after irradiation for 6 hours by each lamp.

The XRD pattern of the TiO₂/Cu₂O thin film showed the strong peak of the anatase-rutile TiO from an upper layer and the weak peak of Cu₂O from lower layer. The suitable photocatalytic effect was obtained by the constitution of TiO₂ with 300 nm and Cu₂O with 200 nm in thickness, when the photocatalytic effect showed about 31 % under an artificial sun lamp and about 90 % under a sterilization lamp. In the case of the TiO₂/TiN/Cu₂O film it was estimated that the diffusion of Cu was prevented by inserting TiN from the XRD pattern, however, the high photocatalytic effect was not obtained. It was considered that the photocatalytic effect depended on thickness of the TiN layer.

SS-TuP8 Atomic Arrangements and Structural Stability of the Mn Adsorbed GaAs(001) Surfaces. A. Hagiwara, The University of Electro-Communications (UEC-Tokyo), Japan, A. Ohtake, National Institute for Materials Science (NIMS), Japan, Y. Kanno, S. Yasumura, J. Nakamura, The University of Electro-Communications (UEC-Tokyo), Japan

Epitaxial growth of MnAs on the zinc-blende (ZB) GaAs substrate has been extensively studied, because MnAs with ZB has been predicted to be half-metallic. In order to understand the growth mechanism of MnAs on GaAs, it is necessary to clarify the initial adsorption sites of Mn and to determine the well-defined structure of the Mn-adsorbed surface. It has been reported that a variety of (2x2) structures on the GaAs(001) surface appears depending on the coverage of Mn and on the pressure of incident As molecular beams [1]. The local structures which appear with the Mn coverage of 0.25 monolayer under the As-rich condition have been analyzed using electron diffraction and scanning tunneling microscopy (STM); this surface consists of the buckled Ga-As dimer and one Mn adatom in a (2x2) unit cell. However, the initial adsorption site for Mn has not been clarified yet. On the other hand, STM experiments have also shown that the configuration of buckled dimers is not well-ordered anywhere between neighboring unit cells: Local (4x2) or (2x4) arrangement is observed. In this study, first, we determine the position of the Mn atom in the (2x2) unit cell using first-principles calculations based on the spin density-functional theory. Next, in order to explore the onset of the local disordering of dimers, we employ (4x2), (2x4), and c(2x4) models as well as (2x2) and evaluate interactions between the Ga-As dimers.

We have revealed that the Mn atom prefers to adsorb at the site between Ga-As dimers along the dimer row of the (2x2) surface and the simulated STM images agree well with the experimental ones. Next, we have calculated the structure models which represent the different configurations of the dimers on the surface. It has been found that the (4x2) configuration, in which the Ga-As dimer and the As-Ga one align alternately along the dimer row, is most stable. In order to test what contributes to the stabilization of this configuration, we decompose the total energy into each constituent energy term. The Hartree and core-electron terms for (4x2) are lower than those for (2x2). The electronic charges transfer from Ga to As in the dimer structure, which results in the dipole formation at the dimer site. From this point of view, the (4x2) configuration, in which the adjacent dipoles are antiparallel with each other, has the energy gain because of the

preferable dipole-dipole interactions. Therefore, the disordered configuration observed locally at the (2x2) surface can be attributed to the stabilization of the local (4x2) unit. This work was partially supported by Grant-in-Aid for Scientific Research (B) (No.22360020).

[1] A.Ohtake *et al.*, submitted.

SS-TuP9 Facets and Surfaces Observed on Si(5 5 12) Studied by using Ultra-High-Vacuum Scanning Tunneling Microscopy. S.-G. Zhao, Y. Li, Y.-B. Song, Y.-Z. Zhu, Yanbian University, China, J.M. Seo, Chonbuk National University, Republic of Korea, S. Zhang, Z.-P. Guo, Yanbian University, China

Si(5 5 12)-2x1 surface, which attracts much attention for one-dimensional (1-D) metal nanowire growth on the surface, usually appears wider area single domain with well ordered 1-D structure. In this work, phenomenon of the facets observed on the Si(5 5 12) surface is studied systematically by using ultra high vacuum scanning tunneling microscopy. On the well defined Si(5 5 12) surface, in addition to (1 1 3) facet and (6 9 17) facet, some components (and/or facets) can be observed on the surface as well, such as (7 7 17), (3 3 7), (1 1 2), (1 1 1)-5x5, (1 1 1)-7x7. It is considered that the surface orientations from Si(7 7 17) to (5 5 12), are stable and have almost the same surface free energy, i.e. it is weak anisotropic on the γ -plot. But the (3 3 7), (1 1 2), (1 1 1)-5x5, and (1 1 1)-7x7 facets are appeared to be confined delicately by the surface tensions and the driving force of the single domain growth of the stable surface and facet, which is accompanied by the process of the reconstruction of the surface. Acknowledgement: This work was supported by the National Natural Science Foundation of China (10964014 and 10864008).

References:

- [1] A. A. Baski, S. C. Erwin, L. J. Whitman, Surf. Sci., 392, 69 (1997).
- [2] S. Jeong, H. Jeong, S. Cho, et al. Surf. Sci., 557, 183 (2004).
- [3] H. Kim, H. Li, Y.-Z. Zhu, J. R. Hahn and J. M. Seo, Surf. Sci. 601, 1831 (2007).
- [4] C. Herring, Phys. Rev. 82, 87-93 (1951).
- [5] V. A. Shchukin and D. Bimberg, Rev. Mod. Phys, 71, 1125 (1999).
- [6] R. J. Phaneuf, N. C. Bartelt, and E. D. Williams, et al., Phys. Rev. Lett. 67, 2986-2989 (1991).
- [7] Y.-Z. Zhu, H. Kim, J.-M. Seo, Phys. Rev. B., 73, 245319 (2006).

SS-TuP10 Photoelectron Spectroscopy and Valence Band Studies of Non-Stoichiometric Superconducting FeSe_{1-x}Te_x. L. Huerta, V. Ortiz, Universidad Nacional Autonoma de Mexico, M. Flores, Universidad de Guadalajara, Mexico, R. Escamilla, Universidad Nacional Autonoma de Mexico

Polycrystalline samples of Fe(Se_{1-x}Te_x), with x = 0.0, 0.25, 0.50, 0.75 and 1.0, were synthesized by solid state reaction. The samples were characterized by x-ray diffraction (XRD), measurements magnetization vs. temperature and photoelectron spectroscopy (XPS). Results of x-ray diffraction shows that the effect of the substitution of Se by Te is increase the lattice parameters. Curves of magnetization vs. temperature shows superconductivity for x = 0.25, 0.5 and 0.75. Whereas, x-ray Photoelectron spectroscopy (XPS) identified the oxidation states of Fe 2p, Se 3d and Te 3d core levels associated with the chemical states Fe(Se_{1-x}Te_x). Finally we compared the Valence Band obtained by XPS for each concentration of tellurium with the density of states electronic (DOS) reported.

SS-TuP11 Photovoltaic Property of Cu₂O/Cu/TiO₂ Thin Films Prepared by Reactive Magnetron Sputtering. Y. Suzuki, I. Takano, Kogakuin University, Japan

Recently, TiO₂ is considered as one of attractive materials. Since the photoinduced decomposition of water on the TiO₂ electrode was discovered, the photocatalysis based on semiconductor property has attracted extensive interest. TiO₂ is an n-type semiconductor with a band gap energy of 3.0 - 3.2 eV and is well known as a versatile material. From the view of solar cells TiO₂ is applied in development of dye-sensitized solar cells (DSSCs) or quasi-one-dimensional TiO₂ nanotube structure. On the other hand Cu₂O is a p-type semiconductor with a direct band gap of 2.0 eV and is a promising material on solar cell applications because of its nontoxicity, low cost and high absorption coefficient in the visible region. In this study, the photovoltaic property of p-Cu₂O/n-TiO₂ solar cells which was prepared by magnetron sputtering was investigated. Furthermore Cu buffer layer between TiO₂ and Cu₂O was used to obtain high efficiency.

Cu₂O/Cu/TiO₂ thin films with p-n heterojunction were fabricated by reactive magnetron sputtering. Firstly, glasses (Corning#1737) and ITO-film coated glasses as a substrate were ultrasonically cleaned by an acetone rinse. The TiO₂ thin film was deposited on glass substrates using pure

metallic titanium (99.99%) as a sputtering target material in an oxygen gas atmosphere. The flow rates of a sputtering argon gas and an oxygen gas were 20 sccm and 1.5 sccm, respectively. Secondly, the Cu thin film was deposited on the TiO₂ thin film using pure metallic copper (99.99%) as a sputtering target material. Thirdly, the Cu₂O thin film was deposited on the Cu/TiO₂ thin film. The flow rates of a sputtering argon gas and an oxygen gas were 15 sccm and 10 sccm, respectively. Each thickness of the TiO₂ and Cu₂O layer was about 100 nm and 200 nm. Composition and microstructure of these films were investigated by the X-ray photoelectron spectroscopy and the X-ray diffraction. Transmittance of the TiO₂ and Cu₂O thin film was measured by a spectrophotometer. The photovoltaic property was evaluated by measuring the current-voltage curve.

The Cu₂O/Cu/TiO₂ thin films with p-n heterojunction were successfully fabricated by reactive magnetron sputtering. The XRD diffraction pattern of TiO₂ layers deposited at an oxygen flow rate of 1.5 sccm showed a mixture structure. The open voltage of Cu₂O/Cu/TiO₂ thin films showed a higher value under artificial sun light than Cu₂O/TiO₂ thin films. It was confirmed that the buffer layer of Cu improved the photovoltaic property of Cu₂O/TiO₂ thin films.

SS-TuP12 Measurement of pH Induced Transition in Redox Potential for Cerium Oxidation States in Nanoceria, S. Saraf, University of Central Florida, *A.S. Karakoti*, Pacific Northwest National Laboratory, *S. Barkam, S.S. Seal*, University of Central Florida

Cerium oxide is an important technological materials and widely used in catalytic converters in automobiles, solid oxide fuel cells, and fuel additives, etc. Recently, it has been discovered that Nanoceria has the ability to kill cancer cells. In addition, it is found that nanoceria can mimic superoxide dismutase (SOD) and catalase activities both of which are essentially the enzymes in the body that are responsible for disproportion of superoxide and peroxide respectively. All of the previously stated applications use the dynamic nature of valence states transition in Nanoceria and makes it electrochemically active. This study is specifically designed to measure nanoceria's redox potential associated with its transition in biological media to fine-tune its further applications. In biological media, the pH also affects the transition characteristics in nanoceria. It is imperative to measure potential-pH diagram for nanoceria as well. In this study we propose to find redox potential of cerium oxide exposed to various pH by the use electrodes made up of nanoceria embedded onto platinum and nickel mesh substrates. Redox reactions are monitored by using cyclic voltammetry experiments. The redox potential of different ceria synthesis is compared at various pHs. Surfaces of Nanoceria are characterized using SEM, XPS and TEM. A complete picture of potential-pH diagram of Nanoceria is presented.

SS-TuP13 XPS and STM Studies of Metal Dopant-Ceria Mixed Oxide Interfaces, J. Zhou, E. Ginting, University of Wyoming, *Y.H. Zhou*, Xiamen University, China

Ceria has attracted great attentions in catalysis due to its unique redox properties and oxygen storage capacity. To improve the properties of ceria, suitable metal dopants such as Ti and Mn can be incorporated into it and form dopant-ceria mixed oxides. The additional metal component can modify the physical/chemical properties of ceria. To understand the intriguing chemistry at the metal dopant-ceria interfaces, we examined their structures at the nano-scale using X-ray photoelectron spectroscopy (XPS) and scanning tunneling microscopy (STM) techniques. Dopants including Ti and Mn were vapor-deposited onto well-ordered reducible CeO₂(111) thin films grown on Ru(0001) under ultrahigh vacuum conditions. Both Mn and Ti are oxidized at the cost of ceria reduction upon deposition at 300 K. Ti is in the +4 formal oxidation state. However, +2 state of Mn is the predominate species on ceria. STM studies show the formation of two-dimensional structures on ceria which can further develop into chain structures or triangular domains upon heating. Our studies suggest a strong interaction between metal dopants and ceria. The nature of dopant-ceria interfaces greatly depends on the dopant type. The research is sponsored by the School of Energy Resources at University of Wyoming.

SS-TuP14 Phosphonic Acids for Surface Initiated Polymerization from Oxide Nanoparticles and Flat Surfaces: Towards Applications in Organic Electronics, S.A. Paniagua, Y. Kim, N. Doubina, Georgia Institute of Technology, *C.K. Luscombe*, University of Washington, *J.W. Perry, S.R. Marder*, Georgia Institute of Technology

In this work, tailor-made phosphonic acids are used as surface initiators for the growth of both dielectric and semiconductor polymers from barium titanate nanoparticles and transparent conductive electrodes respectively. For capacitor applications, grafting the polymer from the barium titanate surface gives a composite with high permittivity due to the inorganic inclusions as well as high breakdown strength, mechanical flexibility, and ease in processability due to the organic polymer. The polymer is grown

using an atom transfer radical polymerization with catalyst in the ppm level and can be done with limited presence of air. The amount of polymer grown can be controlled in order to fabricate devices with varying polymer content to study its influence in device performance. Devices are created by simple blade casting without the need for any ball milling.

For transparent electrodes in solar cells, the growth of the donor phase directly from the substrate could lead to new morphologies, long term stability, and increased charge collection. We recently published a paper describing the growth of polymethylthiophene from ITO and some of its electrochemical properties.[1] Currently we are working on the optimization of the procedure to obtain smooth, thick polymer brushes that can be used to fabricate devices. Ongoing work involves X-ray photoelectron spectroscopy characterization of the starting monolayers and intermediate metallated species.

[1] Doubina, N.; Jenkins, J. L.; Paniagua, S. A.; Mazzio, K. A.; MacDonald, G. A.; Jen, A. K. Y.; Armstrong, N. R.; Marder, S. R.; Luscombe, C. K. *Langmuir* **2011**, *28*, 1900-1908.

SS-TuP15 Determination of Active Surface Region in Pure and Modified TiO₂ Photocatalysts, T. Luttrell, J. Tao, M. Batzill, University of South Florida

A novel approach for determining the photo catalytically active surface region is presented. In this method the photo activity of well-defined epitaxial anatase and rutile TiO₂ thin films is measured by methyl orange decomposition. The photo activity as a function of film thickness then enables to extract the active surface region, which is closely related to the bulk charge carrier diffusion length. Using this methodology we are able to compare differences in the photoactive region of anatase and rutile polymorphs of TiO₂ as well as to investigate the effect of dopants (nitrogen and tungsten) on the depth of the active surface layer. The latter highlights the trade-off between enhanced (visible light) absorption and reduction of active volume of the photocatalyst. These studies are the first that quantifies the differences in rutile and anatase and the influence of dopants on charge carrier diffusion and thus photocatalytic activity.

SS-TuP16 Basic Regimes and Reaction Mechanisms of Chemicurrent Generation during H₂ Oxidation on Catalytic MIM Nanostructures with Porous TiO₂ Support, M. Hashemian, S. Dasari, E. Karpov, University of Illinois at Chicago

Fundamental charge transfer processes and chemical reaction mechanisms at gas-solid interfaces require better understanding for catalysis, advanced sensing, and energy conversion and storage applications. Here, we report on distinct regimes of hydrogen oxidation reaction on catalytic Pt/TiO₂/Ti porous nanostructures with a potential barrier, identified via analysis of long term chemicurrent kinetics recorded in the course of the surface reactions. Three regimes in total have been observed, where the reaction turnover rate, thermal effect and chemicurrent production efficiency vary by orders of the magnitude. One the regimes is characterized with a nearly negligible thermal effect, but a surprisingly high yield of 0.1-0.4 electrons per water molecule produced, being highly encouraging for novel energy conversion applications of the present system. Correlations between occurrence of the distinct regimes and conditions in the gas phase are also established.

SS-TuP17 Photo-patternable Superhydrophobic Porous TiO₂ Films Prepared by Hydrothermal Treatment, S. Nishimoto, M. Becchaku, Y. Kameshima, M. Miyake, Okayama University, Japan

In recent years, highly porous TiO₂ surfaces prepared by hydrothermal treatment using aqueous alkaline solutions have attracted great interest due to their unique architectures, which include TiO₂ nanotubes and nanowires. These nanostructured surfaces can potentially be used as filtration membranes, high-surface-area electrodes, and photocatalysts for environmental purification. In addition to these applications, porous TiO₂ surfaces are considered to be suitable for use as functional surfaces that undergo photostimulated wettability conversion that changes them from being superhydrophobic to being superhydrophilic. However, to the best of our knowledge, no studies have been conducted on potential applications of such superhydrophobic-superhydrophilic surfaces. In this paper, we report the preparation of superhydrophobic TiO₂ surfaces by hydrothermally treating Ti plates with concentrated NaOH solution and then washing them in deionized water and HCl and subjecting them to heat treatment and surface modification with octadecylphosphonic acid (ODP). Rough nanostructured anatase TiO₂ surfaces with many pores were prepared by the hydrothermal treatment. Surface modification with self-assembled monolayers (SAMs) of ODP made the surface superhydrophobic with a static water contact angle (CA) of about 174°. This superhydrophobic surface could be converted into a superhydrophilic surface with a water CA

of nearly 0° by irradiating it with ultraviolet light as the result of photocatalytic decomposition of the ODP SAM. Thus, the large wettability contrast of the surface, with a water CA difference of over 170°, would allow this photostimulated wettability conversion porous films to be used in many applications including offset printing, cell growth, spotting of biomolecules fluidic microchips, site-selective immobilization of functional materials, and so on.

SS-TuP18 High Hydrophobic Surface with Metabolic System using Organic Monolithic Structure, M. Sakai, Kanagawa Academy of Science and Technology, Japan, *T. Kato, A. Nakajima,* Tokyo Institute of Technology, Japan, *A. Fujishima,* Science University of Tokyo, Japan

Recently, the importance of controlling the wettability on the solid surface is recognized in various industries. Superhydrophobic surfaces with water contact angles exceeding 150° are currently the subject of great interest and intensive study. Superhydrophobic coatings that produce rough surfaces at the micro- and nanoscale level with low surface energies have been prepared by several methods. However, the practical applications have been limited, because the superhydrophobic coatings suffered from physical/chemical durability. In the current paper, the super hydrophobic coating with the high physical/chemical durability was designed using organic monolithic structure with TiO₂ photocatalyst and polytetrafluoroethylene particles. The structure was formed by nanoscale frames with 3-dimensional co-continuous, which was composed of epoxy resin. Therefore, the surface with micro structures newly appeared when the top surface was scratched by physical force. Moreover, the organic frame of top surface was slowly decomposed by TiO₂ photocatalyst. Then, the grimy surface could be removed by water fluid (ex. rain). The appearance of fresh micro structure might be similar to metabolic system in a plant. We evaluated the durability performance of the superhydrophobic coating in accelerated weathering test and wear resistance test. In these results, the superhydrophobic coating has kept outdoor durability for 6 years.

SS-TuP19 Adsorption of Water on a Hydrophobic Sb(111) Surface, A. Chakradhar, J. Shan, Z. Yu, U. Burghaus, North Dakota State University

The adsorption of water is studied on Sb(111) single crystals by using temperature programmed desorption (TPD) and molecular beam scattering. The surface of Sb(111) is characterized by auger electron spectroscopy (AES), low energy electron diffraction (LEED), and x-ray photoelectron spectroscopy (XPS). Interestingly, water TPD shows only a single peak at ~155 K while recording the parent mass of water obeying zeroth-order kinetics. The fact that the water monolayer peak is missing, suggests that the Sb(111) surface is hydrophobic. In addition, the results show that the antimony surface is inert towards the adsorption of small molecules such as CO, CO₂, and NO. Moreover, the co-adsorption of n-butane and water shows site blocking effects for n-butane adsorption only at very large pre-exposures of water, indicating the formation of a porous water film, as expected for a hydrophobic surface.

SS-TuP20 Insulating Si(111) Surfaces by Organic Fluorine Compound Molecular Monolayer, F.Y. Tian, A.V. Teplyakov, University of Delaware

Both trifluoroethylamine (TFEA) and p-fluoroaniline (pFA) were modified on Si(111) surfaces as insulators by forming Si-N bond through wet-chemistry. Fluorine functional groups are good chemical building block and tracking label for X-ray photon spectroscopy (XPS). Infrared spectroscopy (IR) was also employed to identify the surface Si-N bonding information. The experiment strategy is starting from native oxidized silicon (111) wafers, hydrogen-terminated Si(111) samples were obtained through modified RCA cleaning method and HF/NH₄F etching. Then, the H-Si(111) wafers were treated with PCl₃ to get Cl-terminated Si(111) surfaces. Finally, the samples were reacted in TFEA and pFA/THF solution, respectively, at inert atmosphere at room temperature for a variety reaction period. The formation of molecular monolayer of TFEA and pFA was confirmed by both XPS and IR. Density functional theory (DFT) was also applied to mimic both TFEA and pFA's behavior on Si(111) surfaces. In addition, due to various basicity and electron drawing capabilities, TFEA and pFA presented different reactivity towards Cl-terminated Si(111) surfaces.

SS-TuP21 Methanol Induced Nanopatterning of Si(111):H – Insights from Density Functional Calculations, P. Thissen, T. Peixoto, K. Roodenko, University of Texas at Dallas, *E. Fuchs,* Zyvex Labs LLC, *W.G. Schmidt,* University of Paderborn, Germany, *Y.J. Chabal,* University of Texas at Dallas

The reaction of methanol with hydrogen terminated Si(111) surfaces has been studied using density functional theory (DFT). Depending on the chemical potentials of hydrogen and methanol several surface configurations with various coverage are found to be stable. The temperature dependence of the chemical potentials as well as the entropy contributions to the surface free energy are found to result in only minor

changes of the calculated surface phase diagram. In contrast, the calculated reaction barriers are found to be strongly dependent on the methoxy coverage of the surface. They strongly increase with increasing methoxy coverage. Our calculations thus suggest that the formation of a nanopatterned Si(111) surface, featuring 1/3 methoxy and 2/3 hydrogen termination as observed experimentally is related to the reaction kinetics rather than the surface thermodynamics. Consequently, we show that higher temperatures are the key parameter to prepare Si(111) surfaces with higher methoxy-group coverage than 1/3. Finally, a Kinetic Monte Carlo algorithm is applied to investigate the adsorption and the desorption rates until the surfaces reaction reaches the temperature-dependent equilibrium state. We find the reaction of methanol with hydrogen terminated Si(111) to be self-limited at temperatures over 400 K, since the methanol starts to react with itself.

SS-TuP22 Reactivity of Propane on Pd Oxide Phases Prepared by Surface Oxidation vs. Reduction, C. Hakanoglu, J.F. Weaver, University of Florida

We used temperature-programmed reaction spectroscopy (TPRS) to study the reactivity of propane on oxidized Pd(111) surfaces that were prepared by partially oxidizing Pd(111) as well as partially reducing a PdO(101) thin film in ultrahigh vacuum. These experiments were motivated in large part by recent observations of multiple phases co-existing during the autocatalytic thermal decomposition of a PdO(101) thin film, and the possibility that such phases exhibit distinct reactive properties. We find that the surface reactivity toward propane oxidation increases monotonically with increasing surface oxygen concentration, but that the reactivity exhibits a slight hysteresis as a function of oxygen coverage for surfaces prepared by Pd(111) oxidation vs. PdO(101) reduction. Based on the observation that propane desorbs in distinct features from different Pd-oxide phases, we determined that the hysteresis in reactivity arises from differences in the amount of PdO(101) domains present on partially oxidized vs. reduced surfaces and present evidence that propane reacts exclusively on PdO(101) domains even when a mixture of surface phases is present. We show that deconvolution of the propane desorption traces also allows us to estimate the relative fractions of surface phases which develop during both oxide growth and reduction, and thus provides a means to quantify the phase evolution as a function of oxygen coverage. The analysis demonstrates that metallic domains as well as phases characteristic of monolayer oxides, so-called surface oxides, develop during the early stages of reduction of a multilayer PdO(101) film and appear to form on top of the multilayer oxide. This finding clarifies the nature of new structures that were observed in prior STM studies of PdO(101) film decomposition, and provides key insights for understanding the processes governing oxide decomposition.

SS-TuP23 Structural Properties of TbO_x Thin Films Grown on Cu(111), W.S. Cartas, University of Florida, *T.E. Miltrey, J.F. Weaver,* University of Florida

The oxides of the rare earth metals Tb, Pr and Ce are desirable for several catalytic applications due to their ability to store and release oxygen atoms. In contrast to ceria, terbium surfaces have not been widely investigated, and may exhibit interesting structural behavior since several bulk Tb oxide phases are known to exist. In this study, we investigated the growth of terbium oxide (TbO_x) thin films on Cu(111) in ultrahigh vacuum, using scanning tunneling microscopy (STM) and low energy electron diffraction (LEED) to characterize the surface structures. We used a stepwise procedure to prepare the TbO_x films, with each step involving Tb deposition onto Cu(111) held at 300 K in an O₂ background to produce an ~1 monolayer (ML) film, followed by annealing in O₂ at 750 K. The TbO_x films grow epitaxially on the Cu(111) substrate to generate TbO_x(111) with unit cell dimensions of about (1.4 x 1.4) relative to the Cu(111) lattice. STM images show that the TbO_x films (~2 - 5 ML) are comprised of large, flat terraces and reveal an atomic-structure consisting of hexagonal, close-packed arrangements of atoms that are separated by rows of oxygen vacancies at a spacing of about 2.2 nm. Estimates of the vacancy concentrations suggest that the oxide stoichiometry corresponds to an O:Tb ratio between 1.67 and 1.71, which agrees well with the composition of the stable iota phase of bulk terbium. The capability of preparing TbO_{1.7}(111) films with well-defined arrangements of vacancies may provide new opportunities for preparing model catalyst surfaces and studying the interactions of molecular reactants with ensembles of vacancies. Such studies are currently in progress.

SS-TuP24 Modeling of Chemical Reaction – Induced Thermal Currents in Metal Nanofilm – Semiconductor Schottky Diodes, I. Nedrygailov, University of Duisburg-Essen, Germany, E. Karpov, University of Illinois at Chicago, E. Hasselbrink, D. Dising, University of Duisburg-Essen, Germany

Chemically induced currents (chemicurrents) in metal nanofilm – semiconductor contacts attracted considerable attention of the surface physics and chemistry community since McFarland, Nienhaus *et al.* reported a direct detection of hot electrons and holes, excited by a surface chemical reaction, using Schottky diodes under zero-bias voltage conditions. This phenomenon is highly promising for studying the dynamics of elementary chemical processes on the interface between the gas phase and a solid surface. The use of the chemicurrents for ultrafast chemical sensing and direct conversion of energy of surface chemical reactions into electricity is also currently discussed. As a matter of fact, the mechanism underlying the chemicurrent generation and detection is a subject of ongoing discussions due to the presence of unavoidable thermal effects, accompanying surface chemical reactions, which hamper an unambiguous identification of the experimental data. In this contribution we report on a simple theoretical model for estimating the

magnitude of the chemical reaction - induced thermal currents in metal nanofilm – semiconductor Schottky diodes. As well, we present a comparison of our calculations with the experimental values of the chemicurrents reported earlier.

SS-TuP25 Synthesis, Characterization and Catalytic Activity of Pt Nanoparticles Supported on γ -Al₂O₃ and WC: Size and Support Effects, M. Ahmadi, L. Merte, B. Roldan Cuenya, University of Central Florida

Direct-methanol fuel cells (DMFC) are one of the promising candidates for alternative clean energy generation. Extensive efforts are going on to improve the efficiency of these cells using different Pt-based catalyst. Although tungsten carbide (WC) shows similar electronic structure as Pt and has promising catalytic properties, it is not extensively used due to its instability. However, it has been observed that one monolayer of Pt on the surface of WC displays a similar performance as bulk Pt and furthermore, it stabilizes the WC, which makes it a very cost-effective alternative for Pt electrodes. In this work we have synthesized size- and shape-selected Pt nanoparticles (NPs) via inverse micelle encapsulation methods. The NPs were then supported on WC and γ -Al₂O₃ nanocrystalline powders as well as on WC/W thin films. We have investigated the size and morphology of our NPs by atomic force microscopy (AFM) and by transmission electron microscopy (TEM) and their chemical composition by X-ray photoelectron spectroscopy (XPS). Methanol oxidation was carried out in a packed-bed mass flow reactor and mass spectrometry was employed to quantify the catalyst's activity as a function of the NP size. The evolution of the structure of the Pt NPs during the oxidation of methanol was investigated under operando conditions using extended X-ray absorption fine-structure spectroscopy (EXAFS).

SS-TuP26 Ligand Functionalized Cerium Oxide Nanoparticles - Investigating the Mode and Energetics of Binding, A.S. Karakoti, Z. Lu, W. Wang, P. Nachimuthu, H. Wang, P. Yang, S. Thevuthasan, Pacific Northwest National Laboratory

Despite the significant amount of work done on functionalization of nanoparticles for various applications, studies on the determining the fundamental molecular level interaction between the various ligands and nanoparticle surfaces have been limited due to the inherent challenges associated with the characterization of highly reactive and dynamic nature of these particles. In order to obtain a fundamental understanding of nanoparticle-ligand interaction, cerium oxide nanoparticles (ceria) functionalized with simple ligands such as carboxylic acids were studied to characterize the nature of bonding, configuration of ligands and the energetics of the ligand-nanoparticle interactions. Mono-disperse ceria nanoparticles were synthesized by thermal hydrolysis process and functionalized with carboxylic acid groups from various organic ligands. The size distribution and morphology of the nanoparticles prior to and following functionalization were characterized by various imaging and spectroscopy tools to ascertain the integrity of nanoparticles. In-situ x-ray photoelectron spectroscopy (XPS) from aqueous solution of functionalized ceria nanoparticles frozen at liquid nitrogen temperature was performed to avoid any surface contamination and preserve the chemistry of the functionalized nanoparticles. XPS data suggests that the following functionalization the ceria nanoparticles predominantly exist in Ce⁴⁺ oxidation state. From XPS elemental quantification it was found that the oxygen from carboxylate molecules becomes a part of the ceria lattice to maintain the stoichiometry and bind to the ceria surface in bidentate orientation. Sum frequency generation vibration spectra (SFG-VS) showed the presence of OCO modes of vibration on the surface of cerium oxide confirming the bidentate mode of bonding between carboxylate and ceria

nanoparticle surface. In addition isothermal titration calorimetry was used to determine energetics of ligand binding on the surface of nanoparticles. Results from these characterizations were combined with the periodic density functional theory (DFT) calculations to develop a complete visualization of the interaction of organic ligands with nanoparticle surfaces.

SS-TuP27 In Situ Coarsening Study of Micellar Pt Nanoparticles Supported on γ -Al₂O₃: Pretreatment and Environmental Effects, J. Matos, L.K. Ono, F. Behafarid, J.R. Croy, S. Mostafa, University of Central Florida, A.T. DeLaRiva, A. Datye, University of New Mexico, A.I. Frenkel, Yeshiva University, B. Roldan Cuenya, University of Central Florida

The thermal stability of micellar Pt nanoparticles (NPs) supported on nanocrystalline γ -Al₂O₃ was monitored in situ under different chemical environments (H₂, O₂, H₂O) via extended x-ray absorption fine-structure spectroscopy (EXAFS) and ex situ via scanning transmission electron microscopy (STEM). Drastic differences in the stability of identically synthesized NP samples were observed upon exposure to two different pretreatments. In particular, exposure to O₂ at 400°C before high temperature annealing in H₂ (800°C) was found to result in the stabilization of the micellar Pt NPs, reaching a maximum overall size after coarsening of ~1 nm. Interestingly, when an analogous sample was pre-treated in H₂ at ~400°C, a final size of ~5 nm was reached at 800°C. The beneficial role of oxygen for the stabilization of small Pt NPs was also observed in situ during annealing treatments in O₂ at 450°C for several hours. In particular, while NPs of 0.5 ± 0.1 nm initial average size did not display any significant sintering (0.6 ± 0.2 nm final size), an analogous thermal treatment in hydrogen lead to NP coarsening (1.2 ± 0.3 nm). The same sample pre-dosed and annealed in an atmosphere containing water only displayed moderate sintering (0.8 ± 0.3 nm). Our data suggest that PtOx species, possibly modifying the NP/support interface, play a role in the stabilization of small Pt NPs. Our study reveals the enhanced thermal stability of micellar Pt NPs and the importance of the sample pre-treatment and annealing environment in the minimization of undesired sintering processes affecting the performance of nanosized catalysts.

SS-TuP28 Synthesis, Characterization and Reactivity of Cu-Zn and Cu-Pd Bimetallic Nanoparticles, H. Mistry, L. Merte, B. Roldan Cuenya, University of Central Florida

Bimetallic nanoparticles have become an important area of study because of their unique catalytic properties. We describe the synthesis and characterization of bimetallic copper-zinc and copper-palladium nanoparticles. The Cu-Zn and Cu-Pd bimetallics are synthesized using inverse micelle encapsulation in PS-P2VP diblock copolymers. The size and morphology of these nanoparticles supported on SiO₂/Si(111) and TiO₂(110) are characterized using atomic force microscopy (AFM), as well as scanning tunneling microscopy (STM) under ultra high vacuum. Characterization of electronic and chemical properties is carried out using x-ray photoelectron spectroscopy (XPS). Applications of these nanoparticles supported on γ -Al₂O₃ for the catalytic synthesis of methanol will be shown.

SS-TuP29 CO Oxidation over Au/TiO₂ Model Catalyst, T. Fujitani, I. Nakamura, AIST, Japan

In this work we have investigated the reaction mechanism and active sites for CO oxidation over the Au/TiO₂ model surface and Au single crystal surfaces, along with the role of moisture CO.

We examined the effect of moisture on the CO₂ formation rate at the reaction temperature of 300 and 400 K. The CO₂ formation rate at 300 K was increased significantly with increasing H₂O partial pressure up to 0.1 Torr, and then gradually decreased with H₂O pressure. In contrast, no promotional effect of H₂O was observed at the reaction temperature of 400 K. The moisture has an essential role to promote the CO oxidation reaction over Au/TiO₂ catalyst at low temperature, whereas the CO oxidation reaction proceeded without moisture with high reaction temperature. This important observation indicates that the CO oxidation mechanism over Au/TiO₂ is different between 300 and 400 K, considering that the activation process of oxygen molecules strongly depended on a reaction temperature. That is, molecular oxygen has been activated directly over the Au surface at the high temperature while the moisture takes part in the activation of the oxygen molecule at low reaction temperature.

Next, we examined the turnover frequencies (TOFs) for CO₂ formation at the two reaction temperatures as a function of mean gold particle diameter. To determine whether the active sites for CO oxidation were exposed gold atoms on the gold particles or perimeter sites at the interface between the gold particles and the TiO₂ support, we calculated the TOFs in two ways: (i) by normalizing the total number of exposed Au atoms at the gold particles (TOF-S) and (ii) by normalizing the the total number of gold atoms at the perimeter interfaces (TOF-P). The results clearly showed that the

relationship between TOF and mean gold particle diameter depended strongly on reaction temperature. At 300 K, TOF-S decreased with increasing mean gold particle diameter, whereas TOF-P remained nearly constant regardless of particle diameter, suggesting that the active sites for CO oxidation were the gold atoms located at the periphery of the gold particles attached to TiO₂. In contrast, TOF-S at 400 K remained nearly constant regardless of the mean gold particle diameter, indicating that the active sites for CO oxidation were newly created on the gold metal surface at the high temperature. Thus, we can conclude that both the reaction mechanisms and the active sites differed between the low temperature region and the high temperature region.

SS-TuP30 Active Sites for H₂ Dissociation on Gold Model Catalyst, I. Nakamura, T. Fujitani, AIST, Japan

Au nanoparticles supported on metal oxides are highly active for various hydrogenation reactions. The dissociation of H₂ molecules is one of the most important elementary steps in hydrogenation reactions, and the nature of H₂ dissociation sites has been the subject of various studies. Recently, we demonstrated using Au/TiO₂(110) that the perimeter interface between Au and TiO₂ was the active sites for H₂ dissociation. However, the oxidation state of Ti and the structure of Ti oxide at the perimeter interface are not entirely clear. Here, we performed H₂-D₂ exchange reaction using TiO_x/Au(111) and TiO_x/Au(100) (x = 0-2), and clarified the influence of the oxidation state of Ti and the Au and TiO₂ structures on the creation of active sites for H₂ dissociation. We found that the presence of stoichiometric TiO₂ was essential for the creation of H₂ dissociation sites over the Au surfaces. The activation energies (E_a) for HD formation over TiO₂/Au(111) and TiO₂/Au(100) were consistent with each other, and these E_a agreed well with that for Au/TiO₂(110). This result shows that the active sites for H₂ dissociation created on TiO₂/Au(111) and TiO₂/Au(100) were identical to those formed on Au/TiO₂(110). Furthermore, we demonstrated that turnover frequencies (TOFs) for HD formation were close among these three surfaces, where TOFs were calculated by normalizing the number of HD molecules formed per second to the total number of Au atoms at the perimeter interfaces. These results clearly indicate that the active sites for H₂ dissociation over TiO₂/Au(111) and TiO₂/Au(100) were the perimeter interface between TiO₂ and Au. Concerning the structure of TiO₂ on Au surfaces, LEED observations showed that the TiO₂ produced on Au(111) was the ordered structure, in contrast to disordered TiO₂ structure on Au(100). Thus, the creation of active sites for H₂ dissociation was independent of the Au and TiO₂ structures consisting perimeter interface. We concluded that local bonds between Au and O atoms of stoichiometric TiO₂ (Au-O-Ti) create the active sites for H₂ dissociation.

SS-TuP31 Image Potential State Mediated Excitation of Rubrene on Graphite, J. Park, Seoul National University, Republic of Korea, T. Ueba, L. Terawaki, T. Yamada, H. Kato, T. Munakata, Osaka University, Japan

Electronic excitation at the interface between an organic molecular film and a substrate is of general importance for the area of organic electronics and light conversion processes. We demonstrate rubrene/HOPG as a model system for an organic film/substrate interface. Many efforts have been devoted to improve the performance of a rubrene thin film transistor after high carrier mobility was achieved for rubrene single crystals. The reasons for the poor efficiency of the thin films are attributed to the molecular geometry on the surface. To understand the mechanisms of charge transportation for organic molecular devices, it is the primary step to unravel the molecular electronic structures of both occupied and unoccupied states at interfaces between the film and the substrate.

We have performed two-photon photoemission (2PPE) spectroscopy for rubrene films formed on HOPG substrate. It is revealed a prominently enhanced unoccupied molecular peak, which is resonantly excited from the highest occupied molecular orbital (HOMO). Interestingly, the enhancement of the peak becomes less significant at the coverage higher than 1 monolayer, where the image potential state (IPS) peak on the substrate disappears. The resonance enhancement is moderate with s-polarization, by which the transition to IPS is completely suppressed. We ascribe that the excitation of the level is mediated by the IPS on HOPG. Though the IPS wave function extends outside the molecules, it interacts with the unoccupied molecular orbital at the edges of molecular islands, causing the strong resonance enhancement of the unoccupied molecular level.

By clarifying the mechanism, the excitation process is expected to be useful to highly enhance the efficiency of organic molecular devices and light conversion processes. The energy of IPS is generally governed by the work function. It may be possible to tune the IPS level nearly resonant to an unoccupied level of organic films. This provides a way to tailor the electronic excitation efficiency.

SS-TuP32 Tribological Properties in a Vacuum of DLC Thin Films Prepared by N₂⁺ Ion Beam Assisted Deposition, H. Nishi, K. Harada, I. Takano, Kogakuin University, Japan

DLC (Diamond-like carbon) classified in new materials is amorphous carbon including hydrogen and has the similar property to diamond. DLC films were formed by the ion beam evaporation method in the early 1970's and after that have been manufactured by various methods. Because the representative property of DLC shows the high hardness and low friction coefficient, DLC is applied in various fields such as motor parts or tools. The ion beam assisted deposition method has many parameters on the film formation condition in comparison with other dry process methods. Therefore this method was anticipated in production of new characteristics such as a high adhesion film.

From the result of our research, DLC thin films prepared by the ion beam assist method using an N₂ gas showed the excellent low friction coefficient in the atmosphere. In this study, the behavior on friction in a vacuum of those DLC films was investigated. The DLC films were formed using N₂⁺ ion beam assisted deposition in a toluene (C₇H₈) atmosphere. The formation conditions of DLC films were changed with an ion beam current density and an accelerating voltage. Stainless steels (304SS) were used for the sample substrate. The mechanical properties of hardness and friction coefficient were measured using the dynamic micro knoop hardness tester and the ball-on-disk tribotester respectively. Atomic concentration and structure of the films were investigated by X-ray photoelectron spectroscopy and Raman spectroscopy. The friction coefficient in a vacuum was measured under 5 x 10⁻⁴ Pa. The conditions of the ball-on-disk test were 0.98 N in a weight and 135 rpm in a sliding speed.

The suitable friction property of DLC films was obtained by the condition with an accelerating voltage of 5 kV at a current density of 10 μA/cm². The minimum friction coefficient in a vacuum was 0.016 for a SUJ2 ball of the counter material, however, the DLC thin film started to cause partial peeling-off in a sliding distance of 52 m. It is anticipated that the property in a vacuum of these DLC films is applied in space technology.

SS-TuP34 Atomic Structure of the Bi-induced (1×3) Surface Reconstruction on GaAs(001), A. Duzik, J.C. Thomas, A. Van der Ven, University of Michigan, N.A. Modine, Sandia National Laboratories, J.M. Millunchick, University of Michigan

Bismuth (Bi) is a nearly ideal surfactant on GaAs owing to its large size relative to Ga and As, smoothing the surface morphology of the GaAs(001) surface. Surface modification in this manner is potentially useful in high-quality device growth, but corresponding atomic structure and its effects on subsequent device growth are unknown. Reflection high-energy electron diffraction indicates that the Bi surfactant induces a (1×3) surface reconstruction. Experimental scanning tunneling microscopy clearly shows a nm-length-scale step structure with a high density of alternating up/down steps and reconstruction rows of ×3 periodicity. From these observations, we propose a mechanism for the Bi surfactant surface smoothing. The alternating step heights on the nm length scale are likely a result of a Bi-induced surface energy change. However, compositional disorder obscures the atomic structure within the rows. Thus, the atomic structure of the (1×3) reconstruction cannot be revealed through experiment, but must be determined from simulation.

Ab-initio density functional theory and cluster expansion calculations were carried out to determine the relative stability of reconstruction in the Bi/GaAs(001) system. Differences in stability originate from two sources: structure, determined by surface bonding topology, and configuration, arising from the arrangement of Ga, As, and Bi species over the surface dimer sites. For the Bi/GaAs system, the (2×1), α2(2×4), β2(2×4), (4×3), and c(4×4) reconstructions and their species configurations were considered. Calculations show the observed (1×3) reconstruction explained by the (4×3) structure first proposed for AlSb and GaSb, which has a large number of stable configurations at 0K. At typical growth temperatures, the calculated Monte Carlo entropy approaches that of ideal mixing, indicating thermal excitations of these configurations produce the experimentally observed disorder.

SS-TuP35 Spectroscopic Study of the Chemical Reaction at the Ca/PMMA Interface, H.X. Ju, J.F. Zhu, University of Science and Technology of China

PMMA is an important thermoplastic material which has been utilized in a variety of engineering areas ranging from aeronautical applications to electronics industries, due to its attractive physical and optical properties. The physical and chemical interactions have been observed at the interfaces between metals and PMMA, which can play a crucial role in the device performance. As a result, significant attention has been paid to the interfaces in order to promote devices performance and stability.

In this work, we investigate in detail the chemical reaction during deposition of Ca on the PMMA surface by applying X-ray photoemission

spectroscopy (XPS) and near-edge X-ray absorption fine structure spectroscopy (NEXAFS), which provide detailed information concerning surface chemical reaction. The changes of the O 1s and C 1s core level XPS spectra indicate a strong interaction between the Ca and the PMMA. The O K-edge NEXAFS spectra give a comprehensive insight into reaction sites. In this way, the pronounced decrease of the π^* (C=O) resonance intensities with deposition of Ca clearly demonstrates that Ca atoms attack carbonyl groups in PMMA. The experimental results confirm the previous work regarding the adsorption microcalorimetry measurements of metal particles adsorption on polymer surfaces, which provide a powerful approach for determining the adsorption energy and understanding interfacial interactions. There is a high heat of Ca adsorption on PMMA surfaces of 780 kJ/mol, attributed to the reaction of each Ca reacts with 2 esters to form the Ca carboxylate. Furthermore, we provide addition information regarding the details of specific chemical interactions at the interface. These will greatly contribute toward further understanding of the interfaces between metals and polymers.

SS-TuP36 Mass Ratio Effects in Hyperthermal Surface Scattering. *D. Kulkarni, C.E. Sosolik*, Clemson University

The forward scattering of heavy ionic projectiles from oriented crystal surfaces gives evidence of collective effects that are far more pronounced than those seen in scattering of light ionic projectiles. For example, molecules containing heavy atoms such as XeF₂ are known to initiate novel surface chemistry effects. To study these kinematic trends, MD and trajectory simulations were performed for hyperthermal energy ions. By sequentially increasing the mass of the projectile across the periodic table, we have observed energy and angle resolved trends that show a clear deviation from standard scattering events, which are typically interpreted as sequential binary collisions. The simulation results were compared to experimental data for alkali ions on metal surfaces, specifically for the cases of K⁺ and Cs⁺ scattered from Cu(001).

SS-TuP37 Ag Nanoparticles on Reducible CeO₂(111) Thin Films: Effect of Nanoscale Ceria. *S.W. Hu, X.F. Feng, D.D. Kong, D.L. Cheng, Y.F. Ye, J.F. Zhu*, University of Science and Technology of China

Ag/CeO₂ is of particular interests because of its importance in technical applications as catalysts for many chemical reactions such as CO and hydrocarbon oxidation. However, there are still some discrepancies remaining in the fundamental recognition of the Ag/CeO₂ catalysts such as the oxidation state of Ag species and the mechanism of Ag-induced the reduction of CeO₂. In order to obtain a detailed insight of the Ag/CeO₂ system, the growth and structures of Ag nanoparticles on CeO_x(111) thin films with different thicknesses, morphologies and reduction degrees have been systematically studied by scanning tunneling microscopy (STM), X-ray photoelectron spectroscopy (XPS) and low energy electron diffraction (LEED). These CeO_x(111) thin films were epitaxially grown on Cu(111). It is found that in most cases Ag exhibits the three-dimensional (3D) growth with constant particle densities on the CeO_x(111) surfaces. Ag only populates the sites at the ceria-ceria step edges, independent of the thicknesses and the reduction degree of the ceria films. Moreover, the particle density is directly proportional to the number of step edges of ceria, which is related to its thickness on Cu(111). On the reduced ceria films, Ag nanoparticles do not nucleate on point defects. Upon heating, the Ag nanoparticles undergo serious sintering before desorption at 800 K on the fully oxidized CeO₂ films. While on the reduced ceria films, the sintering and desorption process are slowed down at the same annealing temperatures as those on CeO₂. This result suggests that although the surface point defects have no influence on the growth behavior of Ag, they can enhance the thermal stability by inhibiting the diffusion of Ag on the ceria surface to form large particles during annealing.

Wednesday Morning, October 31, 2012

Biomaterial Interfaces

Room: 23 - Session BI+SS+NS-WeM

Bio/Nano Interfaces with Applications in Biomedicine and Energy

Moderator: G.J. Leggett, University of Sheffield, UK

8:00am **BI+SS+NS-WeM1 Combining Colloidal Lithography and Photolithography to Create Dual Length-Scale Topographical Features to Study Stem Cell Behavior**, *D.T. Bennetsen, D.C.E. Kraft, R. Ogaki, M. Foss*, Aarhus University, Denmark

It is well known that topographical features influence cellular response. A novel combination of colloidal- and photolithography has been developed to create a dual length scale topographical platform. The presented approach permits rapid parallel fabrication of micro/nanoscale patterns. The aim is to study the response of primary human dental pulp stem cells (hDPSC) to such topographies in a systematic way.

Colloidal lithography is performed using the "lift-off" method, which is applicable to surfaces with a non-flat surface. This enables the combination of using photolithography pre-made wafers as substrates, resulting in a complex topographical structure, spanning two length scales (Figure 1). Topographical patterns are created using the colloidal mask with either evaporation or sputtering via physical vapor deposition (PVD). The principle combination of materials investigated is tantalum covered with tantalum features. These dual scale substrates are exposed to hDPSC and proliferation, attachment and differentiation are examined. Differentiation is examined using osteogenic markers and MyoD1 expression.

Initial cell proliferation data indicates that variations in the colloidal pattern heights do not seem to elicit a statistical significant response (Figure 2). A set of experiments to clarify the effect of the colloidal pattern on the proliferation and cell cycle of the hDPSC is thus currently being performed. Furthermore, the effect of the dual scale topographical substrates on proliferation, differentiation and cell cycle is also being explored.

Concurrently we are investigating the combined effects of topographical/chemical patterns on cellular response. This can be achieved by depositing different materials site-specifically, followed by a material-specific self-assembly route. E.g. silanes and thiols with specific chemical moieties on oxides and gold, respectively. Characterization is performed using atomic force microscopy (AFM), scanning electron microscopy (SEM), X-ray photoelectron spectroscopy (XPS) and time-of-flight secondary ion mass spectrometry (ToF-SIMS).

Our fabrication approach enables the opportunity to increase the complexity of artificial 2D platforms thus by gaining a better understanding of cellular behavior for a range of biomedical and biotechnological applications.

8:20am **BI+SS+NS-WeM2 Genetically Modified Tobacco Mosaic Virus (TMV)-based Electrochemical Detection of 2, 4, 6-trinitrotoluene (TNT)**, *F. Zang, H. Ben-Yoav, X. Fan, A. Brown, J. Culver, R. Ghodssi*, University of Maryland

Detection of chemical hazards and explosive compounds has received growing attention for applications in environmental monitoring, food science, and national security. Explosives, such as TNT, show low vapor pressure, molecular mass, and volume, which makes the detection of these molecules challenging for most mass and refractive index based sensors. Thanks to the redox reaction of nitro groups in TNT molecules, electrochemical methods may be used for detection of low concentrations of TNT in aqueous environments. Electrochemical sensors are suited for on-site explosive detection due to high sensitivity, low volume and convenient integration with miniaturized devices. However, to distinguish TNT from other electrochemically active compounds in complex environments, high selectivity is a more critical factor for development of TNT sensors.

The TMV has a high aspect ratio, rod-like nanostructure that can be genetically modified to express tailored chemical receptors. In this work, a 12-amino acid (WHWQRPLMPVSI) sequence peptide with multivalent recognition properties of TNT was expressed on the coat protein of TMV (TMV-p) which was utilized to develop a sensitive and selective electrochemical sensing mechanism for TNT detection. Selective binding of TMV-p with TNT molecules will decrease the free TNT concentration in solution, reducing the number of nitro groups available for redox reactions.

In preliminary studies, background signals generated from electrolytes were characterized and the signal-to-noise ratio was optimized by long term scans of square wave voltammetry. Three concentration dependent current peaks from the reduction of nitro groups in TNT were observed at the

potentials of -0.53V, -0.72V and -0.86V vs. Ag/AgCl reference electrode, respectively, which agreed with the results in literatures. The initial results showed a stable and reliable electrochemical response by the TMV-p sensing system. By comparing the reduction currents in the mixtures of TMV-p and unmodified TMV with TNT solutions, we will demonstrate that TMV-p preserves the peptide binding affinity to TNT molecules while increasing the binding site density.

The approach described in this study is a sensitive and selective label-free method to detect TNT based on the binding of target molecules with peptide modified TMV. In addition to the highly selective peptide binding with analytes and a high binding site density, the genetically modified TMV is also capable of self-assembly, coating the active surfaces of a wide range of transducers. This work can potentially be implemented in the development of miniature sensors for selective TNT detection in complex environments.

8:40am **BI+SS+NS-WeM3 Nanoparticles in Biology: Engineering the Interface for Sensing and Delivery**, *V. Rotello*, University of Massachusetts **INVITED**

A key issue in the use of nanomaterials is controlling how they interact with themselves and with the outer world. Our research program focuses on the tailoring of nanoparticles of surfaces for a variety of applications, coupling the atomic-level control provided by organic synthesis with the fundamental principles of supramolecular chemistry. Using these engineered nanoparticles, we are developing particles for biological applications, in particular delivery and sensing. This talk will focus on the interfacing of nanoparticles with biosystems, and will discuss our use of nanoparticles for delivery applications including our *in vitro* studies of small molecule, nucleic acid, and protein delivery. This presentation will also feature the use of nanoparticles for diagnostic applications, including the use of array-based sensing paradigms for the sensing and identification of proteins, bacteria and cell type and state.

9:20am **BI+SS+NS-WeM5 Hydrophobic Forces, Electrostatic Steering, and Acid-Base Bridging between Atomically Smooth Self-Assembled Monolayers and End-Functionalized PEGolated Lipid Bilayers**, *M. Valtiner*, Max-Planck-Institut fur Eisenforschung, Germany, *S.H. Donaldson, M.A. Gebbie, J.N. Israelachvili*, University of California, Santa Barbara

A molecular-level understanding of interaction forces and dynamics between *asymmetric* apposing surfaces plays a key-role in utilizing molecular structures for functional surfaces in biological and materials applications. To quantify interaction forces and binding dynamics between apposing surfaces in terms of their molecular architecture we developed a novel surface-forces-apparatus experiment, using self-assembled monolayers (SAMs) on *atomically-smooth* gold. Varying the SAM head-group allowed to quantitatively identify and control which interaction forces dominated between the SAM surfaces and surfaces coated with short-chain, end-functionalized polyethylene-glycol (PEG) polymers extending from lipid-bilayers [1].

Three different SAM-terminations were studied: (a) carboxylic-acid, (b) alcohol, and (c) methyl head-group terminations. These functionalities allowed for the quantification of (a) specific acid-base bindings, (b) steric effects of PEG chains, and (c) adhesion of hydrophobic segments of the polymer-backbone, all as function of the solution pH. The pH-dependent acid-base binding appears to be a *specific, charge-mediated hydrogen bond* between oppositely-charged carboxylic-acid and amine functionalities, above the acid- pK_A and below the amine- pK_A . The long-range electrostatic "steering" of acid-base pairs leads to high binding probability even at distances close-to-full-extension of the PEG tethers, a result which has potentially important implications for protein-folding, enzymatic catalysis and biomaterial development.

[1] M. Valtiner et al., *JACS*, **2012**, 1746

9:40am **BI+SS+NS-WeM6 Viral Encapsulation in Lecithin Liposomes to Enhance the Therapeutic Effect of Oncolytic Viral Therapy**, *N. Mendez, V. Herrera, A.C. Kummel*, University of California San Diego

Oncolytic viruses have emerged as a novel platform for cancer therapeutics due to their tumor-selective replication in cancer cells. In particular, the oncolytic virus TAV-255 has shown viral replication attenuation in normal cells while retaining cytolytic activity in tumor cells by taking advantage of defects in the p53-tumor suppressor pathway. Extensive testing of oncolytic viruses has shown a limited therapeutic effect due to rapid clearance by the reticuloendothelial (RE) system and antibody neutralization. With the aim to overcome an immune response and to enhance localized delivery, an oncolytic virus-liposomal encapsulation method has been designed to increase tumor uptake and the therapeutic efficacy of oncolytic viruses in

cancer cells. An inexpensive, non-toxic liposome has been prepared by self-assembly of Lecithin phospholipid bilayers around the Adenovirus capsid. Cholesterol and DSPE-PEG were incorporated into the lipid formulation to improve retention and stability. The developed method has shown that non-targeted encapsulated viral particles retain their ability to transfect cancer cells. In addition, surface functionalization of the liposomes may be applied to specifically target cancer cells and to compensate for decreased infectivity due to viral encapsulation.

10:40am **BI+SS+NS-WeM9 Engineering Bio-Interfaces using Electric Field-Induced Nanolithography**, S. Zauscher, R.J. Ferris, B. Yellen, Duke University

Field-Induced Nanolithography (FINL) offers a convenient tool to create physically or chemically distinct patterns for bio-interfacial sensing applications. For pattern transfer, FINL merely requires a conductively coated SPM tip or stamp, connected to a conductive substrate via a voltage source. The patterning electrode is placed in contact with the target surface and a bias voltage is applied. Few sub-diffraction limit surface patterning techniques offer FINL's versatility to function in both a serial and parallel fashion. Recently we demonstrated the use of FINL to pattern a range of polymer brushes: poly(acrylic acid) (PAA), poly(N-isopropylacrylamide) (PNIPAAm), poly(sulfobetaine methacrylate) (PSBMA), and poly(oligo(ethylene glycol) methyl methacrylate) (POEGMA). Our results show that FINL of non-fouling polymer brushes provides a novel patterning technique that results in the localized topographical and chemical modification of the polymer brush surface only. The resulting chemical modification allowed selective addressing of the brush surface with aldehyde reactive coupling chemistries. Our approach thus shows significant promise for fabricating large-scale sensing devices, as patterning can be accomplished in a step-and-repeat fashion. Using FINL, we also demonstrated patterning of surface charges onto ferroelectric thin films (FETFs). FETFs are materials that are able to maintain a bi-stable polarization state, and that once polarized, maintain a high surface charge density. Using FINL, it is possible to locally align unit-cell dipole moments within the film to produce nano-scale polarization patterns. Although to date the use of FETFs is isolated to semiconductor and memory applications, we demonstrate that FETFs have great potential for biological and interfacial sensing applications. We show that FETF surface charge patterns can be used to control the lateral extent of electric double layer formation in dilute electrolyte solutions, with clear implications for field assisted particle deposition and programmed self assembly.

11:00am **BI+SS+NS-WeM10 Supramolecular Bioassemblies at Solid-Liquid Interfaces: Binding Control through Redox-Driven Multivalent Host-Guest Interactions**, G.V. Dubacheva, CIC biomaGUNE, Spain, L. Guerente, D. Boturny, Joseph Fourier University, France, R. Auzély, CERMAV, France, R.P. Richter, CIC biomaGUNE, Spain; Joseph Fourier University, France; Max Planck Institute for Intelligent Systems, Germany, P. Labbé, Joseph Fourier University, France

The design of kinetically stable bioassemblies while keeping binding control is of high current interest for bioanalytical and biomedical sciences. The development of tunable biointerfaces is also a key issue in nanobiotechnology as they can be used for modeling cell surface-associated biological processes. In this context, supramolecular host-guest chemistry is particularly attractive as it allows controllable molecular recognition and structural modification at specific areas of a nanoassembly, i.e. purpose-designed molecules can be confined in time and space in a highly controlled manner.

Cyclodextrin (CD) is well-known to form host-guest complexes with hydrophobic molecules while being soluble at physiological conditions. Taking advantage of redox-driven β -CD-ferrocene (Fc) multivalent interactions, we designed stimuli-responsive biomaterials composed of linear polymers, their multilayer assemblies and biomolecules. For this aim, we developed a new method to create β -CD self-assembled monolayers (SAMs) allowing precise varying β -CD surface density.1 We showed that Fc-functionalized polymers can be reversibly attached to such β -CD SAMs.1 We also showed a possibility to build up multilayer host-guest polymer assemblies on β -CD surfaces.2 In addition, we applied these β -CD SAMs for the reversible attachment of biomolecules using orthogonal Fc/ β -CD- and specific bio-interactions under biological conditions.3 Finally, combined with guest-modified polysaccharide hyaluronan, the β -CD surfaces were explored as a model system to understand multivalent interactions at the cell-hyaluronan matrix interface associated to a variety of cellular functions and biological processes.

Physico-chemical properties of supramolecular assemblies were characterized by QCM-D, ellipsometry, cyclic voltammetry and contact angle goniometry. The redox-driven binding of polymers and biomolecules to β -CD surfaces was assessed by *in situ* combining electrochemistry/QCM-D and SPR ellipsometry/microfluidic systems. The developed tunable

biointerfaces can be applied to investigate other topics in soft condensed matter physics, molecular physics and biophysics.

1Dubacheva et al., *Langmuir*, **2010**, 26:13976

2Dubacheva et al., *Soft Matter*, **2010**, 6:3747

3Dubacheva et al., *Chem Commun*, **2011**, 47:3565

11:20am **BI+SS+NS-WeM11 High-resolution *In Situ* Electrochemical STM Imaging of Phospholipid Model Cell Membrane**, H. Shimizu, S. Matsunaga, University of Tokyo, Japan, T. Yamada, T. Kobayashi, RIKEN, Japan, M. Kawai, University of Tokyo, Japan

We obtained molecular-scale images of phospholipid layers spread on a modified Au(111) immersed in a buffer solution, by means of *in situ* electrochemical scanning tunneling microscopy (EC-STM). Real cell membranes consist of a bilayer of phospholipids which continually gather and interact. There are various kinds of phospholipids in the real cell membranes. To understand the action of these molecules, a dynamic molecular-scale method of observation is necessary. Lipkowski [1] first visualized static monolayers of phospholipid on Au(111) by *in situ* EC-STM. Matsunaga *et al.* [2] revealed dynamic, microscopic motion of phospholipid monolayer on alkanethiol-modified Au(111) immersed in a buffer solution. We intended to compose a bilayer of phospholipid on a hydrophilic substrate in order to mimic the real cell membrane more truly. We used a hydrophilically modified Au(111), anticipating that the first lipid monolayer with the hydrophilic head group down to the surface, and the second lipid monolayer with the hydrophobic alkyl chains down, all spontaneously in aqueous buffer solution.

For this purpose, we used 3-mercaptopropionic acid (MPA) self-assembled monolayer (SAM) on Au(111), in which the COOH groups are expected to be exposed out of the surface. We first observed a ($\sqrt{3} \times \sqrt{3}$) type adlattice of MPA SAM by STM. Then the sample was immersed in 50 mM phosphate buffer containing minimal lipid particles of 200 μ M 1-palmitoyl-2-oleoyl-*sn*-glycero-3-phosphocholine (POPC) with or without 50 μ M cholesterol.

We uniquely observed a 2-dimensional adlattice with a parallelogram unit cell of 1.0 nm x 1.9 nm. Along the short segment, bright spots are aligned. The adlattice did not change with or without cholesterol, indicating that it was composed exclusively of pure POPC. The interval of 1.9 nm is apparently shorter than the full length of POPC molecule (≈ 2.5 nm). To interpret the adlattice structure, we considered a model structure composed of tilted POPC, with the head group attached to the MPA SAM. This model involves a strong affinity between the hydrophilic groups.

Although this frozen adlattice does not completely match our target structure of mobile lipid bilayer, we consider we could partly utilize the hydrophobicity/hydrophilicity of the phospholipid molecules to compose a uni-directional membrane. We will further develop this kind of methods by choosing the proper modifier on Au(111), aiming the bilayer structure. By this we expect to go closer to the nanometer-scale reality of cell membranes containing functional proteins.

[1] J. Lipkowski, *Phys. Chem. Chem. Phys.* **12**, 13874 (2010).

[2] S. Matsunaga *et al.*, *Electrochem. Commun.* **9**, 645 (2007).

11:40am **BI+SS+NS-WeM12 Characterization of Polymer/Drug Films as Model for Drug Eluting Coronary Stent Coating Layers**, V. Ciarnelli, M.R. Alexander, M.C. Davies, C.J. Roberts, University of Nottingham, UK

This work describes the characterization of a polymeric based drug eluting stent coating, used in coronary stenting to prevent restenosis [1]. The work examines thin films as models for drug eluting stent coatings. Complementary surface analysis techniques are used to investigate the drug polymer distribution on the surface and throughout the depth of the model films.

The first goal of this project is to establish the feasibility of certain surface analysis techniques in the characterisation of a drug eluting stent coating layer. Secondly, this study will act as a standard reference to determine the ideal operating conditions for characterizing the more complex stent device.

Thin film models were produced varying the substrate materials (silicon or glass), preparation procedures (spin casting or spray coating) and drying methods (oven or warm air). The different drug to polymer ratios used were: 1:3, 1:1 and 3:1 (w:w).

Complementary surface analysis techniques such as atomic force microscopy (AFM), time of flight secondary ion mass spectrometry (ToF-SIMS) and x-ray photoelectron spectroscopy (XPS) were employed for the characterization of the films. Depth profiling has also been performed using XPS and ToF-SIMS.

AFM imaging of the oven dried spun cast films shows domains of drug, characterized by a circular organization with features of 100 - 250 nm in

diameter. These domains are not observed in other samples and appear to be related to phase separation during the drying step.

Surface characterization using XPS shows enrichment of the drug at the surface for all the model films with the exception of the spray coated films at the 1:3 drug-to-polymer weight ratio.

Depth profiling using both ToF-SIMS and XPS confirms that the drug is enriched at the surface, posing significant implications for drug loaded polymer delivery systems.

Complementary surface analysis techniques have proven extremely successful in characterizing the model films. Suitable techniques and their operative conditions have now been established for the characterization of a stent device.

[1] I. Iakovou et al., Incidence, predictors, and outcome of thrombosis after successful implantation of drug-eluting stents. *JAMA*, **293** (2005): p. 2126-2130.

Graphene and Related Materials Focus Topic Room: 13 - Session GR+AS+BI+PS+SS-WeM

Graphene Surface Chemistry, Functionalization, Biological and Sensor Applications

Moderator: D.K. Gaskill, U.S. Naval Research Laboratory

8:00am **GR+AS+BI+PS+SS-WeM1 Structural Analysis of Chemically Functionalized Epitaxial Graphene with High-Resolution X-ray Reflectivity**, *J.D. Emery, Q.H. Wang, M. Zarrouati*, Northwestern University, *P. Fenter*, Argonne National Laboratory, *M.C. Hersam, M.J. Bedzyk*, Northwestern University

For graphene to realize its potential in next-generation electronics it must be incorporated with a variety of materials to form devices. Recently, the use of self-assembled organic monolayers deposited on epitaxial graphene (prepared by graphitization of the 6H-SiC(0001) surface) has been effective in the functionalization of the bare graphene sheet, enabling the additional chemistry necessary for device fabrication. In this work, we present high-resolution X-ray Reflectivity (XRR) studies of perylene-3,4,9,10-tetracarboxylic dianhydride (PTCDA) on epitaxial graphene. Initially, a model-independent vertical electron density profile of the graphene/silicon carbide interface is retrieved with the use of Feinup-based error correction algorithms in order to minimize ambiguities that can arise from model-based methods. This retrieved structure is then used as the foundation for model-based analysis, from which the final structures are extracted. A series of structures comprising 0, 1, and 2MLs of PTCDA deposited on 1-2ML graphene are discussed. The interlayer spacing between the PTCDA and top graphene layer are revealed to be approximately 0.35 nm, which supports the view that the PTCDA molecules are interacting only weakly (van der Waals) with the graphene layer. In addition to the characterization of PTCDA-functionalized graphene, we will also demonstrate the efficacy of these molecules to form a weakly-interacting seeding layer for subsequent growth of high-k dielectrics via atomic layer deposition.

8:20am **GR+AS+BI+PS+SS-WeM2 In Situ FT-IR Study of Graphene Fluorination using XeF₂**, *J.-F. Veyan, N. Shafiq*, University of Texas at Dallas, *K. Novoselov*, University of Manchester, UK, *Y.J. Chabal*, University of Texas at Dallas

Graphene fluorination to obtain fluorographene has been successfully realized by exposing graphene flakes to molecular Xenon-Difluoride¹⁻³. To gain a mechanistic understanding of XeF₂ reaction with the graphene flakes, an all-aluminum custom-made two-stage reaction cell has been designed to fit into the main sample compartment of an FTIR Nicolet 6700 interferometer, for *in situ* infrared absorption spectroscopy. The first stage is a clean expansion chamber to isolate the pure XeF₂ in its gas phase, from solid XeF₂ (powder) stored in a storage vessel. The XeF₂ vapor is extracted by opening the valve V1 to the storage chamber and its pressure (up to ~4 Torr) is controlled by the valve V2. The second stage is a reactor equipped with two KBr windows, allowing the IR beam to penetrate and exit the enclosure. A pneumatic valve allows the transfer of gaseous XeF₂ from stage 1 into stage 2. Pressures in both storage and reactor chambers are measured with Baratron gauges (Ga1, Ga2). To avoid any contamination of the reactor and sample holders during sample preparation and loading, a N₂-purged glove bag is placed over the reactor to maintain a controlled environment. The graphene flakes in suspension in a NMP (N-Methylpyrrolidone) solution, are transferred onto three mechanically polished Aluminum plates at a temperature of 70°C. The plates are then mounted on the specially designed 3-reflection sample holder flange designed to fit stage 2.

By varying the sample temperature from 20 to 200°C as well as the XeF₂ pressure in the reactor stage from 0.1 to 4 Torr, the chemical attachment of fluorine on graphene is identified from a comprehensive FT-IR study performed under industrial conditions. Fluorine attached out of plane can be easily differentiated from fluorine attached at edges (i.e. remaining within the basal plane) and terminating the edge atoms.

¹ R. R. Nair, et al., *Small* **6**, 2877 (2010).

² J. T. Robinson, et al., *Nano Letters* **10**, 3001 (2010).

³ K.-J. Jeon, et al., *Acs Nano* **5**, 1042 (2011).

8:40am **GR+AS+BI+PS+SS-WeM3 Molecularly Resolved Chemical Functionalization of Graphene**, *M.C. Hersam*, Northwestern University **INVITED**

Graphene has emerged as one of the leading materials in condensed matter physics due to its superlative electrical and mechanical properties. With an eye towards expanding its functionality and applications, this talk will highlight our latest efforts to tailor the surface chemistry of graphene [1]. At the molecular scale, we employ ultra-high vacuum (UHV) scanning tunneling microscopy (STM) and conductive atomic force microscopy (cAFM) to characterize chemically modified epitaxial graphene on SiC(0001) [2,3]. For example, a suite of perylene-based molecules form highly ordered self-assembled monolayers (SAMs) on graphene via gas-phase deposition in UHV [4,5]. Due to their noncovalent bonding, these SAMs preserve the superlative electronic properties of the underlying graphene while providing uniform and tailorable chemical functionality [6]. In this manner, disparate materials (e.g., high-*k* gate dielectrics) can be seamlessly integrated with graphene, thus enabling the fabrication of capacitors, transistors, and related electronic/excitonic devices [7]. Alternatively, via aryl diazonium chemistry, functional polymers can be covalently grafted to graphene [8], while exposure to atomic oxygen in UHV enables chemically homogeneous and thermally reversible covalent epoxy functionalization [9]. Beyond UHV STM characterization, this talk will also delineate our most recent efforts to exploit chemically modified graphene in technologically significant applications including photovoltaics [10], transparent conductors [11-13], flexible GHz transistors [14], *in vivo* biomedical applications [15,16], and photocatalysts [17].

[1] Q. H. Wang and M. C. Hersam, *MRS Bull.*, **36**, 532 (2011).

[2] J. A. Kellar et al., *Appl. Phys. Lett.*, **96**, 143103 (2010).

[3] J. M. P. Alaboson et al., *Adv. Mater.*, **23**, 2181 (2011).

[4] Q. H. Wang and M. C. Hersam, *Nature Chemistry*, **1**, 206 (2009).

[5] Q. H. Wang and M. C. Hersam, *Nano Lett.*, **11**, 589 (2011).

[6] J. D. Emery et al., *Surf. Sci.*, **605**, 1685 (2011).

[7] J. M. P. Alaboson, et al., *ACS Nano*, **5**, 5223 (2011).

[8] Md. Z. Hossain et al., *J. Am. Chem. Soc.*, **132**, 15399 (2010).

[9] Md. Z. Hossain et al., *Nature Chemistry*, **4**, 305 (2012).

[10] I. P. Murray et al., *J. Phys. Chem. Lett.*, **2**, 3006 (2011).

[11] A. A. Green and M. C. Hersam, *J. Phys. Chem. Lett.*, **1**, 544 (2010).

[12] A. A. Green and M. C. Hersam, *Nano Lett.*, **9**, 4031 (2009).

[13] Y. T. Liang and M. C. Hersam, *J. Am. Chem. Soc.*, **132**, 17661 (2010).

[14] C. Sire et al., *Nano Lett.*, **12**, 1184 (2012).

[15] M. C. Duch et al., *Nano Lett.*, **11**, 5201 (2011).

[16] J.-W. T. Seo et al., *J. Phys. Chem. Lett.*, **2**, 1004 (2011).

[17] Y. T. Liang et al., *Nano Lett.*, **11**, 2865 (2011).

9:40am **GR+AS+BI+PS+SS-WeM6 Structure of a Peptide Adsorbed on Graphene and Graphite**, *J. Katoch*, University of Central Florida, *S.N. Kim, Z. Kuang, B.L. Farmer, R.R. Naik*, Air Force Research Laboratory, *S.A. Tatulian, M. Ishigami*, University of Central Florida

Non-covalent functionalization of graphene using peptides is a promising method for producing novel sensors with high sensitivity and selectivity. We have performed atomic force microscopy, Raman spectroscopy, infrared spectroscopy and molecular dynamics simulations to investigate peptide-binding behavior to graphene and graphite. We studied a dodecamer peptide, GAMHLPWHMGTL, identified by phage display to possess affinity for graphite.

Optical spectroscopy reveals that the peptide forms secondary structures both in powder form and in an aqueous medium. The dominant structure in the powder form is α -helix, which undergoes a transition to a distorted helical structure in aqueous solution. The peptide forms a complex reticular structure upon adsorption on graphene and graphite, having a helical conformation different from α -helix due to its interaction with the surface. Our observation is consistent with our molecular dynamics calculations and our study paves way for rational functionalization of graphene using

biomolecules with defined structures and, therefore, functionalities. Our results have recently been published [1].

[1] J. Katoch, S.N. Kim, Z. Kuang, B. L. Farmer, R. R. Naik, S. A. Tatulian, and M. Ishigami, dx.doi.org/10.1021/nl300286k, *Nano Letters* (2012).

10:40am **GR+AS+BI+PS+SS-WeM9 Controlling the Spatial Distribution of Graphene Chemistry.** *S.C. Hernández, E.H. Lock, S.G. Walton, C.J. Bennett, R. Stine, P.E. Sheehan, F.J. Bezares, L.O. Nyakiti, R.L. Myers-Ward, J.T. Robinson, J.D. Caldwell, C.R. Eddy, Jr., D.K. Gaskill*, Naval Research Laboratory

Graphene has attracted a widespread of interest because of its unique structural and electronic properties however, manipulation of these properties is necessary before realizing its full potential as the next generation material in a broad range of applications. Precise control of the surface chemistry of graphene can allow for subsequent surface procedures both for device fabrication (i.e. atomic layer deposition) and sensor applications. Chemical composition strongly impacts the electronic properties as well as chemical reactivity, both globally and locally. Electron-beam generated plasmas are capable of imparting a variety of functional group types over a range of coverages with minimal damage to the carbon back bone because of their inherently low ion energies and as such offer a unique approach for large area uniform processing of graphene films with controlled surface chemistry. The ability to manipulate the surface chemistry of this atomically thin material coupled with the capability to regulate the spatial distribution of functional will be discussed. Plasma processing conditions and characteristics, as well as the resulting chemical, structural, and electrical properties of the functionalized graphene will be demonstrated. This work is supported by the Naval Research Laboratory base program.

11:00am **GR+AS+BI+PS+SS-WeM10 Coverage-dependent Ordering of Adsorbed Iron Phthalocyanine on Epitaxial Graphene Grown on SiC(0001)-Si.** *A.A. Sandin, D.B. Dougherty, J.E. Rowe*, North Carolina State University

The crystallographic and electronic structure of monolayer and sub-monolayer Iron-Phthalocyanine (FePc) films are experimentally studied on graphene grown on SiC(0001) using Scanning Tunneling Microscopy and Spectroscopy (STM and STS) as well as Low Energy Electron Diffraction (LEED). At full monolayer coverage of FePc the STM images show that a nearly square overlayer lattice forms with flat-lying molecules and a densely-packed structure oriented 10° relative to the graphene principle lattice directions. This close-packed structure appears to be the same as that previously reported for FePc on graphite surfaces. For sub-monolayer coverage at room temperature, our STM images suggest that FePc forms a unique 2D molecular gas with images that have the hexagonal symmetry of the graphene honeycomb lattice. This is interpreted as suggesting that only a small diffusion barrier exists for molecular motion between neighboring sites in the 3-fold symmetry of the sub-monolayer overlayer lattice. The sub-monolayer gas condenses into islands at liquid Nitrogen temperatures with bare graphene regions and this implies that a weak attractive interaction exists between FePc molecules causing the close-packed ordering. Near defects in the graphene lattice we observe ring-like structures at room temperature that suggest an increased residence time of the mobile 2-D gas of FePc molecules. Our results using Scanning Tunneling Spectroscopy suggest the possibility of a hybrid molecule-graphene state in the unoccupied density of both states near the Fermi level which could possibly be useful in modifying the charge injection into graphene in future devices.

11:20am **GR+AS+BI+PS+SS-WeM11 A Molecular Route to Carbon Nanomembranes, Graphene and Their Hybrids with Tailored Physical and Chemical Properties.** *A. Turchanin*, University of Bielefeld, Germany **INVITED**

Bottom-up approaches via molecular self-assembly have high potential to facilitate the applications of two-dimensional (2D) carbon materials in nanotechnology. In this talk it will be demonstrated how self-assembled monolayers (SAMs) of aromatic molecules can be employed to this end. These monolayers are converted into *carbon nanomembranes* (CNMs) with a thickness of one molecule by electron or photon irradiation. CNMs can be separated from their original substrates and transferred onto various other substrates, fabricated as suspended nanomembranes or stacked into multilayer films with precise control over their thickness and composition. They possess two chemically distinct faces, which can be used for their selective functionalization, opening broad avenues for the engineering of novel materials with tailored on demand properties. High temperature annealing induces the transformation of CNMs into *graphene*, which allows large-area fabrication of the homogenous sheets with tunable electrical, optical and chemical properties. Integration of graphene sheets with CNMs into novel hybrids presents a promising route to flexibly functionalize

graphene for applications as optical, electrical, chemical and biofunctional coating in nanoelectronics and sensors. Various physical and chemical properties of these novel materials, their nanopatterning and functional applications will be presented.

1) A. Turchanin and A. Götzhäuser, *Prog. Surf. Sci.* (2012) in press.

2) A. Turchanin, D. Weber, M. Büenfeld, C. Kisielowski, M. Fistul, K. Efetov, R. Stosch, T. Weimann, J. Mayer, A. Götzhäuser, *ACS Nano* 5 (2011) 3896-3904.

3) C.T. Nottbohm, A. Turchanin, A. Beyer, R. Stosch, A. Götzhäuser, *Small* 7 (2011) 874-883.

4) Z. Zheng, C.T. Nottbohm, A. Turchanin, H. Muzik, A. Beyer, M. Heilemann, M. Sauer, A. Götzhäuser, *Angew. Chem. Int. Ed.* 49 (2010) 8493-8497.

5) A. Turchanin, A. Beyer, C.T. Nottbohm, X. H. Zhang, R. Stosch, A. Sologubenko, J. Mayer, P. Hinze, T. Weimann, A. Götzhäuser, *Adv. Mater.* 21, 1233-1237 (2009).

Nanometer-scale Science and Technology

Room: 12 - Session NS+AS+SS+SP-WeM

Nanoscale Catalysis and Surface Chemistry

Moderator: U.D. Schwarz, Yale University

8:20am **NS+AS+SS+SP-WeM2 Preparation and Performance of Solid Rocket Propellant Containing *In Situ*-Synthesized Nanoparticle Catalysts and Fuels.** *D. Reid, R. Draper*, University of Central Florida, *M. Johnson, T. Allen, A. Demko, E. Petersen*, Texas A&M University, *S.S. Seal*, University of Central Florida

Energetic nanocomposites have the potential to substantially increase the performance of rocket propulsion systems, but adoption outside the laboratory has been slow, largely due to manufacturing difficulties, safety challenges, and performance that falls short of theoretical potentials. In this study, we explore some novel synthesis methods to significantly improve performance and alleviate the difficulties of incorporating nanoparticles into energetic materials. Solid rocket propellants containing in-situ synthesized catalytic TiO₂ and energetic aluminum nanoparticles were prepared. These propellants exhibited significant performance improvements over those containing conventionally prepared nanoparticles. The performance gains are attributed to the small particle sizes, high degree of dispersion, and surface property control afforded by the in-situ synthesis methods.

9:00am **NS+AS+SS+SP-WeM4 Synthesis and Catalytic Activity of WS₂ Nanotube Supported Cobalt and Nickel Catalysts Towards Thiophene Hydrodesulfurization.** *M. Komarneni, Z. Yu, A. Chakradhar, U. Burghaus*, North Dakota State University, *Y. Tsvetkov, R. Popovitz-Biro, Y. Feldman, R. Tenne*, Weizmann Institute of Science, Israel

Inorganic nanotubes (INT) including WS₂ INT are promising materials for heterogeneous catalysis due to their intriguing properties like enhanced surface area, defects, and confinement effects. The promotion effects of Co and Ni combined with novel nanomaterials such as INT-WS₂ may create the next generation hydrodesulfurization (HDS) catalysts. To verify this, M/INT-WS₂ (M = Co or Ni) catalysts were synthesized and their catalytic activity towards HDS of thiophene was characterized by gas chromatography/ambient pressure catalytic tests and ultra-high vacuum (UHV) thermal desorption spectroscopy (TDS) experiments. Synthesis of M/INT-WS₂ involved two steps: Surface activation of INT-WS₂ by palladium seeding process and electroless plating method to coat nanoparticles of M. The deposited nanoparticles of M formed non-uniform layer on the INT surface. Nanoparticles of size 10-20 nm for Co (*hcp* structure) and 10-20 nm for Ni (*fcc* structure) were coated on INT-WS₂. Next, the catalytic activity of M/INT-WS₂ towards thiophene HDS was characterized using an atmospheric flow reactor. M/INT-WS₂ catalysts exhibited enhanced HDS activity when compared to pristine INT-WS₂ mainly due to the promotion effects of Co and Ni. Hydrogen sulfide and hydrocarbons such as 1,3-butadiene, butane, cis-2-butene, and trans-2-butene were formed as HDS products by both pristine and M/INT-WS₂. Commercial HDS catalysts, CoMo and NiMo from Haldor Topsoe were found to show ~ 4 times higher activity than M/INT-WS₂ synthesized in this study. These results are promising and show that further optimization of the nanofabrication process yields better HDS nanocatalysts. Furthermore, the adsorption kinetics of thiophene on M/INT-WS₂ was studied by TDS at UHV conditions. Thiophene adsorbed on internal, external, and groove sites of the M/INT-WS₂ bundles. Binding energies of thiophene on Ni/INT-WS₂ are ~ 10 kJ/mol smaller than that of pristine INT-WS₂. Thiophene also decomposed on M/WS₂ NT at UHV conditions. In addition, catalytic screening of nanocatalysts such as Au and Co-Ni coated INT-WS₂, pristine

MoS₂ nanoparticles with fullerene-like structure (IF), and Re-doped IF-MoS₂ for HDS was also performed. Overall, M/INT-WS₂ catalysts were the best HDS catalysts among the new nanocatalysts studied. The results also reflected the promotion effects of Co and Ni on the M/INT-WS₂ catalysts for higher thiophene conversion rates.

11:20am **NS+AS+SS+SP-WeM11 Charge Exchange and Molecule/Metal Coupling in Fulvalene Surface Chemistry**, *G. Rojas, B.G. Sumpster*, Oak Ridge National Laboratory, *J.A. Schlueter*, Argonne National Laboratory, *P. Maksymovych*, Oak Ridge National Laboratory

Understanding the epitaxy of organic semiconductors on the surface, and the ensuing processes of charge transfer and band-alignment is vitally important for the deterministic design of energy harvesting and light-emitting devices based on molecular heterojunctions. While most of the attention so far has been directed to pi-conjugated aromatic compounds, little is known about the properties of the fulvalene family in contact with metal surface. Here we will present a spectroscopic study of bis(ethylenedithio)tetrathiafulvalene (ET) on Ag(111) in the sub-monolayer to monolayer coverage. Varying coverages of ET adsorption show the molecules dimerize in parallel, bonding to the Ag surface along the long-axis of the molecule. The dimers remain mobile after adsorption, resulting in the formation of a two-phase surface material: unidimensional loosely stacked nanoclusters and finely packed, two-dimensional domains of interlocked molecules. These structures are an intermediate kinetic state, as the molecules further chemically react with the underlying Ag surface following annealing to temperatures as low as 40 C. It is thought based on these data that the dimers form chemical bonds with a single, shared Ag adatom upon adsorption, as observed for other pi orbital dominated aromatic molecules such as PTCDA. Formation of a reactive layer has significant implications for the orbital alignment at the interface. We have therefore probed the properties of the 2D ordered layer and the reacted layers using a combination of current-distance and image-potential state spectroscopy. The interpretation of these results will be presented in conjunction with the first-principles calculations of the respective structures, and correlated with the induced density of interface states (IDIS) model for orbital alignment at metal-molecule interface.

This research was conducted at the Center for Nanophase Materials Sciences, sponsored at the Oak Ridge National Laboratory by the Division of User Facilities, U.S. Department of Energy.

11:40am **NS+AS+SS+SP-WeM12 Subpicosecond-pulse Photoinduced Chemistry on Nanoscale Palladium Model Catalyst Surfaces**, *A. Bhattacharya*, Brookhaven National Laboratory, *R. Palomino, J.C. Lofaro*, Stony Brook University, *H. Park, M.G. White, N. Camillone*, Brookhaven National Laboratory

To date, time-resolved investigations of surface chemical reaction dynamics have almost exclusively been conducted on metal single crystals. However, current and proposed catalysts and photocatalysts generally consist of nanometer-scale metal particles supported on metal oxides. To conduct time-resolved investigations of the surface chemical dynamics of such systems we have synthesized and characterized arrays of palladium nanoparticles (approximately 4 to 10 nm in diameter) supported on clean rutile TiO₂(110). We will present our synthetic approach and the results of chemical and morphological characterization and thermal chemistry experiments on these arrays. We will also discuss the results of subpicosecond-pulse photoinduced desorption of molecular oxygen and carbon monoxide, as well as the photoinduced bimolecular reaction between adsorbed atomic oxygen and carbon monoxide. Comparisons to the same reactions on single crystal Pd(111) surfaces will be made, and the unique features of the chemistry and dynamics at the nanoscale highlighted.

Scanning Probe Microscopy Focus Topic

Room: 16 - Session

SP+AS+BI+ET+MI+NM+NS+SS+TF-WeM

Probe-Sample Interactions, Nano-Manipulation and Fabrication

Moderator: S. Allen, The University of Nottingham, UK, A.-P. Li, Oak Ridge National Laboratory

8:20am **SP+AS+BI+ET+MI+NM+NS+SS+TF-WeM2 Controlled Coupling of Silicon Atomic Quantum Dots at Room Temperature: A Basis for Atomic Electronics?**, *R.A. Wolkow*, University of Alberta and The National Institute for Nanotechnology, Canada, *J. Pitters*, The National Institute for Nanotechnology, Canada, *G. DiLabio, M. Taucer, P. Piva, L. Livadaru*, University of Alberta and The National Institute for Nanotechnology, Canada **INVITED**

Quantum dots are small entities, typically consisting of just a few thousands atoms, that in some ways act like a single atom. The constituent atoms in a dot coalesce their electronic properties to exhibit fairly simple and potentially very useful properties. It turns out that collectives of dots exhibit joint electronic properties of yet more interest. Unfortunately, though extremely small, the finite size of typical quantum dots puts a limit on how close multiple dots can be placed, and that in turn limits how strong the coupling between dots can be. Because inter-dot coupling is weak, properties of interest are only manifest at very low temperatures (milliKelvin). In this work the ultimate small quantum dot is described – we replace an “artificial atom” with a true atom - with great benefit.

It is demonstrated that the zero-dimensional character of the silicon atom dangling bond (DB) state allows controlled formation and occupation of a new form of quantum dot assemblies - at room temperature. Coulomb repulsion causes DBs separated by less than ~2 nm to experience reduced localized charge. The unoccupied states so created allow a previously unobserved electron tunnel-coupling of DBs, evidenced by a pronounced change in the time-averaged view recorded by scanning tunneling microscopy. It is shown that fabrication geometry determines net electron occupation and tunnel-coupling strength within multi-DB ensembles and moreover that electrostatic separation of degenerate states allows controlled electron occupation within an ensemble.

Some speculation on the viability of a new “atomic electronics” based upon these results will be offered.

9:00am **SP+AS+BI+ET+MI+NM+NS+SS+TF-WeM4 Atomic Forces and Energy Dissipation of a Bi-Stable Molecular Junction**, *C. Lotze*, Freie Universität Berlin, Germany, *M. Corso, K.J. Franke, F.V. Oppen, J.I. Pascual*, Freie Universität Berlin, Germany

Tuning Fork based dynamic STM/AFM is a well established method combining the advantages of scanning tunneling and dynamic force microscopy. Using tuning forks with high stiffness, stable measurements with small amplitudes, below 1 Å can be performed. In this way, conductance and frequency shift measurements of molecular junction can be obtained simultaneously [1] with intramolecular resolution [2].

One of the most intriguing aspects of molecular junctions relates to the effect of structural bi-stabilities to the properties of the junction. These lead, for example, to conductance fluctuations, telegraph noise and the possibility to switch the electrical transport through the junction.

In this presentation, we characterize a model bi-stable molecular system using dynamic force spectroscopy. The effect of current-induced stochastic fluctuations of conductance are correlated with fluctuations in force. In our experiment we identified the last from both, frequency shifts and energy dissipation measurements, picturing a regime in which electrical transport and mechanical motion are coupled.

[1] N. Fournier *et. al*, PhysRevB 84, 035435 (2011),

[2] L. Gross *et. al*, Science 324, 1428 (2009)

9:20am **SP+AS+BI+ET+MI+NM+NS+SS+TF-WeM5 Acetylene on Cu(111): Imaging a Molecular Pattern with a Constantly Rearranging Tip**, *Y. Zhu, J. Wyrick, K.D. Cohen, K. Magnone, C. Holzke, D. Salib, Q. Ma, D.Z. Sun, L. Bartels*, University of California Riverside

Abstract: Using variable temperature STM and DFT simulation, we identify the phases of acetylene adsorbed on the Cu(111) surface. Depending on the coverage, a diffraction-derived surface pattern of acetylene on Cu(111) is validated by STM. The modification of the STM image transfer function

through the adsorption of an acetylene molecule onto the tip apex is taken into account. In this case, the images of acetylene patterns on Cu(111) also include direct evidence of the **rotational orientation and dynamics of the acetylene species attached to the tip apex**. DFT modeling of acetylene/Cu(111) reveals that the molecular orientation and separation is governed by a balance of repulsive interactions associated with stress induced in the top surface layer and attractive interactions mediated by the electronic structure of the substrate. Computationally modeling of the substrate with 3 layers obtains the periodicity of the intermolecular interaction that provides a theoretical underpinning for the experimentally observed molecular arrangement.

9:40am **SP+AS+BI+ET+MI+NM+NS+SS+TF-WeM6 Atomic Scale Imaging and Electronic Structure of Trimethylaluminum Deposition on III-V Semiconductor (110) Surfaces, T.J. Kent*, M. Edmonds, E. Chagarov, A.C. Kummel**, University of California San Diego

Silicon based metal oxide semiconductor field effect transistors (Si-MOSFETs) are quickly approaching their theoretical performance limits, as a result many semiconductors are being explored as an alternative channel material for use in MOSFETs. III-V semiconductors are an appealing alternative to Si because of their higher electron mobilities. The limiting factor in III-V based MOSFET performance is defect states which prevent effective modulation of the Fermi level. The InGaAs (001) As-rich (2x4) surface contains two types of unit cells: ideal unit cells with double As-dimers and defect unit cells with single As-Dimers. The missing As-dimer unit cells, which comprise ~50% of the surface, are believed to cause electronic defect states at the semiconductor-oxide interface, specifically at the conduction band edge of the semiconductor. *In-situ* scanning tunneling microscopy and spectroscopy (STM/STS) and density function theory (DFT) modeling show that TMA readily passivates the As-As dimers in the ideal unit cell but the missing InGaAs(001)-2x4 may not be fully passivated by TMA. To improve the electronic structure of the interface, the sidewalls of the finFETs on InGaAs(001) can be fabricated along the (110) direction. The (110) surface contains only buckled III-V heterodimers in which the lower group III atom is sp² hybridized with an empty dangling bond and the upper group V atom is sp³ hybridized with a full dangling bond. This results in an electrically unpinned surface.

To investigate the benefits of using a (110) surface as a channel material, the atomic and electronic structure of the ALD precursor trimethylaluminum (TMA) monolayer deposited on III-V (110) surfaces has been studied using *in-situ* STM and STS. Both GaAs and InGaAs samples were studied. GaAs wafers were obtained from Wafertech with a Si doping concentration of 4x10¹⁸/cm³. The (001) samples were cleaved *in-situ* to expose the (110) surface. Samples were transferred to the STM chamber (base pressure 1x10⁻¹¹ torr) where the atomic bonding structure of the precursor monolayer unit cell was determined. STS, which probes the local density of states (LDOS), was used to determine Fermi level pinning. A model of TMA chemisorption was developed in which TMA chemisorbs between adjacent As atoms on the surface, giving a highly ordered monolayer with a high nucleation density which could allow for aggressive effective oxide thickness (EOT) scaling.

10:40am **SP+AS+BI+ET+MI+NM+NS+SS+TF-WeM9 A New Experimental Method to Determine the Torsional Spring Constants of Microcantilevers, G. Haehner, J.D. Parkin**, University of St Andrews, UK
Cantilever based technologies have seen an ever increasing level of interest since the atomic force microscope (AFM) was introduced more than two decades ago. Recent developments employ microcantilevers as stand-alone sensors by exploiting the dependence of their oscillating properties on external parameters such as adsorbed mass [1], or the density and the viscosity of a liquid environment [2,3]. They are also a key part in many microelectromechanical systems (MEMS) [4]. In order to quantify measurements performed with microcantilevers their stiffness or spring constants have to be known. Following calibration of the spring constants a change in oscillation behavior can be quantitatively related to physical parameters that are probed. The torsional modes of oscillation have attracted significant attention due to their high sensitivity towards lateral and friction forces, and recent developments in torsional-tapping AFM technology [5]. However, the methods available to determine the torsional spring constants experimentally are in general not simple, not very reliable, or risk damage to the cantilever [6].

We demonstrate a new method to determine the spring constants of the torsional modes of microcantilevers experimentally with high accuracy and precision. The method is fast, non-destructive and non-invasive. It is based on measuring the change in the resonance frequencies of the torsional

modes as a function of the fluid flow escaping from a microchannel. Results for rectangular cantilevers will be presented and compared to results obtained with other methods [7].

- [1] J. D. Parkin and G. Hähner, Rev. Sci. Instrum. **82** (3), 035108 (2011).
- [2] N. McLoughlin, S. L. Lee, and G. Hähner, Appl. Phys. Lett. **89** (18), 184106 (2006).
- [3] N. McLoughlin, S. L. Lee, and G. Hähner, Lab Chip, 1057 (2007).
- [4] S. Beeby, G. Ensell, N. Kraft, and N. White, *MEMS Mechanical Sensors*. (Artech House London, 2004).
- [5] O. Sahin and N. Erina, Nanotechnology **19** (44), 445717 (2008).
- [6] M. Munz, Journal of Physics D-Applied Physics **43** (6), 063001 (2010).
- [7] C. P. Green, H. Lioe, J. P. Cleveland, R. Proksch, P. Mulvaney, and J. E. Sader, Rev. Sci. Instrum. **75** (6), 1988 (2004).

11:00am **SP+AS+BI+ET+MI+NM+NS+SS+TF-WeM10 A Torsional Device for Easy, Accurate and Traceable Force Calibration of AFM Cantilevers, J.F. Portoles, P.J. Cumpson**, Newcastle University, UK

Accurate measurement of biologically-relevant forces in the range of pN to µN is an important problem in nanoscience.

A number of force probe techniques have been applied in recent years. The most popular is the Atomic Force Microscope (AFM). Accuracy of force measurement relies on calibration of the probe stiffness which has led to the development of many calibration methods[1], particularly for AFM microcantilevers. However these methods typically exhibit uncertainties of at best 15% to 20% and are often very time consuming. Dependency on material properties and cantilever geometry further complicate their application and take extra operator time. In contrast, one rapid and straightforward method involves the use of reference cantilevers (the "cantilever-on-cantilever" method) or MEMS reference devices. This approach requires that a calibrated reference device is available, but it has been shown to be effective in providing measurement traceability[2].

The main remaining difficulty of this approach for typical users is the positional uncertainty of the tip on the reference device, which can introduce calibration uncertainties of up to around 6%. Here we present a new reference device based on a torsional spring of relatively large dimensions compared to the typical AFM cantilever and demonstrate how it is calibrated. This method has the potential to calibrate the reference device traceably[3] to the SI with a 1% accuracy by applying techniques typically used for the characterisation of micromechanical devices. The large dimensions of the device reduce the positional uncertainty below 1% and simultaneously allow the use of the device as an effective reference array with different reference stiffnesses at different positions ranging from 0.090 N/m to 4.5 N/m

- [1] P J Cumpson, C A Clifford, J F Portolés, J E Johnstone, M Munz Cantilever Spring-Constant Calibration in Atomic Force Microscopy, pp289-314 in Volume VIII of Applied Scanning Probe Methods, Ed. B Bhushan and H Fuchs (Springer, New York, 2009)
- [2] P J Cumpson PJ, J Hedley, Nanotechnology 14 (2003) pp. 1279-1288
- [3] J F Portolés, P J Cumpson, J Hedley, S Allen, P M Williams & S J B Tendler, Journal of Experimental Nanoscience 1 (2006) pp51-62.

11:20am **SP+AS+BI+ET+MI+NM+NS+SS+TF-WeM11 Nanoscale Surface Assembly by Single-Molecule Cut-and-Paste, H.E. Gaub**, Ludwig-Maximilians Universität, Germany

INVITED
Bottom up assembly of functional molecular ensembles with novel properties emerging from composition and arrangement of its constituents is a prime goal of nanotechnology. With the development of Single-Molecule Cut-and-Paste (SMC&P) we provided a platform technology for the assembly of biomolecules at surfaces. It combines the Å-positioning precision of the AFM with the selectivity of DNA hybridization to pick individual molecules from a depot chip and allows to arrange them on a construction site one by one. An overview on different applications of this technology will be given in this talk. One recent example demonstrates the functional of receptors for small molecules. By SMC&P we assembled binding sites for malachite green in a molecule-by-molecule assembly process from the two halves of a split aptamer. We show that only a perfectly joined binding site immobilizes the fluorophore and enhances the fluorescence quantum yield by several orders of magnitude. To corroborate the robustness of this approach we produced a micron-sized structure consisting of more than 500 reconstituted binding sites. To the best of our knowledge this is the first demonstration of a one by one bottom up functional bio-molecular assembly. Figure included in supplemental document. S. Kufer, Puchner E. M., Gump H., Liedel T. & H. E. Gaub *Science* (2008), Vol 319, p 594-S. Kufer, Strackham, M., Stahl S.W., Gump H., Puchner E. M. & H. E. Gaub *Nature Nanotechnology* (2009), Vol 4, p 45-M. Erdmann, R. David. A.N. Fornof, and H. E. Gaub, *Nature*

* ASSD Student Award Finalist

Surface Science

Room: 22 - Session SS+OX-WeM

Synthesis and Characterization of Oxides

Moderator: J.M. Millunchick, University of Michigan

8:00am SS+OX-WeM1 Structure and Dynamics of Oxide Surfaces and Interfaces, X. Pan, University of Michigan INVITED

Ferroelectric materials are characterized by a spontaneous electric polarization that can be reoriented between different orientations by an applied electric field. The ability to form and manipulate domains with different polarization orientations at the nanometer scale is key to the utility of ferroelectric materials for devices such as nonvolatile memories. The ferroelectric switching occurs through the nucleation and growth of favorably oriented domains and is strongly mediated by defects and interfaces. Thus, it is critical to understand how the ferroelectric domain forms, grows, and interacts with defects. In this talk I will present the nanoscale ferroelectric switching of BiFeO_3 and $\text{PbZr}_{0.2}\text{Ti}_{0.8}\text{O}_3$ thin films under an applied electric field using *in situ* transmission electron microscopy with atomic resolution. We follow the kinetics and dynamics of ferroelectric switching at millisecond temporal and subangstrom spatial resolution. We observed localized nucleation events at the electrode interface, domain wall pinning on point defects, the formation of ferroelectric domains localized to the ferroelectric/electrode interface, and domain wall pinning by dislocations. We also find that in writing nanosized domains the domain wall itself can drive backswitching. It was observed that the localized 180° polarization switching in $\text{PbZr}_{0.2}\text{Ti}_{0.8}\text{O}_3$ thin films initially forms domain walls along unstable planes. After removal of the external field, they tend to relax to low energy orientations. In sufficiently small domains this process results in complete backswitching. Our results suggest that even thermodynamically favored domain orientations are still subject to retention loss, which must be mitigated by overcoming a critical domain size.

8:40am SS+OX-WeM3 Capturing Ion-Solid Interactions with MOS Structures, R. Shyam, E.S. Srinadhu, S. Chambers, J.E. Harriss, W.R. Harrell, C.E. Sosolik, Clemson University

We have fabricated metal-oxide-semiconductor (MOS) devices for a study of implantation rates and damage resulting from low energy ion-solid impacts. Specifically, we seek to capture ion irradiation effects on oxides by exposing as-grown SiO_2 layers (50 nm to 200 nm) to incident beams of singly-charged alkali ions with energies in the range of 100 eV to 5 keV. The oxide is analyzed post exposure by encapsulating the irradiated region under a top metallic contact or within a finished MOS device. Characterization of the resulting ion-modified MOS device involves the standard techniques of room temperature and bias-temperature stress capacitance-voltage (C-V) measurements. The C-V results reveal alkali ion-induced changes in the flatband voltage and slope of C-V of irradiated devices which can be used to extract and delineate between implantation probabilities and irradiation effects of the ions. Biased C-V measurements are utilized to confirm the concentration or dosage of ions in the oxide. A triangular voltage sweep (TVS) measurement at elevated temperatures also reveals the total ionic space charge in the oxide and is used to extract mobility for the ions as they pass through the damaged oxide. Our C-V data show changes in flatband voltage which are greater than those expected for mobile charges present at the range calculated by SRIM which implies that stoichiometry, morphological and chemical changes in the SiO_2 layer are introduced by the ion impacts.

9:00am SS+OX-WeM4 Synthesis and Characterization of Yttrium Aluminum Garnet and Lanthanum Zirconate Particles, R.R. Harl*, S.L. Gollub, G. Walker, B.R. Rogers, Vanderbilt University

Rare-earth doped yttrium aluminum garnet (YAG) and lanthanum zirconate (LZO) are luminescent ceramics that have been used in TV's, LED's, metal oxide transistors, and as laser sources. These materials are thermally and chemically stable. Recent work at Vanderbilt by the Walker and Rogers research groups has shown that the emitted spectrum of proton irradiated LZO particles differs from that of non-irradiated particles, suggesting these materials may be used as passive radiation exposure indicators.

We will discuss the combustion synthesis and characterization of YAG and LZO particles. Combustion synthesis involves heating a mixture of metal

nitrate and a fuel until the mixture ignites. If the proper conditions are used, the energy released by the combustion is sufficient to form polycrystalline material. The type and amount of fuel used in the synthesis affect the amount of gaseous by-products produced and flame temperature achieved during a reaction, both of which affect the crystallite size formed. The organic fuels included in this study are urea and glycine with adiabatic flame temperatures 1780°C and 1210°C , respectively. Urea's higher flame temperature makes this fuel attractive for combustion syntheses. However, urea shows signs of degradation beginning around 120°C , well below its ignition temperature. Glycine does not appear to degrade until approximately 230°C much closer to its ignition temperature. The trade-off between degradation and adiabatic flame temperature suggests the temperature ramp rate used will significantly affect the performance of combustion syntheses carried out with these fuels.

We will present results of detailed thermogravimetric analysis and differential scanning calorimetry (TGA/DSC) experiments used to study the effects of heating rate on the combustion process and on the characteristics of the material formed. TGA/DSC-determined heats of combustion and heat capacities of the reactants and products will also be presented.

Characterization results of powders made using conditions determined by the TGA/DSC experiments will also be presented. X-ray photoelectron spectroscopy (XPS) was used to determine chemical bonding information. Rutherford backscattering spectroscopy (RBS) was used to provide quantitative elemental composition of the material. X-ray diffraction (XRD) was used to determine the crystallinity of the material and to estimate crystallite sizes. Photoluminescence spectroscopy (PL) was used to characterize the materials' emission spectra.

9:20am SS+OX-WeM5 X-ray Linear Dichroism of Epitaxial (Fe,N) Co-Doped Rutile TiO_2 Thin Films, T.C. Kaspar, Pacific Northwest National Lab, A. Ney, Univ. of Duisburg-Essen, Germany, A.N. Mangham, Pacific Northwest National Lab, S.M. Heald, Advanced Photon Source, Argonne National Lab, Y. Joly, Institut Néel, CNRS et Univ. Joseph Fourier, France, V. Ney, Univ. of Duisburg-Essen, Germany, F. Wilhelm, A. Rogalev, F. Yakou, European Synchrotron Radiation Facility, S.A. Chambers, Pacific Northwest National Lab

Efficient visible light photocatalysis could revolutionize hydrogen production, chemical synthesis, and pollution mitigation. Binary oxides such as TiO_2 have received much attention for these applications since they are stable under aqueous and oxidizing conditions, and show promise as ultraviolet-light photocatalysts. However, to operate in the visible portion of the solar spectrum, the wide bandgap of these oxides (~ 3 eV for rutile TiO_2) must be reduced. Anion doping of anatase TiO_2 has been widely explored, and shows some promise. However, in nanoparticles and fine powders, it can be difficult to determine the structural and electronic behavior of N dopants. Homoepitaxial $\text{Fe}:\text{TiO}_2$ and $(\text{Fe},\text{N}):\text{TiO}_2$ thin films deposited on rutile $\text{TiO}_2(110)$ were investigated by x-ray absorption spectroscopy (XAS) and associated theoretical simulations to elucidate the detailed structure of the doped materials. Co-doping with N was found to increase the extent of Fe incorporation into the rutile lattice. X-ray absorption near edge spectroscopy (XANES) spectra were collected at the Ti L-edge, Fe L-edge, O K-edge, N K-edge, and Ti K-edge. No evidence of structural disorder associated with a high concentration of oxygen vacancies was observed. Substitution of Fe for Ti could not be confirmed, although secondary phases such as Fe_2O_3 and metallic Fe could be ruled out. The similarity of the N K-edge spectra to O, and the presence of a strong x-ray linear dichroism (XLD) signal for the N K-edge, indicates that N is substitutional for O in the rutile lattice, and is not present as a secondary phase such as TiN . Simulations of the XANES spectra qualitatively confirm substitution, although N appears to be present in more than one local environment. Although optical absorption spectra confirm that substitutional N redshifts optical bandgap of Fe-doped rutile into the visible region, the film surfaces are photochemically inert with respect to hole-mediated decomposition of adsorbed trimethyl acetate.

9:40am SS+OX-WeM6 Unified Picture of the Excess Electron Distribution at the $\text{TiO}_2(110)$ Surface, P. Krueger, Institut Carnot de Bourgogne, France, J. Jupille, Institut des Nanosciences de Paris, France, S. Bourgeois, B. Domenichini, Institut Carnot de Bourgogne, France, A. Verdini, L. Floreano, A. Morgante, Laboratorio TASC, Italy

Titanium dioxide, an inert insulator in stoichiometric form, can be easily reduced into an n-type semiconductor TiO_{2-x} with the many electronic, photocatalytic and chemical properties that make the material of huge technological relevance. Formally associated with $\text{Ti}^{4+} + e^- \rightarrow \text{Ti}^{3+}$, the reduction of titania results in excess electrons (EE) that populate localized Ti 3d band gap states. Puzzling issues are the surface or subsurface distribution of EE and the lattice or interstitial nature (Ti_{int}) of the Ti^{3+} ions. Despite a number of experimental and theoretical studies, the reduced archetypal $\text{TiO}_2(110)$ has not been unambiguously pictured yet. Regarding the location of Ti^{3+} ions, density functional theory (DFT), DFT + U scheme

* Morton S. Traum Award Finalist

and DFT-Hartree-Fock hybrid functionals (the two latter including a better account of self interaction corrections) are far from consensus. EE that are suggested to be trapped either on sixfold (Ti1) and fivefold (Ti2) coordinated surface Ti, or on subsurface beneath Ti1 or beneath Ti2. In such context, the unique capability of resonant photoelectron diffraction (RPED) to map out the spatial distribution of Ti 3d gap states was previously demonstrated in the study of a TiO₂(110) surface involving vacancies in bridging oxygen rows (O_b-vac) [1]. However, our conclusion that EE mostly occupy subsurface Ti sites was later challenged by the suggestion that Ti_{int} atoms play a key role in the formation of EE [2,3]. This has prompted us to analyse the Na-covered TiO₂(110) surface on which Na adatoms are predicted to produce similar EE as by direct injection of electrons [4], while the formation of Ti_{int} is not expected.

The pivotal observation was that the Na/TiO₂ RPED pattern [4] was almost perfectly similar to the O_b-vac RPED pattern [1]. Data were fitted on the basis of the location of the Ti³⁺ ions on the Ti lattice sites. Indeed, attempts to model EE on Ti_{int} failed. A unified model of the reduced TiO₂(110) surface emerges, with EE located on subsurface beneath Ti2 > second subsurface beneath Ti1 > Ti1 [4] (See supplemental document). As shown by the qualitative agreement of the present findings with DFT approaches [5,6], the charge distribution of the Ti 3d states is dictated by electrostatics. It is essentially an intrinsic property of the titania surface that is independent on the way EE are created.

[1] Krueger et al. Phys. Rev. Lett. 100 (2008) 055501.

[2] Wendt et al., Science 320 (2008) 1755.

[3] Papageorgiou et al., Proc. Natl. Acad. Sci. U.S.A. 107 (2010) 2391.

[4] Krueger et al. Phys. Rev. Lett. 108 (2012) 126803.

[5] Albaret et al., Phys. Rev. B 65 (2001) 035402.

[6] Deskins et al., J. Phys. Chem. C 113 (2009) 14583.

10:40am **SS+OX-WeM9 XPS Satellite Structure and Covalent Bonding**, P.S. Bagus, University of North Texas, E.S. Ilton, Pacific Northwest National Laboratory, C.J. Nelin, Consultant

The satellites in X-Ray photoemission spectroscopy, XPS, especially for ionic compounds, are an important part of the spectra [1, 2] and may provide information about the electronic structure. For uranium oxides, they allow the oxidation state of the U cations to be determined. [2] It would be useful to establish and to understand how the satellite intensity may be related to the extent of covalent bonding in an oxide or other ionic material. It is often believed that the intensity lost from the main XPS peaks to satellites is directly related to the covalent bonding, with greater covalent bonding leading to greater losses to satellites. We show that this relationship is not rigorously correct. A more correct relationship is between satellite intensity and the difference of the degrees of covalency in the initial, unionized, state and the final, core-hole states with larger differences leading to larger losses to satellites. Furthermore, the final state covalency is less sensitive to the environment than is the initial state covalency since the bonding in the final state is more appropriate to that for an equivalent, Z+1, impurity atom representing the core-ionized atom. [3] We investigate the extent to which the effects of covalency can be tuned by comparing the Ni 2p XPS between NiO and Ni impurities in MgO.

1. P. S. Bagus, et al., Chem. Phys. Lett. **487**, 237 (2010).

2. E. S. Ilton and P. S. Bagus, Surf. Interface Anal. **43**, 1549 (2011).

3. W. L. Jolly and D. N. Hendrickson, J. Am. Chem. Soc. **92**, 1863 (1970).

11:00am **SS+OX-WeM10 Surface of BaTiO₃ (001): STM and STS Study**, E. Morales, J. Martinez, A.M. Rappe, D.A. Bonnell, University of Pennsylvania

BaTiO₃ is a versatile material that finds applications in sensors and electrooptical devices. Interactions start at the very surface, thus it is necessary to understand at a fundamental level its geometrical and electronic structure. Ferroelectricity is a key property that provides unique opportunities to explore molecular adsorption at a surface and allows investigation of chemical interactions as well. Interaction with gaseous species can be performed in-situ in "as-received" and poled crystals by controlling the poling voltage at the surface. Recent studies with macroscopic measurements show that polarization indeed affects molecular adsorption but mechanisms are not yet understood. Here we present scanning tunneling microscopy (STM) and scanning tunneling spectroscopy (STS) of atomically resolved reconstructions on BaTiO₃ (001) surfaces, ($\sqrt{5} \times \sqrt{5}$)R26.6^o. A comparison of electronic structure determined by STS with theoretical calculations shows that the surface that is Ti terminated. In this and other reconstructions Ti-ad atoms create filled and empty states that are imaged in STM. The interactions of reconstructed surfaces with H₂O is examined with atomic resolution. This is the first atomic scale observation of molecular adsorption on a ferroelectric surface.

11:20am **SS+OX-WeM11 Synthesis and Characterization of White Light Emitting Ca_xSr_{1-x}Al₂O₄:Tb³⁺,Eu³⁺ Phosphor**, S.K. Shaat, H.C. Swart, O.M. Ntwaeaborwa, University of the Free State, South Africa

Today, many researchers are making efforts to develop white light emitting phosphors that can be used in solid state lighting applications such as phosphor lamps and light emitting diodes. Aluminates with a general formula MA₂O₄ (M = Ba, Ca, Mg, Sr) have emerged as preferred hosts for divalent (Mn²⁺ and Eu²⁺) and trivalent (Ce³⁺, Tb³⁺, Dy³⁺) ions to prepare such phosphors. We have prepared a potential white light emitting Ca_xSr_{1-x}Al₂O₄:Tb³⁺,Eu³⁺ (x = 0, 0.3, 0.7, 1) phosphor by combustion method and we are evaluating it for application in solid state lighting. Depending on the concentration of Ca²⁺ or Sr²⁺, the X-ray diffraction data showed that monoclinic structures of either CaAl₂O₄ or SrAl₂O₄ were crystallized and the stretching modes of Sr-Al-O and Ca-Al-O bonds were confirmed from the Fourier transform infrared spectroscopy data. The chemical compositions and electronic states of each element of the Ca_xSr_{1-x}Al₂O₄:Tb³⁺,Eu³⁺ phosphor were determined using X-ray photoelectron spectroscopy. White photoluminescent was observed when Ca_xSr_{1-x}Al₂O₄:Tb³⁺,Eu³⁺ was excited at 227 nm using a monochromatized xenon lamp. This was a result of the combination of blue and green emissions from Tb³⁺ and red emission from Eu³⁺. It is likely that Tb³⁺ and Eu³⁺ ions were simultaneously excited by a single photon of sufficiently high energy absorbed in Ca_xSr_{1-x}Al₂O₄ host.

11:40am **SS+OX-WeM12 A Novel 2-D Cu-Tungstate (CuWO₃) Phase on Cu(110)**, F.P. Netzer, M. Denk, D. Kuhnness, M. Wagner, S. Surnev, University of Graz, Austria, F.R. Negreiros, L. Sementa, G. Barcaro, A. Fortunelli, CNR-IPCF Pisa, Italy

We explore the feasibility to fabricate W-oxide nanostructures on metal surfaces via self-assembly and condensation of (WO₃)₃ clusters, deposited directly from the gas phase: here we report the formation of a novel two-dimensional Cu-tungstate CuWO_x phase on Cu(110). A beam of (WO₃)₃ cluster molecules, formed by sublimation of WO₃ powder at ~900-1000°C in a thermal evaporator, has been directed onto a Cu(110)2x1-O surface oxide at low temperature and the surface has been annealed subsequently at 600 K. At low temperature (< 15 K) the (WO₃)₃ clusters adsorb in intact molecular form, albeit in a somewhat distorted cluster geometry [1]. Upon heating to 600K, the (WO₃)₃ molecules dissociate and react with the Cu-O(2x1) surface oxide, forming a wetting monolayer with a well ordered incommensurate structure. The latter has been structurally characterized by high-resolution STM imaging and LEED. The chemical nature and electronic structure of this novel 2-D W-O-Cu layer has been investigated by high-resolution XPS core level spectroscopy, NEXAFS, and valence band spectra. The unusually sharp W 4f core level spectra, the specific NEXAFS fingerprint and the evolution of the valence band all suggest that this 2-D W surface oxide is of a Cu-tungstate CuWO_x type. Density functional calculations are in progress to help elucidating the physical and chemical nature of this unusual surface oxide phase.

Work supported by the ERC Advanced Grant SEPON

[1] M. Wagner, S. Surnev, M.G. Ramsey, G. Barcaro, L. Sementa, F.R. Negreiros, A. Fortunelli, Z. Dohnalek, F.P. Netzer, J. Phys. Chem. C **115** (2011) 23480

Surface Science

Room: 21 - Session SS-WeM

Chemisorption on Metallic Surfaces

Moderator: C.H. Sykes, Tufts University

8:00am **SS-WeM1 An Atomic-scale Study of the Adsorption, Assembly and Reactivity of Methanol with Model Cu, O/Cu and Pd/Cu Alloy Surfaces with STM, TPD and XPS**, T. Lawton, M. Boucher, A. Baber, G. Kyriakou, C.H. Sykes, Tufts University

Hydrogen is green fuel capable of producing electricity. Methanol is a promising hydrogen storage molecule with a high hydrogen-to-carbon ratio (4:1). My research examines methanol oxidation and decomposition on model catalysts via variable temperature scanning tunneling microscopy (VT-STM) and temperature-programmed reaction (TPR).

Methanol desorption on Cu(111) was studied from 130 K (multilayer desorption) to 165 K (monolayer desorption) with STM. Analysis of STM images reveals several structures that are governed by hydrogen-bonding interactions. From the STM images, hexamers are the most thermodynamically stable structure on Cu(111). Hydroxyl-proton localization on the hexamers leads to two enantiomers.

The Cu surface was chemically modified in two ways to alter methanol reactivity. First, the effect of oxygen at various temperatures on Cu(111)

was studied with STM. STM and XPS of a Cu(111) surface pre-adsorbed with oxygen after exposure to methanol show methoxy forms at the interface of the oxide-like domains and bare Cu.

The second avenue was a Cu-based bimetallic alloy containing small amounts of Pd. The TPD studies on model Pd/Cu catalysts interestingly reveal partial decomposition of methanol to formaldehyde and hydrogen. STM images acquired reveal that at temperatures above MeOH desorption, molecules only occupy sites near Pd atoms, suggesting these are the active sites.

8:20am **SS-WeM2 Imaging the Role of Ligand Groups in Surface Coordination Chemistry/Networks: Cyano- vs. Isocyano Groups**, *L. Bartels, M. Luo, S. Bobek, K.D. Cohen, C. Wang, R. Hooley*, University of California Riverside

We use STM to investigate the adsorption, self assembly and metal-coordination of isocyano- and cyano-based aromatic species on Cu (111). Despite their structural similarity, cyano and isocyano groups are chemically quite different. We investigate the effect of this distinction on the structures on the metal coordination structures they form and on the resultant geometric and electronic state of the metal coordination center. In particular we find very different structures for dicyano- and diisocyano-anthracene molecules. While the former generates a network consisting of trigonally coordinated metal centers, the latter generates molecular rows, i.e. more linear arrangement. Cyano- and Isocyano-naphthalene also generate different distributions of coordination compounds on Cu(111). The combination of these studies highlights the impact of the chemical structure of the ligand on the coordination center. Organic ligands are a common tool for affecting activity in homogeneous catalysis. Our study is aimed at exploring the capabilities of lateral coordination in controlling the activity of a surface.

8:40am **SS-WeM3 Chemisorption, Ordering, and Structural Transitions in the Terephthalic Acid Monolayer and Bilayer on Cu(100)**, *S.L. Tait*, Indiana University - Bloomington

The use of small organic molecules to control structure as well as electronic and chemical functionality of a surface is a critical field of surface chemistry. Interest in problems related to bonding, charge transfer and self-assembly of organic species at metal surfaces has grown, in correlation with stronger needs for inexpensive and highly functional organic technologies in energy conversion, sensors, electronics, and other applications. We have studied a prototypical system, terephthalic acid on Cu(100), using a set of complementary analysis tools to develop a complete picture of the chemisorption and structural transitions in this dynamic system, which is of key importance for structural control and organic-to-metal interface design. Scanning tunneling microscopy has been used to achieve molecular resolution structural characterization of the first layer structural transitions and of the second layer structures. High-resolution electron energy loss spectroscopy reveals orientation of the molecule in each layer and lends insight into the bonding interaction with the surface. X-ray standing wave spectroscopy and density functional theory calculations show a strong chemical bond to the surface and indicate that the apparent attractive interaction between molecules is likely due to a substrate mediated interaction, sufficient to overcome any electrostatic repulsion between the negatively charged carboxylate groups on the molecules. This system has also laid the ground work for related advances in using terephthalic acid layers and related molecules for coordination bonded structures, some of which show high levels of chemical selectivity, and for ionically bonded structures. These results provide general insight in the development of self-assembled organic thin films at surfaces, especially with regard to the nature of the metal/organic interface and growth transitions to obtain a second layer that bridges substrate commensurability and a more bulk-like structure, key issues in organic thin film design.

9:00am **SS-WeM4 Attachment and Nanoscale Patterning of Alkyne Groups on Gold via Non-thermal Pathways**, *Q. Li*, Oak Ridge National Laboratory, *C.B. Han*, North Carolina State University, *M. Fuentes-Cabrera, H. Terrones, B.G. Sumpter, W.C. Lu*, Oak Ridge National Laboratory, *J. Bernholc*, North Carolina State University, *Z. Gai, A.P. Baddorf, P. Maksymovych, M.H. Pan*, Oak Ridge National Laboratory

Self-assembled monolayers are the basis for molecular nanodevices, flexible surface functionalization and dip-pen nanolithography. Yet self-assembled monolayers are typically created by a rather inefficient process involving thermally driven tethering reactions of precursor molecules to a metal surface, followed by a slow and defect-prone molecular reorganization. Here we demonstrate a non-thermal control over the self-assembly of phenylacetylene on gold that produces previously unachievable well-ordered three-dimensional monolayers, where the molecules are attached directly through the alkyne group. While thermal excitation can only desorb the parent molecule due to prohibitively high activation barriers

for attachment, localized injection of hot electrons or holes not only overcomes this problem, but also enables an unprecedented control over subsequent ordering of attached molecules on the surface, including a nanoscale control over the size and shape of the self-assembly, defect structures and the reversible process between flatlying and upright molecular configuration from single molecular level to mesoscopic scale. This work thus demonstrates the feasibility of non-thermal reaction pathways that may lead to unique and controllable self-assembly in supported molecular layers.

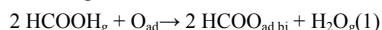
9:20am **SS-WeM5 Molecular Structure of a Mixed NH₃-O₂ Overlayer on Pt(111)**, *Z. Liang*, University of Illinois at Chicago, *H. Kim, Y. Kim*, RIKEN, Japan, *M. Trenary*, University of Illinois at Chicago

The interaction of NH₃ with chemisorbed molecular O₂ on a Pt(111) surface has been studied at the single-molecule level with low temperature scanning tunneling microscopy. Chemisorbed O₂ molecules are found to form an ordered network at high coverages for adsorption temperatures below 50 K. Sites unoccupied by O₂ molecules on Pt(111) appear as holes in the network. Various hole-hole distances among nearest neighbors are observed reflecting variations in the arrangement of O₂ molecules. A hole-hole distance of 0.74 nm is found to be predominant on the surface and is assigned to be the most favorable one as it maintains the 3-fold symmetry of underlying platinum lattice. Ammonia molecules are observed to adsorb in the holes within the ordered network of O₂ molecules, which is also the atop site with respect to the Pt(111) substrate. Further annealing of the ammonia-oxygen overlayer to 400 K results in the formation of a mixed p(2×2) overlayer of N, O and NH. This work provides new insights into the ammonia oxydehydrogenation reaction on platinum surface, which is an important catalytic reaction in the industrial production of nitric acid.

9:40am **SS-WeM6 Enthalpies of Formation of Formate Intermediates Adsorbed on Pt(111) by Microcalorimetry**, *T.L. Silbaugh, E.M. Karp, C.T. Campbell*, University of Washington

Knowing the heats of formation of adsorbed catalytic intermediates is an essential component in gaining the fundamental understanding of reaction mechanisms and the relationships between catalyst structure and activity necessary for rational design of heterogeneous catalysts. The current study utilizes the ultrahigh vacuum technique of single crystal adsorption calorimetry to determine the energetics of adsorbed formate species on Pt(111).

From previous literature, it is known that formic acid dosed on Pt(111) precovered with oxygen adatoms (O_{ad}) at 190K reacts completely to form adsorbed bidentate formate (HCOO_{ad,bi}) and gas phase water (H₂O_g) according to the reaction:



where HCOO_{ad,bi} bonds in a bridging configuration. The heat of Reaction (1) extrapolated to zero coverage was found to be -110 kJ/mol. A simple thermodynamic cycle that uses this and other known adsorption energies provides a heat of formation of HCOO_{ad,bi} of -418 kJ/mol.

Prior studies have shown that submonolayer coverages of formic acid on O-precovered Pt(111) at 130K first produce monodentate formate (HCOO_{ad,mon}) and adsorbed hydroxyl (OH_{ad}) via the reaction:



where HCOO_{ad,mon} forms a single Pt—O bond to the surface. The heat of Reaction (2) extrapolated to zero coverage was found to be -93 kJ/mol, which provides a heat of formation of HCOO_{ad,mon} of -354 kJ/mol. At this same temperature, this monodentate formate converts to bidentate bonding, but at a rate that is slow relative to the 100 ms heat measurement time, so this slower reaction does not complicate thermodynamic measurement of the formation of this monodentate species. Together with our earlier measurements of the heats of formation of -OCH_{3,ad} and -OH_{ad}, these allow us to estimate reaction energies for conversion pathways between formate and methoxy intermediates in Pt catalysis.

10:40am **SS-WeM9 Adsorption Energy of Oxygen on Pt(111): Errors in Calorimetry Values and Consequences for the Enthalpy of Related Hydroxyl Species**, *C.T. Campbell, E.M. Karp*, University of Washington

Beautiful calorimetric measurements of the adsorption enthalpy of O_{2,g} to make 2 O_{ad} on Pt(111) were performed by Fiorin et al. However, we show here that they used a calibration that relied upon a value for the optical reflectivity of Pt(111) that was incorrectly reported in the literature. This error in reflectivity led to a 40% error in the adsorption energies they originally reported. We use here our more accurate reflectivity of 76% to recalibrate their oxygen adsorption enthalpy data and show that it gives nearly identical results to the heats of adsorption below 0.15 ML determined from activation energies for desorption of oxygen from Pt(111) measured with temperature programmed desorption (TPD) by two separate groups (Campbell et al.2 and Parker et al.3). Differences arise above 0.15

ML, but we attribute these to the very low sticking probability of O₂ on Pt(111) (< 0.05) above 0.15ML, which we argue lead to large errors in the adsorption energies measured by calorimetry. Given this, we propose that the most reliable values for the adsorption enthalpy of oxygen on Pt(111) up to ¼ ML are those derived from those TPD experiments, rather than the more recent calorimetry data, except below 0.15 ML where they agree after this calibration correction. The best values are well described by (217-151θ) kJ/mol below ¼ ML, where θ is the O_{ad} coverage in ML (i.e., O_{ad} per Pt surface atom). We further use these corrected adsorption enthalpy data to revise the energetics of hydroxyl species on Pt(111) that we previously measured⁴. This gives revised values for the standard enthalpies of formation of the coadsorbed (DO-D₂O)_{ad} complex and of OD_{ad} on Pt(111) of -511 ± 7 and -210 ± 7 kJ/mol, respectively, and a revised O-Pt bond enthalpy in adsorbed hydroxyl of 248 ± 7 kJ/mol. These three corrected enthalpies are all 16 kJ/mol smaller in absolute value than originally reported.

- (1) Fiorin, V.; Borthwick, D.; King, D. A., *surf. sci.*, 2009, 603, 1360.
- (2) Campbell, C. T.; Ertl, G.; Kuipers, H.; Segner, J., *surf. sci.*, 1981, 107, 220.
- (3) Parker, D. H.; Bartram, M. E.; Koel, B. E., *surf. sci.*, 1989, 217, 489.
- (4) Lew, W.; Crowe, M. C.; Karp, E.; Lytken, O.; Farmer, J. A.; Arnadottir, L.; Schoenbaum, C.; Campbell, C. T., *J. Phys Chem. C.*, 115, 11586.

Work supported by the National Science Foundation.

11:00am **SS-WeM10 Mechanism of Halogenated Solvent Pre-treatment of Polymeric Substrates to Significantly Improve Noble Metal Thin Film Adhesion**, *B.H. Augustine, W.C. Hughes, A.K. Mo, James Madison University, H.M. Meyer, Oak Ridge National Laboratory, T.C. DeVore, James Madison University*

Many emerging microfabrication technologies such as microfluidic devices rely on the deposition of metal features onto polymeric substrates. Au and Pt thin film metallization are particularly important for electrodes, IR reflectors, interconnects and catalytic surfaces in these devices. However, due to the inert nature of Au and Pt, adhesion to polymeric substrates is generally poor. We report on the use of halogenated organic solvents as a pre-treatment onto poly(methyl methacrylate) (PMMA) substrates to improve the adhesion of an array of 121 electron-beam or magnetron sputter deposited 1.5 mm diameter metal dots by up to a factor of five compared to deposition on cleaned PMMA substrates. We have observed improvement by both spin-casting and vapor phase pre-treatment of the PMMA surface. Nearly 90% of the Au dots remain after a standard tape pull-test for samples pre-treated with CHCl₃ compared with only 17% remaining on the untreated samples. The adhesion of CHCl₃, CH₂Cl₂ and CHBr₃ pre-treated samples are also significantly improved compared to remote O₂ plasma pre-treatment (26% adhesion). Atomic force microscopy roughness data shows that this is not due to surface roughening, and we have shown through X-ray photoelectron spectroscopy (XPS) and attenuated total reflection Fourier transform infrared spectroscopy (ATR-FTIR) studies that the halogenated solvent molecules form a Lewis acid-base adduct with the polymer chains leaving a halogen-rich surface. A covalent bond is then formed between the Cr metal adhesion layer and the surface terminated Cl which results in the strong metal adhesion. Molecular modeling has been performed to understand the origin of the enhanced adhesion. DFT calculations are consistent with the presence of adduct formation having a interaction enthalpy of ~35 kJ/mol. The mechanism of improved chemical metal bonding will be discussed.

11:20am **SS-WeM11 HREELS Investigation of Hydrocarbon Dehydrogenation on Oxide-Supported Platinum Nanoparticles**, *M.H.C. Van Spyk, K.A. Perrine, J.C. Hemminger, University of California Irvine*

Factors such as support type and nanoparticle morphology are known to impact catalytic activity, but detailed studies are required to elucidate the effect of nanoparticle size on the mechanism of dehydrogenation over nanoparticles supported on oxides. In this work, high resolution electron energy loss spectroscopy (HREELS) was used to characterize the dehydrogenation of hydrocarbons on platinum nanoparticles supported on an Al₂O₃ film grown by oxidation of a NiAl(110) single crystal. The alumina film is a good representation of the high surface area oxides used as catalyst supports in industry, and the flat surface enables investigation by electron inelastic scattering techniques. The platinum nanoparticles were deposited on a fresh alumina film at cryogenic temperatures, and platinum deposition was monitored by the reduction in elastic peak intensity in the HREEL spectra. Cyclohexane was used as a model hydrocarbon because the dehydrogenation on Pt(111) has been studied extensively and thus provides a good point of comparison for the nanoparticle studies. The HREELS spectra of cyclohexane on Pt(111) show a distinct low frequency peak at 2600 cm⁻¹ which can be monitored to determine the temperature at

which dehydrogenation begins.^{1,2} The HREELS annealing profile from an alumina film does not exhibit cyclohexane adsorption at 170 K, or upon successive annealing. In contrast, the HREEL spectra from platinum nanoparticles on alumina exhibit cyclohexane adsorption at 170 K with the ν_{C-H} stretch energy loss peak observed at 2930 cm⁻¹. Interestingly, HREEL spectra from cyclohexane on platinum nanoparticles do not resemble spectra from cyclohexane on Pt(111). Specifically, the additional ν_{C-H} energy loss peak observed at 2600 cm⁻¹ for cyclohexane adsorbed on Pt(111) is not seen in the case of platinum nanoparticles.^{1,2} In addition, the ν_{C-H} energy loss peak from cyclohexane on platinum nanoparticles does not shift or decrease in intensity upon annealing to room temperature. Our results indicate that cyclohexane dehydrogenates upon adsorption to platinum nanoparticles at 170 K. This dehydrogenation temperature is lower than that on Pt(111), indicating that platinum nanoparticles supported on an alumina film are more catalytically active for the initial stages of dehydrogenation than Pt(111).

1. Land, D. P.; Erley, W.; Ibach, H., HREELS Investigation of the Orientation and Dehydrogenation of Cyclohexane on Pt(111). *Surface Science* **1993**, 289 (3), 237-246.
2. Saeys, M.; Reyniers, M. F.; Neurock, M.; Marin, G. B., Adsorption of cyclohexadiene, cyclohexene and cyclohexane on Pt(111). *Surface Science* **2006**, 600 (16), 3121-3134.

11:40am **SS-WeM12 Scanning Tunneling Microscopy Investigation of the Conversion of Propylene and Butylene to Carbon Clusters on Pt(111)**, *G.F. Sun, S.S. Khan, A.B. De la Ree, J.C. Hemminger, University of California Irvine*

Thermal dehydrogenation of propylene and butylene adsorbed on Pt(111) has been studied under ultra-high vacuum (UHV) conditions

using scanning tunneling microscopy (STM). After heating to 700 K the alkenes dehydrogenated to form flat, uniform sized circular carbon clusters with less than a monolayer coverage. With cycles of continued adsorption and heating, particles grew in number but not in size. The catalytic activity stopped by the third saturation dose, leaving areas of bare Pt. Clusters of propylene and butylene were 12 ± 1.2 Å and 13 ± 1.0 Å in diameter, respectively. Propylene and butylene clusters contain an average of 44 and 51 carbons atoms per cluster, respectively.

Vacuum Technology

Room: 14 - Session VT+AS+SS-WeM

Surface Analysis and Vacuum Manufacturing for Accelerators

Moderator: M.L. Stutzman, Thomas Jefferson National Accelerator Facility

8:00am **VT+AS+SS-WeM1 Manufacturing and Welding Processes for TPS Large Aluminum Bending-Chambers and 14 m Vacuum Cells**, *C.L. Chen, C.C. Chang, C.K. Chan, Y.C. Yang, T.Y. Lee, G.Y. Hsiung, J.R. Chen, NSRRC, Taiwan, Republic of China*

A unique manufacturing and welding technique has been developed for building the 3 GeV Taiwan Photon Source (TPS) large aluminum bending chambers and 14-meter vacuum cells. There are total 48 bending chambers, which are about 3.8 meters long each. Combined with an appropriate manufacturing processes, such as with a precise CNC machine, lubrication with pure alcohol and cleaning with ozonated water, the aluminum chambers have an oil-free interior surface finished for an ultra-high vacuum environment before aluminum welding. Ozonated water has a high oxidation potential and can remove most organic contaminations. It is used to effectively clean aluminum chambers' surfaces, and provides with the lowest outgassing yield. After the bending chambers are cleaned with ozonated water, the chambers are moved to a welding room for following welding processes. A novel automatic gas-tungsten arc-welding (GTAW) system has been established at NSRRC for welding the aluminum bending chambers. This welding system has a XY stage that is built and configured to provide high-performance positioning along multiple welding axes. The automatic welding system comprises six welding torches to implement simultaneously two longitudinal side welds of a bending chamber, and is innovative in using computer-based software to control the welding movements and the welding parameters of the six-torch output. In traditional manual welding, the key success factors focus on elimination as much as possible the distortions of structural assemblies. The six-torch welding and a clamp-free approach together address the issue of reducing distortion and minimizing residual stresses with a novel one-step welding process. In addition, on-site welding sequence is introduced for assembling two straight and two bending chambers into one 14-meter vacuum cell.

From the beginning of CNC machining to the end of vacuum cell assembly, deformations through all process sequences are measured and controlled under 300 μm . In this paper, both the manufacturing sequences, vacuum data and statistical analysis of deformation control are presented in detail.

8:20am **VT+AS+SS-WeM2 A High Power Electron Beam Stop for Cornell ERL Prototype Injector**, *X. Liu, Y. Li, K.W. Smolenski, I. Bazarov, B.M. Dunham*, Cornell University

The electron beam stop for Cornell University's Energy Recovery Linac (ERL) prototype injector was designed and manufactured for 600 kW electron beam power at beam energies between 5 and 15 MeV. To minimize neutron production from high energy electrons, aluminum was chosen over copper for the construction material. It consists of a 20 mm thick main body with machined outer cooling channels and a tight fit jacket, with the thickness mainly determined by the stopping power of the material. The stop body also serves as the vacuum envelope. The stop body is made of three sections, which are electron-beam welded together. It has a cylindrical shape with a cone at the end, about 0.5 m in diameter and 3 m in overall length. Flexibility is allowed at the body-jacket joint to minimize the thermal stress. The naturally small ERL electron beam is enlarged and rastered in a circular pattern using magnets at the entrance. The enlarged electron beam strikes the stop surface at an average angle of about 8 degrees. The electron scattering inside the stop body was simulated using GEANT4, and the inside profile of the body was optimized so that the thermal load is the most evenly distributed over the whole body. A quadrant detector is equipped at the entrance of the stop to monitor the electron beam centering and rastering. An array of thermocouples is installed on the outside surface of the jacket, providing a rough map of the heat load distribution. Gases generated in the close-circuit cooling water by radiolysis are vented and the concentration of hydrogen is monitored. The stop has been in operation since October 2008, and has been tested up to 250 kW to date.

8:40am **VT+AS+SS-WeM3 Ion Pump Starting Behaviour at High Pressures - Influence of Pump Design Diode / Triode and Power Supply**, *M. Thierley, C. Paolini*, Agilent Technologies, Italy

Today ion pumps are broadly seen as pumps for good high vacuum and ultra-high vacuum environments. Operated at these low pressures, the power consumption of ion pumps is also very low, making ion pumps one of the most energy efficient vacuum pump technologies. Power supplies, however, with several hundred Watts of power continue to be used, as in the past decades, often based on the fear of not being able to start the ion pump; historic issues associated with higher pressures. In this presentation/paper, the differences in starting behaviour of Diode and Triode pump elements are discussed, based on experimental data. Questions addressed will include; how does the pumping speed of these elements change while starting with voltage and current? What impact does the power and design of the pump control unit have on the start and the pump down time of the vacuum system? What is the impact of the power supply unit's technology (ie. classic transformer based design vs. more modern switching power supplies)? In addition to controller experimental data and discussion of the operation theory of the pump elements, pictures of the actual plasma development inside the pump will be featured.

9:00am **VT+AS+SS-WeM4 Superconducting Niobium for Accelerator Cavities: Status and Prospects**, *M.J. Kelley*, Jefferson Lab and College of William & Mary **INVITED**

Radiofrequency accelerator cavities of superconducting niobium are the technology of choice for a number of recent and coming particle accelerators, largely because of their cost-for-performance. The principal aspects of performance are the amount of accelerator needed to achieve a required final beam energy (accelerating gradient, E_{acc}) and energy consumption (cavity quality factor, Q_c). The former impacts chiefly initial cost; the latter both initial and operating costs. Research and development efforts are bearing fruit for both. Gaining the benefits need not await the construction of new accelerators or major upgrades, as accelerator modules are regularly cycled out of existing machines. A challenge that is underappreciated by physics researchers, but is well familiar to the AVS community, is the manufacturing excellence needed to translate research progress into hardware on the ground.

Authored by Jefferson Science Associates LLC under US DOE Contract De-AC05-06OR23177

9:40am **VT+AS+SS-WeM6 Niobium Nitride Thin Films and Multilayers for Superconducting Radio Frequency Cavities**, *W.M. Roach*, D.B. Beringer, Z. Li*, The College of William and Mary, *J.R. Skuza*, National Institute of Aerospace, *C. Clavero, R.A. Lukaszew*, The College of William and Mary

Niobium nitride in thin film form has been considered for a number of applications including multilayered coatings onto superconducting radio frequency (SRF) cavities which have been proposed to overcome the fundamental accelerating gradient limit of 50 MV/m in niobium based accelerators [1]. In order to fulfill the latter application, the selected superconductor's lower critical field, H_{c1} , must be larger than that of niobium and separated from the niobium surface by an insulating layer in order to shield the niobium cavity from field penetration, therefore allowing higher field gradients. Thus, for the successful implementation of such a multilayered stack it is important to consider not just the material's inherent properties, but also how these properties may be affected in thin film geometry and also by the specific deposition techniques used. Here, we present the results of our correlated study of structure and superconducting properties in niobium nitride thin films. Additionally, we explore how growth parameters can affect the surface morphology, since the quality of the surface has major implications on the ultimate performance of SRF cavities. Combining our findings on the surface morphology, microstructure, and superconducting properties in niobium nitride thin films, we discuss their potential application in multilayered coatings for accelerator cavities.

[1] A. Gurevich, Appl. Phys. Lett. **88**, 012511 (2006).

This work was funded by the Defense Threat Reduction Agency (HDTRA-10-1-0072).

10:40am **VT+AS+SS-WeM9 Characterization of Anisotropic Surface Morphology in Epitaxial Superconducting Thin Films by Wavelet Analysis**, *D.B. Beringer, J.B. Hackett, W.M. Roach, R.A. Lukaszew*, The College of William and Mary

Surface morphology and interface roughness are critical factors impacting the ultimate performance of many thin film materials and nano-scale devices. Next generation superconducting radio frequency (SRF) materials for particle accelerator cavities depend upon the ability to tailor and finely control the microstructure and morphology of superconducting / insulating /superconducting (SIS) multilayer thin film structures. The evolving surface of grown epitaxial thin films, influenced by nucleation and growth kinetics, may exhibit dendritic or fractal patterning where the resulting anisotropic features dominate a coarsening morphology. As such, a quantitative understanding of superconducting thin film morphology and the thin film deposition parameters leading to optimal SRF surfaces is desirable. Quantitative characterization of surface morphology is typically achieved with Fourier transform (FT) analysis and fractal characterization; however, this approach suffers intrinsic limitations as the FT is localized in the frequency domain and therefore cannot differentiate between specific features with isolated spatial coordinates. Wavelet analysis transcends these limitations by effectively isolating and quantifying surface features belonging to a designated length scale, thus enabling independent analysis of local surface features with varied spatial resolutions. Here we present our work with surface characterization by wavelet analysis of epitaxial superconducting Nb thin films.

11:00am **VT+AS+SS-WeM10 NbN-AlN-Nb Multilayer Thin Films for Superconducting Radio Frequency Cavities**, *Z. Li, W.M. Roach, D.B. Beringer, C. Clavero, R.A. Lukaszew*, College of William and Mary

Linear accelerators that are used in high-energy or nuclear physics experiments use superconducting radio frequency (SRF) cavities made with bulk Nb. However, as technology is improved for bulk Nb cavities, the accelerating gradient for these cavities is reaching the fundamental limit of 50 MV/m. Since the critical surface of Nb in SRF cavities is less than one micron, it is possible to use thin films and multilayers to overcome the accelerating gradient limit. It has been proposed to apply a superconductor-insulator-superconductor (SIS) multi-layer structure onto Nb based cavities in order to provide an improved lower critical field (H_{c1}) that will shield the Nb and therefore allow for an increase in the accelerating gradient [1]. NbN is one of the superconductors that may be implemented in this SIS structure. However, the choice of insulator is crucial in determining the performance of NbN thin films. Here, we present our study of epitaxial thin films prepared on both MgO and AlN templates. The effect of substrate choice on microstructure and superconducting properties is explored in order to

* ASSD Student Award Finalist

determine which insulator provides optimal performance of NbN thin films for SRF applications.

[1] A. Gurevich, Appl. Phys. Lett. **88**, 012511 (2006).

Wednesday Afternoon, October 31, 2012

Applied Surface Science

Room: 20 - Session AS+NS+SS+TF-WeA

3D Imaging & Nanochemical Analysis - Part 2 (2:00-3:20 pm)/ Advanced Data

Analysis and Instrument Control (4:00-6:00 pm)

Moderator: V.S. Smentkowski, General Electric Global Research Center, M.R. Linford, Brigham Young University, S.J. Pachuta, 3M Company

2:00pm AS+NS+SS+TF-WeA1 From Atomic Scale to Materials Behavior: Using Atom-Probe Tomography to Understand the Behavior of Alloys and Ceramics, E.A. Marquis, University of Michigan INVITED

The ability to improve the performance of functional materials is driven by how well microstructure can be understood and controlled. The three-dimensional distribution of solutes, dopants or impurities in particular, in relation to structural features determines such properties as fracture toughness, strength, ductility, as well as electrical and magnetic response. After a brief introduction to atom-probe tomography, I will illustrate how high resolution characterization approaches can be used systematically to understand the atomic scale processes controlling materials microstructures and their evolution, focusing on alloys and ceramic systems. Several topics will be presented: precipitation and coarsening behavior of Al-based alloys, grain boundary chemistry and role of impurities during irradiation in ferritic steels which may play an important role in fracture and corrosion resistance, the development of oxide-dispersion strengthened steels for structural applications in future nuclear reactors and the role of minor elements in controlling the oxidation behavior of Ni-base alloys for high temperature power generation applications.

2:40pm AS+NS+SS+TF-WeA3 Three Dimensional Atomic Scale Characterization of Binary and Complex Oxides using Atom Probe Tomography, A. Devaraj, R. Colby, D.E. Perea, S. Thevuthasan, EMSL, Pacific Northwest National Laboratory

The development of three dimensional, high spatial and mass resolution characterization techniques is important for several materials used in applications ranging from catalysis, sensors to optoelectronics. Laser assisted atom probe tomography (APT) technique offers such an opportunity to perform atomic scale three dimensional analysis of materials including metals, semiconductors and dielectrics, with subnanometer spatial resolution and sub-ppm level mass resolution. The Cameca LEAP 4000XHR Atom Probe equipped with 355nm UV pulsed laser is used to analyze technologically important binary bulk oxides like MgO, Al₂O₃, TiO₂ and CeO₂. A strong correlation between applied UV laser energy and measured stoichiometry was observed for all these binary oxides. Using those results the importance of laser energy optimization on obtaining accurate stoichiometric composition analysis for oxides will be highlighted. Extension of such laser parametric investigation to complex oxides including SrTiO₃, LaCrO₃ and LaSrMnO₃ will also be presented. In addition the impact of laser pulsing on atomic scale structure of the oxide APT sample surface was studied by a direct cross correlation with aberration corrected TEM. The information on the atomic scale structure of the field evaporated oxide APT samples will be utilized to postulate the laser-oxide material interaction occurring during APT analysis of such oxides leading to the dependency of applied laser energy on measured stoichiometry.

3:00pm AS+NS+SS+TF-WeA4 Atom Probe Tomography of Complex Heterogeneous Low Dimensional Materials, S. Thevuthasan, A. Devaraj, R. Colby, D.E. Perea, V. Subramanian, V. Shutthanandan, Pacific Northwest National Laboratory

EMSL, a national scientific user facility of the DOE, is developing a comprehensive chemical imaging capability combining atom probe tomography with high resolution (scanning) transmission electron microscopy(HR(S)TEM) and high resolution Rutherford back scattering spectrometry (HRRBS) to provide solutions to problems pertaining to energy and environmental applications. We will emphasize on a chemical imaging effort aimed at atomically-resolved composition and structural analysis of low dimensional materials such as nanowires and embedded metal nanoparticles highlighting the benefits and challenges for APT. A unique benefit of APT is the ability to characterize the ppm level concentration and distribution of dopants across semiconducting nanowire heterojunctions. The preferential incorporation of dopants at specific atomic facets at the heterojunction interface in Si-Ge nanowires can only be characterized by using APT. Another important class of low dimensional

materials includes embedded metal nanoparticles in oxides with applications in catalysis, sensors and optoelectronic applications. In order to extent APT analysis capability to such materials a cross correlative approach of combining APT with aberration corrected HRSTEM is employed. The results from the model system of ion beam synthesized Au and Ag nanoparticles embedded in MgO will be presented.

4:00pm AS+NS+SS+TF-WeA7 Upgrading a 25 Year Old ims-4f Magnetic Sector SIMS Instrument: Teaching an Old Dog New Tricks and Keeping Research in its Future, A.J. Fahey, B.E. Naes, G. Hager, Pacific Northwest National Laboratory

The CAMECA ims-4f at PNNL is nearly 25 years old. Although much of the vacuum system, electrostatic optics and associated apertures and slits have been maintained and remain operational the electronics that control the critical components of this machine has gone beyond the typical "mean-time-between failure" of nearly all components, which is typically 10 years.

The original electronics designs, many of which are no longer employed on the newer CAMECA models, incorporated multiple series of relays to control lens voltages that allowed isolation of low control and high voltage output. These relays, among other components, are failing.

Some components of the electrostatic optics and vacuum system are targeted to be replaced to upgrade the capabilities of the instrument and to use physical components from our "surplus" ims-4f system than would enhance the operation of the PNNL ims-4f giving in near-equivalence to the operation of an ims-7f.

The upgraded electronics and control systems are being designed in a modular way using as many commercial components as possible, such as modular high voltage power supplies and commercially available high-voltage operational amplifiers. The new system will allow for complete control of all subsystems on the instrument and will improve repeatability of settings and measurements. We will be able to perform measurements sets and sequences that are currently not possible on any existing SIMS instrument. In addition, the new computer controlled system should make operation of the SIMS instrument more accessible to other investigators as it should reduce the level of training needed to operate the instrument. Currently, the operator must adjust "knobs" to tune the instrument and reproduce prior operating conditions. With the upgraded system conditions will be recalled from saved files.

All modular components are being housed in ANSI-standard DIN modules and sub-racks. Control, monitoring and data acquisition will largely be performed via PXI subsystems. The Vacuum will be controlled and monitored via a commercial process control system. Also, several other individual instruments will be used in critical positions around the instrument.

Details of the upgrade will be discussed as well as improvements to the flexibility of measurements and the performance of the system. An outline of the types of measurements that should be available with all modern systems will be presented and discussed as well as the results of improvements implemented to the PNNL ims-4f SIMS instrument.

4:20pm AS+NS+SS+TF-WeA8 Automated Processing of X-ray Photo-Electron Spectra, K. Macak, E. Macak, S.J. Coultas, S.J. Hutton, A.J. Roberts, R. Raso, S.J. Page, C.J. Blomfield, Kratos Analytical Ltd, UK

Modern XPS instruments are capable of generating a large amount of data in a hands-off automated fashion. Many new material challenges are increasingly reliant upon XPS for sample screening and other high throughput, low operator intervention applications.

The interpretation of XPS data and reliable quantification from the acquired results presents an opportunity to improve the whole experimental automation still further. We present an algorithm for fully automated processing of X-ray photo-electron spectra. The analysis is split into three stages: background subtraction, peak identification and quantification of element composition.

Each step can be carried out separately and the user can provide prior knowledge of the sample by manually selecting regions, assigning their labels and/or explicitly include/exclude specific elements. This additional information then helps to improve the accuracy of the results.

The algorithm was tested on more than 1000 spectra, selected from a wide range of different materials; including steels, polymers, semiconductors and ceramics. These spectra were processed using the automated procedure and the outcomes were compared to those determined by expert users. The average element detection success rate was 87 %.

The influence of various experimental conditions (such as signal-to-noise ratio and operating conditions) on the identification procedure is also discussed.

4:40pm AS+NS+SS+TF-WeA9 Correlating Structure and Chemistry – A Multitechnique Study using Light Microscopy (LM), SEM and XPS, M.L. Pacholski, P.Y. Eastman, The Dow Chemical Company

Understanding the distribution of carbon-rich chemistries on organic substrates can be very difficult, particularly when the substrates are not uniform, such as cellulose fibers. Recently we have been challenged to measure the distribution of an olefin polymer on a fibrous cellulose sheet. In order to verify that measured chemical distributions were definitively from polymer, as well as to understand the morphology of the deposited polymer, it was highly desired to study identical areas using SEM and other imaging techniques. Although several chemical imaging methods were investigated, it became apparent that XPS imaging was the only chemical technique capable of obtaining distributions over the desired fields of view (1 mm-3 mm). Registry of the SEM images with XPS images proved to be difficult since many of the traditional registry methods, such as marking with ink or gluing markers to the surface are ill-suited to absorbent cellulose. The first step was to align relatively low magnification light microscope images from a stereoscope with optical images captured directly in the XPS instrument. These images were then used as a “bridge” to align the higher magnification SEM and XPS images. With this method, deposited polymer and chemical information were correlated with high spatial accuracy. Composite images showing the chemical information as colored overlays on the SEM images were generated to clearly display the correlation.

**Graphene and Related Materials Focus Topic
Room: 13 - Session GR+AS+EM+NS+SS-WeA**

Dopants and Defects in Graphene; Graphene Interfaces with Other Materials

Moderator: D. Gunlycke, Naval Research Laboratory

2:00pm GR+AS+EM+NS+SS-WeA1 Increasing Interface Bonding and Tuning Doping Behavior at Metal-Graphene-Metal Sandwich Contact, C. Gong, R.M. Wallace, K.J. Cho, Y.J. Chabal, The University of Texas at Dallas

Two types of interfaces can be formed between metals and graphene depending on the strength of the metal-graphene interaction: weak (metal physisorption) and strong (metal chemisorption) interfaces. “Physisorption” interfaces (e.g., with Al, Ag, Cu, Ir, Pt and Au) are characterized by a larger metal-carbon distance ($>3 \text{ \AA}$) with some charge transfer between metal and graphene (i.e. doping of graphene) that maintains its overall π -band dispersion. “Chemisorption” interfaces (e.g. with Ni, Co, Pd, and Ti) are characterized by a smaller metal-carbon distance ($<2.5 \text{ \AA}$) and strong orbital hybridization between metal- d and carbon- p_z orbitals, resulting in the destruction of the graphene’s π -band dispersion around the Dirac point. Till now, only a small fraction of all available metals has been used as electrode materials for carbon-based devices due to metal-graphene interface debonding problems. The issue therefore is to keep graphene’s intrinsic π bandstructure by using weakly interacting metals while enhancing the interface stability.

We report an enhancement of the bonding energy of weakly interacting metals by using a metal-graphene-metal sandwich geometry, without sacrificing the intrinsic π -electron dispersions of graphene that is usually undetermined by strong metal-graphene interface hybridization. This sandwich structure further makes it possible to effectively tune the doping of graphene with an appropriate selection of metals. Density functional theory calculations reveal that the strengthening of the interface interaction is ascribed to an enhancement of interface dipole-dipole interactions. Raman scattering studies of metal-graphene-copper sandwiches are used to validate the theoretically predicted tuning of graphene doping through sandwich structures.

2:20pm GR+AS+EM+NS+SS-WeA2 Defects in Two-Dimensional Materials and their Heterostructures, L. Adamska, I.I. Oleynik, University of South Florida

Recent developments in graphene electronics have stimulated an interest in other two dimensional materials such as hexagonal boron nitride (BN) and molybdenum disulfide (MoS_2). In contrast to graphene, BN and MoS_2 possess appreciable band gap and may form good interfaces with graphene, which opens up exciting opportunities for development of novel nanoelectronic devices. For practical applications, it is important to

understand the effect of defects, which appear during growth and processing, on resulting electronic properties. The defects in graphene, BN, MoS_2 and their heterostructures have been investigated by first-principles density functional theory. Their effect on electronic properties including density of states and simulated STM images will be discussed.

4:00pm GR+AS+EM+NS+SS-WeA7 Metal Oxide Growth and Characterization on CVD Graphene, A. Matsubayashi, College of Nanoscale Science and Engineering, University at Albany

Thin metal oxide layers deposited on graphene can be utilized as dielectric barriers between metals and graphene to help isolate a metal contact from the graphene channel. This is important for graphene based spintronic devices as dielectric layers between the ferromagnetic electrode and graphene have been shown to increase the spin relaxation time measured utilizing non-local detection and spin precession measurements^[1]. However, simply depositing metal oxide layers such as aluminum oxide on graphene results in non-uniform film lowering the quality of the interface barrier^[2]. In addition it is important to understand the stoichiometry of the resulting film. We will present a systematic study of aluminum oxide layers grown on CVD (chemical vapor deposition) graphene under ultra-high vacuum conditions with and without titanium seed layers. The aluminum oxide layers with the titanium seed layers showed reduced surface roughness. The chemical and structural composition determined by XPS (X-ray photoelectron spectroscopy) will be also presented that shows full oxidation of the aluminum and partial oxidation of the titanium.

References:

- (1) E. I. Rashba, Phys. Rev. B, **62**, 16267 (2000)
- (2) W. Han *et al*, Phys. Rev. Lett., **105**, 167202 (2010)

4:20pm GR+AS+EM+NS+SS-WeA8 Bi-layer Graphene Growth on Ni(111): The Role of Monolayer Graphene Rotation, A. Dahal, A. Rafik, University of South Florida, P.W. Sutter, Brookhaven National Laboratory, M. Batzill, University of South Florida

Bi-layer graphene synthesis by chemical vapor deposition is of importance for field effect devices because the band gap can be tuned in bi-layer graphene by an applied electric field. Here, we demonstrate that bi-layer graphene can be synthesized above 650°C by chemical vapor deposition on thin Ni(111) films grown on YSZ(111) substrates in ultra high vacuum (UHV). We characterize the bi-layer graphene growth by low energy electron microscopy (LEEM), Auger electron spectroscopy (AES) and low energy electron diffraction (LEED). Below 600°C graphene grows in registry with the Ni(111) lattice and no second layer graphene is formed upon cooling. At 650°C rotationally misaligned graphene domains are formed on Ni(111) and we observe second layer graphene to grow by carbon-segregation under those rotated monolayer graphene domains. The difference in second layer graphene nucleation and growth is explained by the graphene-Ni interaction, which is much stronger for graphene in registry with the substrate than for rotated graphene. The segregated second layer graphene sheet is in registry with the Ni(111) substrate and this suppresses further carbon-segregation, effectively self limiting graphene formation to two layers.

4:40pm GR+AS+EM+NS+SS-WeA9 Energetic and Kinetic Factors of Graphene Nucleation on Cu, N. Safran, M.S. Arnold, University of Wisconsin-Madison

Chemical Vapor Deposition (CVD) of graphene on Cu substrates uniquely allows for growth of uniform monolayer graphene and is a promising route for its scalable production for many industrial applications due to low cost. The growth is a purely surface driven process, due to carbon’s low solubility in the Cu substrate, and relies on the Cu surface catalytically decomposing a carbon precursor (methane). As the growth of graphene proceeds across the surface, the reactivity of the Cu is passivated by the graphene, making the growth self-limiting to monolayer coverage. Research interest on the control of nucleation is intensifying, as the polycrystalline character of the graphene films can limit mobility, thermal conduction, and mechanical strength via grain boundaries.

In this paper, we study the nucleation dependencies of graphene at ambient pressure CVD in the context of surface nucleation theory. At low methane partial pressures, the concentration of carbon on the surface on the copper is low and carbon clusters cannot grow to a critical size for nucleation. As the partial pressure is increased, the methane partial pressure reaches a critical value and nucleation occurs. Tracking the critical pressure as a function of temperature from 880 to 1075°C , we have determined the formation energy of the critical graphene nucleus to be $\sim 1.5 \text{ eV/carbon atom}$, via the relation $c_{\text{mc}} \sim \exp(-E_{\text{form}}/k_B T)$. Additionally, we have found that the nucleation density of the graphene varies by 5 orders of magnitude over this temperature range at the critical methane concentration. The results are

described under the desorption controlled regime of surface cluster nucleation.

Growths near the critical methane concentration yield hexagonal growing graphene domains characteristic of attachment limited kinetics, while at higher rates yield other growth shapes. Characterization by Raman Spectroscopy has been used to identify defects in the graphene layers. We find that the Raman defect band (D-Band) scales with the root of the nucleation density, indicating the majority of defects are located at the domain boundaries and the D-band intensity scales with the distance between them. Electrical mobility measurements show nearly constant values in samples across the range of temperatures indicating other limiting factors besides internal defects. Growths at 900^o C yield $\mu > 1000$ cm²/Vs, ON/OFF ratio ~10, and Raman D/G ratio <1, demonstrating high quality of growth even at relatively low temperatures.

5:00pm GR+AS+EM+NS+SS-WeA10 Magnetic Spin Reorientation Transition in Graphene Covered Cobalt on Iridium(111), A.T. N'Diaye, Lawrence Berkeley National Laboratory, *J. Coraux, N. Rougemaille, C. Vo-Van, O. Fruchart,* Institut NÉEL, CNRS & Université Joseph Fourier, France, *A.K. Schmid,* Lawrence Berkeley National Laboratory

One of graphene's promises is to be material for spintronic applications. While the influence of a magnet on graphene is under intense investigation by many groups little attention is given to the influence of graphene on a magnet.

With spin polarized low energy electron microscopy (SPLEEM) we studied thickness dependent spin reorientation transition on this system and compare with Co/Ir(111) without graphene. Monitoring the spin orientation in three dimensions while increasing the film thickness by one ML at a time, we find that the presence of graphene on the film at least doubles the thickness at which the spin reorientation from out-of-plane to in-plane occurs from 6ML Co to transition to 12ML-13ML at 300°C and to between 14ML and 20ML at room temperature.

We attribute the significant contribution of the graphene/Cobalt interface to the magnetic anisotropy energy to a strong hybridization of graphene with Cobalt in directional bonds.

This work was supported by the U.S. Department of Energy under Contract No. DE-AC02-05CH11231, by the French ANR contract ANR-2010-BLAN-1019-NMGEM and by the Alexander von Humboldt Foundation.

5:20pm GR+AS+EM+NS+SS-WeA11 Nucleation and Growth of Rh and Au Clusters on Graphene Moiré/Ru(0001), B. Habenschicht, Oak Ridge National Laboratory, *D. Teng,* Georgia Institute of Technology, *L. Semidey-Flecha,* Oak Ridge National Laboratory, *D. Sholl,* Georgia Institute of Technology, *Y. Xu,* Oak Ridge National Laboratory

Nanometer and sub-nanometer sized metal clusters may possess electronic and catalytic properties that differ greatly from those of the corresponding bulk metals. For potential applications, dense arrays of uniform metal clusters are desirable. However, the synthesis of such cluster materials remains a formidable challenge. Moiré superstructures that develop in graphene supported on certain metals have been shown to be viable templates for driving the formation of uniform metal clusters.[1] On graphene moiré (GM) on Ru(0001), dispersed clusters are obtained for Rh whereas Au coalesces into very large 2D islands.[2,3] We carry out a computational study to understand the disparate morphologies of Rh and Au clusters on GM/Ru(0001) via a multi-scale approach. DFT calculations are performed to study the adsorption and diffusion of the adatom and ad-clusters of Rh and Au on GM/Ru(0001) and the bonding mechanism between the metals, graphene, and Ru substrate. The potential energy landscape is then used to perform kinetic Monte Carlo simulations for the diffusion, nucleation, and growth of Rh and Au clusters. This approach allows us to predict the spatial and size distribution of the metal clusters and may be generally applicable to identifying the conditions necessary for obtaining desired cluster morphologies on GM.

(1) N'Diaye, A. T.; Bleikamp, S.; Feibelman, P. J.; Michely, T. *Phys. Rev. Lett.* **2006**, *97*, 215501.

(2) Zhou, Z.; Gao, F.; Goodman, D. W. *Surf. Sci.* **2010**, *604*, L31.

(3) Xu, Y.; Semidey-Flecha, L.; Liu, L.; Zhou, Z.; Goodman, D.W. *Faraday Discuss.*, **2011**, *152*, 267.

5:40pm GR+AS+EM+NS+SS-WeA12 Graphitic and Pyridinic N Species on N-doped HOPG Studied by STM, STS, PES and DFT, M. Sakurai, T. Shikano, D. Ushigome, T. Suzuki, University of Tsukuba, Japan, *Y. Harada, M. Oshima,* University of Tokyo, Japan, *S. Casolo,* University of Milan, Italy, *M.I. Trioni,* ISTM, Italy, *G.F. Tantardini,* University of Milan, Italy, *T. Kondo, J. Nakamura,* University of Tsukuba, Japan

Nitrogen doped graphene and carbon nanotube have been reported to show superior catalytic activity or superior support effect in the fuel cell. However, effects of the dopant nitrogen on the modification of the electronic structure of such graphite-related materials have not been clarified because a wide variety of defects with different types of C-N bonding configurations can coexist in nitrogen doped graphite.

Here, we report comprehensive atomic-resolution characterization of the defects in a nitrogen-doped graphite surface by scanning tunneling microscopy (STM), scanning tunneling spectroscopy (STS), Photoemission spectroscopy (PES) and first-principles calculations based on the density functional theory (DFT). Nitrogen-doped graphite was produced by nitrogen ion bombardment of the HOPG (highly oriented pyrolytic graphite) followed by thermal annealing at about 900 K.

Two types of nitrogen species were identified at the atomic resolution. One is pyridinic N (N having two C nearest neighbors) with single-atom vacancy. The other is graphitic N (N having three C nearest neighbors). In the case of pyridinic N with single vacancy, the local electronic states of the non-bonding pz orbital of carbon are found to appear at occupied region near the Fermi level at the carbon atoms around pyridinic N. On the other hand, the local electronic states of the non-bonding pz orbital of carbon are found to appear at unoccupied region near the Fermi level at the carbon atoms around graphitic N.

These results indicate that in both cases more than 300 carbon atoms are found to be modified by the dopant N to show the non-bonding pz orbitals. Moreover, these results suggest that the graphitic-N and pyridinic-N as well as their surrounding carbon atoms may act as "acid" and "base", because their non-bonding pz orbitals appear at empty and occupied region, respectively.

Surface Science

Room: 22 - Session SS+EM-WeA

Semiconductor Surfaces

Moderator: M.A. Hines, Cornell University

2:00pm SS+EM-WeA1 Local Characterization of Laterally Patterned GaN Polar Surfaces, J.D. Ferguson, Virginia Commonwealth University, *J.K. Hite, M.A. Mastro, C.R. Eddy, Jr.,* U.S. Naval Research Laboratory, *A.A. Baski,* Virginia Commonwealth University

Using scanning probe microscopy techniques, we have investigated the topographic and electrical properties of lithographically defined Ga- and N-polar regions grown on the same surface of a GaN epilayer. These unique structures were created on N-polar substrates grown by either hydride vapor phase epitaxy (HVPE) or metalorganic chemical vapor deposition (MOCVD). A patented selective epitaxy process [1,2] was used to prepare the alternating polarity surfaces on the two separate substrate types. To produce adjacent stripes of alternating polarity on a single substrate, a thin inversion layer comprising AlN was selectively grown inside a nitride mask. After removing the mask, Ga- and N-polar GaN were simultaneously grown over the inversion layer and bare N polar substrate, respectively, using MOCVD. Atomic force microscope (AFM) topography images reveal that Ga-polar regions are smoother than N-polar ones by about two orders of magnitude (rms of ~0.5 nm and ~50 nm, respectively). Local current/voltage (I/V) spectra obtained by conductive AFM indicate a lower turn-on voltage and higher conductivity for N polar regions, whereas Ga polar regions are insulating. Scanning Kelvin probe microscopy (SKPM) data show a surface potential drop of ~0.5 V across the interface domain boundary (< 200 nm lateral resolution) from the N- to the Ga polar regions on the HVPE substrate. A lower potential drop (~0.2 V) is seen across the N- to Ga- interface on the template, as well as inconsistent surface potential values (+/-0.1 V) for Ga-polar stripes. Using SKPM, the surface photovoltage (SPV), or the change in surface potential upon exposure to above-bandgap light, may also be measured for both surfaces simultaneously. Both samples show similar characteristics to previously studied polar GaN surfaces, where Ga-polar regions have higher initial SPV values (~0.3 V for HVPE, ~0.5 V for MOCVD) than N-polar regions (~0.2 V for HVPE, ~0.3 V for MOCVD). Restoration of the SPV signal after

illumination is faster for Ga-polar regions, which is not consistent with previously studied bulk Ga-polar films. In summary, scanning probe methods can be used to distinguish Ga- versus N-polar GaN surface regions grown on the same GaN epilayer.

1. J.K. Hite, M.E. Twigg, M.A. Mastro, C.R. Eddy, Jr. and F.J. Kub, "Initiating Polarity Inversion in GaN Growth Using an AlN Interlayer", *Physica Status Solidi A* 208, 1504-1506 (2011).

2. J.K. Hite, N.D. Bassim, M.E. Twigg, M.A. Mastro, F.J. Kub and C.R. Eddy, Jr., "GaN Vertical and Lateral Polarity Heterostructures on GaN Substrates", *Journal of Crystal Growth* 332, 43-47 (2011).

2:20pm **SS+EM-WeA2 Systematic Prediction of Entropic Surface Reconstruction Stabilization on GaAs(001) from First Principles**, J.C. Thomas, A. Van der Ven, University of Michigan, N.A. Modine, Sandia National Laboratories, J.M. Millunchick, University of Michigan

Increasing evidence linking bulk material properties to surface structure has made critical the development of a comprehensive understanding of atomic-scale surface structure. This is particularly true in low-temperature-grown (LTG) GaAs, where As anti-site defects are incorporated at the As-rich growth surface. Unfortunately, GaAs(001) reconstruction stability is poorly characterized in this regime, where, in addition to the well-studied $\beta 2(2 \times 4)$ and $c(4 \times 4)$ reconstructions, a " $\times 3$ " reconstruction is also observed. This " $\times 3$ " reconstruction has been difficult to characterize experimentally, and theoretical calculations have failed to identify a stable " $\times 3$ " reconstruction on GaAs(001). We have developed a systematic, rigorous procedure for predicting equilibrium surface structure and ordering behavior at finite temperature. By combining new and established techniques, our method overcomes difficulties of studying multicomponent surfaces from first principles, which has traditionally followed a painstaking trial-and-error approach.

Using our approach of directed structural enumeration and density functional theory calculation, we can efficiently identify stable and near-stable reconstructions of the GaAs(001) surface in order to identify the structure of the missing " $\times 3$ " reconstruction. Accounting for lattice vibrations and configurational entropy from first principles, we predict finite-temperature stability of a (4×3) reconstruction over a range of A_s partial pressure at low temperature. Our results reveal a competition between vibrational entropy of the (4×3) reconstruction and configurational entropy of the $c(4 \times 4)$ reconstruction, which becomes entropically stabilized at higher temperatures. We find that this same (4×3) reconstruction features prominently in calculated reconstruction phase diagrams for the wetting layer systems Bi/GaAs(001) and InAs/GaAs(001).

2:40pm **SS+EM-WeA3 3D Atomic Scale Structure Analysis of Semiconductor Nanostructures by Atom Probe Tomography and Cross-Sectional STM**, P.M. Koenraad, Eindhoven University of Technology, Netherlands **INVITED**

Present day semiconductor science depends heavily on the construction of precise nanostructures in which atomic scale details are of key importance in the understanding and utilization of such nanostructured semiconductor materials. It is thus of key importance to have techniques that allow such details to be assessed by novel microscopy techniques that can obtain, preferable in 3D, atomic resolution. In this presentation I will present recent results that we have obtained by two exciting techniques that allow for an atomic scale resolution. We have used cross-sectional Scanning Tunneling Microscopy (X-STM) and Atom Probe Tomography (APT) on a range semiconductor nanostructures such as quantum dots and rings. The X-STM technique offers a superb 2D true atomic resolution in a single atomic plane intersecting the nanostructure. Atom Probe Tomography is a technique that has recently become available for the analysis of semiconductor nanostructures. Laser induced field emission is used to get a full atomically resolved 3D map of the composition of semiconductor nanostructure. In the presentation I will apply and compare these techniques on quantum dots and rings that have been obtained by various growth procedures such as the traditional Stransky-Krastonow process, droplet epitaxy or by applying Sb during the dot formation process.

4:20pm **SS+EM-WeA8 Coverage-dependent Adsorption of a Bifunctional Molecule with a Rigid Spacer on the Ge(100)- 2×1 Surface**, B. Shong, S.F. Bent, Stanford University

Direct chemical functionalization of semiconductor surfaces with organic molecules has been gaining attention, in part due to its potential applications based on forming organic-inorganic interfaces with tailorable properties. Attachment of bifunctional molecule is important because of the possibility for manipulating the chemical properties of the surface to allow for successive reaction, for example by molecular layer deposition (MLD). Whether dual or single reaction occurs during adsorption of a bifunctional molecule is of critical interest. It is known that more singly-tethered

adsorbates typically form at higher coverages, but most previous studies focused only on a few discrete coverages.

In this study, we investigate coverage-dependent adsorption behavior of resorcinol (1,3-benzenediol) on the Ge(100)- 2×1 surface. *In situ* X-ray photoelectron spectroscopy and Fourier transform infrared spectroscopy experiments along with density functional theory calculations are combined to determine the products and reaction pathways. First, the results support our previous conclusion that molecular geometry is an important factor in the reactivity and stereoselectivity of rigid bifunctional adsorbates.¹ Resorcinol is found to dually and singly attach on Ge(100) through its two hydroxyl groups, and the dually reacted adsorbate assumes only one configuration due to geometrical restrictions. Moreover, a detailed study with respect to coverage shows that the product distribution is strongly dependent on coverage in a nonlinear fashion with two distinct adsorption regimes. In the low coverage regime, a constant fraction of singly-attached adsorbates is observed, independent of coverage. On the other hand, the fraction of singly-bound adsorbates increases with coverage in the high coverage regime. The increase in singly-bound species at higher coverages is explained by surface crowding, with existing adsorbates blocking reactive sites. This study provides fundamental knowledge about the reactivity of bifunctional molecules on semiconductor surfaces.

¹B. Shong, K. T. Wong, and S. F. Bent, *J. Phys. Chem. C* **116**, 4705 (2012).

4:40pm **SS+EM-WeA9 2012 AVS Medard Welch Award Lecture: Chemical Functionalization of H-terminated Silicon Surfaces**, Y.J. Chabal*, The University of Texas at Dallas **INVITED**

Silicon is best known for its oxide because of its propensity to oxidize and the remarkable properties of the Si/SiO₂ interface. Yet, oxidation is ill-defined and hard to control. Moreover, modification of chemically stable oxide surfaces mostly involves silanization, typically characterized by disorder and poor chemical stability in solution. The ability to functionalize oxide-free Si surfaces opens new opportunities for a broader range of applications. Precise modification of clean Si surfaces in an ultra-high vacuum environment leads to interesting chemistry but is not widely applicable. In contrast, wet chemical preparation of well-defined H-terminated Si surfaces provides a platform for both fundamental science and further applications. Much work has been done to functionalize H/Si using well known chemical procedures, such as UV- or catalyst-induced hydrosilylation with alkene molecules or halogens followed by Grignard chemistry. Relatively little attention has been placed on the role of structure in H-terminated surfaces for selective modification. Yet, just as structure is important in etching, it also plays a role during chemical modification of surfaces, as illustrated by the reaction of ammonia on stepped Si(111) surfaces.¹ Understanding the role of structure during HF etching is also critical to devise new methods for expanding the functionality of H-terminated surfaces. This talk illustrates this concept and shows that thermal chemistry is well suited to explore such effects. It discusses, for instance, the use of methoxylation of H-terminated Si(111) surfaces to provide a well-defined template for interesting surface chemistry and a broader range of functionalization,² such as the grafting of phosphonates, amines, and metal complexes.

¹ Dai, M., Y. Wang, J. Kwon, M.D. Halls, and Y.J. Chabal, *Nitrogen interaction with hydrogen-terminated silicon surfaces at the atomic scale*. *Nature Materials* **8**, 825 (2009).

² Michalak, D.J., S.R. Amy, D. Aureau, M. Dai, A. Esteve, and Y.J. Chabal, *Nanopatterning Si(111) surfaces as a selective surface-chemistry route*. *Nature Materials* **9**, 266 (2010).

5:20pm **SS+EM-WeA11 Wet Chemical Approach for Amino Functionalization of Oxide-free Si(111) Surfaces**, T. Peixoto, P. Thissen, Y.J. Chabal, University of Texas at Dallas

The ability to functionalize H-terminated Si surfaces with NH₂ groups is crucial for a number of applications, such as biomedical (bio-sensors), solid diffusion barrier films, single electron devices, MOSFETs and MEMS. The Si-N bond provides a versatile functionality for chemical modification. Although the creation of a well-defined and stable interface for the Si-N bonds has remained elusive, chlorosilanes have been shown to easily react with gas-phase or liquid ammonia and primary and secondary amines to achieve a stable silicon nitride bond¹.

For fluorosilane surfaces, we have performed DFT calculations indicating that the kinetic barrier for the NH₃ reaction with Si-F surfaces is only slightly higher than for Si-Cl surfaces, suggesting the reaction should occur at moderate temperatures (<70°C). The 1/3 ML Si-F and 2/3 ML Si-H nanopatterned² model surface has a tailorable distance between Si-F groups (from 6.8 Å for 1/3ML to 3.9 Å at higher coverages) allowing the adsorption mechanism to be investigated in detail (and evaluated by DFT

* Medard W. Welch Award Winner

calculations) and the role of NH_x-NH_x interactions explored. We further show that the Si-F surface reacts with amino containing molecules (NH₂-R-NH₂), as evidenced by the reaction between Si-F and ethylenediamine at room temperature. Using these reactions we demonstrate that the amidation for the nanopatterned surface takes place for both small molecules (NH₃) and larger amino chains (NH₂-CH₂-CH₂-NH₂) with similar kinetics. The surfaces were characterized using Fourier-transform infrared spectroscopy (FTIR) and x-ray photoelectron spectroscopy (XPS) to verify reaction mechanisms.

These results provide a fundamental understanding of the amidation reaction mechanism for achieving stable Si-N bonds using fluorosilanes surfaces. Achieving a well-defined and stable Si-N interface is significant for a number of important technological applications.

References:

[1] Tian, F.; Taber, D.F.; Teplyakov, A.V. *J. Am. Chem. Soc.* **2011**, *133*, (20769)

[2] Michalak, D. J.; Amy, S. R.; Aureau, D.; Dai, M.; Esteve, A.; Chabal, Y. *J. Nat. Mater.* **2010**, *9*, (266).

5:40pm **SS+EM-WeA12 Ammonia- and Amine-based Chemical Modification of Silicon Surfaces**, A.V. *Teplyakov*, University of Delaware
Stable silicon-nitrogen bonds on surface of single crystalline silicon substrates can serve a variety of practical purposes. The main problem is that creating and controlling the formation of these bonds is done predominantly in the controlled ultra-high vacuum conditions. Here the formation of stable Si-N-based interfaces will be compared for vacuum procedures and for the wet chemistry-based methods. A number of compounds, including ammonia, amines, azides and nitro- and nitroso-compounds, dosed onto a clean silicon surface can yield stable Si-N bonds. However, designing surface reactions leading to contaminant-free interfaces that contain these bonds by wet chemistry methods has been a challenge. We will use multiple spectroscopy and microscopy techniques supplemented by density functional theory investigations to build interfacial systems based on Si-N bonds with ammonia and amines reacting with Cl-covered single crystalline silicon surfaces in a solvent at room temperature. Further transformations of the produced functionalized surfaces will also be discussed.

Surface Science

Room: 21 - Session SS-WeA

Catalysis on Metals and Alloys

Moderator: G. Fisher, University of Michigan

2:00pm **SS-WeA1 A Novel MoS_x Structure with High Affinity to Adsorbate Binding**, D.Z. *Sun*, W.H. *Lu*, University of California Riverside, D. *Le*, University of Central Florida, Q. *Ma*, University of California Riverside, M. *Amanpour*, University of Central Florida, S. *Bobek*, J. *Mann*, University of California Riverside, T. *Raman*, University of Central Florida, L. *Bartels*, University of California Riverside

MoS₂ is a semiconducting material consisting of sulfur-molybdenum-sulfur tripledecker layers loosely bound by van der Waals interactions. Single layer MoS₂ can be exfoliated mechanically similar to graphene. This presentation shows an alternative avenue for the fabrication of MoS₂ monolayers at comparatively low temperature and mild conditions through sulfur loading of a copper substrate using thiophenol followed by the evaporation of Mo atoms and annealing. Here we also demonstrate that another MoS_x structure can be formed in this fashion, which has a far higher affinity to adsorbate interaction. Using anthraquinone and formic acid as test molecules, we titrate the various MoS_x and copper-based structures presented on our substrate in order to determine the relative strength of adsorbate interaction.

2:20pm **SS-WeA2 Atomic-Scale Determination of the Crystallographic Stacking at the Technologically-Important Cobalt-Copper Interface**, E.A. *Lewis*, C.H. *Sykes*, Tufts University

The deposition of Co on Cu has been studied extensively due to the use of layered Co/Cu systems in giantmagnetoresistance devices and the application of magnetic Co nanostructures in spintronics. Co deposited on Cu follows a Volmer-Weber type growth mechanism, forming bilayer-high, triangular islands. These islands grow in two orientations that are rotated 60° with respect to each other. The formation of triangular islands is dictated by the six-fold symmetry of the underlying Cu lattice, and triangular growth is preferred to hexagonal growth due to favored diffusion of Co from the (100) to the (111) facet of the islands during deposition. The consequence of this diffusion is that there must be a difference in the

crystallographic packing between the two orientations of the islands. It is thought that one packing configuration of the Co islands is fcc, in which Co follows the stacking of the underlying Cu, but the second packing structure is still debated. Here we use low-temperature scanning tunneling microscopy to explore the stacking of these islands through adsorption of hydrogen on their surfaces.

Hydrogen adsorbs dissociatively on Co, and prefers to bind to fcc three-fold hollow sites, although it is calculated that there is only a 0.01 eV difference in the binding energy of hydrogen to fcc hollows vs. hcp hollows. We show that at 80 K, hydrogen is present on the Co surface in both adsorption sites, and that there is an electronic difference between the two states that is apparent in our STM images. Through high-resolution imaging of the hydrogen at the boundary between the two adsorption sites, we have been able to deduce the stacking of the underlying Co island lattice. We confirm that the majority orientation of the islands is indeed fcc stacking, and the minority of the islands follow Co's native hcp stacking. This has important ramifications in the development of Co/Cu/Co systems for GMR devices, as the interface between the two metals can significantly affect electron scattering.

2:40pm **SS-WeA3 Understanding the Growth and Surface Activity of Oxide-supported Bimetallic Clusters**, R.P. *Galhenage*, H. *Yan*, A. *Duke*, K. *Xie*, D.A. *Chen*, University of South Carolina **INVITED**

The nucleation, growth and surface composition of bimetallic clusters on titania have been investigated as model systems for understanding how surface chemistry can be controlled by bimetallic composition and interactions between the clusters and the oxide support. Specifically, we have focused on Au-based bimetallic systems (Au-Pt, Au-Ni, Au-Co) as well as Co-Pt systems. Scanning tunneling microscopy studies demonstrate that bimetallic clusters can be formed via sequential deposition when there is a difference in mobility between the two metals; the more mobile atoms (i.e. Au) can be nucleated at existing Ni, Pt and Co clusters. The surfaces of the Au-containing bimetallic clusters are almost pure Au at Au compositions greater than 50% due to the lower surface free energy of Au compared to other metals. In contrast, the Co-Pt clusters are rich in Pt despite the lower surface energy of Co. In the Au-containing bimetallic clusters, CO and methanol adsorbates induce diffusion of Pt and Ni to surface, whereas this effect is not observed for CO on Au-Co. The activity of these model surfaces have been studied in a prototype recirculating loop microreactor.

4:00pm **SS-WeA7 Synchrotrons, Catalysts and UOP: from Imaging to In Situ Spectroscopy**, S.R. *Bare*, UOP LLC, a Honeywell Company **INVITED**

The characterization methods available at today's synchrotron light sources are ideally suited to unravel the complexity of a practical working catalyst. This will be illustrated using examples from our work using a combination of synchrotron techniques including: (i) X-ray micro- and nano-tomography, (ii) X-Ray microprobe fluorescence and X-ray microprobe absorption fine structure (XAFS), and (iv) in situ XAFS combined with density functional theory (DFT) and DFT/MD calculations. Indeed, the use of in situ XAFS is now an integral catalyst characterization technique at UOP. The method provides detailed element-specific atomic-level structural and chemical information of the active catalyst. Often this information cannot be obtained by any other method. We have developed and implemented the appropriate equipment to allow these in situ studies to be performed. This equipment ranges from a plug flow reactor that operates at high pressure, to equipment that allows rapid collection of XAFS data from multiple samples simultaneously. These reactors are coupled to an automated gas manifold combined with on-line product analysis. Examples of our recent work will be presented. Each example will highlight a different aspect of the use of in situ XAFS in an industrial research environment. These examples will include in situ sulfidation of experimental hydroprocessing catalysts, and operando XAFS of rhenium-based catalysts. The talk will end with a look to the future.

4:40pm **SS-WeA9 Glycolaldehyde as a Probe Molecule for Biomass-derivatives**, W. *Yu*, M. *Barteau*, J. *Chen*, University of Delaware

Controlling the activity and selectivity of converting biomass-derivatives to syngas (H₂ and CO) is critical for the utilization of biomass feedstocks as renewable sources for chemicals and fuels. One key chemistry in the conversion is the selective bond scission of the C-OH and C=O functionalities, which are present in many biomass-derivatives. Because of the high molecular weight and low vapor pressure, it is relatively difficult to perform fundamental surface science studies of C₆ sugars, such as glucose and fructose, using ultrahigh vacuum (UHV) techniques. Glycolaldehyde (HOCH₂CH=O) is the smallest molecule that contains both the C-OH and C=O functional groups, as well as the same C/O ratio as C₆ sugars, and thus is selected as a probe molecule in the current study to determine how the

presence of the C=O bond affects the reaction mechanism. Using a combination of density functional theory calculations and experimental measurements, our results indicate that the reaction pathway of glycolaldehyde to produce syngas can be enhanced by supporting monolayer Ni on a Pt substrate, which shows higher activity than either of the parent metals. Based on the comparison of the activity and reaction intermediates of ethylene glycol and glycolaldehyde, the presence of the C=O functionality enhances the activity on the Pt(111) surface. On the other hand, for surfaces with high activity toward the O-H bond scission, such as NiPtPt(111), the presence of C=O does not significantly affect the activity or reaction pathway of C2 oxygenates. Furthermore, the Pt substrate can be replaced by tungsten monocarbide (WC) to achieve similar activity and selectivity, indicating the possibility of using Ni/WC to replace Ni/Pt as active and selective catalysts with higher stability and lower cost.

5:00pm **SS-WeA10 Modifying Selectivity of Hydrocarbon Conversion Reactions by Alloying Sn and Pt: Benzene Formation from Acetylene**, *X. Yang*, Princeton University, *J. Gao*, *S. Podkolzin*, Stevens Institute of Technology, *B. Koel*, Princeton University

Bimetallic catalysts involving Sn and Pt have important applications in hydrocarbon conversion catalysis. We have performed experiments probing chemisorption and reaction kinetics on well-defined, ordered Pt-Sn surfaces in order to aid developments needed for improving catalyst selectivity and overall performance. One specific example from investigations of benzene formation from acetylene on Pt-Sn alloys with HREELS, TPD, and DFT calculations will be discussed. On Pt(111), $\mu_3\text{-}\eta^2$ -acetylene chemisorbed in a three-fold site is the most stable configuration, as indicated by DFT calculations, and has a C-C stretching frequency (ν_{CC}) of 1310 cm^{-1} . This configuration becomes less thermodynamically favorable in the presence of Sn compared to the bridge-bonded $\mu_3\text{-}\eta^2$ configuration ($\nu_{CC} = 1495 \text{ cm}^{-1}$). The ν_{CC} peaks at $\sim 1600 \text{ cm}^{-1}$ are assigned to π -bonded acetylene, which dominate the spectra collected at 90 K. Absence of three-fold Pt sites on the Pt₂Sn alloy inhibits the transformation of acetylene to CCH₂, and the ν_{CC} peak at 1412 cm^{-1} assigned to CCH₂ appears only in the spectra of the Pt₅Sn alloy. DFT calculations show that the destabilizing effect of Sn alloying is more significant for CCH₂ and CCH + H than for acetylene. This change in relative stability increases the barrier for acetylene decomposition and makes associative reactions more likely. Results from DFT calculations indicate that benzene formation on the Pt-Sn alloys proceeds through the formation of an upright cyclic C₄H₄ intermediate, which is predicted to produce benzene by reacting with an additional surface acetylene. This closely integrated experimental-computational study has enabled us for the first time to characterize the adsorption modes of acetylene on Pt-Sn alloys. In addition, we developed a molecular level reaction mechanism for benzene formation by consolidating HREELS and TPD experimental results with DFT calculations. The presence of Sn changes the preferential adsorption sites for hydrocarbons, decreases the stability of adsorbed species to varying degrees, and favors associative reactions, thus, enabling benzene production by cyclotrimerization of acetylene.

B.E.K. acknowledges support by NSF Grant No. CHE-1129417.

5:20pm **SS-WeA11 Composition Spread Alloy Films for Study of Alloy Catalysis Across Composition Space**, *A.J. Gellman*, *B. Fleutot*, *P. Kondratyuk*, *J.B. Miller*, *G. Gumuslu*, Carnegie Mellon University

Composition spread alloy films (CSAFs) are alloy libraries that contain a continuous distribution of alloy compositions ($A_xB_yC_{1-x-y}$). Spatially resolved measurements of catalytic reactivity across CSAF libraries map catalytic reactivity as function of alloy composition. In many implementations CSAFs span continuous regions of ternary alloy composition space, but not the entire composition space. We describe the design and implementation of a method for deposition of a 1x1 cm^2 CSAF that contains all possible compositions of a ternary alloy ($A_xB_yC_{1-x-y}$ with $x = 0 \rightarrow 1$ and $y = 0 \rightarrow 1-x$), all three binary alloys (A_xB_{1-x} , A_xC_{1-x} , and B_xC_{1-x} with $x = 0 \rightarrow 1$) and all three pure component species. These CSAFs can be characterized using a number of methods including energy dispersive spectroscopy, electron back scatter diffraction, x-ray photoemission spectroscopy, and low energy ion scattering spectroscopy. The bulk structure of Cu_xPd_{1-x} binary CSAFs matches that of the bulk phase diagram. XPS and LEISS show that the surface is enriched in Cu across the entire composition space. The catalytic reactivity of Cu_xPd_{1-x} binary CSAFs a Cu_xAu_yPd_{1-x-y} ternary CSAF have been mapped across composition space using a 100 channel microreactor array. The reactivity changes with bulk composition can be correlated to the electronic structure of the alloys. The suite of methods allows a comprehensive study and understanding of alloy catalysis across composition space.

5:40pm **SS-WeA12 Role of Dissociated Hydrogen in Stabilizing Catalytic Sites and Regulating Surface Reactions for Hydrogen Storage in Metal Hydrides**, *I. Chopra*, University of Texas at Dallas, *S. Chaudhuri*, Washington State University, *J.-F. Veyan*, *Y.J. Chabal*, University of Texas at Dallas

There has been an ongoing quest to find cheaper hydrogen activation routes based on aluminum. Recently it was shown that aluminum doped with very small amounts of Ti can activate molecular hydrogen at temperatures as low as 90K. The method is based on the ability to introduce a high flux of molecular hydrogen seeded with a guest molecule (CO) to probe the catalytic activity and H₂dissociation. Once dissociated, hydrogen forms a complex with adsorbed CO (CO-H), characterized by a substantially and uniquely blue-shifted CO internal frequency.

We use this new method to determine that Titanium when present on the surface is catalytically more active ($\sim 30\%$) than subsurface Titanium. Dissociated hydrogen stabilizes Ti on the surface and as the surface becomes saturated with hydrogen it is possible for Ti atoms sitting in originally sub surface configurations to be pulled out of their original positions by the dissociated hydrogen into surface configurations. These "pulled" Ti atoms then contribute towards additional hydrogen activation when Ti is present in specific (nearest neighbor and next nearest neighbor) configurations.

Finally we show that this dissociated hydrogen protects the CO in the CO-H complex from additional reactions as is demonstrated by no isotopic exchange between CO16 and CO18. Dissociated hydrogen is present in the hollow sites around the Ti and protects the Ti-Al back-bond from further chemical activation. Similar experiments performed on surfaces with no hydrogen (Al/Ti, AlO/TiOx) show isotopic exchange reactions between CO16 (of the complex) and adsorbed CO18. The barrier for this isotopic exchange is the lowest for adsorbed CO on TiOx (desorption temperature $\sim 140\text{K}$) and highest for CO on Ti (desorption temperature $\sim >300\text{K}$).

These results provide critical information about the role of dissociated hydrogen in stabilizing Ti catalytic sites and the CO-H complex. A complete understanding of such mechanisms will help enhance material performance for hydrogen activation using cheap catalyst materials.

References:

[1] Chopra, I. S., Chaudhuri, S., Veyan, J.-F., and Chabal, Y. J., Nature Materials, 10, 884–889 (2011)

Thursday Morning, November 1, 2012

Electronic Materials and Processing

Room: 14 - Session EM+SS+AS+NS-ThM

Nanoelectronic Interfaces, Materials, and Devices

Moderator: M. Filler, Georgia Institute of Technology

8:00am EM+SS+AS+NS-ThM1 **Tensilely Strained Ge Nanomembranes for Applications in Group-IV Infrared Photonics**, *R. Paiella*, Boston University **INVITED**

Single-crystal semiconductor nanomembranes have emerged as a new materials platform offering unique opportunities for strain engineering, by virtue of their ultrasmall thicknesses that result in extremely high thresholds for plastic deformation under stress. This talk will review our recent work aimed at exploiting this property for the development of CMOS-compatible group-IV semiconductor light sources for the technologically important short-wave infrared spectral region. It is well known that Si, Ge, and related alloys are very inefficient light emitters and generally unsuitable for laser action, due to the indirect nature of their fundamental energy bandgap. A possible solution to this important drawback is provided by the ability of biaxial tensile strain in Ge to lower the conduction-band edge at the direct (G) point relative to the L-valley minima, until at a strain of about 1.9% the fundamental bandgap becomes direct. In our work, mechanically stressed Ge nanomembranes capable of accommodating the required strain levels have been developed, and used to demonstrate strong strain-enhanced photoluminescence. A maximum biaxial tensile strain of over 2% in a 24-nm-thick nanomembrane has been measured, above the accepted threshold for the formation of direct-bandgap Ge. A detailed theoretical model of the light-emission and optical gain properties of tensilely strained Ge has also been developed and applied to the measured luminescence spectra, providing evidence of population inversion at strain levels as low as about 1.4%. More recent work is focused on integrating optical cavities on these strained nanomembranes for the development of infrared photonic active devices.

8:40am EM+SS+AS+NS-ThM3 **Self-activating and Self-limiting Features of the Thermally Assisted Growth Mechanisms of Thin Oxide-, Nitride- and Carbide Films on Si Surfaces at Low Gas or Plasma Pressures**, *P. Morgen, J. Drews, R. Dhiman*, University of Southern Denmark, *Z.S. Li*, Aarhus University, Denmark

The thermally assisted growth of oxide-, nitride-, and carbide films on Si surfaces, in direct reactions, carried out with neutral gases or remote plasmas under ultrahigh vacuum background conditions, are self-limiting processes, reaching different thicknesses. The mechanisms have been studied using photoelectron spectroscopies with synchrotron radiation or conventional x-ray induced photoelectron spectroscopy (XS). For the oxidation with neutral oxygen molecules, or microwave-excited remote oxygen plasmas, and for the nitride formation reaction with microwave-excited remote nitrogen plasmas, the "kinetics" (uptake versus exposure plots) is well described with a Hill-function. For the nitrogen reaction, the variation of the temperature causes the Hill parameters to vary because this reaction has more latitude than the oxidation, in temperature range and final thickness, as well as in the resulting structure of the nitride, going from amorphous to crystalline at higher temperatures. One known instance of the "Hill reaction" is a self-activating enzymatic-like reaction, and such a mechanism is believed to be relevant also in our systems. The carbide reaction is different, due to defects in the growing film, which allow a relatively unhindered transport of Si to the surface, where it reacts with carbon species arriving at the surface, from remote microwave-excited plasmas of methane. Thus the limiting thickness of SiC/Si (111) is around 100 nm, while the thickness of oxide is 0.8 nm, and the nitrides between 1 and 3 nm.

9:00am EM+SS+AS+NS-ThM4 **Functional Conductive Polymer to Inexpensive and Portable Chemiresistive Biosensor**, *D. Bhattacharyya, K.K. Gleason*, Massachusetts Institute of Technology

Extensive research has focused on developing different types of biosensors for detecting bio-threat risks and the occurrence of toxins in the food supplies. However, these food screening processes involve many steps, have high labor costs, reagent costs and time delays of at least 2-3 days to obtain reliable data. Despite the current availability of various types of sensors, limitations of the current state-of-the-art biosensors for molecular recognition of biomolecules are well known. Among these limitations are the unacceptably long process times required for detection and user non-compliance as a result of the excessive weight of the sensor modules coupled with the inflexibility of the sensor platforms for routine uses.

Chemiresistive biosensors detect changes in resistance when analyte molecules specifically bind to the sensor surface. Chemiresistive biosensing technique is attractive because it is label-free and can be developed for faster detection of analytes. In this work, oxidative chemical vapor deposition (oCVD) technique is employed for deposition of functional conductive copolymer thin films on the electro-spun fiber mats. The dry oCVD process allowed us to deposit uniform and conformal conducting -OH functional copolymeric film on the electro-spun fiber mat in a single step. For the proof-of-concept of the biosensor application, avidin molecules were covalently immobilized to the -OH functional groups. Various concentrations of biotin solutions were employed as the analytes. The responses and the response times of the devices were significantly improved when the high surface area electro-spun mat were used as a substrate in contrast to a flat substrate.

9:20am EM+SS+AS+NS-ThM5 **Semiconductor Nanomembranes for Biomedical Applications**, *J.A. Rogers*, University of Illinois at Urbana Champaign **INVITED**

Biology is curved, soft and elastic; silicon wafers are not. Semiconductor technologies that can bridge this gap in form and mechanics will create new opportunities in devices that adopt biologically inspired designs or require intimate integration with the human body. This talk describes the development of ideas for electronics that offer the performance of state-of-the-art, wafer-based systems but with the mechanical properties of a rubber band. We explain the underlying materials science and mechanics of these approaches, and illustrate their use in bio-integrated, 'tissue-like' electronics with unique capabilities for mapping cardiac electrophysiology, in both endocardial and epicardial modes, and for performing electrocorticography. Demonstrations in live animal models illustrate the functionality offered by these technologies, and suggest several clinically relevant applications.

10:40am EM+SS+AS+NS-ThM9 **Structure, Dynamics and Mechanism of a Single-Molecule Electric Motor**, *C.J. Murphy, C.H. Sykes*, Tufts University

Future nano-electronic devices, such as fluid pumps, sensors and switches, will rely on rotating molecules bound to surfaces as key components. To operate these devices, it is important to understand and direct molecular rotation at this interface. We utilized a Low Temperature Scanning Tunneling Microscope (LT-STM) to both drive and measure the rotation of a single asymmetric thioether molecule bound to a copper (111) surface. Due to the hexagonal arrangement of the underlying Cu atoms the rotor molecule has six favorable orientations, with an asymmetrical barrier to rotation around the Cu-S bond. The symmetry of this barrier is dependent on the surface bound chirality. Rotation of the molecule can be driven by either thermal or electrical means. In thermally driven systems, there is no preferred direction of rotation. In order to measure the rate of anisotropic rotation, the system is cooled to 5 K, and a tunneling current is applied to periodically excite the molecule, resulting in a flashing ratchet like mechanism of molecular rotation. The progression of molecular orientations relative to the tip can be determined by the exponential dependence of tunneling current on distance. This allows evaluation of the rate, direction and magnitude of rotation between these orientations in real time. We aim to further interrogate this novel mechanism for electrically-driven motion by quantifying the lifetime of the rotor in each stable orientation and the transitions between these states as a function of tunneling current and voltage.

11:00am EM+SS+AS+NS-ThM10 **Semiconductor Nanostructures for Efficient Thermoelectric Energy Conversion**, *Z. Aksamija*, University of Wisconsin Madison

Thermoelectric (TE) refrigeration using semiconductor-based nanostructures, such as nanowires, nanoribbons, and superlattices, is an attractive approach for targeted cooling of local hotspots inside integrated circuits due to inherently no moving parts, ease of miniaturization and on-chip integration, and the nanostructures' enhanced TE conversion efficiency. In addition, thermoelectric power generation enables the reuse of waste heat in a variety of applications, from low-power and energy-efficient designs to internal combustion engines and solar cells. Thermoelectric efficiency, measured by the figure-of-merit ZT , is dictated by the ratio of electronic power factor $S^2\sigma$ over the total thermal conductivity. Consequently, largest gains in TE conversion efficiency have come from the ability to reduce thermal conductivity. This is especially true in nanostructures, where small physical dimensions lead to reduced thermal transport due to the scattering of lattice waves, or phonons, with the boundaries of the nanostructure. The design of efficient semiconductor thermocouples requires a thorough understanding of both charge and heat

transport; therefore, thermoelectricity in semiconductor-based nanostructures requires that both electronic and thermal transport are treated on equal footing. SOI nano-membranes and membrane-based nanowires and ribbons show promise for application as efficient thermoelectrics, which requires both high electronic power factor and low thermal conductivity. I will present numerical simulation and modeling of both carrier and phonon transport in ultrathin silicon nanomembranes and gated nanoribbons. We show that the thermoelectric response of Si-membrane-based nanostructures can be improved by employing the anisotropy of the lattice thermal conductivity, revealed in ultrathin SOI nanostructures due to boundary scattering, or by using a gate to provide additional carrier confinement and enhance the thermoelectric power factor. Furthermore, we explore the consequences of nanostructuring on silicon/germanium and SiGe alloy superlattices, and show that the drastic reduction of thermal conductivity in these structures comes from the increased interaction of lattice waves with rough interfaces and boundaries. Finally we demonstrate reduced thermal conductivity in both suspended and supported graphene nanoribbons (GNRs), which exhibit strong anisotropy due to interaction of lattice waves with line edge roughness (LER) and the competition between LER and substrate scattering. The talk will conclude with an outlook for future nanostructured thermoelectric based on nanocrystalline and nanocomposite semiconductors, and nanopatterned graphene.

11:20am **EM+SS+AS+NS-ThM11 UV Ozone Irradiation Induced Defect Formation in Graphene/PZT Devices**, C.X. Zhang, D.M. Fleetwood, M.L. Alles, R.D. Schrimpf, Vanderbilt University, E.B. Song, S. Kim, K. Galatsis, K.L. Wang, University of California at Los Angeles, E.X. Zhang, Vanderbilt University

Graphene based materials are promising candidates for integration into future integrated circuit technologies. Initial studies of the effects of electron-beam and proton irradiation have been performed on graphene materials, but there remain significant questions about the nature of the conductivity and the defects that influence its material and electronic properties. We have found that low-energy x-ray irradiation can lead to significant shifts in the charge neutral point and increases in resistance of suspended graphene layers and graphene layers on SiO₂. For graphene-on-SiO₂ structures, the reaction oxygen atoms may be supplied either by ozone in the ambient air, or by the adjacent SiO₂ substrate. Similar reactions may be observed for hydrogen, for devices exposed to x-ray and/or UV ozone (UVO) irradiation. Moreover, we also have found that graphene/PZT ferroelectric field-effect transistors (FFETs) are sensitive to UVO irradiation. The conducting channel in these devices is a single graphene layer. The device functions as a nonvolatile memory with reverse hysteresis, where charge trapping and detrapping in the PZT layer leads to a large memory window that is robust to x-ray irradiation and/or memory state cycling. When these devices are exposed to UVO irradiation, the memory window of the device decreases slightly with exposure time. In addition, an increase is observed in the slope of the I-V curves, along with a small positive shift in current-voltage characteristics. These results are consistent with the formation of negatively charged surface states on the graphene layer during the UVO exposure, which are most likely associated with adsorbed oxygen. The degradation in the I-V characteristics recovers somewhat with room temperature annealing. At the AVS meeting, the detailed electrical response will be described, and a physical model will be presented for the UVO degradation and recovery mechanisms.

11:40am **EM+SS+AS+NS-ThM12 Switching Molecular Kondo Effect by Chemical Reactions**, H. Kim, ISSP, University of Tokyo, Japan, Y.H. Chang, KAIST, Korea, M.H. Chang, Korea University, Y.-H. Kim, KAIST, Korea, S.-J. Kahng, Korea University

Motivated by spintronics applications, the methods to control Kondo effect have been actively studied in magnetic adsorbates on metal surfaces using scanning tunneling microscopy, but they were limited to the processes that required external energy supply from scanning tunneling microscope tip. We report new methods to control molecular Kondo effect by using bimolecular chemical reactions. A chemical binding between diatomic molecules and Co-porphyrin was exploited to switch off, or reset the molecular Kondo effect. The Kondo effect was switched back on using scanning tunneling microscope manipulation as well as thermal desorption. These methods rely on the hybridized pairing of unpaired spins in d₂ and π* orbitals of Co-porphyrin and diatomic molecules, respectively, as supported by our density functional theory calculation results. Our study opens up ways to control the molecular Kondo effect using an enormous variety of bimolecular chemical reactions.

12:00pm **EM+SS+AS+NS-ThM13 Quantifying the Local Seebeck Coefficient using Scanning Thermoelectric Microscopy (SThEM)**, J.C. Walrath, Y.H. Lin, K.P. Pipe, R.S. Goldman, University of Michigan

Thermoelectric (TE) devices allow reliable solid-state conversion of heat to electricity. The efficiency of a TE device is determined by the figure of

merit, ZT, which is sensitive to the Seebeck coefficient, S. Traditional S measurements are used to quantify thermally-induced electron transport on a macroscopic scale. A promising alternative method for nanoscale measurements of S is scanning thermoelectric microscopy (SThEM). In SThEM, an unheated scanning tunneling microscopy (STM) tip acts as a high-resolution voltmeter to measure the thermally-induced voltage, V, induced by a temperature gradient in a heated sample. SThEM has been utilized to measure V across a GaAs p-n junction [1], with the spatial profile of S determined through a comparison of the measured V with a simulation of a network of resistors and voltage sources, based upon a theoretical S-value [2]. Although this approach is useful for predicting the measured V, it does not provide a method for direct conversion of the measured V to a local S. We have developed a Fourier heat conduction model to calculate a temperature profile matrix, thereby enabling direct conversion between the measured V and the local S. According to our model, SThEM can be optimized by fine-tuning several parameters, including the cone angle of the STM tip and the relative thermal conductivity of the tip and sample. We applied our model to SThEM data across a GaAs p-n junction [1] and improved the agreement between the measured and theoretical S by 40%. Our progress towards SThEM measurements of CoSb₃ and InAs quantum dots will also be discussed. This material is based upon work supported by the Department of Energy under Award Number DE-PI0000012. Y.H. Lin and R.S. Goldman are supported in part by DOE under contract No. DE-FG02-06ER46339.

[1] H.K. Lyeo, A.A. Khajetoorians, L. Shi, K.P. Pipe, R.J. Ram, A. Shakouri, and C. K. Shih, *Science* **303**, 816 (2004).

[2] Z. Bian, A. Shakouri, L. Shi, H.K. Lyeo and C.K. Shih, *Appl. Phys. Lett.* **87**, 053115 (2005)

Graphene and Related Materials Focus Topic

Room: 13 - Session GR+AS+NS+SS-ThM

Graphene Nanostructures

Moderator: A. Kis, EPFL, Switzerland

8:00am **GR+AS+NS+SS-ThM1 Atomic and Electronic Structures of Graphene Nanoribbon made by MBE on Vicinal SiC Substrate**, F. Komori, K. Nakatsuji, T. Yoshimura, University of Tokyo, Japan, T. Kajiwara, K. Takagi, S. Tanaka, Kyushu University, Japan

Electronic states of graphene nanoribbon attract much interest because its intrinsic metallic band is modified to have a gap or a one-dimensional edge state at the Dirac energy E_D. Actually, microfabricated graphene [1] showed an energy gap at E_D, and the gap size increases with decreasing the width. Fabrication of well-controlled graphene nanoribbons on macroscopic area of a semiconductor substrate is, however, still one of the challenging issues in graphene research. Here, we report characterizations of graphene nanoribbon made by carbon molecular beam epitaxy (MBE) and a hydrogen treatment on a vicinal SiC(0001) substrate. Use of MBE is essential because graphene is made over the step edges of the SiC substrate in the case of graphene formation by widely-used thermal decomposition.

In the experiment, a 6√3 x 6√3 structure was first made by MBE on the anisotropic terrace of the Si-terminated surface of a nitrogen-doped 6H-SiC(0001) substrate vicinal to the [1-100] direction. The tilting angle of the substrate was 4 degree, and a well-ordered step-and-terrace structure was made after cleaning the substrate by annealing in hydrogen as confirmed by atomic force microscopy. We optimized the substrate temperature and the carbon deposition rate to make a homogeneous 6√3 x 6√3 structure on the terraces without thermal decomposition of the substrate. The surface structure was *in situ* monitored by reflection high energy electron diffraction, and the width of the 6√3 x 6√3 area on the terrace was adjusted by monitoring the 6√3 x 6√3 spots. After stopping the growth, the sample was exposed to hydrogen molecules at 600 °C to transform the surface 6√3 x 6√3 layer to single-layer graphene by inserting hydrogen atoms at the interface. [2]

Graphene honeycomb lattice without the 6√3 x 6√3 structure was confirmed by low energy electron diffraction and scanning tunneling microscopy (STM). Few point defects are seen at the graphene on the terrace in the STM images of atomic resolution. The width of graphene nanoribbon on the substrate terrace is 10-15 nm, depending on the growth condition. The electronic states of the graphene nanoribbon were studied using angle-resolved photoemission spectroscopy (ARPES) at 130 K as in the previous report. [3] The top of the π band of the graphene nanoribbon was 0.05 ~ 0.25 eV below the Fermi energy. No signal from the π* band was detected by ARPES above the top of the π band, indicating the gap formation at E_D.

References

1. M. Y. Han *et al.*, *Phys. Rev. Lett.* **98**, 206805 (2007).

2. C. Riedl *et al.*, Phys. Rev. Lett. **103**, 246804 (2009).
 3. K. Nakatsuji *et al.*, Phys. Rev. **B82** 045428 (2010).

8:20am GR+AS+NS+SS-ThM2 Carrier Transport Behavior of Carbon Nanotube Transistors with Single Semiconducting and Metallic Tube, P. Sakalas, M. Schroter, Technische Universität Dresden, Germany

The high interest in using carbon nanotube FETs in advanced electronics is based on their unique 1D transport properties such as quasi-ballistic transport. The high carrier velocity together with the quasi 1D tube geometry yield a very low intrinsic capacitance per tube of approximately 80 aF/mm in multitube structures. Those properties makes CNTFETs very interesting for high frequency and power applications.

CNTFETs with a single semiconducting tube yield too low current (25 μ A) for useful applications and thus the transistors with thousands tubes in parallel are being fabricated [1][2]. Unfortunately, following theory 1/3rd of all tubes are metallic. Carrier scattering is better understood for metallic tubes and it is believed that for semiconducting tubes, despite more complexity, the same scattering mechanisms are applicable: CNTs defect scattering, physical bends and phonon scattering are present. Investigation of CNTFETs with a single semiconducting (ST), single metallic (MT) and metallic+semiconducting (MST) tubes at different lattice temperature environment was never done before and enables a deeper insight of CNT transport properties to further improve the application-oriented device behavior. It was shown that multifinger CNTFETs exhibited a weak temperature dependence of IV, RF and NF indicating a very weak electron-phonon interaction and the absence of charge-carrier freeze-out known for conventional doped semiconductors [3],[4].

In this work transistors with single ST, single MT and double MST were selected. Transistors have 800 nm channel length and features n-type behavior. IV characteristics were measured on wafer for manufacturable CNTFET process selected single CNTs at different lattice temperatures. The investigated structures have a fixed gate length of 0.35 μ m and gate width of 40 μ m. The source-drain spacing (channel length) is 800 nm. A 20 nm thick HfO₂ was used for the gate oxide. The devices were fabricated with the process technology described in [1][2]. The CNTFETs were embedded in DC pads for on-wafer measurements. Transfer characteristics of ST and MT transistor structures at ambient temperature T₀ = 300 K, are shown in Fig.1 and Fig.2, Fig.3, Fig.4. The drain current show saturation for ST device, typical for MOSFETs. Nevertheless the carrier transport is very different. The dependence of drain current over the temperature will enable the analysis of transport behavior of single ST and MT and coupled MST. As it is seen from Fig.3 and Fig.4 the MT transistor structure behaves as nonlinear resistor.

8:40am GR+AS+NS+SS-ThM3 Fabrication of Chemically-isolated Graphene Nanoribbons (GNRs) by Scanning Probe Nanolithography using a Heated Probe, W.K. Lee, J.T. Robinson, R. Stine, C.R. Tamanaha, D. Gunlycke, Naval Research Laboratory, *M. Haydell, E. Cimpotiasu*, U.S. Naval Academy, *W. King*, University of Illinois at Urbana Champaign, *P.E. Sheehan*, Naval Research Laboratory

One route to realizing graphene as a material for digital-type devices is through the lithographic patterning of graphene nanoribbons (GNRs). GNRs enable band gap engineering that is dependent on nanoribbon width and edge state. We employed two complementary AFM-based lithography techniques to pattern GNRs: (1) thermal dip-pen nanolithography (tDPN)¹ and (2) thermochemical nanolithography (TCNL)². Though inverse in approach, both techniques generate GNRs into a larger sheet of insulating chemically-modified graphene. Both lithographies were performed on CVD-grown single-layered graphene (SLG) on SiO₂/Si substrates using heated AFM probes. The first approach, tDPN, used the heated probe to deposit narrow polystyrene (PS) ribbons on pristine graphene. The areas of the graphene not protected by the polymer were then fluorinated, converting them to a highly insulating state, which leaves behind a chemically isolate GNR channel. We show that the PS protected ribbon was the only conductive pathway for active device. Secondly, we use the converse approach by using the heated AFM probe to locally reduce fluorographene back to graphene, leaving behind a conductive GNR channel. Both techniques can generate a wide range of nanoribbon widths while avoiding electron beams which can damage graphene. We discuss the relative merits of each strategy, as well as their impact on electrical properties (e.g., doping).

1. WK Lee *et al.*, *Nano Letters*, 11, 5461, 2011
 2. Z Wei *et al.*, *Science*, 328, 1371, 2010

9:20am GR+AS+NS+SS-ThM5 Growth of a Linear Topological Defect in Graphene as a Gate-tunable Valley Valve, A. Zettl, J.-H. Chen, N. Alem, Univ. of California at Berkeley, Lawrence Berkeley Lab, *G. Autes, F. Gargiulo*, Ecole Polytechnique Fédérale de Lausanne (EPFL), Switzerland, *A. Gautam, M. Linck*, Lawrence Berkeley National Lab, *C. Kisielowski*, Lawrence Livermore National Lab, *O.V. Zazyev*, Ecole Polytechnique Fédérale de Lausanne (EPFL), Switzerland, *S.G. Louie*, Univ. of California at Berkeley, Lawrence Berkeley Lab

INVITED

The valleytronics, a zero-magnetic-field equivalent of spintronics, could be realized in graphene if a simple scheme can be conceived to generate and to detect valley polarization in the material. Here we provide the first direct experimental observation of the self-sustained, atomically controlled growth of a peculiar linear defect structure in suspended graphene. The structure consists in units of octagon and pentagon pairs (termed 5-5-8 defect) and can be grown from a single pentagon seed in graphene under electrical bias. First-principle simulations show that the 5-5-8 defect can act as a gate-tunable valley valve. The result represents a critical step towards realizing valleytronics in graphene.

10:40am GR+AS+NS+SS-ThM9 Crystalline and Electrical Properties of Vertically-Laminated Carbon Nanowalls formed by Two-Step Growth Method, H. Kondo, T. Kanda, Nagoya University, Japan, *M. Hiramatsu*, Meijo University, Japan, *K. Ishikawa, M. Sekine, M. Hori*, Nagoya University, Japan

Carbon nanowall (CNW) is one of carbon nanomaterials consisting of stacked graphene sheets, which are vertically standing on the substrate. Due to the unique properties of graphene sheets, such as high carrier mobility, large current carrying capability, and so forth, it is expected that the CNW also have such the excellent electrical and physical properties. On the other hand, in the CNWs, the bending and branching graphene sheets take a maze-like form. Therefore, due to their unique morphology and properties, the CNWs are promising as channel and electrode materials in the various types of the future nanoelectrics devices. At the construction of the CNW devices, vertical lamination of different types of CNWs is one of the useful and important technique as basic elements of the devices.

In this study, we investigated sequential two-step growth of CNWs to form the vertically-laminated structures. In this experiment, two types of CNW growth processes with different conditions were sequentially performed on Si substrate by an electron beam excited plasma-enhanced chemical vapor deposition (EBEP-CVD) using CH₄/H₂ mixture gas. Firstly, the CNW was grown at 600°C and 2.67 Pa for 10 min. Then, the second-step growth process was performed at 480°C for 10 min. The CNW samples formed only by the single-step growth at 480°C or 600°C were also prepared for comparison. Morphology and crystalline structures of CNWs were analyzed by scanning electron microscopy and Raman spectroscopy.

In the case of the single-step growth, only after the growth at 600°C, about 600 nm-thick CNWs were formed, although CNWs hardly grew at 480°C. On the other hand, in the case of the step-growth, about 1200 nm-thick CNWs were formed after the second-step growth at 480°C, compared to the single-step growth at 600°C. No boundary was found between the lower and upper region. The stacks of graphene sheets formed seamless structures. According to the Raman spectra, the crystalline structures of the CNWs were hardly changed even after the first-step growth at 600°C and the second-step growth at 480°C. This result means that the nanographene can restart to grow easily and continuously at the edges of the previously-grown graphene even at 480°C without the nucleation. These results indicate the possibility to realize the vertical junction of different types of CNWs, such as a p-n junction. At the session, the interfacial structures and electrical properties of the vertically-laminated CNWs will also be discussed.

11:00am GR+AS+NS+SS-ThM10 Surface Modification of Vertically Oriented Graphene Electrochemical Double-Layer Capacitors, R.A. Quinlan, Naval Surface Warfare Center, Carderock Division, *M. Cai*, The College of William and Mary, *A.N. Mansour*, Naval Surface Warfare Center, Carderock Division, *R.A. Outlaw*, The College of William and Mary

Previously reported efforts have identified the potential of vertically oriented graphene nanosheets in electrochemical double-layer capacitors (Miller *et al.*, Science 2010) for efficient AC line-filtering performance. Continued investigations to improve performance suggest that the availability of a high edge and surface defect density could be the dominant mechanism. Furthermore, charge/discharge profiles over time show that performance can actually increase as the device ages. In an effort to understand these findings, X-ray photoelectron spectroscopy, Auger electron spectroscopy and near edge absorption fine structure spectroscopy have been utilized to study the interaction of the electrolytes and solvents with the graphene-based electrode materials. The EDL capacitance of graphene nanosheets has been measured before and after Ar plasma bombardment for various times and after exposure to water, isopropanol,

methanol, NaOH and KOH. Graphene nanosheet electrochemical capacitors have been disassembled and analyzed following short term and long term operation.

11:20am **GR+AS+NS+SS-ThM11 Electronic Properties and Device Applications of Wafer-Scale Graphene Nanoribbons**, *D. Jena*, University of Notre Dame **INVITED**

Graphene boasts unique physical, electronic, and optical properties. For conventional electronic device applications, the zero band gap of 2-dimensional graphene is an impediment. Opening of effective band gaps can be achieved by field-effect in bilayer graphene, or by using Klein-tunneling properties of graphene p-n junctions. However, these methods appear not to effectively scale to small dimensions. Another way to open band gaps in graphene is to make graphene nano ribbons (GNRs) and use size quantization. Though many of the properties of 2D graphene are lost in the process, GNRs become similar to semiconducting carbon nanotubes, but with planar structures and compatibility with conventional lithographic processes. In this talk, I will present our group's research progress in making such wafer-scale GNR transistors. Band gaps ~ 0.15 eV appear in ~ 10 nm wide single GNRs, and band gaps are preserved in parallel arrays of GNRs. Based on these GNRs, we measure current drives as high as 10mA/micron, which far exceeds all other semiconductor materials and seems attractive for both logic and interconnect applications. The effects of edge roughness on scattering and mobility, and the progress towards making GNR-based tunneling transistors will also be presented.

Surface Science

Room: 21 - Session SS+EN+OX-ThM

Catalysis and Photocatalysis on Oxides

Moderator: Z. Dohnalek, Pacific Northwest National Laboratory

8:00am **SS+EN+OX-ThM1 Photoelectrochemical Water Splitting under Sunlight Irradiation using Oxynitride Electrodes Fabricated by Particle Transfer Method**, *K. Domen, J. Kubota*, The University of Tokyo, Japan **INVITED**

Hydrogen production through the photoelectrochemical (PEC) water splitting is one of the attractive ways to convert solar energy to storable chemical energy. The availability of powder semiconductor materials through coating methods for preparing photoelectrodes is a one of strong point of PEC cells. Even if the surface is a rough particle layer, the electrolyte solution automatically forms the desirable solid-liquid interface for whole semiconductor surfaces, where photoexcited carriers are separated by electric field.

Oxynitride and oxysulfide materials are promising candidates for photoelectrodes for water splitting. Among them, LaTiO_2N has a proper band structure from the view point of driving solar water splitting. The material shows photocatalytic hydrogen and oxygen evolutions in half reactions using sacrificial reagents, indicating that the material have a proper band structure to drive PEC water splitting. LaTiO_2N absorbs visible light up to 600 nm ($E_g = 2.1$ eV), so that they can capture more solar energy than oxide photocatalysts, which typically have absorption in the UV region. Photoelectrodes based on the material have been studied extensively, however, the photocurrent was low due to the lack of good preparation method of the electrode.

In the present study, we report a novel fabrication method of photoelectrodes for PEC water splitting using semiconductor powders. This method, which we have termed the particle transfer (PT) method, is shown to be applicable to a variety of semiconductor powders. LaTiO_2N was demonstrated to exceed those prepared by the conventional method of photoelectrode fabrication from powder materials.

8:40am **SS+EN+OX-ThM3 Multi-step Photooxidation of CO on $\text{TiO}_2(110)$** , *G.A. Kimmel, N.G. Petrik*, Pacific Northwest National Laboratory

TiO_2 is an important photocatalyst with many practical applications. However, a detailed understanding of the relevant physical and chemical processes for the photocatalysis remains elusive. We have studied the photooxidation of CO adsorbed on rutile $\text{TiO}_2(110)$ during UV irradiation with ~ 1 ms time resolution. Previous investigations with ~ 0.1 s resolution found that the maximum CO_2 photon-stimulated desorption (PSD) signal occurred for the first data point and then decreased monotonically with increasing irradiation time. However our experiments with improved time resolution show that the initial rate of CO_2 production is zero, and then increases smoothly to a maximum before decreasing at longer irradiation

times. Experiments varying the UV photon flux show that the CO_2 PSD kinetics are proportional to the photon fluence but are independent of the photon flux (for the range investigated). The photon fluence required to reach the maximum CO_2 PSD signal increases as the initial coverage of chemisorbed O_2 increases – an effect that we attribute to changes in the initial charge state of the chemisorbed O_2 . These results demonstrate that the production of CO_2 proceeds through the formation of stable precursor. The angular distribution of the photodesorbing CO_2 , which is peaked at $\sim 40^\circ$ with respect to the surface normal perpendicular to the BBO rows, is also consistent with the production of CO_2 from a precursor state. Previously, the photooxidation of CO on $\text{TiO}_2(110)$ was believed to occur in a single non-thermal reaction step: $\text{CO} + \text{O}_2 + h\nu \rightarrow \text{CO}_2 + \text{O}_{ad}$. However, our results show that the photooxidation of CO requires at least two non-thermal reaction steps – one to form the precursor and a second to produce the CO_2 . We will compare the experimental results to DFT calculations and discuss the role of photo-generated electrons and holes in the photooxidation of CO. These results show that the photooxidation of CO on TiO_2 is more complicated than previously appreciated.

9:00am **SS+EN+OX-ThM4 Design of Band Engineered Photocatalysts using Titanium Dioxide**, *S.W. Ong, D.E. Barlaz, E.G. Seebauer*, University of Illinois at Urbana Champaign

Difficulties in achieving control over carrier concentration have impeded progress toward tailoring the electric fields in semiconducting oxide photocatalysts based upon principles of electronic band engineering drawn from classical optoelectronics. The present work demonstrates such principles using the model case of methylene blue photo-oxidation over thin-film anatase TiO_2 grown by atomic layer deposition. The carrier concentration in the polycrystalline semiconductor is controlled over a range of 2.5 orders of magnitude via an unconventional means - film thickness, which indirectly influences the concentration of electrically active donor defects at grain boundaries. Over this range, the reaction rate constant varies by more than a factor of 10, and is well described by a quantitative one-dimensional model for photocurrent. The model suggests that the changes in rate result fundamentally from variations in the width of the space charge layer near the surface. Electrical characterization of the films by capacitance-voltage measurements and ultraviolet photoelectron spectroscopy, together with detailed physical characterization by a variety of techniques, confirm this picture. Prospects for better control of grain boundary donor defects through film synthesis procedures are discussed.

9:20am **SS+EN+OX-ThM5 Adsorption of CO_2 on Oxygen Precovered $\text{TiO}_2(110)$ Surfaces**, *X. Lin, Y. Yoon, N.G. Petrik, G.A. Kimmel, Z. Li, Z.-T. Wang, B.D. Kay, I. Lyubintsky, R. Rousseau, Z. Dohnalek*, Pacific Northwest National Laboratory

Rutile $\text{TiO}_2(110)$ was employed as a model oxide surface to investigate the adsorption behavior of CO_2 by means of scanning tunneling microscopy (STM) and density functional theory (DFT). STM images of partially reduced $\text{TiO}_2(110)$ surfaces obtained before and after *in-situ* dosing of CO_2 molecules at 50 K show that CO_2 adsorbs preferentially on oxygen vacancy (V_O) sites. Since the reaction of CO_2 with oxygen adatoms (surface hydroxyl groups) may lead to the formation of carbonate (bicarbonate), O_2 (H_2O) was pre-dosed to form oxygen adatom (hydroxyl) covered TiO_2 surfaces. On the oxygen precovered surfaces, CO_2 molecules were found to preferentially bind on the Ti sites next to oxygen adatoms (O_a 's) and form $\text{CO}_2/\text{O}_\text{a}$ complexes, while on hydroxylated surfaces no interactions were observed between CO_2 and hydroxyl groups. CO_2 binding to O_a 's is weak as revealed by the dissociation of the $\text{CO}_2/\text{O}_\text{a}$ complexes at 50 K where CO_2 diffuses away along the Ti row. The weak binding indicates that CO_2 is bound to O_a only via dispersion forces. Temperature dependent studies (100 - 150 K) show that the CO_2 binding energy next to O_a 's is smaller by ~ 20 mV than that on V_O 's. At 50 K, however, the adsorption of CO_2 on V_O is partially hindered by the higher adsorption barrier. CO_2 molecules diffusing between two $\text{CO}_2/\text{O}_\text{a}$ complexes are found to move fast compared to the STM sampling rate and are imaged as a time average of all CO_2 binding configurations on Ti sites. DFT studies reveal the rotation-tumbling mechanism for CO_2 diffusion with a very low diffusion barrier (~ 50 meV) in agreement with the experiment.

X.L. is grateful for the support of the Linus Pauling Distinguished Postdoctoral Fellowship Program at PNNL. This work was supported by the US Department of Energy, Office of Basic Energy Sciences, Division of Chemical Sciences, Geosciences & Biosciences. A portion of the research was performed using EMSL, a national scientific user facility sponsored by the Department of Energy's Office of Biological and Environmental Research and located at Pacific Northwest National Laboratory (PN NL). PNNL is a multiprogram national laboratory operated for DOE by Battelle.

9:40am **SS+EN+OX-ThM6 Probe of NH₃ and CO Adsorption on the Very Outermost Surface of a Porous TiO₂ Adsorbent Using Photoluminescence Spectroscopy**, A. Stevanovic, J.T. Yates, Jr., University of Virginia

The photoluminescence (PL) of powdered TiO₂ at 529.5 nm (2.34 eV) has been found to be a sensitive indicator of UV-induced band structure modification. As UV irradiation occurs, the positive surface potential changes and shifts the depth of the depletion layer. It was found that UV light (3.88 eV) induces a positive surface potential which diminishes band bending in n-type TiO₂ and enhances PL. Also, adsorbates modify the PL intensity by exchanging charge with TiO₂, producing a change in the surface band bending structure.

In addition, we employ photoluminescence (PL) spectroscopy to probe the development of adsorbed layers on the very outermost surface sites of a porous solid adsorbent (TiO₂) in a depth of 20 nm where the meso-pores, separating 30-80 nm TiO₂ particles, join the gas phase. In parallel, we also employ transmission infrared (IR) spectroscopy to gain insight into the extent of adsorption averaged over the entire depth of the diffusion process. The combination of the two surface spectroscopies (PL and IR) allows one to observe the kinetics of transport of adsorbate molecules between the very outermost surface region (where adsorption first occurs) and the interior of the powdered substrate. The transport is governed by the surface mobility of the adsorbate molecules, and hysteresis effects in adsorption/desorption are observed.

References:

1. Stevanovic, A.; Buttner, M.; Zhang, Z.; Yates, J. T., Jr., Photoluminescence of TiO₂: effect of UV light and adsorbed molecules on surface band structure. *Journal of the American Chemical Society* **2012**, *134*, (1), 324-32.
2. Stevanovic, A.; Yates, J. T., Jr., Probe of NH₃ and CO Adsorption on the Very Outermost Surface of a Porous TiO₂ Adsorbent Using Photoluminescence Spectroscopy. *Langmuir: the ACS journal of surfaces and colloids* **2012**, *28*, (13), 5652-9.

Work supported by the Army Research Office.

10:40am **SS+EN+OX-ThM9 Site-Specific Photocatalytical Reactions of O₂ on TiO₂(110)**, Z.-T. Wang, Pacific Northwest National Laboratory, N.A. Deskins, Worcester Polytechnic Institute, I. Lyubinsky, Pacific Northwest National Laboratory

Photo-stimulated reactions on TiO₂ have attracted much attention due to the variety of potential applications ranging from a hydrogen production by water splitting to environmental remediation through organic pollutant oxidation. In majority of these processes, the oxygen plays a crucial role. A better understanding of the fundamental aspects of oxygen on TiO₂ can potentially lead to improvements or developments of the TiO₂ applications. We present the direct observation at an atomic level with high-resolution scanning tunneling microscopy of photostimulated reactions of single O₂ molecules on reduced TiO₂(110) surfaces at 50 K. The critical relation between photoreactivity and adsorption sites on TiO₂ is demonstrated. Two distinct reactions of O₂ desorption and dissociation occur at different active sites of terminal Ti atoms and bridging O vacancies, respectively. These two reaction channels follow very different kinetics. While hole-mediated O₂ desorption is promptly and fully completed, electron-mediated O₂ dissociation is much slower and is quenched above some critical O₂ coverage. Density functional theory calculations indicate that both coordination and charge state of an O₂ molecule chemisorbed at specific site largely determine a particular reaction pathway.

11:00am **SS+EN+OX-ThM10 Bond Selectivity in the Activation of n-alkanes on PdO(101)**, J.F. Weaver, A. Antony, C. Hakanoglu, F. Zhang, University of Florida, A. Asthagiri, The Ohio State University

We have investigated initial C-H bond selectivity in the activation of propane and n-butane on PdO(101) both experimentally and computationally. Temperature-programmed experiments using different propane isotopologues reveal a strong preference toward primary C-H bond cleavage of propane on PdO(101); about 90% of the propane molecules which react do so by primary C-H bond activation. Direct measurements of the initial dissociation probability of various n-butane isotopologues also demonstrate a high selectivity for primary C-H bond activation of n-butane on PdO(101) at low coverages. Unlike propane, however, TPRS experiments show that the preference for primary C-H bond cleavage of n-butane diminishes with increasing molecular coverage. Calculations using dispersion-corrected DFT reproduce the selectivity toward primary C-H bond cleavage of propane and n-butane on PdO(101), and predict that alkane C-H bond scission occurs heterolytically on the oxide surface. The calculations suggest that greater substituent polarization in the 1-alkyl

transition structures is responsible for the lower energy barriers for primary vs. secondary C-H bond activation of alkanes on PdO(101).

11:20am **SS+EN+OX-ThM11 Photoresponse, Electronic Transport and Magnetic Properties of Ti-doped (Cr_xFe_{1-x})₂O₃**, S.E. Chamberlin, T.C. Kaspar, M.E. Bowden, V. Shuthanandan, S.A. Chambers, M.A. Henderson, Pacific Northwest National Laboratory

There is widespread interest in discovering materials that can effectively harvest sunlight in the visible region of the electromagnetic spectrum in order to drive chemical processes on surfaces. Hematite (Fe₂O₃) has received renewed interest recently as the active photoanode in photoelectrochemical (PEC) water splitting to store solar energy as H₂. Hematite has three key advantages which make it appealing: it is very abundant, it has a bandgap of 2.2 eV, which is suitably narrow to harvest incident solar radiation, and it is sufficiently stable in the aqueous solutions required for PEC water splitting. However, hematite is a charge-transfer insulator with extremely poor electron and hole mobilities, which results in short hole diffusion lengths and ultrafast recombination of photogenerated electron/hole pairs before charge separation can occur. Substitutional Ti(IV) at an Fe(III) site should be a donor, and epitaxial Ti-doped α-Fe₂O₃ exhibits significantly enhanced conductivity relative to pure hematite when grown under certain conditions by oxygen-assisted molecular beam epitaxy (OAMBE) on α-Al₂O₃(0001) substrates.¹ In addition, Mashiko *et al.*² have shown that the bandgap of pure hematite can be reduced to 1.7 eV by alloying with Cr(III) in epitaxial films. Combining these approaches is expected to result in material with both a reduced bandgap and favorable electrical conductivity, which will facilitate visible-light photoactivity. Heteroepitaxial thin films of (Fe_{1-x}Cr_x)₂O₃ and (Fe_{1-x-y}Cr_xTi_y)₂O₃ were deposited on α-Al₂O₃(0001) substrates by OAMBE. Film quality was monitored *in situ* by reflection high energy electron diffraction (RHEED). *In situ* x-ray photoemission spectroscopy (XPS) was utilized to characterize the charge states of the cations. Film crystallinity and lattice parameters were determined *ex situ* by high resolution x-ray diffraction (HRXRD). Rutherford backscattering spectrometry (RBS) in both random and channeling geometries confirmed the film stoichiometry, and elucidated the degree of substitution of the cations in the lattice. Preliminary optical absorption measurements and photochemistry experiments will be presented.

1. B. Zhao, T. C. Kaspar, T. C. Droubay, J. McCloy, M. E. Bowden, V. Shuthanandan, S. M. Heald, and S. A. Chambers, *Phys. Rev. B* **84**, 245325 (2011).

2. H. Mashiko, T. Oshima, and A. Ohtomo, *Appl. Phys. Lett.* **99**, 241904 (2011).

11:40am **SS+EN+OX-ThM12 A Nonadiabatic Mechanisms of Inequilibrium Charge Carriers Production in Pd/n-GaP Schottky Nanodiode Exposed to Atomic Hydrogen**, S.V. Simchenko, V. Styrov, Azov State Technical University, Ukraine

Since the recent discovery of production of electronic flows in Schottky diodes with nanosized "top" metal layer due to ballistic metal-to-semiconductor transport of hot electrons formed by the surface exoergic chemical reaction, e.g. [1], this effect attracts attention of scientists owing to its fundamental and practical potential. Here we investigate a new system of that kind, namely Pd-(n)GaP planar Schottky diode (15 nm Pd-layer) placed in the atmosphere of atomic hydrogen. We found the steady-state current flow through the system under consideration in perpendicular direction to the metal surface on which the hydrogen atoms stationary recombine into molecules.

We elaborated a new approach to detect production of the inequilibrium charge carriers via nonadiabatic channel by observing the current-voltage characteristic of the Schottky diode in the presence and absence of the atomic flux incident on the structure. The nonequilibrium nature of the additional carriers is confirmed by kinetics measurements: the current drops to its initial value in the absence of atoms practically momentarily once the atoms are "switched off" and jumps immediately to its excited value when atoms are "switched on" (at the given temperature of the structure and the fixed forward voltage bias on the structures). We were able to draw some quantitative information about the processes of generation of nonequilibrium electron-hole pairs in the reaction of recombination of hydrogen atoms on Pd-surface and their transport in the metal film. The short circuit current is expressed in terms of yield of the chemoexcited carriers and probability of their survival while traveling through the Pd-film.

For a 1V forward bias the current drastically grows from 3 nA to 950 uA; thus the bias allows gaining chemicurrent value as large as five orders of magnitude. This result can be of significant importance for the practical applications of the nonequilibrium chemiconductance and chemicurrents in Schottky nanostructures including sensing and chemical-to-electricity energy conversion.

[1] B. Georgen, H.Nienhaus, W.H. Weinberg, E. McFarland. *Science*, 294, 2521 (2003)

Surface Science

Room: 22 - Session SS-ThM

Molecular Films: Chirality & Electronic Features

Moderator: A.J. Gellman, Carnegie Mellon University, S.L. Tait, Indiana University - Bloomington

8:00am **SS-ThM1 Smooth and Transparent Organic Surfaces showing Exceptional Dynamic Dewetting Behavior Toward Nonpolar Liquids ~ Oleophobicity is Independent on Length of Perfluoroalkyl Groups ~**, A. Hozumi, J. Park, D.F. Cheng, B. Masheder, C. Urata, AIST, Japan

Perfluorinated compounds such as perfluoroalkylsilanes (FASs) and related materials have been widely employed in a wide variety of engineering fields by taking advantages of their excellent hydrophobic/oleophobic properties. However, their chemical and physical effects on human health and the environment have been lately viewed with suspicion. In particular, the use of long-chain perfluorinated chemicals (LCPFCs) is going to phase out by the end of 2015. An alternative hydrophobic/oleophobic treatment method not requiring LCPFCs has been strongly demanded.

In this study, we report smooth and transparent organic surfaces showing unusual dynamic dewetting behavior toward nonpolar liquids. We prepared two different surfaces on glass slides: one, organic surfaces consisting of self-assembled monolayers (SAMs) of FASs with different chain length [CF₃(CF₂)_nCH₂CH₂Si(OR)₃, n = 0, 3, 5, 7, R=CH₃ or C₂H₅], and the other, organic surfaces derived from a mixture of FASs and tetramethoxysilane (TMOS). Oleophobicity on the former surfaces was markedly depended on the length of perfluoroalkyl chains, but the latter exhibited excellent dynamic oleophobicity toward various kinds of nonpolar liquids, independent of the length of the perfluoroalkyl chains. Due to the addition of TMOS, condensed silica species most likely acted as spacer moieties such that an appropriate distance now separated the perfluoroalkyl chains allowing them to rotate freely and confer liquid-like properties on the surface [1,2]. This leads to the exceptional dynamic dewetting behavior toward various nonpolar liquids.

[1] A. Hozumi and T. J. McCarthy, *Langmuir*, 26 (2010) 2567-2573.

[2] D. F. Cheng, C. Urata, M. Yagihashi and A. Hozumi, *Angew. Chem. Int. Ed.*, 51 (2012) 2956-2959.

8:20am **SS-ThM2 Enantioselective Separation on Chiral Au Nanoparticles**, N. Shukla, N. Khosla, N. Ondeck, A.J. Gellman, Carnegie Mellon University

Adsorption of chiral compounds on chiral surfaces is the initial step in enantioselective processes such as separations and catalysis. There has been a significant effort over the past decade aimed at the preparation of chiral nanoparticles based on metallic cores modified by chiral ligands. In principle, these can serve as the basis for enantioselective chemical processing. In this work we demonstrate a simple measurement of enantioselective adsorption on chiral metal nanoparticles using a method that can yield quantitative measures of the enantiospecific adsorption equilibrium constants [1].

The surfaces of chemically synthesized Au nanoparticles have been modified with D- or L-cysteine to render them chiral and enantioselective for adsorption of chiral molecules. Their enantioselective interaction with chiral compounds has been probed by optical rotation measurements when exposed to racemic propylene oxide. The ability of optical rotation to detect enantiospecific adsorption arises from the fact that the specific rotation of polarized light by R- and S-propylene oxide is enhanced by interaction Au nanoparticles. This effect is related to previous observations of enhanced circular dichroism by Au nanoparticles modified by chiral adsorbates. More importantly, chiral Au nanoparticles modified with either D- or L-cysteine selectively adsorb one enantiomer of propylene oxide from a solution of racemic propylene oxide, thus leaving an enantiomeric excess in the solution phase. Au nanoparticles modified with L-cysteine (D-cysteine) selectively adsorb the R-propylene oxide (S-propylene oxide). A simple model has been developed that allows extraction of the enantiospecific equilibrium constants for R- and S-PO adsorption on the chiral Au nanoparticles.

[1] N. Shukla, M.A. Bartel, A.J. Gellman "Enantioselective separation on chiral Au nanoparticles" *Journal of the American Chemical Society*, 132(25), (2010), 8575-8580

8:40am **SS-ThM3 2012 AVS Peter Mark Award Lecture: Effects of Chirality in Electron Tunneling, Molecular Excitation and Rotation**, C.H. Sykes*, Tufts University **INVITED**

Industrially, the selective conversion of prochiral reagents to chiral products is a crucial step in the production of a variety of asymmetric pharmaceuticals. While this feat is accomplished using either chiral catalysts or crystallization, many external influences have been shown to be capable of inducing such symmetry breaking including circularly polarized light, spin-polarized electrons, and combinations of unpolarized light and magnetic fields. Pioneering studies have made great strides towards explaining these various interactions, however many of the fundamental mechanisms by which chirality is transferred at the molecular-level are not yet fully understood. It is also a great challenge to design experimental setups with which to study these phenomena in a quantitative and reproducible manner. We report a simple thioether system in which symmetry breaking can be both induced and measured in situ at the single-molecule level. We demonstrate that electrical excitation of a prochiral molecule on an achiral surface produces large enantiomeric excesses in the chiral adsorbed state of up to 40%, whereas thermal annealing produces racemic mixtures as expected. These effects arise from a previously unreported phenomenon that standard polycrystalline metal scanning probe tips can possess intrinsic chirality.

Thioethers also constitute a simple, robust system with which to study molecular rotation as a function of temperature, electron energy, applied fields, and proximity of neighboring molecules. In order for molecules to be used as components in molecular machines, methods are required to couple individual molecules to external energy sources and to selectively excite motion in a given direction. Studying the rotation of molecules bound to surfaces offers the advantage that a single layer can be assembled, monitored and manipulated using the tools of surface science. We report that a butyl methyl sulfide (BuSMe) molecule adsorbed on a copper surface can be operated as a single-molecule electric motor. Electrons from a scanning tunneling microscope are used to drive directional motion of the BuSMe molecule in a two terminal setup. Moreover, the temperature and electron flux can be adjusted to allow each rotational event to be monitored at the molecular-scale in real time. The direction and rate of the rotation are related to the chiralities of the molecule and the tip of the microscope (which serves as the electrode), which again illustrates the importance of the symmetry of the metal contacts in atomic-scale electrical devices.

9:20am **SS-ThM5 Single-Site Studies of Chirality Transfer Complexes on Chirally Modified Pt(111)**, J.-C. Lemay, P.H. McBreen, V. Demers-Carpentier, G. Goubert, Y. Dong, Université Laval, Canada, B. Hammer, A.M.H. Rasmussen, L. Ferrighi, Aarhus University, Denmark, F. Masini, Université Laval, Canada

Stereoselective catalytic sites on achiral metallic surfaces may be prepared by adsorbing optically active compounds described as chiral modifiers. A fundamental understanding of the stereodirecting forces in such systems is necessary to develop more efficient enantioselective catalysts. We will present data for chirality transfer complexes formed by the chiral modifier (*R*)-(+)-1-(1-naphthyl)ethylamine ((*R*)-NEA) and pro-chiral α -phenylketone and α -ketoester substrates on Pt(111). Time-lapsed scanning tunneling microscopy allowed us to isolate individual chiral modifier/substrate complexes. The structure of the diastereomeric complexes were separately determined using DFT calculations. The extremely good convergence between the calculated structures and visual STM data, as well as supporting surface spectroscopy data, shows that prochiral steering on chirally modified Pt(111) can be followed with submolecular resolution at the reaction temperature (room temperature), thus enabling conformational, regiospecific and enantiospecific characterisation. The study reveals the contributions of steric repulsion, non-covalent attractive interactions and site-specific chemisorption to stereoinduction. We will conclude with a short description of the targeted design of new chiral modifiers.

9:40am **SS-ThM6 Chirality in Flatland: 2D Crystallization, Single-Molecule Dynamics and Unidirectional Rotors**, K.-H. Ernst, EMPA, Switzerland

A promising approach to study chiral molecular recognition is studying two-dimensional (2D) crystallization phenomena on well-defined surfaces via scanning tunneling microscopy (STM). We present studies on different two-dimensional chiral systems and discuss their tendency to undergo

* Peter Mark Memorial Award Winner

enantiomeric separation. A special surface enantiomorphism is observed via STM after adsorption of the enantiomers of a helical aromatic hydrocarbon on Cu(111). Instead of crystallization into homochiral 2D domains on the surface, racemic enantiomorphs are observed. In this situation, a small excess of one enantiomer is sufficient to create domains possessing single handedness throughout the entire surface layer. The induction of homochirality by chiral doping has also been observed for succinic acid and achiral (*R,S*)-tartaric acid. Our findings are explained by cooperative interactions between many chiral units, similar to the mechanism of chiral amplification observed in helical polymers and coined as "Sergeants-and-soldiers" principle. Another recently observed phenomenon is single enantiomorphism due to chiral conflict. Depending on the handedness of a chiral adduct to a racemic situation suppresses one enantiomorph during crystal growth, but supports the other by forming a quasiracemic solid solution. Finally, we present chirality aspects in single molecule surface dynamics, including conversion of adsorbate handedness and linear, unidirectional propulsion of a molecular car with chiral "wheels".

10:40am **SS-ThM9 Functional Molecular Layers for Energy Applications**, *R.J. Hamers*, University of Wisconsin-Madison **INVITED**

Electrode materials for renewable energy applications are largely based on materials such as metal oxides and various forms of carbon because of their intrinsically high stability. However, the properties can be markedly enhanced through the integration of "smart" molecular functionalities. We have been investigating the development and application of new chemistry for fabricating novel types of electrochemically and photoelectrochemically active molecular structures on surfaces of metal oxides and on thin-film diamond. One area of interest has been the use of "click" chemistry as a versatile approach to functionalizing surfaces with redox-active molecules that can be used either as potential catalysts or as light-harvesting molecules. By using complementary functionalization on two different nanostructured oxides, it is also possible to make chemically-assembled oxide-oxide heterojunctions, such as TiO₂/SnO₂. In these cases the formation of a heterojunction can provide a built-in potential to enhance charge transfer at the interface.

A key question in these studies has been understanding how the presence of alkyl chain, ranging from ~4 atoms to ~12 atoms, impacts the electron transfer. While most previous work on molecular layers has been performed on densely packed layer on coinage metals such as gold and silver, when molecular layers are tethered to covalent materials such as diamond or metal oxides, the resulting layers have a high degree of disorder due to the mismatch between the native packing of the alkyl chains and the distribution of available surface sites. We have investigated the electron-transfer properties at these functionalized interfaces and find that the electron transfer rates are surprisingly high and only weakly dependent on the length of the alkyl chain, which we explain as a result of the increased conformational disorder. Our data suggest that the "best" molecular layers for electron-transfer applications are those that have a controlled degree of conformational disorder. We demonstrate these effects using recent measurements of electroactive Ru(bpy)-based complexes on diamond and on metal oxides.

11:20am **SS-ThM11 Atomic Study for P-type Doping Process of CuPc Molecules with STM**, *J.H. Park, K. Tyler, C.T. William, A.C. Kummel*, University of California San Diego

Metal phthalocyanines (MPc) have been widely employed as channel materials in organic thin film transistor (OTFT) for chemical vapor sensing, due to their novel gas adsorption properties. Theoretically, MPc molecules act electron donors during reaction with oxidative analytes and are the basis of their chemical sensing. However, this sensing reaction has not been understood fully. This study presents molecular scale observation of NO adsorption onto CuPc monolayers using ultra-high vacuum (UHV) scanning tunneling microscopy (STM). CuPc monolayers were deposited on Au(111) surfaces by organic molecular beam epitaxy in ultra-high vacuum (UHV) and subsequently dosed at 150 K substrate temperature with NO (5% : diluted by He of 95 %) via a supersonic molecular beam source (MBS). After dosing NO for 1 min, STM images reveal small NO chemisorption sites on the CuPc metal centers and ~4 % of CuPc molecules are reacted with NO. Un-reacted central Cu²⁺ ion of CuPc appears as dark hole in both of empty and filled states STM images. Conversely, after chemisorption of NO, the topographic appearance of core metal ion is modified into a bright spot, while the 4-leaf pattern of ring still remain. As dosing duration increases to 10 min, the coverage of NO chemisorption sites increases to ~7 %. However this coverage increase is sublinear and further dosing does not increase the coverage consistent with a chemisorption induced change in electronic structure. In order to study the electronic structure of NO chemisorption onto CuPc molecules, scanning tunneling spectroscopy (STS) data was also obtained. Unreacted CuPc has a Fermi level (E_F) almost in the middle of the band gap. However, after NO chemisorption, this central E_F shifts to the highest occupied molecular

orbital (HOMO) and this transition indicates CuPc molecules is doped to 'p-type' by NO. This 'doping' process of NO is in good agreement with previously published theoretical predictions and is consistent with the high sensitivity of CuPc film to strong oxidants in CuPc OTFT chemical sensors.

11:40am **SS-ThM12 Formation of 2D Superstructure with Wide Band-gap n-type Behavior**, *T.K. Shimizu, J. Jung*, RIKEN, Japan, *T. Otani*, University of Tokyo, Japan, *Y.-K. Han*, Korea Basic Science Institute, *M. Kawai*, University of Tokyo, Japan, *Y. Kim*, RIKEN, Japan

A two-dimensional superstructure of molecules with high electron affinity was successfully formed on Au(111), and it indicated wide band-gap n-type behavior. The molecule used was fluorinated fullerene (C₆₀F₃₆). Although there exist three isomers (C₃, C₁, and T) in our molecular source, scanning tunneling microscopy (STM) images and density functional theory (DFT) calculations suggested that the molecules in the well-ordered region consisted of only the C₃ isomer. Its LUMO distribution governs the adsorption orientation due to partial electron transfer from Au to the molecule. The intermolecular C-F...p electrostatic interactions determines the lateral orientation of C₆₀F₃₆ molecules.

[Ref] Shimizu et al., ACS Nano 6, 2679-2685 (2012).

Thursday Afternoon, November 1, 2012

Electron Transport at the Nanoscale Focus Topic

Room: 16 - Session ET+SS+GR+SP-ThA

Electron Transport at the Nanoscale: Molecules and Defects

Moderator: S. Allen, The University of Nottingham, UK, J. Wendelken, Oak Ridge National Laboratory

2:00pm **ET+SS+GR+SP-ThA1 Molecule Substrate Interactions Probed by Scanning Tunneling Microscopy, H.-J. Gao, Chinese Academy of Sciences** **INVITED**

Molecule substrate interactions play an important role in constructing nanostructures of functionalities and controlling of the physical properties and thus have stimulated a great interest in the past decades. One of the challenges in this top is to make a single molecule or small quantum systems stably connected to a single metal atom on metal surfaces, and further to make the nanostructure create electric energy and optical/electro radiation. In the talk, I will present that by using Au adatoms of the Au(111) surface we have successfully formed a single molecule rotor array, isolated tetra-*tert*-butyl Zinc Phthalocyanine ((*t*-Bu)₄-ZnPc) molecules sticking to the Au adatoms of the Au(111) and rotating on the surface at 78 K. This kind of single molecular rotor was also found to be controlled by the different sites of the Au(111) surface using low temperature scanning tunneling microscopy (STM). Furthermore, by changing the molecular structure the same molecular family of the Pc, ZnPc and FePc can also modulate the rotation behavior of the molecular rotors. Given that the lateral structure of a molecule/substrate interface can be modified by the attachment of ligands, our results will be helpful for opening up the possibility to tailor physical properties of a single molecule or complex aggregates to the desired specifications.

2:40pm **ET+SS+GR+SP-ThA3 Electron Localization in Single Mixed-Valence Molecules, R.C. Quardokus, N.A. Wasio, Y. Lu, S.A. Kandel, University of Notre Dame**

Scanning tunneling microscopy (STM) is used to study two dinuclear organometallic molecules, meta-Fe₂ and para-Fe₂. These molecules share identical molecular formulas but differ in their positions of connectivity to the central phenyl ring. STM images of neutral meta-Fe₂ and para-Fe₂ show symmetrical distribution of electron density across the two metal centers. Chemical oxidation of these molecules leads to mixed-valence species. STM images of mixed-valence meta-Fe₂ show an asymmetric distribution of the electron density between the two metal centers. Despite the greater distance between the two metal centers, the electron density remains symmetric in mixed-valence para-Fe₂. Comparison with constrained density functional (CDFT) calculations leads to the conclusion that through-bond coupling of the two metal centers is more prevalent than through-space coupling. Further investigation of mixed-valence dinuclear organometallic molecules with asymmetric electron state density may open up the possibility for their use in molecularly based electronic devices.

3:00pm **ET+SS+GR+SP-ThA4 Rectification by a Single Molecular Diode, L. Adamska, University of South Florida, M. Kozhushner, Institute of Chemical Physics, Russian Academy of Sciences, I.I. Oleynik, University of South Florida**

Single-molecule rectification has been recently observed using the STM modulated break-junction technique in non-symmetric diblock dipyrimidinyl-diphenyl molecule covalently bound to metallic electrodes. To provide an insight to the nature of the rectification, first-principles calculations of atomic, electronic and transport properties of gold/molecule/gold junctions have been performed for both symmetrical tetraphenyl and asymmetrical dipyrimidinyl-diphenyl diblock molecules. The charge transport was found to occur by hole resonant tunneling mechanism via positively-charged hole states of the molecule, which are very susceptible to the external electric field and dispersive interactions with the metallic electrodes. It was found that the rectification effect in chemically-asymmetric dipyrimidinyl-diphenyl molecule is due to strong localization of the hole wave function at one end of the diblock under applied electric field. Such behavior is contrasted by symmetric I-V curves exhibited by symmetric tetraphenyl molecule.

3:40pm **ET+SS+GR+SP-ThA6 Electron Transport Study of Graphene Grain Boundaries Using Scanning Tunneling Potentiometry, K. Clark, X.-G. Zhang, I. Vlasiouk, A.-P. Li, Oak Ridge National Laboratory**

Graphene, due to its unique electronic structures, has quickly become one of the most notable "super-materials" poised to transform the electronics and nanotechnology landscape. The symmetry of the graphene honeycomb lattice is a key element for determining many of graphene's unique electronic properties, such as the linear energy-momentum dispersion and the reduced backscattering (i.e., high carrier mobility). However, topological lattice defects, such as grain boundaries and step edges, break the sublattice symmetry and can affect the electronic properties, especially in transport of graphene in unexpected ways. To utilize the full potential of graphene a complete understanding of the physical and electronic properties of defects in this system is needed. By using a scanning tunneling potentiometry method with a low temperature four-probe scanning tunneling microscope, two-dimensional maps of electrochemical potentials have been measured across individual grain boundaries on the graphene films grown on copper foil and transferred to SiO₂. An Atomic Force Microscope (AFM) is implemented to image the grain boundary that forms between individual graphene flakes that grow on the surface. The AFM imaging along with scanning tunneling potentiometry characterize the grain boundaries formed between coalesced grains on the SiO₂ surface. Results of the influence of the grain boundary on the electronic transport across this potentially revolutionary new electronic system will be presented. This research was conducted at the Center for Nanophase Materials Sciences, which is sponsored at Oak Ridge National Laboratory by the Office of Basic Energy Sciences, U.S. Department of Energy.

4:00pm **ET+SS+GR+SP-ThA7 Static and Dynamic Conductance in Topological Defects in Ferroelectrics, S.V. Kalinin, Oak Ridge National Laboratory** **INVITED**

Topological defects in ferroic materials are attracting much attention both as a playground of unique transport, magnetic, and ferroic phenomena and due potential applications in reconfigurable electronic devices. In this presentation, I will summarize recent studies of transport phenomena in 2D (domain walls) and 1D (vortexes and antivortexes) in ferroelectric materials by combination of piezoresponse force microscopy, phase-field modelling, and density functional theory. In particular, the observations such as memory effects and hysteresis in domain wall conductance, metallic conductivity of ferroelectric walls, and conductivity in vortex cores will be discussed. For domain walls, these observations are consistent with carrier accumulation due to presence of charged wall segments. We further demonstrate that a continuum of non-volatile metallic states across decades of conductance can be encoded in the size of ferroelectric nanodomains using electric field. For vortexes, modelling predicts that the core structure can undergo a reversible transformation into a metastable twist structure, extending charged domain walls segments through the film thickness. The vortex core is therefore a dynamic conductor controlled by the coupled response of polarization and electron/mobile vacancy subsystems with external bias. This controlled creation of conductive 1D channels opens a pathway for design and implementation of integrated oxide electronic devices based on domain patterning. Finally, recent insight on domain walls structure from combination of aberration corrected scanning transmission electron microscopy and phase-field theory will be discussed. Research supported (SVK) by the U.S. Department of Energy, Basic Energy Sciences, Materials Sciences and Engineering Division and partially performed at the Center for Nanophase Materials Sciences, a DOE-BES user facility.

4:40pm **ET+SS+GR+SP-ThA9 Transport and Mechanical Properties of Molecular Junctions formed by Acetophenon Deposited on Si (100) Surface, M. Setvin, Z. Majzik, O. Krejci, P. Hapala, P. Jelinek, Institute of Physics of ASCR, Czech Republic**

One of the main challenges of Molecular electronics is to understand and control charge transfer through a reproducible single molecule contact between electrodes. Most investigations of electron transport through molecules have been performed in "blind" junction experiments, where the molecular conformation and contact geometry cannot be probed. Therefore large gaps in our knowledge remains since in molecular electronics the atomic-scale structure of the entire junction including the leads is important for its conductance properties.

Our goal is to study electrical transport through well-defined molecular junction on semiconductor surfaces. Formation of molecular junctions using organic molecules on semiconductor surfaces might lead to interesting phenomena. For example, the presence of the band gap in electrodes can

lead to the negative differential resistance observed in transport through molecules bonded to dangling-bond sites[1].

In this contribution, we investigate formation of molecular junction consisting of a single acetophenone molecule deposited on Si(100) surface in upright position by means of simultaneous AFM/STM measurements and DFT calculations. We used a modified UHV VT STM/AFM Omicron machine allowing simultaneous acquisition of the current and forces with atomic resolution using a tuning fork sensor[2]. The simultaneous acquisition of the tunneling current and force during tip approach allows precise control of contact formation and its consequence on the charge transport through molecular junction[3]. On other hand, DFT simulations provide more insight into interaction mechanism between probe and molecule. It also helps to understand induced structural and electronic relaxations during tip approach.

References

- [1] T. Rakshit et al. Nanoletters 4, 1803–1807 (2004).
- [2] Z. Majzik et al, Beilstein J. Of Nanotech. 3, 249 (2012).
- [3] N. Fournier et al Phys. Rev. B 84, 035435 (2011).

5:00pm ET+SS+GR+SP-ThA10 Experimental Determination of the Charge Neutrality Level (CNL) of Conjugated Polymers, *W. Wang, R. Schlaf*, University of South Florida

The charge neutrality levels (CNL) of poly-(3-hexylthiophene) (P3HT) and poly-[2-methoxy-5-(2'-ethylhexyloxy)-p-phenylene vinylene] (MEH-PPV) were determined. This was achieved by investigating a number of interfaces between these conjugated polymers and metals with varying work function. The interfaces were fabricated using the electrospray deposition technique, which allows the direct deposition of polymers from solution into vacuum environment without interference of significant surface contamination. This enabled the measurement of the charge injection barriers at clean polymer interfaces without contamination interlayer with photoemission spectroscopy. The results of these measurements enabled the establishment of the correlation between barrier heights and substrate. The results indicate that conjugated polymer interfaces form in a similar fashion as small molecular materials interfaces to metals as described by the 'induced density of states' (IDIS) model. In contrast, the presented results also suggest that the 'integer charge transfer' (ICT) model, which was developed for polymer/metal interfaces, only describes interfaces prepared under atmosphere or inert environment, where the presence of contamination weakens the interaction between the materials in contact.

5:20pm ET+SS+GR+SP-ThA11 Investigation on the Electronic Structure of Arylthio (ArS)-functionalized CdSe Nanoparticle Hybrid Materials, *Z. Li*, University of South Florida, *K. Mazzi*, University of Washington, *S. Gutmann*, University of South Florida, *C.K. Luscombe*, University of Washington, *R. Schlaf*, University of South Florida

CdSe nanoparticles are a promising material for 3D heterojunction solar cells due to their tunable electronic and optical properties through size control. By covalently bonding these nanoparticles to organic ligands, a novel light absorption, charge separation and transportation system can be formed. This presentation will discuss efforts to measure the hybrid-internal orbital line-up at the nanoparticle/ligand junction. Photoemission spectroscopy was used to characterize a prototypical arylthio (ArS)-functionalized CdSe molecule nanoparticle/ligand hybrid. Generally, in such hybrid molecules, the highest occupied molecular orbital (HOMO) emission is a superposition of the emissions of the nanoparticles and that of the organic ligands. This superposition makes the direct study of the orbital line-up through PES measurements impossible. Hence, a new technique needed to be developed to delineate the orbital line-up at such inner-molecular contacts. This was achieved through the additional investigation of the isolated components, which yielded detailed information of their electronic structure. Combination of this data with measurements on the assembled hybrid molecules enabled the determination of the orbital line-up at the interface. The influence of the covalent bond on the orbital line-up was investigated by comparing the hybrid line-up with the electronic structure of a physisorbed interface formed between the hybrid components. This interface was prepared through in-vacuum electrospray deposition of a thin film sandwich of CdSe and ArSH films, while measuring the transition from the CdSe to the ArSH electronic structure.

Graphene and Related Materials Focus Topic Room: 13 - Session GR+EM+NS+SS+TF-ThA

Beyond Graphene: BN and Other 2D Electronic Materials; 2D Heterostructures

Moderator: I.I. Oleynik, University of South Florida

2:00pm GR+EM+NS+SS+TF-ThA1 X-ray Photoelectron Spectroscopy Investigation of the Valence and Conduction Band Offset at Hexagonal a-BN:H/Si Interfaces, *S. King, M. French, J. Bielefeld*, Intel Corporation, *M. Jaehnig*, Intel Corporation, *M. Kuhn, B. French*, Intel Corporation

Due to a wide band gap (~ 6 eV) and close lattice matching, hexagonal boron nitride (h-BN) is of interest as a potential gate dielectric in graphene channel transistor devices. A key property for the success of h-BN as a gate dielectric in such devices is the valence and conduction band offsets at the h-BN/graphene and h-BN/gate electrode interfaces. In many graphene channel devices, amorphous or poly-Si is a desirable gate electrode material for compatibility in standard CMOS processing. In this regard, we have utilized x-ray photoelectron spectroscopy (XPS) to determine the valence band offset present at the interface between plasma enhanced chemically vapor deposited hexagonal a-BN:H and a (100) Si substrate. Combined with Reflection Electron Energy Loss Spectroscopy measurements of the a-BN:H band gap, we have also been able to determine the conduction band offset at this interface. The combined measurements indicate a type I alignment with valence and conduction band offsets of 1.95 ± 0.1 and 2.15 ± 0.17 eV respectively.

2:20pm GR+EM+NS+SS+TF-ThA2 Monolayer Graphene-Boron Nitride 2D Heterostructures, *R. Cortes, J. Lahiri, E. Sutter, P.W. Sutter*, Brookhaven National Laboratory

Unusual electronic properties have been predicted for monolayer graphene-boron nitride heterostructures, but access to these properties depends on methods for controlling the formation of graphene-boron nitride interfaces [1]. Here we report on the growth and interface formation of monolayer graphene (MLG)-hexagonal boron nitride (h-BN) 2D heterostructures on Ru(0001), investigated by a combination of real-time low-energy electron microscopy (LEEM) and scanning tunneling microscopy (STM).

LEEM observations of sequential chemical vapor deposition growth show that h-BN attaches preferentially to the edges of existing MLG domains, while nucleation of h-BN on the Ru surface away from MLG is not observed at the conditions considered here. With increasing coverage, h-BN expands anisotropically and, ultimately, the substrate is covered by a continuous 2D membrane of MLG domains embedded in h-BN. The study of the 1D interface between MLG and h-BN in these membranes by STM demonstrates that, following sequential growth at high temperatures, the interface is not abrupt, but contains an intermixed zone consisting of h-BN with embedded carbon atoms. Using quantitative LEEM, we have identified processes that eliminate this intermixing and pave the way to atomically sharp graphene-boron nitride boundaries, as confirmed by STM. The application of a similar growth procedure to terminate the edges of atomically controlled graphene nanoribbons with h-BN, embedding them in a h-BN membrane, will be considered.

[1] P. Sutter, R. Cortes, J. Lahiri, and E. Sutter. *Submitted* (2012).

2:40pm GR+EM+NS+SS+TF-ThA3 Large Area Vapor Phase Growth and Characterization of MoS₂ Atomic Layers, *J. Lou, S. Najmaei, Z. Liu, Y. Zhan, P. Ajayan*, Rice University

INVITED

Monolayer Molybdenum disulfide (MoS₂), a two-dimensional crystal with a direct bandgap, is a promising candidate for 2D nanoelectronic devices complementing graphene. Unlike conductive graphene and insulating h-BN, atomic layered MoS₂ is a semiconductor material with a direct bandgap, offering possibilities of fabricating high performance devices with low power consumption in a more straight-forward manner.

In this talk, we will discuss our recent efforts on the large area growth of MoS₂ atomic layers by a scalable chemical vapor deposition (CVD) method. The as-prepared samples can either be readily utilized for further device fabrication or be easily released from the growth substrate and transferred to arbitrary substrates. High resolution transmission electron microscopy and Raman spectroscopy on the as grown films of MoS₂ indicate that the number of layers range from single layer to a few layers.

Our results on the direct growth of MoS₂ layers on dielectric leading to facile device fabrication possibilities show the expanding set of useful 2D atomic layers, on the heels of graphene, which can be controllably synthesized and manipulated for many applications.

3:40pm GR+EM+NS+SS+TF-ThA6 Formation of Silicene and 2D Si Sheets on Ag(111): Growth Mode, Structural and Electronic Properties. *P. Vogt*, Technical University of Berlin, Germany, *T. Bruhn*, *A. Resta*, *B. Ealet*, CNRS CiNAM, Marseille, France, *P. De Padova*, CNR-ISM, Rome, Italy, *G. Le Lay*, CNRS CiNAM, Marseille, France

Since the discovery of graphene enormous efforts have been invested to discover other similar 2-dimensional materials, like e.g. silicene. These 2D materials share similar structural, electronic and optical properties as graphene but are expected to differ in terms of their respective chemical reactivity and thus their applicability for electronic devices. In particular silicene could more easily be integrated into current Si-based electronics than graphene. Silicene has been predicted theoretically [1,2] but does not seem to exist in nature.

Recently, we could synthesize silicone layers grown epitaxially by depositing Si on Ag(111) surfaces. The electronic properties of these silicene layers were shown to behave as theoretically predicted [3] and the structural and electronic properties are very similar to graphene. In STM images the hexagonal 2D silicene sheet gives rise to triangular structures situated in a honeycomb arrangement with (4×4) symmetry with respect to the Ag(111) surface. A structural model derived from the STM measurements showed a very good agreement with DFT results and exhibited a downward conical electronic dispersion resembling that of relativistic Dirac fermions at the Si K-points [3]. Depending on the growth conditions the formation of different 2D silicon arrangements can be observed: 1) Si-clusters at low deposition temperatures, 2) the formation of less ordered 2D hexagonal Si-based structures at temperatures up to 180°C, 3) the formation of the (4×4) silicene sheet around 220°C and 4) a 2D Si structure with a ($\sqrt{13}\times\sqrt{13}$)-like periodicity at higher growth temperatures exhibiting a very regular, wide range ordered Moiré-like surface pattern in STM.

Here, we will discuss the formation and epitaxial growth mode of these different 2D Si structures and the dependence on the growth parameters. We will also investigate whether these different 2D Si layers all refer to similar silicene sheets which give rise to different appearances in STM due to a varying rotation with respect to each other.

Keywords: silicene, 2D materials, graphene, Dirac fermions

References:

- [1] S. Cahangirov et al., Phys. Rev. Lett. **102**, 236804 (2009)
- [2] G. G. Guzman-Verri and L. C. Lew Yan Voon, Phys. Rev. B **76**, 75131 (2007)
- [3] P. Vogt et al., Phys. Rev. Lett. **108**, 155501 (2012)

4:00pm GR+EM+NS+SS+TF-ThA7 Yttria-monolayer on Pt(111) Supported Graphene: A Novel Two Dimensional Heterostructure and its Affect on Charge Doping of Graphene. *R. Addou*, *A. Dahal*, *M. Batzill*, University of South Florida

Yttrium oxide (Y₂O₃) is a high-k dielectric material, with promising wetting behavior of graphene [1]. In our study we grew yttria by reactive MBE on Pt(111) supported graphene to investigate the structural and electronic properties of the graphene/yttria interface. Photoemission measurements indicate that the graphene layer is covered by yttria. Scanning tunneling microscopy (STM) and low energy electron diffraction reveal that at annealing temperatures higher than 600 °C yttria forms an ordered monolayer on top of graphene. In STM, a moiré pattern is observed that is a consequence of super-positioning of a hexagonal yttria monolayer lattice with that of graphene. X-ray photoemission indicates a shift of the C1s peak by 1 eV to higher binding energy upon depositing of the yttria film. This peak shift is explained by charge doping of graphene by the underlying Pt substrate due to the change in the work function of the yttria coated graphene.

[1] Z. Wang et al. Nano Lett. **2010**, *10*, 2024–2030; L. Ding et al. Nano Lett. **2009**, *9*, 4209–4214.

4:20pm GR+EM+NS+SS+TF-ThA8 Probing the BCN-triangle by Computations—Outside the Carbon Corner. *Yakobson*, Rice University
INVITED

We will discuss recent work on modeling 2D-materials “beyond graphene” [1-2]: two dimensional hexagonal h-BN, pure B polymorphs, MoS₂, etc. Lessons from graphene studies remain invaluable as they offer general approach and views on the edges [3] and interface structures and energies, and especially organization of the grain boundaries [4,5]. New dislocation

cores in BN (both 5/7 and 4/8 types) lead to accordingly new physical properties of emerging polar GB [6]. Similarly, we identify the dislocation cores and the grain boundary structure for more complex polar layer-material, MoS₂ (X. Zou, unpublished). Our analysis of edge and cleavage energies helps to explain fracture patterns emerging in the course of synthesis. In principle, computations suggest possibility of metastable 2D-layers of GaN or ZnO or even their hybrids. Finally, it is important to mention clear opportunities of designing 2D-circuits by combining 2D-materials in specific functional patterns like proposed nanoroads and quantum dots [7-8] which now become a subject of experimental laboratory work.

- [1] Y. Liu et al. Nano Lett. **11**, 3113 (2011).
- [2] E. Penev, et al, Nano Lett. **12**,2441 (2012).
- [3] Y. Liu et al. Phys. Rev. Lett. **105**, 235502 (2010).
- [4] BIY and F. Ding, ACS Nano **5**, 1569 (2011).
- [5] Ajayan and BIY, Nature Mater. **10**, 415 (2011).
- [6] Y. Liu et al. ACS Nano (2012).
- [7] A. Singh and BIY, Nano Lett., **9**, 1540 (2009).
- [8] A. Singh, E. Penev, and BIY, ACS Nano, **4**, 3510 (2010).

5:00pm GR+EM+NS+SS+TF-ThA10 Single-layer MoS₂ Devices and Circuits. *A. Kis*, EPFL, Switzerland
INVITED

Single layer MoS₂ is a recent addition to the family of 2D materials and is reminiscent of graphene except that it is an intrinsic direct band gap semiconductor with a 1.8 eV gap. We have exfoliated single layers 6.5 Angstrom thick from bulk crystals of semiconducting MoS₂, using the micromechanical cleavage technique commonly used for the production of graphene. Our nanolayers are mechanically and chemically stable under ambient conditions. We have fabricated transistors based on single-layer MoS₂ which demonstrate that this material has several advantages over silicon for potential applications in electronics. Our transistors have room-temperature current on/off ratios higher than 10⁸, mobility higher than 780 cm²/Vs and leakage currents in the fA range. Integrated circuits based on MoS₂ have the capability to amplify signals and perform logic operations. Finally, I will show our work on suspended MoS₂ membranes that show ripples similar to those observed in graphene. MoS₂ also has superior mechanical properties: higher stiffness than steel and 30 times its breaking strength which makes it suitable for integration in flexible electronics.

References

1. B. Radisavljevic, A. Radenovic, J. Brivio, V. Giacometti, and A. Kis. Single-layer MoS₂ transistors. Nature Nanotechnology **6**, 147, 2011. doi: 10.1038/nnano.2010.279
2. M.M. Benameur, B. Radisavljevic, J.S. Heron, S. Sahoo, H. Berger, and A. Kis. Visibility of dichalcogenide nanolayers. Nanotechnology **22**, 125706, 2011. doi: 10.1088/0957-4484/22/12/125706
3. B. Radisavljevic, M.B. Whitwick, and A. Kis. Integrated circuits and logic operations based on single-layer MoS₂. ACS Nano **5**, 9934, 2011. doi: 10.1021/nn203715c
4. J. Brivio, D.T.L. Alexander, and A. Kis. Ripples and Layers in Ultrathin MoS₂ Membranes. Nano Letters **11**, 5148, 2011. doi: 10.1021/nl2022288
5. S. Bertolazzi, J. Brivio, and A. Kis. Stretching and Breaking of Ultrathin MoS₂. ACS Nano **5**, 9703, 2011. doi: 10.1021/nn203879f

Surface Science

Room: 21 - Session SS+NS-ThA

Surface Science of Nanostructures

Moderator: J.M. Millunchick, University of Michigan

2:00pm SS+NS-ThA1 Direct Atomic Scale Imaging and Spectroscopy of III-V Semiconductor Nanowire Surfaces. *A. Mikkelsen*, Lund University, Sweden
INVITED

Free-standing III-V nanowires have the potential to become central components in future electronics and photonics with applications in IT, life-science and energy[1]. The atomic scale structure and morphology of semiconductor nanowire surfaces are central in determining both growth and function of the wires. Surface diffusion and nucleation will directly influence the final appearance of the wires, and transport and optical properties of semiconductor nanowires is often governed by their surfaces.

We develop and use scanning probe and synchrotron based microscopy/spectroscopy to completely determine structure, chemistry and physical properties of III-V nanowire surfaces with extreme precision. We use our novel methods to directly image both interior and exterior surfaces of the nanowires down to the single atom level, revealing geometric structure as well as both electrical and mechanical properties[2-4]. With our rather diverse toolbox we can obtain a real understanding of the connections between nanowire structure, growth and function.

We present recent Scanning Tunneling Microscopy/spectroscopy (STM/S) results, on nanowires consisting of various III-V materials and of polytypic heterostructures with wurtzite (WZ) and zincblende (ZB) crystal segments - only possible in nanowires. We have obtained images of the atomic scale structure for all common WZ and ZB facets as well as information about the electronic structure using STS. We are now developing these methods to perform STM/S on individual nanowires under device operation. Further, we show that STM, can be used for direct top view imaging of the micrometer high free-standing nanowires. We then determine mechanical resonances up to hundreds of MHz with sub Ångström precision[4].

Finally, using synchrotron based Photo Emission / Low Energy Electron Microscopy/Spectroscopy (PEEM/LEEM/XPS) we have characterized III-V nanowire surface chemistry and electronic properties and investigated the influence of various ultra-thin dielectrics to reduce surface band-bending effects[5-8]. A complete picture of oxide thicknesses, effects on bandbending and information on axial and radial doping is obtained.

1. C.M. Lieber and Z.L. Wang, *MRS Bull.* **32**, 99 (2007), and other papers in this issue.
2. A. Mikkelsen et al, *Nature Mater.* **3**, 519 (2004) ; L. Ouattara et al, *Nano Lett.* **7**, 2859 (2007)
3. E. Hilner, et al, *Nano Lett.* **8**, 3978 (2008)
4. A. Fian, et al, *Nano Lett.* **10**, 3893 (2010)
5. R. Timm et al., *Appl. Phys. Lett.* **99**, 222907 (2011).
6. B. Mandl et al., *Nano Lett.* **10**, 4443 (2012)
7. R. Timm et al., *Microelectron. Eng.* **88**, 1091 (2011).
8. M. Hjort et al, *Appl. Phys. Lett.* **99**, 233113 (2011)

2:40pm SS+NS-ThA3 Spontaneous Assembly of Ordered Atomic Wires with a Long Interwire Distance on a Stepped Nanotemplate. B.G. Shin, M.K. Kim, D.-H. Oh, C.-Y. Park, J.R. Ahn, Sungkyunkwan University, Republic of Korea

Atomic wires do not interact directly with each other and are therefore ordered by an indirect substrate mediated interaction, whereas molecular structures can be assembled spontaneously by a direct interaction with each other. Such interwire interactions were very short and subsequently an interwire distance of ordered atomic wires were a few Å. Because of the interwire interaction, atomic wires have been described as a quasi 1D system rather than an ideal 1D system. Therefore, an atomic wire with a long interwire distance needs to study an ideal 1D system but, as mentioned before, atomic wires were not ordered with a long interwire distance. Assembly of a long interwire distance atomic wire is thus very challenging and demanded to widen experimental scope of studies on one-dimensional physics. In this study, indium atomic wires with a long interwire distance of 5.7 nm were ordered spontaneously at room temperature on a stepwise nanotemplate, a Si(557) surface. In general, interwire interactions are required to produce ordered nanowires so that other ordered atomic wires have a short interwire distance of a few Å, as described above. The long interwire distance of the ordered indium atomic wires is therefore very unique. Indium atoms were mobile at room temperature and were adsorbed on a only specific step among four steps, one (111) and three (112) steps of the reconstructed Si(557) surface, maintaining the stepwise nanotemplate structure, as observed by scanning tunneling microscopy (STM), despite the fact that the triple steps have similar local atomic structures. The energetic stability of the indium atomic wires was calculated by first-principles calculations. The reconstructed Si(557) structure model was based on the dimer-atom-stacking fault (DAS) model and atom-parallel dimer (AD) model of (111) and (112) facets, respectively.[1, 2] Total energy differences between indium atomic wires on the three (112) steps was very small and the most stable atomic structure was located at the second (112) step, which was consistent with STM images. STM simulations also reproduced the x2 periodicity of the In-induced atomic wires along the wire direction.

- [1] K. Takayanagi, Y. Tanishiro, M. Takahashi, and S. Takahashi, *J. Vac. Sci. Technol. A* **3**, 1502 (1985)
- [2] D. Oh, M. Kim, J. Nam, I. Song, C. Park, S. Woo, H. Hwang, C. Hwang, J. Ahn, *Phys. Rev. B*, **77**, 155430 (2008)

3:00pm SS+NS-ThA4 Influence of Surface Steps on the Initial Oxidation of TiN (100). M. Hong, S.R. Phillpot, S.B. Sinnott, University of Florida

Titanium nitride (TiN) film has extreme hardness, high chemical reactivity and high electrical conductivity and thus is widely used for wear and corrosion resistant coatings as well as diffusion barriers and gate electrodes in microelectronic devices. They are thus routinely subjected to extreme conditions such as high pressure and temperature, corrosive environments,

and consequently undergo oxidation. Here, density functional theory calculations are used to determine the mechanisms associated with step-related oxidation process and the formation of TiO_x induced by both the dissociation of O₂ and Ti surface diffusion on TiN (100). Preliminary calculations reveal stable adsorption sites near surface steps for O₂ molecules and single O adatoms, both of which have adsorption energies larger than on terraces. This indicates that the dissipated energy during O₂ dissociation near the surface step is larger than that on (100) terraces so that consequent oxidation reactions can occur more easily. The calculations reveal potential O₂ dissociation paths with activation energies in the range of 1-2 eV. This work is supported by the National Science Foundation (DMR-1005779).

3:40pm SS+NS-ThA6 Growth of Ag/Ge(111) Phases Studied with LEEM and LEED. S. Chiang, C. Mullet, UC Davis

Low energy electron microscopy (LEEM) and low energy electron diffraction (LEED) were used to study the growth of structural phases of Ag deposited on Ge(111) above and below the Ag desorption temperature. Ag deposited on Ge(111) formed three main surface phases above 100°C: (4x4), (√3x√3)R30°, and (3x1). At a given coverage, (4x4) island size increased with deposition temperature and decreased with deposition rate. The (4x4) structure nucleated at steps edges and grew only at steps for samples with very high step density. While the √3 structure did not show a preference for nucleating at steps, its growth was bounded by substrate step bunches. The (3x1) was the only Ag phase on the surface for deposition at 370°C and coverage Θ < 0.1 ML, forming domains large enough to be resolved in LEEM images. The (3x1) and (4x4) phases coexisted for T < 350°C and 0.1 < Θ < 0.38 ML, while the (3x1) and √3 phases coexisted for T > 400°C and Θ > 0.4 ML. LEEM images of Ag desorption from Ge(111) at T > 575°C showed that Ag (4x4) and √3 phases reversibly transform to a disordered (1x1) phase, with desorption proceeding from the edges of disordered (1x1) domains and the (1x1) phase being slightly less dense than the (4x4) phase. For sufficiently high deposition rates, Ag was observed to accumulate on Ge(111) above the 575°C desorption temperature. For deposition between 580 and 640°C, a silver layer formed with a (3x1) LEED pattern; upon completion of that layer, a √3 layer formed. For deposition at 660°C, only the (3x1) layer formed. Desorption proceeded by the reverse sequence of phases.

Funded by NSF CHE-0719504 and NSF PHY-1004848

4:00pm SS+NS-ThA7 A Synchrotron XPS Study of the Radio-Frequency SF₆ Plasma Fluorination of Single-Walled Carbon Nanotubes. A.J. Barlow, NEXUS XPS Facility, Newcastle University UK, A.J. Blanch, A.D. Slattery, J.S. Quinton, Flinders University, Australia

With the ever increasing utilisation of carbon nanostructures across many fields, researchers are continuously looking for new and more efficient methods for the reliable and controllable functionalisation of these materials, in a way that is easily scalable. This is particularly true for the one dimensional carbon nanotube (CNT). While plasma science is not a new field, its application towards the covalent attachment of chemically reactive species to the sidewalls of the initially somewhat inert CNT structure has only more recently been investigated. Furthermore, in-depth studies of the plasma functionalisation of CNTs using fluorine-rich species such as sulphur hexafluoride (SF₆) are limited for a process that is capable of not only providing reactive sites for further chemical attachment but also the modification of the electronic structure of the nanotube [1, 2].

In this presentation research efforts into the fluorination of single-walled CNTs (SWCNTs) in a controlled manner using SF₆ plasma will be discussed. Control over the amount of fluorine attached to the CNT surfaces is demonstrated through variation in experimental conditions such as plasma power. Furthermore, the type of fluorine bonding present on the surface (covalent or semi-ionic) is shown to be controllable through the addition of oxygen containing species into the fluorination mechanism. This can be achieved through either the doping of the plasma itself with oxygen or water vapour, or by an oxidative surface pretreatment of the CNTs through wet-chemical or plasma methods. With this level of control, greatly enhanced C-F covalency can be achieved over a pure SF₆ plasma treatment alone. Results will be presented from lab-based XPS analysis of SWCNT surfaces performed at Flinders University, South Australia, as well as synchrotron-based XPS analysis performed at the Australian Synchrotron.

1. Park, K.A., Y.S. Choi, and Y.H. Lee, *Atomic and electronic structures of fluorinated single-walled carbon nanotubes*. *Phys. Rev. B*, 2003. **68**: p. 045429.
2. Plank, N.O.V., et al., *Electronic properties of n-type carbon nanotubes prepared by CF₄ plasma fluorination and amino functionalisation*. *J. Phys. Chem. Lett. B*, 2005. **109**: p. 22096-22101.

4:20pm **SS+NS-ThA8 Solving the Shape of Micellar Pt Nanoparticles Supported on TiO₂(110) and γ -Al₂O₃: A STM, TEM and EXAFS Study, F. Behafarid, B. Roldan Cuenya, University of Central Florida**

Nanoparticles (NPs) with well-defined sizes and shapes were synthesized via inverse micelle encapsulation methods. For 2-4 nm Pt and Au NPs supported on TiO₂(110), the shape was resolved by scanning tunneling microscopy (STM). Geometrical information on smaller Pt NPs supported on nanocrystalline γ -Al₂O₃ was extracted by a combination of transmission electron microscopy (TEM) and extended x-ray absorption fine-structure spectroscopy (EXAFS) measurements. It will be shown that the size, interparticle distance, and the geometry (2D vs 3D) of the NPs can be tuned via our micellar synthesis.

Pt NPs in the size range of 2-4 nm supported on TiO₂(110) were studied by STM after heating in UHV at high temperature (>1000°C). This thermal treatment facilitates the melting of the NPs and the formation of NP-support epitaxial interfaces. High resolution STM images allowed us to determine the shape of the NPs as well as facet orientations. Three different shape types were observed, and each category of shapes was found to appear within a particular NP size regime. In addition, the epitaxial relationship between the NPs and the TiO₂(110) surface was investigated in order to explain the specific orientation of the NPs observed in our study. It was also found that due to interface-induced strain, the NP shapes obtained do not follow the Wulff theorem, namely {100}/{111} facet area ratios deviating from the value obtained for support-free clusters.

Pt NPs in the size range of 0.8-1.5 nm supported on γ -Al₂O₃ were studied by EXAFS, and the nearest neighbor coordination numbers up to the 4th shell were obtained following multiple scattering analysis. These coordination numbers, together with the NP diameter obtained by TEM were examined against a theoretically generated database of possible NPs shapes to determine the most representative shape of Pt NPs in each of the samples. Correlations between the reactivity and the shape of the Pt NPs were established.

4:40pm **SS+NS-ThA9 Geometrical, Electronic, and Vibrational Properties of Bare and H-covered Pt_n(n=22, 33, 44, 55, and 85) Nanoparticles, G. Shafai, S. Hong, M. Alcantara, T.S. Rahman, University of Central Florida**

We have performed systematic density functional theory (DFT) calculations of the geometrical, electronic, and vibrational properties of small Pt_n nanoparticles (NPs) (n=22, 33, 44, 55, and 85) and their changes with NP size and adsorbate (H₂) coverage. We find our calculated H adsorption energy to be in range of -0.42 eV and -0.62 eV, and with increasing hydrogen coverage the H adsorption energy decreases due to adsorbate-adsorbate interactions. We find increase of Pt-Pt bond length upon hydrogen adsorption and, strikingly, the red shift of the center of the *unoccupied* d-bands of the bare Pt clusters turns to a blue shift upon hydrogen adsorption in good agreement with experiment [1]. We also find that there is a net charge transfer from all Pt atoms within the NPs to all hydrogen atoms of 0.55 (Pt₂₂H₂₂) and 1.37 electrons (Pt₄₄H₄₄). Thus, the remarkable hydrogen effect on the electronic structure of Pt NPs can be attributed to charge transfer from the Pt NPs to hydrogen. Regarding the optimal H coverage on Pt NPs, our calculated free-energy phase diagram shows non-zero H coverage even at beyond 600K under ambient H₂ pressure. This work is supported in part by US-DOE under Grant No. DE-FG02-07ER46354.

[1] F. Behafarid, L.K. Ono, S. Mostafa, J. R. Croy, G. Shafai, S. Hong, T. S. Rahman, Simon R. Bare, and B. Roldan Cuenya, submitted.

5:00pm **SS+NS-ThA10 The Effect of S to Se Substitution in SAMs: Odd-Even Polymorphism of Biphenyl-Substituted Alkaneselenolate on Au(111), M. Dendzik, Jagiellonian University, Poland, A. Terfort, Goethe University, Germany, P. Cyganik, Jagiellonian University, Poland**

To fabricate aromatic self-assembled monolayers (SAMs) of practical importance for molecular electronics and other applications, high level of control over the SAMs properties should be achieved. In particular, besides monitoring the electronic properties, the control of structure and stability, is an issue of equal importance. As demonstrated previously one way to improve structure and stability of these systems can be achieved by the substitution of the headgroup atom (S versus Se, which binds SAMs constituent to the substrate) [1-3]. In the present study [4], to elucidate how the S to Se substitution influences SAMs structure and stability, we investigate influence of the BPnSe/Au(111) (BPnSe, CH₃-(C₆H₄)₂-(CH₂)_n-Se-, n=2-6) formation temperature and compare obtained results with the corresponding data obtained for their thiol analogues i.e. for BPnS/Au(111) SAMs. Obtained STM data are discussed and analysed in view of the spectroscopic [2] and spectrometric [3] results reported by us recently for these systems, as well as compared to the previously reported STM data [1]. Observed odd-even effect in polymorphism for BPnSe/Au(111) indicates that bonding configuration at the molecule-substrate interface contributes

significantly to the energetics of the SAM. We conclude that S to Se substitution increases strength of the molecule-substrate bonding at the expense of reducing strength of the Au_{surface}-Au_{bulk} and Se-C bonding.

References

- (1) P. Cyganik, K. Szelagowska-Kunstman, et al. *J. Phys. Chem. C* **2008**, *112*, 15466.
- (2) K. Szelagowska-Kunstman, P. Cyganik, et al. *Phys. Chem. Chem. Phys.* **2010**, *12*, 4400.
- (3) S. Wyczawska, P. Cyganik, A. Terfort, P. Lievens, *ChemPhysChem* **2011**, *12*, 2554.
- (4) M. Dendzik, A. Terfort, and P. Cyganik *in preparation*

5:20pm **SS+NS-ThA11 Molecular Self-Assembly by Ionic Bonding in a Series of Carboxylate Species on the Cu(100) Surface, D. Skomski, S.L. Tait, Indiana University - Bloomington**

To expand the catalogue of available interactions for the efficient self-assembly of highly-ordered nanoscale structures, we have investigated the formation of high-stability supramolecular networks constructed with anionic carboxylate species and sodium cations. Our experiments demonstrate that these two-component approaches can steer organic molecules towards efficient self-assembly, even with molecules that do not show a strong tendency towards long-range, two-dimensional ordering when deposited alone. Biphenyl-3,3',5,5'-tetracarboxylic acid (BTA) on Cu(100) serves as a model system to illustrate this effect. Ionic structures have been resolved with molecular and atomic resolution using scanning tunneling microscopy (STM). Chemical shifts in the Na 1s, C 1s, and O 1s core level binding energies, measured by X-ray photoelectron spectroscopy, confirm the active chemical interactions inferred from the STM results.

Ionic self-assembly has been achieved on the Cu(100) surface with terephthalic acid, trimesic acid, as well as BTA. We have shown that the carboxylate and sodium chloride undergo a replacement reaction producing a new salt with long range periodic structure. Chemical shifts in the sodium 1s photoelectron peak have been observed upon addition of the organic species to the surface, confirming a direct interaction. Resulting extended network structures demonstrate very high stability, maintaining their supramolecular structure up to at least 165 °C. The formation of new structures illustrates the interplay between adsorbate-substrate and ionic interactions and opens new possibilities for ionic self-assemblies at surfaces with highly-ordered structure and specific chemical function.

Surface Science

Room: 22 - Session SS-ThA

Liquid/Surface Interactions

Moderator: G.A. Kimmel, Pacific Northwest National Laboratory

2:00pm **SS-ThA1 Interface Properties of Aqueous Nitrile Solutions, K.A. Perrine, A. Margarella, M.H.C. Van Spyk, University of California Irvine, B. Winter, Helmholtz-Zentrum Berlin für Materialien und Energie, Germany, H. Bluhm, Lawrence Berkeley National Laboratory, J.C. Hemminger, University of California Irvine**

It is important to understand the molecular-level properties of aqueous organic mixtures that can affect the environment as well as a variety of chemical systems. Mixtures of acetonitrile and water solutions have been shown to have different properties at the surface and in the bulk at different bulk acetonitrile concentrations. According to surface sensitive studies and molecular dynamic simulations, at 0.07 mole fraction, hydrogen bonding is lost at the interface with increasing acetonitrile concentration, leading to a reorientation of the acetonitrile at the surface. In addition, water and acetonitrile clusters have been shown to coexist and interact by dipole interactions between 0.2 and 0.8 mole fraction of acetonitrile. The reorientation of another nitrile at the surface, propionitrile, by hydrogen bonding has also been observed, but for this molecule, there is a lack of bulk studies of water-nitrile solutions.

In our studies, liquid-jet X-ray photoelectron spectroscopy was used to determine the nature of aqueous solutions of these two nitriles. The C1s, N1s and O1s regions suggest that clustering of the nitrile and water is apparent at the surface as well as the bulk. A full range of nitrile concentrations was studied. In addition, we made comparisons between experiments in which the liquid jet is in contact with a few torr of vapor and experiments in which the jet is exposed to high vacuum. The surface and bulk properties, as determined by XPS, are the same under these two

experimental conditions. Our results also allow us to compare the differences between solubility of the two nitrile aqueous solutions and their hydrogen bonding properties at the surface and in the bulk.

2:20pm SS-ThA2 Photoelectron Spectroscopy of Sulfuric Acid Aqueous Solutions, A. Margarella, K.A. Perrine, University of California Irvine, T. Lewis, Lawrence Livermore National Laboratory, M. Faubel, Max-Planck-Institut für Dynamik und Selbstorganisation, Germany, B. Winter, Helmholtz-Zentrum Berlin für Materialien und Energie and BESSY, Germany, J.C. Hemminger, University of California Irvine

The air-liquid interface of aerosols is an important site for heterogeneous chemistry in the atmosphere, associated, for instance, with the formation of reaction products relevant for ozone depletion. Concentrated (5-14 M) super-cooled aqueous solutions of sulfuric acid are known as sulfate aerosols and are one of the most abundant types of atmospheric aerosols. Fully understanding the dissociation of sulfuric acid, on the molecular level, is important because heterogeneous chemistry occurring on the surface of sulfate aerosols depends on the availability, speciation, location, and solvation structure of the species in solution. Aqueous solutions of sulfuric acid and the subsequent acid dissociation are useful models for sulfate aerosols. As a strong acid, the bulk of an aqueous solution of sulfuric acid will have H_3O^+ , HSO_4^- and SO_4^{2-} , and at high concentrations when the water concentration is very low, un-dissociated H_2SO_4 may be present. The bulk species composition is a function of the initial solution concentration, as well as temperature, and this composition has been well characterized by a variety of methods, such as sum frequency generation and Raman spectroscopy. Here, the chemistry of sulfuric acid aqueous solutions is explored by photoelectron spectroscopy on a liquid micro-jet. Experiments were performed at Beamline U41-PGM at the BESSY II synchrotron facility. A series of sulfuric acid aqueous solutions is measured at a low temperature of 6°C. Deconvolution of the photoelectron spectra yields electronic information on the ionization species of sulfuric acid.

2:40pm SS-ThA3 Using Nanoscale Amorphous Solid Water Films to Create and Study Deeply Supercooled Liquid Water, S.R. Smith, B.D. Kay, Pacific Northwest National Laboratory **INVITED**

Vapor deposition of water on cryogenic substrates is known to produce amorphous solid films. When heated above their glass transition (136 K) these films transform into deeply supercooled liquid water which subsequently crystallizes around 160 K. These nanoscale liquid films can be used to study processes such as diffusion, isotope exchange, and crystallization at cryogenic temperatures not attainable by conventional supercooling of the bulk liquid. Molecular beam scattering, programmed desorption (both TPD and isothermal), and vibrational spectroscopy are used to study the thermodynamics and chemical kinetics of these processes in unprecedented detail. This talk will highlight our recent advances in this area. This work was supported by the U.S. Department of Energy (DOE), Office of Basic Energy Sciences, Division of Chemical Sciences, Geosciences, and Biosciences. The research was performed using EMSL, a national scientific user facility sponsored by DOE's Office of Biological and Environmental Research and located at Pacific Northwest National Laboratory, which is operated by Battelle, operated for the U.S. DOE under Contract DE-AC05-76RL01830.

3:40pm SS-ThA6 DFT Study of Water Dissociation and Diffusion on Metal Surfaces, Kinks and Step, L. Arnaudottir, Oregon State University
Surface defects play a critical role in many surface processes, for example in the formation of a water layer on Pt(111). In this DFT study, we describe water adsorption, diffusion, dissociation and early cluster formation on terrace, steps and kinks on Pt(111). The adsorption energy of a single water molecule increase as it moves from the flat terrace up to the step edge and then atop a kink atom. The highest activation barrier along this path is only 0.22 eV. The stronger binding on the step and kinks makes the reverse barriers much larger and, therefore, the diffusion from the step or kink back to the flat terrace less likely. This suggests that at approximately 100 K, water will diffuse to lower energy adsorption sites on the steps and kinks and form chains on step edges before wetting the lower terrace, in agreement with STM measurements by Morgenstern, M. et al. [1].

Surface defects also play an important role in the dissociation of water molecules. The calculated reaction energy for water dissociation, $\text{H}_2\text{Oads} \rightarrow \text{OHads} + \text{Hads}$, on flat terrace, step and kink shows an interesting trend where the reaction energy on the flat terrace is almost twice the energy at a kink and three times the energy on a step. Water molecule dissociation on flat Pt(111) terrace is therefore less likely than at defects. The reaction energy is 0.21 eV on the (221) step and 0.37 eV on the (854) kink, making the defect sites significantly more promising for water dissociation.

The activation energy for dissociation is also lowest at a step site, 0.80 eV. An oxygen assisted dissociation on the step ($\text{H}_2\text{Oads} + \text{Oads} \rightarrow 2 \text{OHads}$) has even lower reaction energy but the activation barrier is similar.

Although the reaction energy at the kink was not so high, the activation barrier for dissociation is very high, 1.4 eV. The energy landscape is quite complicated around the kink but we consistently get this high barrier for the various dissociative pathways that have been tried. The high barrier may be the result of the strong adsorption at the kink sites.

1. Morgenstern, M., Michely, T. and Comsa, G., *Phys. Rev. Lett.* **77** 703 (1996).

4:20pm SS-ThA8 Adsorption and One-Dimensional Chain Formation of Water on TiO₂(110), J. Lee, D.C. Sorescu, X. Deng, National Energy Technology Laboratory, K.D. Jordan, University of Pittsburgh

The adsorption of water molecule on a reduced rutile TiO₂(110)-(1×1) surface has been investigated using scanning tunneling microscopy (STM) and density functional theory (DFT) calculations. STM results indicate that water monomer adsorbs on top of Ti(5f) atom on the Ti row. The DFT calculations show that the most stable configuration of adsorbed water on TiO₂(110) has the binding energy of 23.6 kcal/mol. In this configuration, the oxygen atom is positioned on top of a Ti(5f) atom with one of the O-H bonds pointing toward a bridging oxygen via H-bonding and the other pointing along the Ti row direction. The water monomer can be dissociated by the electron injection from the STM tip into an oxygen adatom on Ti row. As the coverage increases, water molecules start to form one-dimensional chains via H-bonding along the Ti row direction. Thermal annealing after the adsorption of water at low temperature on TiO₂(110) is also found to be effective in the formation of the one-dimensional water chain. The effects of other coadsorbates such as CO₂ and O₂ in the formation of water chain will also be discussed.

4:40pm SS-ThA9 Characterization of Surface and Adsorbate Chemistry on TiO₂; Particle Ensembles and Atmospherically Prepared TiO₂; Single Crystalline Surfaces, C. Kunze, B. Torun, G. Grundmeier, University of Paderborn, Germany

Titanium dioxide (TiO₂) plays a crucial role for modern technical applications such as the design of new catalysts or biomaterials. TiO₂ particles in the modifications of rutile or anatase are a widely used material as an inorganic white pigment. In particle processing the force interactions within particle collectives are of utmost interest in terms of bulk flow properties and agglomerate dispersibility. As the adhesion between small particles is mostly driven by capillary- and van der Waals forces, the investigation of surface chemistry plays a crucial role to understand interactions at TiO₂ particle surfaces. For studies of particle ensembles a new experimental setup was developed to investigate particle parameters under both control of relative humidity (capillary forces) and UV light exposure (hydrophobic to hydrophilic transition). By combined Fourier Transform Infrared Spectroscopy (FTIR) and quartz crystal microbalance (QCM) we studied the influence of surface hydroxyl densities and molecular adsorbates on the formation of surface water adsorbate films in environments of defined relative humidity.

To study the formation of adsorbates on a model surface, TiO₂(100) and TiO₂(110) single crystalline surfaces were prepared by a wet chemical etching procedure followed by an annealing step. The crystal surface and the native adsorbate layer were studied by means of angle resolved photoelectron spectroscopy (XPS), low energy electron diffraction (LEED) and atomic force microscopy (AFM).

The surface analysis by AFM and LEED revealed a single crystalline TiO₂ surface for both crystal orientations. An ad-layer of surface-hydroxides and specifically adsorbed water additionally to the native contamination layer of low-weight (hydro)carbon species formed under ambient conditions could be proven by angle resolved XPS experiments.

As a model of the carboxy-functional, (hydro)carbon contamination film the adsorption of nonadecylcarboxylic acid (NDCA) on the crystal surface was studied by AFM and angle resolved XPS experiments. Here a significantly different mechanism of adsorption was found comparing the TiO₂(100) and TiO₂(110) surfaces. AFM investigations showed a micellar adsorption of NDCA on the (100) surface forming a dense layer of NDCA micelles which could be removed from the surface by AFM based "nanoshaving"-experiments. In comparison the (110) surface showed very weak interactions with NDCA leading to a coverage of less than one monolayer as a result of different surface termination in comparison to the (100) crystal.

5:00pm SS-ThA10 The Critical Marangoni Number Dependence with Different Aspect Ratio Comparing Microgravity Experiments and Numerical Simulation, S. Yoda, ISAS, Japan, S. Matsumoto, IASA, Japan, H. Kawasaki, I. Ueno, Tokyo University of Science, Japan

Marangoni experiments with a large diameter, 50 mm, were carried out under microgravity condition in Japanese Experiment Module to make clear critical Marangoni number dependence in liquid bridge configuration such

as liquid bridge aspect ratios (length/diameter of liquid bridge). The experiments with the different aspect ratios (length/diameter of liquid bridge) were changed from 0.25 to 1.2 which determined each critical Marangoni numbers. The critical Marangoni numbers decreased up to around 0.4, and after that the number increased monotonically up to 1.2. The most smallest number is observed at critical Mac(20000) at 0.4 and the maximum is Mac (50000) at 1.2. The large liquid bridge was vibrated by crew activity, so that all experiments were done during crew sleeping. This behavior can be qualitatively explained by considering thermal boundary layers which form at both heating and cooling desks of the liquid bridge. The experimental data were good agreement with the numerical results.

Thin Film

Room: 11 - Session TF+AS+SS-ThA

Thin Films: Growth and Characterization-III

Moderator: M.R. Davidson, University of Florida

2:00pm **TF+AS+SS-ThA1 Atomic Force Microscopy (AFM)-Based Nanografting for the Study of Self-Assembled Monolayer Formation of Organophosphonic Acids on Al₂O₃ Single Crystal Surfaces.** *B. Torun, B. Oezkaya, G. Grundmeier*, University of Paderborn, Germany

The surface chemistry of aluminum oxides plays a crucial role in the field of catalysis, corrosion and adhesion. Alumina (Al₂O₃) covered aluminum alloys are employed in the construction of lightweight automotive and aerospace parts. In order to protect these materials from environmental factors organic coatings are commonly used. In this context the adhesion between polymer and oxide surfaces is of outmost importance to improve the longevity of industrial parts. Using self-assembled adhesion promoting monolayers the complexity of surface pretreatment processes could be reduced tremendously. Long aliphatic phosphonic acids, such as octadecylphosphonic acid (ODPA), were found to be suitable for forming dense self-assembled monolayers on native oxide covered aluminum substrates. However in contrast to amorphous oxide films, single crystal surfaces provide a much more well-defined experimental and theoretical platform for studies on the adsorption mechanisms and the stability of organophosphonic acids.

In the presented study^[1], adsorption, stability, and organization kinetics of organophosphonic acids on single-crystalline alumina surfaces were investigated by means of atomic force microscopy (AFM)-based imaging, nanoshaving, and nanografting. The latter, nano-shaving and -grafting, are rather new techniques to study self-assembly processes. Since they were first reported^[2] in 1997, atomic force microscopy based nanografting has been used as a tool to investigate the adsorption of organic monolayers mostly on noble metals, such as gold.^[3] Moreover recent studies focused on influences of the confinement between AFM-tip and background monolayer on the adsorption of molecules during the grafting process. [about:blank#_ENREF_1]

AFM friction and phase imaging have shown that chemical etching and subsequent annealing led to heterogeneities on single-crystalline surfaces with (0001) orientation indicating differences in the local surface termination. These findings were supported by angle resolved X-Ray photoelectron spectroscopy (AR-XPS) measurements suggesting a partially hydroxide terminated surface. Self-assembly and stability of ODPA were shown to be strictly dependent upon the observed heterogeneities of the surface termination, where it was locally shown that ODPA can loosely or strongly bind on different terminations of the crystal surface. Furthermore, organization kinetics of ODPA was monitored with nanografting on (0001) surfaces. Supported by measurements of surface wettability and diffuse reflectance infrared Fourier transform spectroscopy (DRIFTS), it was demonstrated that the lack of organization within the protective adsorbed hexylphosphonic acid (HPA) monolayer on alumina surfaces facilitated the reduced confinement effect during nanografting, such that kinetics information on the organization process of ODPA could be obtained.

[1] Torun, B. et al., *Langmuir* **2012**, 28, (17), 6919-6927.

[2] Xu, S. et al., *Langmuir* **1997**, 13, (2), 127-129.

[3] Yu, J. et al., *Langmuir* **2008**, 24, (20), 11661-11668.

[4] Xu, S. et al., *J. Amer. Chem. Society* **1998**, 120, (36), 9356-9361.

2:20pm **TF+AS+SS-ThA2 SIMS as a Method for Probing Stability of the Molecule-Substrate Interface in SAMs.** *J. Ossowski, J. Rysz, Jagiellonian University, Poland, A. Terfort, Goethe University, Germany, P. Cyganik, Jagiellonian University, Poland*

Despite the numerous structural studies of Self-Assembled Monolayers (SAMs) available nowadays, the structure and stability of the SAM-

substrate interface is still poorly understood and controversial even for the most simple SAM system. As a consequence, the experimental and theoretical analysis of the bonding geometry and the stability of the molecule-substrate interface for technologically relevant, and therefore more complicated SAMs, is extremely difficult.

In this presentation we report extensive static secondary ion mass spectrometry (SIMS) studies¹ on homologous series of thiols (BPnS, CH₃-C₆H₄-C₆H₄-(CH₂)_n-S-Au(111), n = 2-6) and selenols (BPnSe, CH₃-C₆H₄-C₆H₄-(CH₂)_n-Se-Au(111), n = 2-6) where structure and stability of molecule-substrate interface was systematically modified as verified by our previous experiments²⁻⁵. Correlating SIMS data with previous microscopic², spectroscopic³ and very recent neutral mass spectrometry studies^{4,5} we show that SIMS can be successfully applied to monitor fine changes in the molecule-substrate interface stability of these model SAMs. Further, to demonstrate general applicability of SIMS for such analysis, we report use of this method for monitoring influence of S versus Se substitution in purely aliphatic (heksadecanethiol/selenol) and aromatic (anthracenethiol/selenol) SAMs on Au(111). In summary our experiments show that a new approach for probing the stability of molecule-substrate interface in SAMs can be proposed by using SIMS. Importantly, this technique is relatively fast and can be applied for virtually all complicated and technologically relevant SAMs.

References

(1) J. Ossowski, P. J. Rysz, A. Terfort and P. Cyganik *in preparation*.

(2) P. Cyganik, K. Szelagowska-Kunstman, et al. *J. Phys. Chem. C* **2008**, *112*, 15466.

(3) K. Szelagowska-Kunstman, P. Cyganik, et al. *Phys. Chem. Chem. Phys.* **2010**, *12*, 4400.

(4) S. Wyczawska, P. Cyganik, A. Terfort, P. Lievens, *ChemPhysChem* (communication) **2011**, *12*, 2554.

(5) F. Vervaecke, S. Wyczawska, P. Cyganik, et al. *ChemPhysChem* (communication) **2011**, *12*, 140.

2:40pm **TF+AS+SS-ThA3 Wet Chemical Surface Modification of Silicon Oxide and Oxide Free Silicon by Aluminum Oxide.** *P. Thissen, A. Vega, T. Peixoto, Y.J. Chabal*, University of Texas at Dallas

Wet chemical surface modification is a powerful method to change the chemical properties of surfaces. Although it has been used extensively, there are still many issues that limit the applicability of these reactions. Substrate dip coating in aqueous solutions is particularly useful to facilitate both organic and inorganic layer functionalization. For instance, the bonding of phosphonic acid to silicon oxide is weak in water because the Si-O-P bond is easily hydrolyzed. We demonstrate here that this problem is alleviated by the addition of an ultra-thin aluminum oxide layer to the silicon oxide surface via dip-coating a silicon substrate in an aqueous solution of aluminum chloride. The growth kinetics of the aluminum oxide layer are characterized by several surface sensitive techniques and found to follow a Stranski-Krastanov mechanism. Once the aluminum oxide layer is in place, a self assembled monolayer (SAM) of octadecylphosphonic acid (ODPA) is attached by the "tethering by aggregation and growth" (T-BAG) method performed in a controlled environment. We demonstrate that this ODPA layer grafted on the aluminum oxide interlayer remains stable in water. We also show that, following the same wet chemical approach, we are able to attach aluminum hydroxyl directly on oxide-free silicon surfaces previously functionalized with 1/3 monolayer OH. [1] Finally, we show that our approach can easily be transferred to other metal oxides and discuss the most influencing parameters.

[1] Michalak, D. J.; Amy, S. R.; Aureau, D.; Dai, M.; Esteve, A.; Chabal, Y. J. *Nat. Mater.* **2010**, *9*, 266-271.

3:00pm **TF+AS+SS-ThA4 Static and Dynamic Depth Profiling of Thin Films with Low Energy Ion Scattering (LEIS).** *H.R.J. ter Veen, M. Fartmann, Tascon GmbH, Germany, T. Grehl, ION-TOF GmbH, Germany, B. Hagenhoff, Tascon GmbH, Germany*

With the ever increasing demand of thinner and better defined thin layer structures, good depth resolution becomes more and more critical in depth profiling techniques. Low Energy Ion Scattering (LEIS) is known as the most surface sensitive chemical analysis technique (see [1] for a review of LEIS technique). It is considerably less known that LEIS can also be applied for so called "static depth profiling" by interpreting the backgrounds on the low energy side of the LEIS peaks. The energy that the particles lose while travelling through the sample is a measure for the depth of the scattering atom, in a way similar to Rutherford Back Scattering (RBS) but for a much smaller depth range. New models have been developed to understand the process that gives rise to these backgrounds and that contains the information from layers below the surface up to depths of 10 nm. These models will be presented.

The models for this static depth profiling can be verified by dynamic (sputter) depth profiling. After each sputter step a full LEIS spectrum is recorded, which contains the surface information as well as the static depth profile at that point in the dynamic depth profile. In this way, the static depth profile can forecast the dynamic depth profile. This technique will be demonstrated for an Si/SiO₂/W/Al₂O₃ system.

LEIS is particularly suited for dynamic depth profiling. Since LEIS is so surface specific, the depth resolution is excellent, as long as the sputter conditions are chosen with care. Furthermore, LEIS can be quantified easily, in many cases - such as in depth profiles - without the use of references. However, any dynamic depth profile suffers from artifacts, such as preferential sputtering and ion beam mixing. By combining the dynamic depth profiling with static depth profiling there is an independent check on these artifacts. Furthermore, it will be shown how static depth profiling can give relevant information also at shallow depths where in a dynamic depth profile sputter equilibrium will not have been reached yet.

[1] H.H. Brongersma et al, Surf. Sci. Rep. 62 (2007)63

3:40pm **TF+AS+SS-ThA6 Paul Holloway Award Talk: Surface Chemistry and Structure of Alloy Thin Films under Reaction Conditions and their Correlations to Catalytic Performances of CO₂ Conversion and Methane Partial Oxidation, F. Tao***, University of Notre Dame **INVITED**

Formation of alloys is one of the important approaches to design of new catalysts with high activity and selectivity as a second metal could tune electronic structure of the first metal or/and create thermodynamically favorable sites for an ideal reaction channel. Co-Ru alloys are active catalysts for conversion of CO₂ into fuel molecules CH₄. Pd-based alloys are important catalysts for methanol partial oxidation to produce hydrogen. Thin films of model catalysts of alloys Co-Ru and Pd-Co were prepared through e-beam evaporation in UHV. In-house ambient pressure X-ray photoelectron spectroscopy using monochromatic Al K α were used to examine the evolution of surface compositions of alloy catalysts and the oxidation states of the constituting elements under reaction conditions and during catalysis in contrast to those before or after a reaction; Surface chemistry (composition and oxidation state) of active phases of Co-Ru and Pd-Co was revealed. High pressure STM provided visible information of surface structure at nano and atomic scale under reaction conditions. These studies clearly suggest a modification of the electronic state through coordinating Ru atoms and thus tuning the adsorption energy of intermediates on Co in CO₂ conversion, which enhances the selectivity to production of CH₄. The formed Co_{0.85}Ru_{0.15} alloy exhibits 100% selectivity to the production of CH₄ and a conversion of 40% which is higher than both pure Co and pure Ru. The promotion effect of the alloy film for CO₂ conversion was rationalized by electronic effects of Ru to Co in the alloy thin films under reaction conditions. In terms of Pd-Co alloy catalysts, segregation of Co to surface under reaction conditions was observed. Through the measurement of surface composition using AP-XPS and the coordination of Pd on surface visualized with STM, a correlation between surface chemistry and structure of Pd-Co alloy surface under reaction conditions and the corresponding catalytic performances were built. The modification of Co to the catalytic behaviors of Pd was identified.

4:20pm **TF+AS+SS-ThA8 Time-resolved and Surface Plasmon Resonance Studies in Metal-Insulator Phase Transition in VO₂ Thin Films, L. Wang, C. Clavero, K. Yang, E. Radue, M.T. Simons, I. Novikova, R.A. Lukaszew,** College of William and Mary

Vanadium dioxide (VO₂) is a prominent example for a material exhibiting a metal-insulator transition (MIT) as a function of temperature with a phase transformation around 340 K from a low-temperature insulator state to a high-temperature conducting state. During the MIT the lattice structure of VO₂ transforms from a monoclinic (insulator) to a tetragonal structure (conductor). Whether these structural changes are solely responsible for the nature of the transition or whether correlation effects also play a role, has been a subject of much debate. Two mechanisms have been generally considered to explain the origin of the MIT in VO₂. The Mott-Hubbard mechanism suggests that electron-electron correlation drives the first-order MIT whereas the Peierls mechanism proposes that a strong electron-lattice interaction leads to the MIT. In order to have a better understanding of the phase transition mechanism and the optical properties of this material across the MIT, we present our research studies on epitaxial VO₂ thin films. We have investigated the optical transmission of a VO₂ thin film during the thermally induced MIT in two different optical spectral regions, with cw THz light and low power (1 mW) IR light (1520 nm HeNe), to identify different mechanisms at play. We have found that the transmission of the THz light starts to decrease at higher temperature than that of the IR light thus probing different stages during the thermally induced MIT. We also

investigated surface plasmon polariton excitation in VO₂ thin films in the IR region, and observed a clear trend from non-absorption in the insulator phase to a high absorption in the metallic phase while changing the VO₂ temperature. Our studies are aimed at helping to understand the evolution of the metallic phase in VO₂ thin films after the MIT and relaxation back to the insulator phase upon the MIT which is of paramount importance for ultra-fast switch applications. Finally, we note that Cavalleri *et al.* [1] reported that the light-induced phase transition happens in less than half a pico-second thus hinting at electronic processes, although they also found that it strongly depended on pump-laser power which is suggestive of lattice interactions. We will compare our time-resolved measurements also using pump-probe techniques but with the sample held at low-temperature vs. room-temperature to illustrate the role of the pump-power on the photo-induced MIT.

[1] A. Cavalleri, Cs. Tóth, C.W. Siders, J. A. Squier, F. Ráksi, P. Forget and J. C. Kieffer, Phys. Rev. Lett. **87** (23), 237401 (2001).

4:40pm **TF+AS+SS-ThA9 Growth, Microstructure and Optical Properties of Sputter-Deposited Gallium Oxide Thin Films, S.K. Samala, C.V. Ramana,** The University of Texas at El Paso

Gallium oxide (β -Ga₂O₃), which is a stable oxide of gallium, is a wide band gap material. The high melting point coupled with stable structure makes of β -Ga₂O₃ the best candidate for high temperature sensing. β -Ga₂O₃ thin films can be used for developing oxygen sensors operating at higher temperatures (≥ 900 °C). This feature opens the possibility of developing the integrated of β -Ga₂O₃ based oxygen sensors for power generation systems. The present work was performed on the analysis of growth behavior, microstructure, and optical properties of β -Ga₂O₃ films grown by sputter deposition. Ga₂O₃ thin film were deposited on Si(100) and quartz substrate by varying the growth temperature from room temperature to 800 °C. The characteristic analysis of the samples was performed employing grazing incidence X-ray diffraction (GIXRD), scanning electron microscopy (SEM), and spectrophotometry measurements. GIXRD analyses indicate that the samples grown at lower temperatures were amorphous while those grown at ≥ 400 °C. SEM results indicate that the morphology evolution is dependent on the temperature. The characteristic shape of the grains changed from triangular to square and finally to spherical morphology with increasing temperature. Optical characterization indicates that the band gap varies from 4.1 to 5.1 eV as a function of increasing temperature. The correlation between growth conditions, microstructure and band gap is established.

5:00pm **TF+AS+SS-ThA10 Optical and Structural Properties of Hafnium Oxide Thin Films Prepared Using Different Deposition Techniques, L. Sun, N.R. Murphy, J.T. Grant, J.G. Jones, R. Jakubiak,** Air Force Research Laboratory

The high dielectric constant and optical transparency of hafnium oxide makes it a useful component in leading-edge integrated circuitry and optical coatings. The optical and structural properties of stoichiometric HfO₂ films vary significantly depending on the deposition mechanism. We prepared 200 nm thick films of HfO₂ on silicon (100) substrates derived from DC magnetron sputtering (DCMS), high power impulse magnetron sputtering (HiPIMS) and pulsed laser deposition (PLD). Analysis of x-ray diffraction data revealed that films deposited via PLD are amorphous, while those deposited using the magnetron sputtering methods had peaks at 2θ of 28.3°, 31.3°, 34.3° and 50.0° indicative of polycrystalline monoclinic HfO₂. This is further supported by the FT-IR data collected in the far-IR regime where absorption bands at 258, 341, 410 and 514 cm⁻¹ were present. AFM and SEM images indicate that the sputtered samples had rougher surface morphology and larger grain sizes than the PLD films where the surface was uniform and smooth (RMS surface roughness less than 0.1 nm). The degree of surface roughness and grain size is inversely proportional to the refractive index. At 632 nm PLD films had an index of refraction of 2.10 while the index of the sputter coated films was 1.98, presumably due to presence of voids. The high refractive index and homogeneity of the PLD films indicate that they were highly packed without voids during growth. Additionally, the influence of the O₂/Ar ratio, working pressure, HiPIMS pulse profile and duty cycle on optical properties, surface roughness, particle size and structural properties of the HfO₂ thin films were characterized and evaluated.

* Paul Holloway Award Winner

5:20pm **TF+AS+SS-ThA11 Nitrogen Induced Changes in the Structure and Electronic Properties of WO₃ Thin Films**, C.V. Ramana, R.S. Vemuri, The University of Texas at El Paso, M. Engelhard, S. Thevuthasan, Pacific Northwest National Laboratory

Tungsten oxide (WO₃) is a wide band gap semiconductor (~ 3.2 eV), which exhibits excellent physical, chemical and electronic properties. WO₃ thin films have been widely used in electrochromics and chemical sensors. Recently, the band gap modification with anionic and cationic doping of WO₃ was gained importance to utilize these materials in photo-catalysis for energy production and utilization. The present work was performed on nitrogen incorporated WO₃ (N-WO₃) films to explore the options to engineer the microstructure and electronic properties. Specifically, the effect of nitrogen incorporation and processing parameters on the microstructure evolution and band gap of WO₃ thin films is investigated. The samples were grown using reactive RF magnetron sputtering where the nitrogen concentration in the films is varied by varying partial pressure of nitrogen during deposition while keeping all other process parameters constant. Quantitative measurements employing X-ray photoemission spectroscopy indicate the nitrogen content increases with increasing nitrogen partial pressure. Structural analysis employing grazing incidence X-ray diffraction demonstrated that the nitrogen atoms embedded in WO₃ crystal matrix changes the crystal-texturing and thus induce changes in the physical properties. Optical spectrophotometry analysis on the N-WO₃ films revealed a shift in the fundamental absorption edge which is in linear relation with the corresponding nitrogen concentration. The correlation between microstructure, dopant profile, dielectric constant and band gap in WO₃ films will be presented and discussed.

Thin Film

Room: 10 - Session TF+EM+SS-ThA

Applications of Self-Assembled Monolayers and Layer-by-Layer Assemblies

Moderator: M.R. Linford, Brigham Young University

2:00pm **TF+EM+SS-ThA1 Light-Directed Nanosynthesis: Near-Field Optical Approaches to Integration of the Top-Down and Bottom-Up Fabrication Paradigms**, G.J. Leggett, University of Sheffield, UK

INVITED

The integration of top-down (lithographic) and bottom-up (synthetic chemical) methodologies remains a major goal in nanoscience. At larger length scales, light-directed chemical synthesis, first reported two decades ago, provides a model for this integration, by combining the spatial selectivity of photolithography with the synthetic utility of photochemistry. Work in our laboratory has sought to realise a similar integration at the nanoscale, by employing near-field optical probes to initiate selective chemical transformations in regions a few tens of nm in size. A combination of near-field exposure and an ultra-thin resist yields exceptional performance: in self-assembled monolayers, an ultimate resolution of 9 nm (ca. 1/30) has been achieved. A wide range of methodologies, based on monolayers of thiols, silanes and phosphonic acids, and thin films of nanoparticles and polymers, have been developed for use on metal and oxide surfaces, enabling the fabrication of metal nanowires, nanostructured polymers and nanopatterned oligonucleotides and proteins. Strategies based upon the use of nitrophenyl-based photocleavable protecting groups have enabled the introduction of synthetic chemical methodology into nanofabrication. Nanoscale control of chemistry over macroscopic areas remains an important challenge. Recently parallel near-field lithography approaches have demonstrated the capacity to pattern macroscopic areas at high resolution, yielding feature sizes of ca. 100 nm over an area four orders of magnitude larger; they have also demonstrated the ability to function under fluid, yielding feature sizes of ca. 70 nm in photoresist under water and suggesting exciting possibilities for surface chemistry at the nanoscale. Finally, the monolayer patterning methods we have developed are by no means restricted to near-field lithography; all that is required is a suitable means of confining the optical excitation. For example, SAM photochemistry has been combined with interferometric exposure to facilitate the fabrication of periodic nanostructures over macroscopic areas in fast, simple, inexpensive processes, underlining the versatility of photochemistry as a nanofabrication tool.

2:40pm **TF+EM+SS-ThA3 Molecular Layer Deposition (MLD) of Polymer Multiple Quantum Dots on TiO₂**, T. Yoshimura, S. Ishii, Tokyo University of Technology, Japan

[Introduction] We previously proposed oxide-semiconductor-based sensitized solar cells, in which polymer multiple quantum dots (MQDs) are utilized for sensitizing layers, and fabricated the polymer MQDs on glass

substrates by Molecular Layer Deposition (MLD) [1]. In the present study, we grew polymer MQDs on TiO₂ by MLD. The polymer MQD growth on TiO₂ was confirmed by photoluminescence (PL) spectra.

[Proposed Solar Cells Sensitized by Polymer MQDs] The proposed sensitized solar cell consists of an oxide semiconductor layer and polymer MQDs on the surface. The polymer MQD contains different-length quantum dots (QDs) in the backbone wire, and consequently, a wide absorption band is obtained by superposition of narrow absorption bands of the individual QDs. This spectral division with the narrow bands can reduce the energy loss arising from the heat generation due to excess photon energy in light absorption processes.

[Absorption/Photoluminescence Spectra of Polymer MQDs] Reference samples of poly-azomethine (AM) and polymer MQDs: OTPTPT, OTPT, and OT were grown on glass substrates by connecting terephthalaldehyde (TPA), *p*-phenylenediamine (PPDA), and oxalic dihydrazide (ODH) with designated orders using MLD. The QD lengths in OTPTPT, OTPT and OT are respectively ~3, ~2 and ~0.8 nm. With decreasing the QD length, while the absorption peak shifts to high-energy side due to the quantum confinement, the PL peak shifts to low-energy side due to the Stokes shift. Namely, in the order of poly-AM to OT, the electrons become highly localized to increase the surrounding atoms' displacement caused by the electron transitions, resulting in the Stokes shift enhancement.

[Growth of Polymer MQDs on TiO₂] We performed MLD to grow poly-AM on ZnO and TiO₂ powder layers. A yellow film of poly-AM was observed on TiO₂. For ZnO, however, no film growth was observed because of weak hydrophilic characteristics of ZnO surfaces. We grew poly-AM and polymer MQDs of TO on the TiO₂ powder layers by MLD, and measured their PL spectra. The PL spectrum of TO was located at lower-energy side than that of poly-AM, which is parallel to the tendency observed in the PL spectra of the reference samples. From this result, it is concluded that polymer MQDs can be grown on TiO₂ by MLD as the sensitizing layers for solar cells.

[1] T. Yoshimura, R. Ebihara, A. Oshima, "Polymer Wires with Quantum Dots Grown by Molecular Layer Deposition of Three Source Molecules for Sensitized Photovoltaics," *J. Vac. Sci. Technol. A*, **29**: 051510-1-6 (2011).

3:00pm **TF+EM+SS-ThA4 Thiol-yne Click Chemistry: Old Concept & New Applications in Surface Science**, N.S. Bhairamadgi, H. Zuilhof, Wageningen University, Netherlands

Click chemistry reactions have opened new horizons in the field of surface chemistry, as these reactions are easy to perform on surfaces. A nice example is the addition of thiol moieties onto C=C bonds, which have been shown to be highly efficient, orthogonal to many other reactions, highly selective, etc. Recently we and others have shown that thiol-ene click reactions can be used efficiently for the modification of semiconductor surfaces and nanoparticles with a wide range of materials. In the current presentation we show an improved procedure involving C≡C bonds, i.e. thiol-yne click reactions.

We modified oxide-free Si(111) surfaces with alkene-terminated and alkyne-terminated monolayers, and these surfaces were further modified with various thiols such as thioglycolic acid, thioacetic acid, thioglycerol, thio-β-D-glucose tetraacetate lactose and 9-fluorenylmethoxy-carbonyl cysteine by using thiol-ene and thiol-yne click reactions. Upon detailed surface analysis it was found that after some optimization the thiol-yne click reaction yielded 20 – 80 % more surface coverage compared to thiol-ene click reactions. Thus surface modification with thiol-yne click reactions promise to be the next step in surface-bound thiol click chemistry.

References:

1. Campos, M. A. C.; Paulusse, J. M. J.; Zuilhof, H., Functional monolayers on oxide-free silicon surfaces via thiol-ene click chemistry. *Chem. Commun.* 2010, 46 (30), 5512-5514.
2. Lowe, A. B.; Hoyle, C. E.; Bowman, C. N., Thiol-yne click chemistry: A powerful and versatile methodology for materials synthesis. *J. Mater. Chem.* 2010, 20 (23), 4745-4750.
3. Ruizendaal, L.; Pujari, S. P.; Gevaerts, V.; Paulusse, J. M. J.; Zuilhof, H., Biofunctional Silicon Nanoparticles by Means of Thiol-Ene Click Chemistry. *Chem. Asian J.* 2011, 6 (10), 2776-2786.
4. Wendeln, C.; Ravoo, B. J., Surface Patterning by Microcontact Chemistry. *Langmuir* 2012, 28 (13), 5527-5538.
5. Wendeln, C.; Rinnen, S.; Schulz, C.; Arlinghaus, H. F.; Ravoo, B. J., Photochemical Microcontact Printing by Thiol-Ene and Thiol-Yne Click Chemistry. *Langmuir* 2010, 26 (20), 15966-15971.

3:40pm **TF+EM+SS-ThA6 Attachment of Conjugated Diruthenium Alkynyl Compounds by Click Chemistry**, *S. Pookpanratana*, National Institute of Standards and Technology, *S.P. Cummings, T. Ren*, Purdue University, *C.A. Richter, C.A. Hacker*, National Institute of Standards and Technology

Attaching electrochemically-active molecules to a variety of different surfaces is of particular interest for applications in photovoltaic devices, catalysis, and molecular electronics. The family of diruthenium 2-anilinoipyridinate (ap) molecules is redox active [1], which makes it an ideal candidate to incorporate on surfaces for molecular catalysis, photoelectrochemical cells for water splitting, and as an active component in molecular electronic devices. Often times, the attachment of a tailored-molecule requires the additional design challenge to incorporate a specific anchoring group (e.g., thiol). Click chemistry has been demonstrated as an effective method to incorporate bulky and complex molecules to a variety of surfaces [2-6]. This route has introduced numerous possibilities of tailoring molecular surfaces.

Here, we have employed a Cu-catalyzed azide-alkyne cycloaddition (CuAAC) click reaction to attach Ru₂(ap)₄-(C≡C-C₆H₄-C≡CH), (henceforth referred to as Ru₂-alkynyl) to Au and SiO₂ surfaces. First, we form an azide-terminated monolayer on Au and SiO₂ by using azidoundecanethiol and azidoundecyl trimethoxysilane, respectively. Next, the Ru₂-alkynyl is linked to the azide-containing monolayers via a CuAAC reaction (adapted from Ref. 4). The clicked-on Ru₂-alkynyl molecule was physically characterized by X-ray photoelectron spectroscopy (XPS) and infrared (IR) spectroscopy. The formation of the azide monolayer on Au and SiO₂ surfaces is confirmed by IR measurements. After the CuAAC click reaction of the Ru₂-alkynyl to the azide-treated surfaces, there is a reduction of the azide stretch in the IR which indirectly confirms the progress of the click reaction. The incorporation of Ru₂-alkynyl is confirmed by XPS, where we estimate the Ru₂-alkynyl covers about 10% of the azide sites.

The formation of molecular electronic junctions (Au/Ru₂-alkynyl/Si structures) by flip-chip lamination [7] for electrical and backside IR [8] characterizations is currently ongoing. With these results, we are able to obtain a thorough picture linking electrical properties with physical and chemical structure of the diruthenium molecular junctions.

S. P. Cummings et al., *Organometallics* 29, (2010) 2783 – 2788.

R. Chelmoski et al., *Langmuir* 25, (2009) 11480-11485.

G. Qin et al., *J. Am. Chem. Soc.* 132, (2010) 16432-16441.

R. E. Ruther et al., *J. Am. Chem. Soc.* 133, (2011) 5692 – 5694.

A. C. Cardiel et al., *ACS Nano* 6, (2012) 310-318.

P. K. B. Palomaki and P. H. Dinolfo, *Langmuir* 26, (2010) 9677 – 9685.

M. Coll et al., *J. Am. Chem. Soc.* 131, (2009) 12451-12457.

C. A. Richter et al., *J. Phys. Chem. B* 109, (2005) 21836 - 21841.

4:00pm **TF+EM+SS-ThA7 Vapor Phase Surface Functionalization using Hybrid SAMs / ALD Heterostructures**, *L. Lecordier, M.J. Dalberth, G. Sundaram, J.S. Becker*, Cambridge Nanotech, Inc.

Self-assembled monolayers and atomic layer deposition are two methodologies commonly used to tailor surface properties at the atomic scale and achieve thin films with excellent electrical, chemical, mechanical or optical performances thus leading to a broad portfolio of applications from thin films for flexible electronics to biological surface functionalization.

While ALD film growth is the result of a discretized process where inorganic monolayers are built upon one another through a sequence of reactant exposure/purge cycles until the desired film thickness is achieved (typically 1-100nm), SAMs on the other hand allow the deposition of a single ordered organic monolayer. Both processes are driven by self-limited chemisorbed surface reactions and can be deposited under vacuum conditions at relatively low temperatures, facilitating the integration of these two processes on a single platform.

The current work was implemented on a commercial Cambridge Nanotech hybrid ALD/SAMs platform. The tool is based on a Savannah S200 ALD reactor and integrates a SAMs kit for the accurate delivery of a variety of SAMs reactants. Stable SAMs monolayers are deposited under vacuum conditions using exposure mode (EXPO) characteristic of Cambridge Nanotech ALD tools. Key process metrics such as precursor pulse and exposure times, source and reactor temperatures were investigated for a variety of precursors including non-polar hydrophobic alkylsilanes (DTS), oleophobic fluorinated silanes (FOTS), hydrophilic polyethylene glycol (PEG) and thiols. In all cases, the self-limited surface saturation was achieved within 1 to 15 min minute exposures to the precursor at temperature ranging from 50 to 110°C.

In some instances, oxide ALD films were used to deposit a very thin seed layers (<5Å) to promote the adhesion of a SAM without prior surface cleaning/conditioning. Heterostructures based on oxide ALD (Al₂O₃, ZrO₂, SiO₂) and SAMs were also obtained to develop efficient water moisture barriers to be used for encapsulation. Overall the integration of these processes in a single platform provides a versatile and scalable method to surface functionalization where surface properties such as wettability can be tuned by controlling at the atomic level the structures of these hybrid coatings.

4:20pm **TF+EM+SS-ThA8 Chemically and Mechanically Stable Hydrophobic Thin Films Prepared by Combination of Layer-By-Layer Approach and Thiolene Chemistry**, *N. Madaan, J.A. Tuscano, N.R. Romriell, M.R. Linford*, Brigham Young University

The current aim of our research is to create robust hydrophobic thin films, for glass/silicon substrates, which can withstand extreme pH conditions and temperatures, have good release properties, and at the same time are mechanically durable. This approach consists of deposition of 3-aminopropyltriethoxy silane (APTES) on a silicon substrate followed by layer-by-layer deposition and cross-linking of alternating layers of poly(acrylic acid) (PAA) and poly(allylamine hydrochloride) (PAH). These nylon-like cross-linked layers have already been demonstrated to possess stability in extreme pH conditions. Their permeability can be controlled by the extent of crosslinking, which depends on the time and temperature of crosslinking. A careful study using X-ray photoelectron spectroscopy in our lab showed 71% cross-linking when these assemblies were heated at 250 °C for 2 h. We also found that the ratio of ammonium to amine groups in these bilayers is 2:1, and that there is a potential to impart additional properties to the films by utilizing these residual amine groups. This was part of an experimental design over a series of times and temperatures. These substrates can further be modified using a variety of chemistries. One approach is to expose these substrates to basic NaOH solution (pH ~ 10) in order to deprotonate the ammonium groups of the terminal PAH layer followed by treatment with Traut's reagent to convert amine groups into thiol groups. The thiol groups are then reacted with 1,2-polybutadiene and a perfluoroalkane thiol using thiol-ene chemistry. Another approach is to use hydrolyzed poly(maleic anhydride alt 1-octadecene) as a terminal electrostatic anionic layer. A chemical and tribological stability comparison will be performed between the above prepared films and a perfluoroalkane silane film on Si substrates. The effect of the total thickness of cross-linked PAH-PAA bilayers on the stability of prepared films will be studied. The substrates are thoroughly analyzed at each surface modification step using X-ray photoelectron spectroscopy, time-of-flight secondary ion mass spectrometry, ellipsometry, water contact angles, and atomic force microscopy.

4:40pm **TF+EM+SS-ThA9 A Detailed Investigation of the Conditions for Monolayer Deposition from Silane Precursors**, *J. Knauf*, Advanced Molecular Films GmbH / RWTH Aachen University, Germany, *L. Reddemann*, Advanced Molecular Films GmbH / Universität zu Köln, Germany, *A. Böker*, RWTH Aachen University, Germany, *K. Reihls*, Advanced Molecular Films GmbH, Germany

We have systematically investigated the process parameters for the vapor-phase deposition of monolayers from fluoroalkylated silane precursors. Our study reveals the influence of many process parameters on the molecular structure of the monolayers. Of particular interest to us are wetting and frictional properties of the monolayer obtained from the variation of process conditions. For reproducibly preparing high quality films particular parameters have to be meticulously controlled in a very narrow range which is not achievable without advanced deposition equipment.

Although the deposition of monolayers from silane precursors has been accomplished by various methods and has been subject to numerous studies, the properties and reproducibility of the resulting films remain unsatisfying for many applications. As an example, fluid wall slippage strongly depends on small changes in monolayer processing conditions which sensitively influence the structure of the monolayer deposited on structured surfaces [1].

Self-assembled monolayers (SAMs) were prepared by controlling a variety of process parameters, such as processing sequence and partial pressures of reactive compounds, deposition temperatures, adsorption/desorption times. These conditions were investigated for linear fluoroalkylated silane precursors of different chain lengths.

SAMs were deposited from fluoroalkylated silane precursors on pre-treated Si-wafers. Samples were examined by dynamic contact angle measurements, x-ray photoelectron spectroscopy (XPS), and static

secondary ion mass spectrometry (sSIMS). The precursors applied were linear 1H,1H,2H,2H-Perfluoroalkyltrichlorosilanes and varying chain lengths of the fluoroalkyl part were used for comparative studies based on detailed investigations using 1H,1H,2H,2H-Perfluorodecyltrichlorosilane. Short-chain precursors were commercially available in ready-to-use quality whereas longer-chain compounds starting from 1H,1H,2H,2H-Perfluorododecyltrichlorosilane were synthesized in our labs. While the short-chain compounds could be processed by routine measures special precautions had to be applied for storage and handling of longer-chain compounds due to their higher reactivity.

Results of the study of deposition conditions will be presented and discussed and may serve as a guideline for the reproducible preparation of well-defined monolayers from silane precursors.

[1] L. Reddemann, J. Knauf, A. Böker, K. Reihls, 14th International Conference on Organized Molecular Films (ICOMF14) - LB14, Abstract 146 (2012)

5:00pm **TF+EM+SS-ThA10 Self Limiting Behavior in the Directed Self-Assembly of Mounds on Patterned GaAs(001)**, *C.-F. Lin*, University of Maryland, *C.J.K. Richardson*, Laboratory for Physical Science, *H.-C. Kan*, University of Maryland, *N.C. Bartelt*, Sandia National Laboratories, *R.J. Phaneuf*, University of Maryland

We present results demonstrating directed self assembly of nm scale mounds during molecular beam epitaxial growth on patterned GaAs(001) surfaces. In the initial stages of growth, a lithographically-defined pattern directs the spontaneous formation of multilayer islands at the centers of bridges between near-neighbor nanopyls along [110] crystal orientation, seemingly due to the presence of an Ehrlich-Schwoebel barrier. As growth continues, the heights of mounds at these 2-fold bridge sites "self-limit". Beyond this point mounds at other, 4-fold bridge sites dominate the topography, but these self-limit as well. This behavior suggests the existence of a minimum, 'critical terrace width' for nucleation of islands during growth, and provides a physical mechanism for understanding the transient nature of the observed instability during growth on these patterned surfaces

5:20pm **TF+EM+SS-ThA11 Characterization of Fully Functional Spray-on Antibody Thin Film**, *J.J. Figueroa*, *S. Magana*, *D. Lim*, *R. Schlaf*, University of South Florida

Physical adsorption (solid-liquid interface) is known as a simple and rapid option to immobilize biomolecules on various surfaces. Proteins, receptors and antibodies are attached via physisorption to different surfaces by various attachment protocols. However, physical adsorption has been often labeled in the past with disadvantages like variability, reversibility and low surface density of immobilized biomolecules. In contrast, the presented research demonstrates that spray deposition with a pneumatic nebulizer can be used to immobilize fully functional and stable physisorbed antibody coatings on glass surfaces with high reproducibility.

The experiments were performed using a low flow concentric nebulizer (commonly used on mass spectrometry), regular glass slides as a substrate and *E. coli* O157:H7 antibody as prototypical test system. The antibody films were examined for functionality, specificity and shelf life. A series of films with varying thickness and deposition conditions was characterized with respect to functionality, mechanical stability, surface morphology and antibody density. The results demonstrate that the films are comparable to films prepared with the standard covalent attachment protocol (avidin-biotin). They show low denaturation or conformational changes, minimal loss during the rinsing process suggesting good attachment to the surface, and they perform as well with regard to sensitivity, specificity and shelf-life. The morphology studies suggest that the non-oriented attachment of the spray deposited antibodies (compared to the oriented attachment achieved with the covalent attachment scheme) is compensated by a higher antibody density enabled by the non-equilibrium spray deposition process.

Friday Morning, November 2, 2012

Energy Frontiers Focus Topic

Room: 15 - Session EN+SS-FrM

Photocatalysis and Solar Fuels

Moderator: N.G. Petrik, Pacific Northwest National Laboratory

8:20am EN+SS-FrM1 **Atomic Layer Deposition for Electronic Band Engineering of Silicon Photoelectrochemical Cells**, *B. Kalanyan, M.D. Losogo, D.H. Kim, G.N. Parsons*, North Carolina State University

Nanostructured semiconductor materials are generating considerable interest for application in photoelectrochemical cells (PEC) for solar water splitting. A key challenge is improving the long-term chemical and operational stability of semiconductor electrodes. Our research in PEC devices focuses on utilizing atomic layer deposition (ALD) as a means to engineer the semiconductor-liquid interface of photoelectrodes. ALD modification can both impart chemical stability and tune the electronic band structure at the semiconductor's surface. P-type silicon photocathodes are a model PEC system capable of high photocurrents (>10 mA/cm²) in aqueous electrolytes under AM 1.5 illumination. Here we will detail our efforts to improve the reproducibility of silicon photocathode fabrication and to use TiO₂ ALD coatings for band engineering that permits planar catalyst integration.

This talk will discuss silicon photocathodes fabricated from p-type Si (100) wafers with ~ 1 cm² functional area. Electrodes were tested in a three-electrode electrochemical cell containing sulfuric acid electrolyte (0.5M, pH ~ 0), a Pt mesh (>5 cm²) counter electrode, and a Ag/AgCl reference electrode. To ensure similar dopant profiles, experiments were run using a range of silicon samples from the same wafer. We will first discuss the effects of varying the processing schemes for forming an ohmic back contact. We find a large and distinct effect on both the photocurrent saturation value and the photocurrent onset potential with the size and composition of this back contact. Through contact optimization, series resistance of the back contact can be reduced by 5x, as measured by impedance spectroscopy.

The second portion of our talk will describe our results using ALD TiO₂ thin films to engineer the electronic band structure at the photocathode/electrolyte interface. Deposition of a coalesced Pt thin film catalyst layer directly on p-type silicon is well known to form an Ohmic contact that pins the silicon's Fermi level in a nearly flat band state. Without the internal bias caused by surface carrier depletion, photoelectrode activity is eliminated. However, by inserting an interfacial TiO₂ layer with sub-nanometer thickness control, a p-n junction can be formed which generates the necessary electric field for photoelectrode operation. Here, we will demonstrate how uniform ALD layers are capable of providing the necessary electronic band engineering to form completely planar p-Si/TiO₂/Pt structures with photocurrents exceeding 10 mA/cm² with no applied bias.

8:40am EN+SS-FrM2 **Photochemical Hole Scavenging Reactions of Methanol on TiO₂: Identification of Active Species and Water Coadsorption Study**, *M. Shen, M.A. Henderson*, Pacific Northwest National Laboratory

Molecular and dissociative forms of adsorbed methanol were prepared on the rutile TiO₂(110) surface to study their relative photocatalytic activity for hole-mediated oxidation. Molecular methanol is the dominant surface species on the vacuum-annealed TiO₂(110) surface in ultrahigh vacuum (UHV). Coadsorption of methanol with oxygen results in $\sim 20\%$ of the adsorbed methanol decomposing to methoxy and OH. Subsequent heating of the surface to 350 K leaves a surface with only adsorbed methoxy groups. Using temperature-programmed desorption, we show that adsorbed methoxy is at least an order of magnitude more reactive than molecularly adsorbed methanol for hole-mediated photooxidation. Methoxy photodecomposes through cleavage of a C-H bond forming adsorbed formaldehyde and a surface OH group. These results suggest that methoxy, and not molecular methanol, is the effective hole scavenger in photochemical reactions of methanol on TiO₂. Same reactions were also studied with water coadsorption.

9:00am EN+SS-FrM3 **Nanostructured Antimony Doped Tin Oxide Enhances Photoelectrochemical Water Splitting by Supported TiO₂**, *Q. Peng*, Duke University, *B. Kalanyan*, North Carolina State University, *M. Andrew, P. Hoertz*, Research Triangle Institute, *L. Alibabaei*, University of North Carolina at Chapel Hill, *J. Liu*, Duke University, *T.J. Meyer*, University of North Carolina at Chapel Hill, *G.N. Parsons*, North Carolina State University, *J.T. Glass*, Duke University

Photoelectrochemical (PEC) water splitting devices hold great promise for harvesting solar energy, however, existing electrodes suffer from either stability or efficiency limitations. Owing to its low production cost, environmental compatibility, and remarkable stability, TiO₂ has been widely investigated as a PEC electrode since 1972. However, the solar-to-fuel conversion efficiency of TiO₂ PEC electrodes is still much lower than the theoretical value. This is partially due to the dilemma of short minority carrier diffusion length and long optical absorption length, as well as the low electron mobility. Nanostructured conductive scaffolds show promise to solve this challenge by decoupling light absorption and charge carrier diffusion while enhancing conductivity. In this research, we synthesized TiO₂ PEC electrodes on a conductive scaffold comprised of antimony doped tin oxide particles (ATO-particle film). These structures, which are a cost effective alternative to semiconductor supported TiO₂ electrodes, yielded a photocurrent density of 0.58 mA/cm². This is approximately 3 \times the corresponding current density for planar TiO₂ PEC electrodes on FTO glass. Our results have shown that the porosity of ATO-particle film has limited the further efficiency improvement, which can be addressed by optimizing particle size, thickness, and assembly strategy for ATO-particle films. Owing to its transparency in a wide range of wavelengths, the ATO-particle scaffold also has great potential to boost the efficiency of devices using other narrow bandgap PEC materials, e. g. Fe₂O₃.

9:20am EN+SS-FrM4 **Plasmon-Mediated Charge Transfer in Au-TiO₂ Heterostructures for Visible Light Water-Splitting**, *J. DuChene, B. Sweeny*, University of Florida, *A. Johnston-Peck, D. Su*, Brookhaven National Laboratory, *W.D. Wei*, University of Florida

Solar water splitting to produce hydrogen represents a potential approach to satisfy the global energy demand in a sustainable manner. Recently it has been reported that the incorporation of plasmonic nanoparticles into semiconductor architectures offers a potential route to increase the efficiency of photoelectrochemical water splitting due to the unique optical properties of plasmonic nanomaterials. We investigated the energetics and dynamics of electron flow in Au-TiO₂ heterostructures following excitation of the Au nanoparticles surface plasmon resonance with visible light. Our results show that the incorporation of Au nanoparticles into wide band gap semiconductors has promise for use as visible light sensitizers. Moreover, we have studied the role of the hole scavenger methanol in the plasmon-mediated charge transfer process in order to ascertain the nature of possible thermodynamic or kinetic limitations involved in this process. These results demonstrate that the excited-state lifetime of these hot electrons in the TiO₂ conduction band is dramatically extended relative to direct band gap excitation within the semiconductor itself, suggesting a possible strategy for improving the efficiency of photocatalytic reactions.

9:40am EN+SS-FrM5 **Narrowing of Band Gap in 1D Arrays of TiO₂ Nanoparticles for Photocatalysis: Studies using X-ray Spectroscopies with In Situ Water Exposure and Heating**, *Y. Liu, J. Taing*, University of California Irvine, *C.C. Chen*, SLAC National Accelerator Lab, *A. Sorini*, Lawrence Livermore National Lab, *M.H. Cheng*, University of California Irvine, *H. Bluhm, Z. Liu*, Lawrence Berkeley National Lab, *T. Devereaux*, SLAC National Accelerator Lab, *J.C. Hemminger*, University of California Irvine

Titanium(IV) oxide (TiO₂) has a wide range of applications in energy science and acts as a stable support for photocatalysts and sensitizers. Utilizing ambient pressure synchrotron x-ray photoelectron and absorption spectroscopies, we explore the properties of TiO₂ thin films and ordered linear arrays of TiO₂ nanoparticles under *in situ* water vapor exposure and heating. Our nondestructive depth profiles (obtained by varying the photoelectron kinetic energy) of electronic and surface structures, combined with density-functional theory calculations, indicate an enhancement of the density of states (DOS) near the Fermi level due to surface Ti³⁺ and oxygen vacancies. Introducing water on the interface suppresses this DOS enhancement. The Ti L-edge and O K-edge absorption spectra, in combination with atomic multiplet calculations, provide information on crystal field effects and multiplet interactions, helping to determine the phases of the TiO₂ particles. Our *in situ* studies suggest that isolated TiO₂ nanoparticles may enhance solar absorption efficiency, and the TiO₂ band gap can be tuned reversibly under water exposure and heating.

10:00am **EN+SS-FrM6 A Theoretical Study of Carbon Dioxide Reduction on Catalysts**, *T. Liang, Y.-T. Cheng, S.R. Phillpot, S.B. Sinnott*, University of Florida

Catalytic reduction of carbon dioxide into fuels would provide an ideal storage medium for intermittent renewable energy sources. Copper and copper oxides electro-catalysts have been found to be capable of producing significant quantities of hydrocarbons or alcohols from CO₂ in aqueous solutions. Selectivity to methanol is speculated to be due to Cu(I) species in electrochemical systems; however, these pathways have not been experimentally verified. Here, the third-generation charge optimized many body (COMB3) potentials, which are proven to be successful to characterize different types of bonding in the heterogeneous systems, are employed to investigate the atomic scale mechanisms associated with catalytic reactions on Cu surfaces and clusters supported on metal oxide surfaces. In particular, the reaction free energies of selected CHO molecules on the Cu (211) surface are investigated and validated with density functional theory calculations. The electrochemical systems are simulated with room temperature, low-energy (5 or 10 eV) deposition of CO₂ or CO₂+H₂O on the Cu (211) surface and Cu cluster interface with the ZnO (101-1) surface. The results suggest that the higher incident energy and the presence of water molecules facilitate CO₂ dissociation. The charge state of the Cu cluster and the charge transfer process are predicted to play significant roles in the selectivity of the catalysts. In particular, the Cu(I) species at the Cu/ZnO interface are predicted to be preferable sites for CO₂ reduction and dissociation, which is consistent with experimental observations. This work was supported as part of the Center for Atomic Level Catalyst Design, an Energy Frontier Research Center funded by the U.S. Department of Energy, Office of Science, Office of Basic Energy Sciences under award number DE-SC0001058.

10:20am **EN+SS-FrM7 Doping Effects on the Electronic Structure of Graphitic C₃N₄ Photocatalysts: Insights from First Principles**, *S. Zuluaga, S. Stolbov*, University of Central Florida

Band gap engineering and facilitating charge separation in the graphitic C₃N₄ semiconductors are promising means for improving the photocatalytic activity of these materials. A number of experiments suggest that doping of C₃N₄ is an efficient way to increase the rate of hydrogen production from water using this photocatalyst. In this work we apply a first principles computational approach to reveal the main factors controlling the S and P doping effects on the properties of C₃N₄. Our density-functional-theory-based calculations show that these dopants are bound to the edges of the triazine elements rather than substituting N or C. Valence charge density analysis provides detailed description of the charge transfer upon doping. We show, for example, that S does not work as an anion in these materials: it does not accept, but donates electronic charge to the C - N system. Using the GW method we calculate with high accuracy the electronic structure, including the band gap, of the pristine and doped C₃N₄. We show that sufficiently large S doping make the system a conductor. The obtained results shed light on how doping affect the catalytic properties of C₃N₄.

Electron Transport at the Nanoscale Focus Topic Room: 16 - Session ET+SS+GR+SP-FrM

Electron Transport at the Nanoscale: Development of Theories and Techniques

Moderator: C. Su, Bruker Nano

8:20am **ET+SS+GR+SP-FrM1 What is Missing in the Space Charge Limited Current Theory?**, *X.-G. Zhang*, Oak Ridge National Laboratory, *S.T. Pantelides*, Vanderbilt University

INVITED

Space-charge-limited currents are important in energy devices such as solar cells and light-emitting diodes, but the available theory from the 1950's finds it necessary to postulate defect states that are distributed in energy in order to match data. This has prevented the theory to be used in extracting reliable defect information such as energy level and trap density from measurements. Here we revisit the theory and show that this postulate is not warranted. Instead, we demonstrate that dopants and the concomitant Frenkel effect, which have been neglected, control the shape of measured current-voltage characteristics. For highly disordered material, there is a significant inter-trap tunnelling current in the Ohmic regime, which accounts for the observed peak in the noise power. The new theory can anchor efforts to develop experimental techniques to measure deep-trap levels.

This research was conducted at the Center for Nanophase Materials Sciences, sponsored at ORNL by the Division of Scientific User Facilities (XGZ), and by Division of Material Science and Engineering, Basic Energy

Sciences, U.S. Department of Energy (STP), and the McMinn Endowment at Vanderbilt University (STP).

9:00am **ET+SS+GR+SP-FrM3 Mapping Solar Cell Internal Fields and Band Offsets**, *H. Cohen, Y. Itzhaik, G. Hodes*, Weizmann Institute of Science, Israel

The internal fields and band offsets across device interfaces are key features in various applications and, yet, this information is generally inaccessible by standard electrical tools. A systematic approach addressing this problem is demonstrated here, based on chemically resolved electrical measurements (CREM). Studying nanoporous photovoltaic cells, we resolve the internal details layer-by-layer and, thus, extract a realistic band diagram for the multi-interfacial structure. We show the spontaneous evolution of two p-n-like junctions and quantify the associated band bending at corresponding domains. An account for the 'real' working conditions of the device is attempted by exposing the cell to optical and electrical stimuli, revealing the charge trapping at each specific layer and showing how certain sample treatments affect the trapping mechanisms. Our methodology overcomes a critical missing link in device characterization and in fundamental studies of nanoscale solid-state devices.

9:20am **ET+SS+GR+SP-FrM4 Quantum Degeneracy Revealed by the Relation between the Tunneling Current and the Chemical Force**, *P. Jelinek, M. Ondracek*, Institute of Physics of ASCR, Czech Republic, *F. Flores*, Universidad Autonoma de Madrid, Spain

Recent progress has allowed merging AFM and STM into a new experimental setup where tunneling current and atomic forces are recorded simultaneously. The possibility to collect both quantities simultaneously opens new horizons not only in advanced characterization at the atomic scale but also in understanding fundamental relations between the electron transfer and formation of the chemical bond between two bodies.

Actually, there is a long-standing debate in the scientific community about the relation between the chemical force and the tunneling current (see e.g. [1]) on the atomic scale. Both the tunneling current and the short-range component of the force, induced by the formation of the chemical bond, exhibit in atomic contacts an exponential decay with increasing distance in the range of several angstroms. As the quantities depend directly on the wave-function overlap between outermost atoms of tip and surface, the corresponding exponential functions should have similar characteristic decay length. In particular, the relation between the chemical force F and the tunneling current I follows the law $F^n \sim I$, where n is an integer number. Over the last 10 years, several different scaling factors n , varying from 1 to 4, have been proposed by different groups based on both theoretical analysis and experimental measurements (see reference in [2]); still there is no consensus on the relation between the chemical force and the tunneling current.

In this contribution, we explain the relation between the tunneling current and the interaction force at the atomic scale using a simple analytical model [2]. The model unveils the existence of two characteristic scaling regimes, where the tunneling current is either proportional to the chemical force $I \sim F$ or to the square of the chemical force, i.e. $I \sim F^2$. We show that the existence of a given regime is basically controlled by two parameters: (i) the electronic level degeneracy and (ii) the hopping between electronic levels involved in the interaction process. Finally, we will collate our theoretical prediction with experimental AFM/STM measurements of single-atom point contacts and complex DFT simulations [3] to confirm the existence of these two characteristic regimes.

[1] W. Hofer and A.J. Fisher, *Phys. Rev. Lett.* 91, 036803 (2003) and the reply in by C.J. Chen

[2] P. Jelinek et al, *J. Cond. Mat. Phys.* 24, 084001 (2012).

[3] M. Ternes et al *Phys. Rev. Lett.* 106, 016802 (2011).

9:40am **ET+SS+GR+SP-FrM5 Understanding the Influence of the Tunneling Current and the Chemical Force on the Contrast Formation in KPFM**, *Z. Majzik, M. Ondráček, M. Švec, J. Berger, P. Jelinek*, Institute of Physics of ASCR, Czech Republic

Kelvin Probe Force Microscopy (KPFM) [1] senses the variation in the electrostatic force. The electrostatic force is $F_{el} = -dCTS/dz(V_{bias} - V_{lcpd})^2$, where V_{lcpd} denotes to the local contact potential difference (LCPD). Atomic scale resolution was achieved by KPFM on the prototypical Si(111)- 7×7 surface [2]. It was shown that the formation of a chemical bond between the closest tip-surface atoms induces significant variation in the LCPD [2]. Lately it was observed that the tunneling current leads to the raise of an additional electrostatic (phantom) force [3]. Consequently, the total electrostatic force must be the combination of several components where the contribution of each component is defined by the tip-sample separation.

Recent progress in Scanning Probe Microscopy opens the possibility of simultaneous acquisition of the tunneling current, atomic forces and local potential difference with atomic resolution [4]. The aim of this contribution is to discuss the origin of electrostatic force contribution at different tip-sample separations. In particular, we performed simultaneous site-specific AFM/STM measurements on Si(111)-7×7 using a modified Omicron qPlus (tuning fork based) system [5]. We found that along the tip approach three characteristic regions can be well distinguished. At large tip-sample separations, the capacitance is a function of tip geometry and the tip-sample distance. Approaching the tip closer towards the surface, quantum effects become to play important role. The overlap between the tip and sample wave functions produces electron tunneling, which induces additional electrostatic force. Formation of the chemical interaction between the tip apex atom and the adatoms of the 7×7 surface induces changes in the electron charge distribution reflected in variation of the LCPD [2] and the permittivity in the tunneling gap. Hence the capacitance is modified accordingly. In order to have better understanding of the impact of the chemical interaction, atomic hydrogen was deposited to saturate the dangling bonds of adatoms. Over the hydrogenated adatoms, no strong shift in the LCPD or sudden change in the capacitance was observed. Further to gain more insight into ongoing processes we carried out DFT calculations for tip-sample interaction to understand affect of the formation of covalent bond between tip apex and surface adatoms on the Si 7×7 surface.

References

- [1] M. Nonnenmacher et. al, App. Phys. Lett. 58, 2921 (1991)
- [2] S. Sadewasser et. al, Phys. Rev. Lett. 103, 266103 (2009)
- [3] A. J. Weymouth et. al, Phys. Rev. Lett. 106, 226801 (2011)
- [4] F.J. Giessibl, Appl. Phys. Lett. 73, 3956 (1998)
- [5] Z. Majzik et. al. B. J. Nano 249, 3 (2012)

10:00am **ET+SS+GR+SP-FrM6 An *In Situ* Technique for Using Ballistic Electron Emission Microscopy to Measure Hot Electron Transport at Metal Semiconductor Interfaces, R. Ralsano, V.P. LaBella,** University at Albany-SUNY

Ballistic electron emission microscopy (BEEM) is a scanning tunneling microscopy (STM) technique that can measure transport of hot electrons through materials and interfaces with high spatial and energetic resolution. BEEM requires an additional contact to ground the metal base layer of a metal semiconductor junction. Performing BEEM *in situ* with the sample fabrication requires a custom built STM or modifying a commercial one to facilitate the extra contact, which leaves the technique to highly trained experts. This presentation will describe our work to develop a special silicon substrate that has the extra contact and oxide hard mask built in to enable *in situ* BEEM without modifications to the STM. Electrically isolated contact traces are lithographically patterned *ex situ* onto the silicon substrate. Then a hard mask is grown and lithographically patterned and connected to the BEEM sample plate which is then inserted into the ultra-high vacuum chamber. The metal is then deposited on top of the hard mask and then mounted *in situ* onto the STM for BEEM measurements. BEEM measurements comparing both *in situ* and *ex situ* deposited films will be presented.

10:20am **ET+SS+GR+SP-FrM7 Electronic Transport on the Nanoscale, R. Moeller,** University of Duisburg-Essen, Germany **INVITED**

To study the transport through objects at the nanoscale a scanning tunneling microscope with several tips is used. Two different configurations will be discussed. The lateral transport of electrons may be studied by using two tips to drive a current parallel to the surface. A third tip enables to map the corresponding electrochemical potential. Measurements for a 2D conducting layer will be discussed. To analyze the transport perpendicular to the surface, a thin metallic layer is placed on a semiconducting surface. At the interface a Schottky barrier is formed, which can only be overcome by electrons of sufficient energy. This may be used to split the current of electrons coming from the tip of the microscope into two parts, the ballistic electrons and the electrons which have been scattered. This technique has been applied to study the ballistic transport of electrons through individual molecules. On the other hand inelastic processes may be revealed by analyzing the fluctuations in the tunneling current observed at different positions of the tunneling tip above an adsorbed molecule.

Authors Index

Bold page numbers indicate the presenter

— A —

Abdallah, L.S.: EL+TF+AS+EM+SS-TuP2, 24;
EL+TF+BI+AS+EM+SS-MoA9, 9
Abel, J.: GR+AS+NS+SP+SS-TuA11, 21
Adam, T.N.: EL+TF+AS+EM+SS+PS+EN+NM-
MoM9, 3
Adamiv, V.T.: AC+TF+SS+MI-MoA7, 8
Adamska, L.: ET+SS+GR+SP-ThA4, **57**;
GR+AS+EM+NS+SS-WeA2, 45
Addou, R.: GR+EM+NS+SS+TF-ThA7, **59**
Adib, K.: SS-TuM4, **18**
Ahmadi, M.: SS-TuP25, **29**
Ahn, J.R.: GR+EM+NS+PS+SS+TF-MoM11, 5;
GR+EM+NS+PS+SS+TF-MoM4, 4; SS+NS-
ThA3, 60
Ajayan, P.: GR+EM+NS+SS+TF-ThA3, 58
Aksamija, Z.: EM+SS+AS+NS-ThM10, **50**
Alaboson, J.M.P.: GR+AS+NS+SP+SS-TuA9, 21
Albrecht, P.M.: SS-TuM11, **18**
Alcantara, M.: SS+NS-ThA9, 61
Alem, N.: GR+AS+NS+SS-ThM5, 52
Alexander, M.R.: BI+SS+NS-WeM12, 33
Alexander, W.A.: SS-MoA1, 11
Alibabaei, L.: EN+SS-FrM3, 68
Allen, S.: BI+SS+AS-TuM5, **14**
Allen, T.: NS+AS+SS+SP-WeM2, 35
Alles, M.L.: EM+SS+AS+NS-ThM11, 51
Altman, E.I.: OX+SS+TF+MI-MoA2, **9**
Alves, E.: AC+TF+SS+MI-MoA9, 8
Amanpour, M.: SS-WeA1, 48
Andersen, J.N.: GR+AS+NS+SP+SS-TuA7, 20;
IS+AS+SS+EN-TuM12, 17
Andrew, M.: EN+SS-FrM3, 68
Antony, A.: SS+EN+OX-ThM10, 54
Aoki, Y.: SS-MoA8, **12**
Arahara, S.: SS-TuP7, 26
Arman, M.A.: GR+AS+NS+SP+SS-TuA7, 20;
IS+AS+SS+EN-TuM12, 17
Arnadottir, L.: SS-ThA6, **62**
Arnebrant, T.: BI+SS+AS-TuM3, **14**
Arnold, M.S.: GR+AS+EM+NS+SS-WeA9, 45
Artyushkova, K.: IS+AS+SS+EN-TuM6, **16**
Aryal, P.: EL+TF+AS+EM+SS+PS+EN+NM-
MoM1, 2
Asthagiri, A.: SS+EN+OX-ThM10, 54
Atanassov, P.: IS+AS+SS+EN-TuM6, 16
Attygalle, D.: EL+TF+AS+EM+SS+PS+EN+NM-
MoM1, 2
Auerbach, D.J.: SS-MoM4, **6**
Augustine, B.H.: SS-WeM10, **41**
Autes, G.: GR+AS+NS+SS-ThM5, 52
Auzély, R.: BI+SS+NS-WeM10, 33
Axnanda, S.: IS+AS+SS+EN-TuM4, **16**

— B —

Baber, A.: SS-WeM1, 39
Baddorf, A.P.: SS-WeM4, 40
Bagus, P.S.: SS+OX-WeM9, **39**
Barcaro, G.: SS+OX-WeM12, 39
Bare, S.R.: SS-WeA7, **48**
Barkam, S.: SS-TuP12, 27
Barlaz, D.E.: SS+EN+OX-ThM4, **53**
Barlow, A.J.: SS+NS-ThA7, **60**
Barrett, N.: GR+AS+NS+SP+SS-TuA1, 20
Barteau, M.: SS-WeA9, 48
Bartels, C.: SS-MoM4, 6
Bartels, L.: SP+AS+BI+ET+MI+NM+NS+SS+TF-
WeM5, 36; SS-WeA1, 48; SS-WeM2, **40**
Bartelt, N.C.: TF+EM+SS-ThA10, 67
Barton, D.: EL+TF+AS+EM+SS+PS+EN+NM-
MoM10, 3
Bartynski, R.A.: OX+SS+TF+MI-MoA6, 10
Baski, A.A.: SS+EM-WeA1, 46
Batzill, M.: GR+AS+EM+NS+SS-WeA8, 45;
GR+EM+NS+SS+TF-ThA7, 59; SS-TuP15, 27
Bazarov, I.: VT+AS+SS-WeM2, 42

Becchaku, M.: SS-TuP17, 27
Becker, J.S.: TF+EM+SS-ThA7, 66
Bedzyk, M.J.: GR+AS+BI+PS+SS-WeM1, **34**;
GR+AS+NS+SP+SS-TuA9, 21
Beechem, T.E.: GR+AS+NS+SP+SS-TuA8, 20
Behafarid, F.: SS+NS-ThA8, **61**; SS-TuP27, 29
Benavidez, T.: EL+TF+BI+AS+EM+SS-MoA3, 8
Bennetsen, D.T.: BI+SS+NS-WeM1, **32**
Bennett, C.J.: GR+AS+BI+PS+SS-WeM9, 35
Bent, S.F.: SS+EM-WeA8, 47
Ben-Yoav, H.: BI+SS+NS-WeM2, 32
Berger, J.: ET+SS+GR+SP-FrM5, 69
Beringer, D.B.: VT+AS+SS-WeM10, 42;
VT+AS+SS-WeM6, 42; VT+AS+SS-WeM9,
42
Bernholc, J.: SS-WeM4, 40
Besnier, J.-F.: EL+TF+AS+EM+SS+PS+EN+NM-
MoM3, 2
Bezares, F.J.: GR+AS+BI+PS+SS-WeM9, 35
Bhairamagdi, N.S.: TF+EM+SS-ThA4, **65**
Bhattacharya, A.: NS+AS+SS+SP-WeM12, 36
Bhattacharyya, D.: EM+SS+AS+NS-ThM4, **50**
Biegalski, M.D.: IS+AS+SS+EN-TuM5, 16
Bielefeld, J.: GR+EM+NS+SS+TF-ThA1, 58
Blanch, A.J.: SS+NS-ThA7, 60
Blomfield, C.J.: AS+NS+SS+TF-WeA8, 44
Bluhm, H.: EN+SS-FrM5, 68; IS+AS+SS+EN-
TuM1, **15**; IS+AS+SS+EN-TuM5, 16; SS-
ThA1, 61
Bobek, S.: SS-WeA1, 48; SS-WeM2, 40
Bockowski, M.: AC+TF+SS+MI-MoA9, 8
Böker, A.: TF+EM+SS-ThA9, 66
Bonnell, D.A.: SS+OX-WeM10, 39
Bora, D.: IS+AS+SS+EN-TuM3, 15
Boturyn, D.: BI+SS+NS-WeM10, 33
Boucher, M.: SS-WeM1, 39
Bourgeois, S.: SS+OX-WeM6, 38
Bowden, M.E.: SS+EN+OX-ThM11, 54
Brant, A.T.: AC+TF+SS+MI-MoA7, 8
Braun, A.: IS+AS+SS+EN-TuM3, 15
Brewer, J.R.: EL+TF+AS+EM+SS-TuP1, 24
Brown, A.: BI+SS+NS-WeM2, 32
Bruhn, T.: GR+EM+NS+SS+TF-ThA6, 59
Brumbach, M.T.: OX+SS+TF+MI-MoA9, **10**
Buchanan, D.A.: AC+TF+SS+MI-MoA7, 8
Buchholz, M.: OX+SS+TF+MI-MoA10, **10**
Burak, Ya.V.: AC+TF+SS+MI-MoA7, 8
Burghaus, U.: NS+AS+SS+SP-WeM4, 35; SS-
TuP19, 28
Bürstel, D.: SS-MoM2, 5
Busse, C.: GR+AS+NS+SP+SS-TuA7, 20
Butorin, S.M.: AC+MI+SS+TF-MoM5, **1**

— C —

Cai, M.: GR+AS+NS+SS-ThM10, 52
Caillard, L.: EL+TF+BI+AS+EM+SS-MoA2, 8
Caldwell, J.D.: GR+AS+BI+PS+SS-WeM9, 35
Calzolari, L.: BI+SS+AS-TuM12, 15
Camillone, N.: NS+AS+SS+SP-WeM12, **36**
Campbell, C.T.: SS-TuM12, 19; SS-WeM6, 40;
SS-WeM9, **40**
Cartas, W.S.: SS-TuP23, **28**
Casolo, S.: GR+AS+EM+NS+SS-WeA12, 46
Castner, D.G.: BI+SS+AS-TuM6, **14**
Ceccone, G.: BI+SS+AS-TuM12, **15**
Chabal, Y.J.: EL+TF+BI+AS+EM+SS-MoA2, 8;
GR+AS+BI+PS+SS-WeM2, 34;
GR+AS+EM+NS+SS-WeA1, 45; SS+EM-
WeA11, 47; SS+EM-WeA9, **47**; SS-TuP21, 28;
SS-WeA12, 49; TF+AS+SS-ThA3, 63
Chagarov, E.:
SP+AS+BI+ET+MI+NM+NS+SS+TF-WeM6,
37
Chakradhar, A.: NS+AS+SS+SP-WeM4, 35; SS-
TuP19, **28**
Chamberlin, S.E.: SS+EN+OX-ThM11, **54**

Chambers, S.: SS+OX-WeM3, 38
Chambers, S.A.: SS+EN+OX-ThM11, 54; SS+OX-
WeM5, 38
Chan, C.K.: VT+AS+SS-WeM1, 41
Chang, C.C.: VT+AS+SS-WeM1, 41
Chang, M.H.: EM+SS+AS+NS-ThM12, 51
Chang, Y.H.: EM+SS+AS+NS-ThM12, 51
Chaudhuri, S.: SS-WeA12, 49
Chen, C.C.: EN+SS-FrM5, 68
Chen, C.L.: VT+AS+SS-WeM1, **41**
Chen, D.A.: SS-WeA3, **48**
Chen, J.: EL+TF+AS+EM+SS+PS+EN+NM-
MoM4, 2; GR+AS+NS+SP+SS-TuA2, 20; SS-
TuP3, 24; SS-WeA9, 48
Chen, J.-H.: GR+AS+NS+SS-ThM5, 52
Chen, J.R.: VT+AS+SS-WeM1, 41
Chen, S.: GR+AS+NS+SP+SS-TuA11, 21
Cheng, D.F.: SS-ThM1, 55
Cheng, D.L.: SS-TuP37, 31
Cheng, M.H.: EN+SS-FrM5, 68
Cheng, Y.-T.: EN+SS-FrM6, 69
Chiang, S.: SS+NS-ThA6, **60**
Chitre, K.: OX+SS+TF+MI-MoA6, 10
Cho, K.J.: GR+AS+EM+NS+SS-WeA1, 45
Choi, J.Y.: GR+EM+NS+PS+SS+TF-MoM11, 5
Chopra, L.: SS-WeA12, **49**
Christen, H.M.: IS+AS+SS+EN-TuM5, 16
Chumbuni-Torres, K.: EL+TF+BI+AS+EM+SS-
MoA3, 8
Chung, B.W.: AC+MI+SS+TF-MoM9, 1
Chupas, P.: IS+AS+SS+EN-TuM9, 16
Ciarnelli, V.: BI+SS+NS-WeM12, **33**
Cimpoiasu, E.: GR+AS+NS+SS-ThM3, 52
Clark, K.: ET+SS+GR+SP-ThA6, **57**;
GR+EM+NS+PS+SS+TF-MoM2, 4
Clavero, C.: TF+AS+SS-ThA8, 64; VT+AS+SS-
WeM10, 42; VT+AS+SS-WeM6, 42
Coh, S.: OX+SS+TF+MI-MoA6, 10
Cohen, H.: ET+SS+GR+SP-FrM3, **69**
Cohen, K.D.:
SP+AS+BI+ET+MI+NM+NS+SS+TF-WeM5,
36; SS-WeM2, 40
Colby, R.: AS+NS+SS+TF-WeA3, 44;
AS+NS+SS+TF-WeA4, 44
Collins, R.W.: EL+TF+AS+EM+SS+PS+EN+NM-
MoM1, 2; EL+TF+AS+EM+SS+PS+EN+NM-
MoM4, 2
Conrad, E.: GR+AS+NS+SP+SS-TuA1, 20
Constable, E.C.: IS+AS+SS+EN-TuM3, 15
Cook, K.: EL+TF+BI+AS+EM+SS-MoA10, **9**
Cooper, R.: SS-MoM4, 6
Copel, M.W.: GR+EM+NS+PS+SS+TF-MoM8, 4
Coraux, J.: GR+AS+EM+NS+SS-WeA10, 46
Corso, M.: SP+AS+BI+ET+MI+NM+NS+SS+TF-
WeM4, 36
Cortes, R.: GR+EM+NS+SS+TF-ThA2, **58**
Coultais, S.J.: AS+NS+SS+TF-WeA8, 44
Creatore, M.: EL+TF+AS+EM+SS+PS+EN+NM-
MoM6, 2
Croad, O.: BI+SS+AS-TuM5, 14
Croy, J.R.: SS-TuP27, 29
Crumlin, E.: IS+AS+SS+EN-TuM5, **16**
Cui, S.: GR+AS+NS+SP+SS-TuA2, 20; SS-TuP3,
24
Culbertson, J.C.: GR+EM+NS+PS+SS+TF-
MoM3, 4
Culver, J.: BI+SS+NS-WeM2, 32
Cummings, S.P.: TF+EM+SS-ThA6, 66
Cumpson, P.J.:
SP+AS+BI+ET+MI+NM+NS+SS+TF-
WeM10, 37
Cyganik, P.: SS+NS-ThA10, **61**; TF+AS+SS-
ThA2, 63

— D —

Dadap, J.: SS-TuP2, 24

Dahal, A.: GR+AS+EM+NS+SS-WeA8, 45;
GR+EM+NS+SS+TF-ThA7, 59
Dalberth, M.J.: TF+EM+SS-ThA7, 66
Darackchieva, V.: AC+TF+SS+MI-MoA9, 8
Dasari, S.: SS-MoM10, 6; SS-MoM11, 6; SS-TuP16, 27
Datye, A.: SS-TuP27, 29
Davies, M.C.: BI+SS+NS-WeM12, 33
De la Ree, A.B.: SS-WeM12, 41
De Padova, P.: GR+EM+NS+SS+TF-ThA6, 59
DeLaRiva, A.T.: SS-TuP27, 29
Demers-Carpentier, V.: SS-ThM5, 55
Demko, A.: NS+AS+SS+SP-WeM2, 35
Dendzik, M.: SS+NS-ThA10, 61
Deng, X.: SS-ThA8, 62
Denk, M.: SS+OX-WeM12, 39
Deskins, N.A.: SS+EN+OX-ThM9, 54; SS-TuM5, 18
Detslefs, B.: GR+AS+NS+SP+SS-TuA9, 21
Devaraj, A.: AS+NS+SS+TF-WeA3, 44;
AS+NS+SS+TF-WeA4, 44
Devereaux, T.: EN+SS-FrM5, 68
DeVore, T.C.: SS-WeM10, 41
Dhiman, R.: EM+SS+AS+NS-ThM3, 50
Dickinson, J.E.: SS-TuM4, 18
Diebold, A.C.:
EL+TF+AS+EM+SS+PS+EN+NM-MoM9, 3;
GR+AS+NS+SP+SS-TuA11, 21
Diesing, D.: SS-MoM2, 5; SS-MoM3, 5; SS-TuP24, 29
DiLabio, G.:
SP+AS+BI+ET+MI+NM+NS+SS+TF-WeM2, 36
Dimitrakopoulos, C.: GR+AS+NS+SP+SS-TuA11, 21
Dohnalek, Z.: SS+EN+OX-ThM5, 53; SS-TuM1, 17
Domen, K.: SS+EN+OX-ThM1, 53
Domenichini, B.: SS+OX-WeM6, 38
Donaldson, S.H.: BI+SS+NS-WeM5, 32
Dong, Y.: SS-ThM5, 55
Doris, B.: EL+TF+AS+EM+SS+PS+EN+NM-MoM9, 3
Dornstetter, J.-C.:
EL+TF+AS+EM+SS+PS+EN+NM-MoM3, 2
Doubina, N.: SS-TuP14, 27
Dougherty, D.B.: GR+AS+BI+PS+SS-WeM10, 35; GR+AS+NS+SP+SS-TuA11, 21
Dowben, P.A.: AC+TF+SS+MI-MoA1, 7;
AC+TF+SS+MI-MoA7, 8
Draper, R.: NS+AS+SS+SP-WeM2, 35
Drews, J.: EM+SS+AS+NS-ThM3, 50
Du, Y.G.: SS-TuM5, 18
Dubacheva, G.V.: BI+SS+NS-WeM10, 33
DuChene, J.: EN+SS-FrM4, 68
Duke, A.: SS-WeA3, 48
Dunham, B.M.: VT+AS+SS-WeM2, 42
Durakiewicz, T.: AC+MI+SS+TF-MoM8, 1
Duzik, A.: SS-TuP34, 30

— E —

Ealet, B.: GR+EM+NS+SS+TF-ThA6, 59
Eastman, P.Y.: AS+NS+SS+TF-WeA9, 45
Eddy, Jr., C.R.: GR+AS+BI+PS+SS-WeM9, 35;
GR+AS+NS+SP+SS-TuA9, 21;
GR+EM+NS+PS+SS+TF-MoM1, 3;
GR+EM+NS+PS+SS+TF-MoM3, 4; SS+EM-WeA1, 46
Edmonds, M.:
SP+AS+BI+ET+MI+NM+NS+SS+TF-WeM6, 37
Edwards, P.R.: AC+TF+SS+MI-MoA9, 8
Elam, J.W.: IS+AS+SS+EN-TuM9, 16
Emery, J.D.: GR+AS+BI+PS+SS-WeM1, 34;
GR+AS+NS+SP+SS-TuA9, 21
Engelhard, M.: TF+AS+SS-ThA11, 65
Enta, Y.: GR+EM+NS+PS+SS+TF-MoM10, 5
Ernst, K.-H.: SS-ThM6, 55; SS-TuM9, 18
Escamilla, R.: SS-TuP10, 26

— F —

Fahey, A.J.: AS+NS+SS+TF-WeA7, 44
Fan, X.: BI+SS+NS-WeM2, 32
Faradzhev, N.S.: SS-TuM3, 17
Farmer, B.L.: GR+AS+BI+PS+SS-WeM6, 34
Fartmann, M.: TF+AS+SS-ThA4, 63
Faubel, M.: SS-ThA2, 62
Feenstra, R.: GR+AS+NS+SP+SS-TuA10, 21
Feldman, Y.: NS+AS+SS+SP-WeM4, 35
Felhofer, J.L.: EL+TF+BI+AS+EM+SS-MoA3, 8
Feng, X.F.: SS-TuP37, 31
Fenter, P.: GR+AS+BI+PS+SS-WeM1, 34
Ferguson, G.S.: EL+TF+BI+AS+EM+SS-MoA10, 9
Ferguson, J.D.: SS+EM-WeA1, 46
Ferrighi, L.: SS-ThM5, 55
Ferris, R.J.: BI+SS+NS-WeM9, 33
Figueroa, J.J.: TF+EM+SS-ThA11, 67
First, P.N.: GR+AS+NS+SP+SS-TuA3, 20
Fleetwood, D.M.: EM+SS+AS+NS-ThM11, 51
Fleutot, B.: SS-WeA11, 49
Flood, A.: SS-MoA3, 11
Floreano, L.: SS+OX-WeM6, 38
Flores, F.: ET+SS+GR+SP-FrM4, 69
Flores, M.: SS-TuP10, 26
Fortunelli, A.: SS+OX-WeM12, 39
Foss, M.: BI+SS+NS-WeM1, 32
Franke, K.J.:
SP+AS+BI+ET+MI+NM+NS+SS+TF-WeM4, 36
French, B.: GR+EM+NS+SS+TF-ThA1, 58
French, M.: GR+EM+NS+SS+TF-ThA1, 58
Frenkel, A.I.: SS-TuP27, 29
Fromm, F.: GR+EM+NS+PS+SS+TF-MoM10, 5
Fruchart, O.: GR+AS+EM+NS+SS-WeA10, 46
Fuchs, E.: SS-TuP21, 28
Fuentes-Cabrera, M.: SS-WeM4, 40
Fujishima, A.: SS-TuP18, 28
Fujitani, T.: SS-TuP29, 29; SS-TuP30, 30
Fukidome, H.: GR+EM+NS+PS+SS+TF-MoM10, 5
Fukutani, K.: SS-MoA9, 12

— G —

Gai, Z.: SS-WeM4, 40
Gajdardziska-Josifovska, M.:
GR+AS+NS+SP+SS-TuA2, 20; SS-TuP3, 24
Galatsis, K.: EM+SS+AS+NS-ThM11, 51
Galhenage, R.P.: SS-WeA3, 48
Galoppini, E.: OX+SS+TF+MI-MoA6, 10
Gao, H.-J.: ET+SS+GR+SP-ThA1, 57
Gao, J.: SS-WeA10, 49
Garces, N.Y.: GR+EM+NS+PS+SS+TF-MoM1, 3;
GR+EM+NS+PS+SS+TF-MoM3, 4
Garcia, C.D.: EL+TF+BI+AS+EM+SS-MoA3, 8
Gargiulo, F.: GR+AS+NS+SS-ThM5, 52
Gartstein, Yu.N.: EL+TF+BI+AS+EM+SS-MoA2, 8
Gaskill, D.K.: GR+AS+BI+PS+SS-WeM9, 35;
GR+AS+NS+SP+SS-TuA9, 21;
GR+EM+NS+PS+SS+TF-MoM1, 3;
GR+EM+NS+PS+SS+TF-MoM3, 4
Gaub, H.E.:
SP+AS+BI+ET+MI+NM+NS+SS+TF-WeM11, 37
Gautam, A.: GR+AS+NS+SS-ThM5, 52
Ge, Q.: SS-TuM10, 18
Gebbie, M.A.: BI+SS+NS-WeM5, 32
Gellman, A.J.: SS-MoA6, 11; SS-ThM2, 55; SS-WeA11, 49
Gerber, T.: GR+AS+NS+SP+SS-TuA7, 20
Ghodssi, R.: BI+SS+NS-WeM2, 32
Gilliland, D.: BI+SS+AS-TuM12, 15
Giner, I.: OX+SS+TF+MI-MoA11, 11
Ginting, E.: SS-TuP13, 27
Glass, J.T.: EN+SS-FrM3, 68
Gleason, K.K.: EM+SS+AS+NS-ThM4, 50
Goldman, R.S.: EM+SS+AS+NS-ThM13, 51
Goldoni, A.: AC+TF+SS+MI-MoA3, 7

Golibrzuch, K.: SS-MoM4, 6
Gollub, S.L.: SS+OX-WeM4, 38; SS-TuP5, 25
Gonçalves, A.: AC+TF+SS+MI-MoA6, 7
Gong, C.: GR+AS+EM+NS+SS-WeA1, 45
Gorovikov, S.: AC+TF+SS+MI-MoA3, 7
Goubert, G.: SS-ThM5, 55
Grånäs, E.: GR+AS+NS+SP+SS-TuA7, 20;
IS+AS+SS+EN-TuM12, 17
Grant, J.T.: TF+AS+SS-ThA10, 64
Grätzel, M.: IS+AS+SS+EN-TuM3, 15
Greeley, J.: IS+AS+SS+EN-TuM9, 16
Grehl, T.: TF+AS+SS-ThA4, 63
Greiner, M.T.: OX+SS+TF+MI-MoA7, 10
Grill, A.: GR+AS+NS+SP+SS-TuA11, 21
Grundmeier, G.: OX+SS+TF+MI-MoA11, 11; SS-ThA9, 62; TF+AS+SS-ThA1, 63
Grunze, M.H.: BI+SS+AS-TuM2, 14
Guereute, L.: BI+SS+NS-WeM10, 33
Gumuslu, G.: SS-WeA11, 49
Gunlycke, D.: GR+AS+NS+SS-ThM3, 52
Guo, J.H.: IS+AS+SS+EN-TuM3, 15
Guo, Z.-P.: SS-TuP9, 26
Gutmann, S.: ET+SS+GR+SP-ThA11, 58

— H —

Habenicht, B.: GR+AS+EM+NS+SS-WeA11, 46
Hacker, C.A.: TF+EM+SS-ThA6, 66
Hackett, J.B.: VT+AS+SS-WeM9, 42
Haehner, G.:
SP+AS+BI+ET+MI+NM+NS+SS+TF-WeM9, 37
Hagenhoff, B.: TF+AS+SS-ThA4, 63
Hager, G.: AS+NS+SS+TF-WeA7, 44
Hagiwara, A.: SS-TuP8, 26
Hakanoglu, C.: SS+EN+OX-ThM10, 54; SS-TuP22, 28
Halevi, B.: IS+AS+SS+EN-TuM6, 16
Hammers, R.J.: SS-ThM9, 56
Hammer, B.: SS-ThM5, 55
Han, C.B.: SS-WeM4, 40
Han, Y.: SS+NS-TuA11, 23
Han, Y.-K.: SS-ThM12, 56
Handa, H.: GR+EM+NS+PS+SS+TF-MoM10, 5
Hannon, J.B.: GR+EM+NS+PS+SS+TF-MoM8, 4
Hao, Y.: GR+AS+NS+SP+SS-TuA11, 21
Hapala, P.: ET+SS+GR+SP-ThA9, 57
Harada, K.: SS-TuP32, 30
Harada, Y.: GR+AS+EM+NS+SS-WeA12, 46
Harl, R.R.: SS+OX-WeM4, 38; SS-TuP5, 25
Harrell, W.R.: SS+OX-WeM3, 38
Harriss, J.E.: SS+OX-WeM3, 38
Hashemian, M.: SS-MoM10, 6; SS-MoM11, 6; SS-TuP16, 27
Hasselbrink, E.: SS-MoM3, 5; SS-TuP24, 29
Havela, L.: AC+TF+SS+MI-MoA6, 7
Haydell, M.: GR+AS+NS+SS-ThM3, 52
Hayden, B.E.: SS+NS-TuA9, 22
He, G.: GR+AS+NS+SP+SS-TuA10, 21
Heald, S.M.: SS+OX-WeM5, 38
Hemminger, J.C.: EN+SS-FrM5, 68; SS+NS-TuA3, 22; SS-ThA1, 61; SS-ThA2, 62; SS-WeM11, 41; SS-WeM12, 41
Henderson, C.: EL+TF+BI+AS+EM+SS-MoA6, 8
Henderson, M.A.: EN+SS-FrM2, 68; SS+EN+OX-ThM11, 54; SS-TuM5, 18
Herdiech, M.W.: OX+SS+TF+MI-MoA2, 9
Hernández, S.C.: GR+AS+BI+PS+SS-WeM9, 35;
GR+EM+NS+PS+SS+TF-MoM1, 3
Herrera, V.: BI+SS+NS-WeM6, 32
Hersam, M.C.: GR+AS+BI+PS+SS-WeM1, 34;
GR+AS+BI+PS+SS-WeM3, 34;
GR+AS+NS+SP+SS-TuA9, 21
Hill, S.B.: SS-TuM3, 17
Hiramatsu, M.: GR+AS+NS+SS-ThM9, 52
Hirayama, H.: SS-MoA8, 12
Hirsch, B.: SS-MoA3, 11
Hirschmugl, C.: GR+AS+NS+SP+SS-TuA2, 20;
SS-TuP3, 24
Hite, J.K.: SS+EM-WeA1, 46
Hodes, G.: ET+SS+GR+SP-FrM3, 69

Hoertz, P.: EN+SS-FrM3, 68
 Holzke, C.: SP+AS+BI+ET+MI+NM+NS+SS+TF-WeM5, 36
 Hong, M.: SS+NS-ThA4, 60
 Hong, S.: SS+NS-ThA9, 61
 Hong, S.-Y.: SS-TuP2, 24
 Hong, W.T.: IS+AS+SS+EN-TuM5, 16
 Hooley, R.: SS-WeM2, 40
 Hori, M.: GR+AS+NS+SS-ThM9, 52
 Horsfall, A.B.: GR+EM+NS+PS+SS+TF-MoM1, 3
 Hou, J.B.: SS+NS-TuA11, 23
 Howe, J.: GR+EM+NS+PS+SS+TF-MoM3, 4
 Hozumi, A.: SS-ThM1, 55
 Hsiung, G.Y.: VT+AS+SS-WeM1, 41
 Hu, S.W.: SS+NS-TuA11, 23; SS-TuP37, 31
 Huerta, L.: SS-TuP10, 26
 Hughes, W.C.: SS-WeM10, 41
 Hussein, R.: BI+SS+AS-TuM12, 15
 Hutton, S.J.: AS+NS+SS+TF-WeA8, 44

— I —

Iacobucci, S.: AC+TF+SS+MI-MoA3, 7
 Ianno, N.J.: EL+TF+AS+EM+SS-TuP1, 24
 Ide, T.: GR+EM+NS+PS+SS+TF-MoM10, 5
 Ilton, E.S.: SS+OX-WeM9, 39
 Ishigami, M.: GR+AS+BI+PS+SS-WeM6, 34
 Ishii, S.: TF+EM+SS-ThA3, 65
 Ishikawa, K.: GR+AS+NS+SS-ThM9, 52
 Ismail-Beigi, S.: OX+SS+TF+MI-MoA2, 9
 Israealachvili, J.N.: BI+SS+NS-WeM5, 32
 Itzhaik, Y.: ET+SS+GR+SP-FrM3, 69

— J —

Jaehnig, M.: GR+EM+NS+SS+TF-ThA1, 58
 Jakubiak, R.: TF+AS+SS-ThA10, 64
 Jelinek, P.: ET+SS+GR+SP-FrM4, 69; ET+SS+GR+SP-ThA9, 57
 Jelinek, P.: ET+SS+GR+SP-FrM5, 69
 Jena, D.: GR+AS+NS+SS-ThM11, 53
 Jewell, A.D.: SS-MoA7, 11; SS-TuP1, 24
 Ji, S.-H.: GR+EM+NS+PS+SS+TF-MoM8, 4
 Johnson, M.: NS+AS+SS+SP-WeM2, 35
 Johnston-Peck, A.: EN+SS-FrM4, 68
 Joly, Y.: SS+OX-WeM5, 38
 Jones, J.G.: TF+AS+SS-ThA10, 64
 Jordan, K.D.: SS-ThA8, 62
 Ju, H.X.: SS-TuP35, 30
 Jung, J.: SS-ThM12, 56
 Juppille, J.: SS+OX-WeM6, 38

— K —

Kahng, S.-J.: EM+SS+AS+NS-ThM12, 51
 Kajiwaru, T.: GR+AS+NS+SS-ThM1, 51
 Kakekhanian, A.: OX+SS+TF+MI-MoA2, 9
 Kalanyan, B.: EN+SS-FrM1, 68; EN+SS-FrM3, 68
 Kalinin, S.V.: ET+SS+GR+SP-ThA7, 57
 Kameshima, Y.: SS-TuP17, 27
 Kan, H.-C.: TF+EM+SS-ThA10, 67
 Kanda, T.: GR+AS+NS+SS-ThM9, 52
 Kandel, S.A.: ET+SS+GR+SP-ThA3, 57
 Kandratsenka, A.: SS-MoM4, 6
 Kanno, Y.: SS-TuP8, 26
 Karakoti, A.S.: SS-TuP12, 27; SS-TuP26, 29
 Karim, A.M.: IS+AS+SS+EN-TuM10, 16
 Karmel, H.J.: GR+AS+NS+SP+SS-TuA9, 21
 Karp, E.M.: SS-WeM6, 40; SS-WeM9, 40
 Karpov, E.: SS-MoM10, 6; SS-MoM11, 6; SS-TuP16, 27; SS-TuP24, 29
 Kasouit, S.: EL+TF+AS+EM+SS+PS+EN+NM-MoM3, 2
 Kaspar, T.C.: SS+EN+OX-ThM11, 54; SS+OX-WeM5, 38
 Kasuya, A.: SS-MoA10, 12
 Kato, H.: SS-MoA10, 12; SS-TuP31, 30
 Kato, T.: SS-TuP18, 28
 Katoch, J.: GR+AS+BI+PS+SS-WeM6, 34
 Kawai, M.: BI+SS+NS-WeM11, 33; SS-ThM12, 56
 Kawai, Y.: GR+EM+NS+PS+SS+TF-MoM10, 5
 Kawasaki, H.: SS-ThA10, 62
 Kay, B.D.: SS+EN+OX-ThM5, 53; SS-ThA3, 62

Kelley, M.J.: VT+AS+SS-WeM4, 42
 Kellogg, G.L.: GR+AS+NS+SP+SS-TuA8, 20
 Kelly, T.D.: AC+TF+SS+MI-MoA7, 8
 Kent, T.J.: SP+AS+BI+ET+MI+NM+NS+SS+TF-WeM6, 37
 Kessels, W.M.M.: EL+TF+AS+EM+SS+PS+EN+NM-MoM6, 2
 Khan, S.S.: SS-WeM12, 41
 Khosla, N.: SS-ThM2, 55
 Kiefer, B.: IS+AS+SS+EN-TuM6, 16
 Kim, D.H.: EN+SS-FrM1, 68
 Kim, H.: EM+SS+AS+NS-ThM12, 51; SS-WeM5, 40
 Kim, M.K.: SS+NS-ThA3, 60
 Kim, S.: EM+SS+AS+NS-ThM11, 51
 Kim, S.N.: GR+AS+BI+PS+SS-WeM6, 34
 Kim, Y.: SS-ThM12, 56; SS-TuP14, 27; SS-WeM5, 40
 Kim, Y.-H.: EM+SS+AS+NS-ThM12, 51
 Kimmel, G.A.: SS+EN+OX-ThM3, 53; SS+EN+OX-ThM5, 53; SS-TuM5, 18; SS-TuM6, 18
 Kim-Ngan, N.-T.: AC+TF+SS+MI-MoA6, 7
 King, S.: GR+EM+NS+SS+TF-ThA1, 58
 King, W.: GR+AS+NS+SS-ThM3, 52
 Kinoshita, T.: GR+EM+NS+PS+SS+TF-MoM10, 5
 Kis, A.: GR+EM+NS+SS+TF-ThA10, 59
 Kisielowski, C.: GR+AS+NS+SS-ThM5, 52
 Knauf, J.: TF+EM+SS-ThA9, 66
 Knoops, H.C.M.: EL+TF+AS+EM+SS+PS+EN+NM-MoM6, 2
 Knudsen, J.: GR+AS+NS+SP+SS-TuA7, 20; IS+AS+SS+EN-TuM12, 17
 Kobayashi, T.: BI+SS+NS-WeM11, 33
 Koel, B.: SS-WeA10, 49
 Koenraad, P.M.: SS+EM-WeA3, 47
 Koirala, P.: EL+TF+AS+EM+SS+PS+EN+NM-MoM4, 2
 Komarneni, M.: NS+AS+SS+SP-WeM4, 35
 Komori, F.: GR+AS+NS+SS-ThM1, 51
 Kondo, H.: GR+AS+NS+SS-ThM9, 52
 Kondo, T.: GR+AS+EM+NS+SS-WeA12, 46
 Kondoh, H.: IS+AS+SS+EN-TuM12, 17
 Kondratyuk, P.: SS-WeA11, 49
 Kong, D.D.: SS-TuM9, 18; SS-TuP37, 31
 Kotsugi, M.: GR+EM+NS+PS+SS+TF-MoM10, 5
 Kozhushner, M.: ET+SS+GR+SP-ThA4, 57
 Kraft, D.C.E.: BI+SS+NS-WeM1, 32
 Krejci, O.: ET+SS+GR+SP-ThA9, 57
 Kroemker, B.: GR+AS+NS+SP+SS-TuA1, 20
 Krueger, P.: SS+OX-WeM6, 38
 Kuang, Z.: GR+AS+BI+PS+SS-WeM6, 34
 Kubota, J.: SS+EN+OX-ThM1, 53
 Kuhn, M.: GR+EM+NS+SS+TF-ThA1, 58
 Kuhness, D.: SS+OX-WeM12, 39
 Kulkarni, D.: SS-TuP36, 31
 Kumar, A.: EL+TF+BI+AS+EM+SS-MoA8, 9
 Kumar, S.: EL+TF+BI+AS+EM+SS-MoA8, 9
 Kummel, A.C.: BI+SS+NS-WeM6, 32; SP+AS+BI+ET+MI+NM+NS+SS+TF-WeM6, 37; SS-ThM11, 56
 Kunze, C.: SS-ThA9, 62
 Kyriakou, G.: SS-MoA7, 11; SS-TuP1, 24; SS-WeM1, 39

— L —

Labbé, P.: BI+SS+NS-WeM10, 33
 LaBella, V.P.: ET+SS+GR+SP-FrM6, 70; GR+AS+NS+SP+SS-TuA11, 21
 Laera, S.: BI+SS+AS-TuM12, 15
 Lahiri, J.: GR+EM+NS+SS+TF-ThA2, 58
 Lawton, T.: SS-WeM1, 39
 Le Lay, G.: GR+EM+NS+SS+TF-ThA6, 59
 Le, D.: SS-WeA1, 48
 Lecordier, L.: TF+EM+SS-ThA7, 66
 Lee, J.: SS-ThA8, 62
 Lee, T.Y.: VT+AS+SS-WeM1, 41
 Lee, W.K.: GR+AS+NS+SS-ThM3, 52
 Lee, Y.K.: SS-MoM1, 5

Leggett, G.J.: TF+EM+SS-ThA1, 65
 Lei, Y.: IS+AS+SS+EN-TuM9, 16
 Leick, N.: EL+TF+AS+EM+SS+PS+EN+NM-MoM6, 2
 Lemay, J.-C.: SS-ThM5, 55
 Lewis, E.A.: SS-WeA2, 48
 Lewis, T.: SS-ThA2, 62
 Li, A.-P.: ET+SS+GR+SP-ThA6, 57; GR+EM+NS+PS+SS+TF-MoM2, 4
 Li, Q.: SS-WeM4, 40
 Li, Y.: SS-TuP9, 26; VT+AS+SS-WeM2, 42
 Li, Z.: ET+SS+GR+SP-ThA11, 58; SS+EN+OX-ThM5, 53; SS+NS-TuA4, 22; VT+AS+SS-WeM10, 42; VT+AS+SS-WeM6, 42
 Li, Z.S.: EM+SS+AS+NS-ThM3, 50
 Liang, T.: EN+SS-FrM6, 69; OX+SS+TF+MI-MoA1, 9
 Liang, Z.: SS-WeM5, 40
 Lim, D.: TF+EM+SS-ThA11, 67
 Lin, C.-F.: TF+EM+SS-ThA10, 67
 Lin, X.: SS+EN+OX-ThM5, 53
 Lin, Y.H.: EM+SS+AS+NS-ThM13, 51
 Linck, M.: GR+AS+NS+SS-ThM5, 52
 Lindh, L.: BI+SS+AS-TuM3, 14
 Linford, M.R.: TF+EM+SS-ThA8, 66
 Liu, B.: IS+AS+SS+EN-TuM9, 16
 Liu, J.: EN+SS-FrM3, 68
 Liu, X.: VT+AS+SS-WeM2, 42
 Liu, Y.: EN+SS-FrM5, 68; SS+NS-TuA3, 22
 Liu, Z.: EN+SS-FrM5, 68; GR+EM+NS+SS+TF-ThA3, 58; IS+AS+SS+EN-TuM4, 16; IS+AS+SS+EN-TuM5, 16
 Livadaru, L.: SP+AS+BI+ET+MI+NM+NS+SS+TF-WeM2, 36
 Lock, E.H.: GR+AS+BI+PS+SS-WeM9, 35
 Lofaro, J.C.: NS+AS+SS+SP-WeM12, 36
 Lorenz, K.: AC+TF+SS+MI-MoA9, 8
 Losego, M.D.: EN+SS-FrM1, 68
 Losovyj, Ya.B.: AC+TF+SS+MI-MoA1, 7; AC+TF+SS+MI-MoA7, 8
 Lotze, C.: SP+AS+BI+ET+MI+NM+NS+SS+TF-WeM4, 36
 Lou, J.: GR+EM+NS+SS+TF-ThA3, 58
 Lou, Y.: SS+NS-TuA4, 22
 Louie, S.G.: GR+AS+NS+SS-ThM5, 52
 Lu, G.: GR+AS+NS+SP+SS-TuA2, 20; SS-TuP3, 24
 Lu, J.: IS+AS+SS+EN-TuM9, 16
 Lu, W.C.: SS-WeM4, 40
 Lu, W.H.: SS-WeA1, 48
 Lu, Y.: ET+SS+GR+SP-ThA3, 57
 Lu, Z.: SS-TuP26, 29
 Lu, Z.-H.: OX+SS+TF+MI-MoA7, 10
 Lucatorto, T.B.: SS-TuM3, 17
 Lukaszew, R.A.: TF+AS+SS-ThA8, 64; VT+AS+SS-WeM10, 42; VT+AS+SS-WeM6, 42; VT+AS+SS-WeM9, 42
 Luo, H.: EL+TF+BI+AS+EM+SS-MoA9, 9
 Luo, M.: SS-WeM2, 40
 Luscombe, C.K.: ET+SS+GR+SP-ThA11, 58; SS-TuP14, 27
 Luttrell, T.: SS-TuP15, 27
 Lyubinetsky, I.: SS+EN+OX-ThM5, 53; SS+EN+OX-ThM9, 54; SS-TuM5, 18

— M —

Ma, Q.: SP+AS+BI+ET+MI+NM+NS+SS+TF-WeM5, 36; SS-WeA1, 48
 Macak, E.: AS+NS+SS+TF-WeA8, 44
 Macak, K.: AS+NS+SS+TF-WeA8, 44
 Madaan, N.: TF+EM+SS-ThA8, 66
 Magana, S.: TF+EM+SS-ThA11, 67
 Magnone, K.: SP+AS+BI+ET+MI+NM+NS+SS+TF-WeM5, 36
 Magnuson, C.W.: GR+AS+NS+SP+SS-TuA11, 21
 Maidecchi, G.: EL+TF+BI+AS+EM+SS-MoA8, 9
 Majzik, Z.: ET+SS+GR+SP-FrM5, 69; ET+SS+GR+SP-ThA9, 57

Maksymovych, P.: NS+AS+SS+SP-WeM11, 36; SS-WeM4, 40
 Malko, A.V.: EL+TF+BI+AS+EM+SS-MoA2, 8
 Mangham, A.N.: SS+OX-WeM5, 38
 Mann, J.: SS-WeA1, 48
 Mansour, A.N.: GR+AS+NS+SS-ThM10, 52
 Mao, B.: IS+AS+SS+EN-TuM4, 16
 Marder, S.R.: SS-TuP14, 27
 Margarella, A.: SS+NS-TuA3, 22; SS-ThA1, 61; SS-ThA2, 62
 Marquis, E.A.: AS+NS+SS+TF-WeA1, 44
 Marsillac, S.: EL+TF+AS+EM+SS+PS+EN+NM-MoM1, 2; EL+TF+AS+EM+SS+PS+EN+NM-MoM4, 2
 Martin, R.L.: AC+MI+SS+TF-MoM3, 1
 Martin, R.W.: AC+TF+SS+MI-MoA9, 8
 Martinez, J.: SS+OX-WeM10, 39
 Masheder, B.: SS-ThM1, 55
 Masini, F.: SS-ThM5, 55
 Mastro, M.A.: SS+EM-WeA1, 46
 Matos, J.: SS-TuP27, 29
 Matsubayashi, A.: GR+AS+EM+NS+SS-WeA7, 45
 Matsumoto, S.: SS-ThA10, 62
 Matsunaga, S.: BI+SS+NS-WeM11, 33
 Matsushita, S.Y.: SS-MoA10, 12
 Mattson, E.: GR+AS+NS+SP+SS-TuA2, 20; SS-TuP3, 24
 Mavrikakis, M.: SS-MoA7, 11; SS-TuP1, 24
 Maxisch, M.: OX+SS+TF+MI-MoA11, 11
 Mazzio, K.: ET+SS+GR+SP-ThA11, 58
 McBreen, P.H.: SS-ThM5, 55
 McClory, J.W.: AC+TF+SS+MI-MoA1, 7; AC+TF+SS+MI-MoA7, 8
 McDonald, K.: SS-MoA3, 11
 McHale, S.R.: AC+TF+SS+MI-MoA1, 7
 McNeilan, J.D.: GR+AS+NS+SP+SS-TuA11, 21
 Medikonda, M.: EL+TF+AS+EM+SS+PS+EN+NM-MoM9, 3
 Medina, A.A.: EL+TF+AS+EM+SS-TuP2, 24
 Mei, W.N.: AC+TF+SS+MI-MoA1, 7
 Melese, Y.G.: EL+TF+AS+EM+SS+PS+EN+NM-MoM6, 2
 Mendez, N.: BI+SS+NS-WeM6, 32
 Menzel, D.: SS+NS-TuA1, 22
 Merte, L.: SS-TuP25, 29; SS-TuP28, 29
 Meyer, H.M.: SS-WeM10, 41
 Meyer, T.J.: EN+SS-FrM3, 68
 Mhatre, B.S.: SS-MoA6, 11
 Michely, T.W.: GR+AS+NS+SP+SS-TuA7, 20; GR+EM+NS+PS+SS+TF-MoM5, 4
 Mikkelsen, A.: SS+NS-ThA1, 59
 Miller, G.P.: SS-TuP4, 25
 Miller, J.: IS+AS+SS+EN-TuM9, 16
 Miller, J.B.: SS-WeA11, 49
 Millunchick, J.M.: SS+EM-WeA2, 47; SS-TuP34, 30
 Milstrey, T.E.: SS-TuP23, 28
 Minton, T.K.: SS-MoA1, 11
 Mirmelstein, A.: AC+MI+SS+TF-MoM9, 1
 Mistry, H.: SS-TuP28, 29
 Miyake, M.: SS-TuP17, 27
 Miyashita, H.: GR+EM+NS+PS+SS+TF-MoM10, 5
 Mo, A.K.: SS-WeM10, 41
 Modine, N.A.: SS+EM-WeA2, 47; SS-TuP34, 30
 Moeller, R.: ET+SS+GR+SP-FrM7, 70
 Monya, Y.: IS+AS+SS+EN-TuM12, 17
 Moon, J.S.: GR+EM+NS+PS+SS+TF-MoM1, 3
 Moore, R.: GR+AS+NS+SP+SS-TuA11, 21
 Morales, E.: SS+OX-WeM10, 39
 Morgante, A.: SS+OX-WeM6, 38
 Morgen, P.: EM+SS+AS+NS-ThM3, 50
 Mostafa, S.: SS-TuP27, 29
 Mowll, T.: GR+EM+NS+PS+SS+TF-MoM2, 4
 Mullet, C.: SS+NS-ThA6, 60
 Mullins, D.R.: SS-TuM11, 18
 Munakata, T.: SS-TuP31, 30
 Munson, A.: GR+AS+NS+SP+SS-TuA11, 21

Murphy, C.J.: EM+SS+AS+NS-ThM9, 50
 Murphy, N.R.: TF+AS+SS-ThA10, 64
 Muthinti, G.R.: EL+TF+AS+EM+SS+PS+EN+NM-MoM9, 3
 Mutoro, E.: IS+AS+SS+EN-TuM5, 16
 Myers-Ward, R.L.: GR+AS+BI+PS+SS-WeM9, 35; GR+AS+NS+SP+SS-TuA9, 21; GR+EM+NS+PS+SS+TF-MoM1, 3; GR+EM+NS+PS+SS+TF-MoM3, 4
 — N —
 Nachimuthu, P.: SS-TuP26, 29
 Naes, B.E.: AS+NS+SS+TF-WeA7, 44
 Nagareddy, V.K.: GR+EM+NS+PS+SS+TF-MoM1, 3
 Naik, R.R.: GR+AS+BI+PS+SS-WeM6, 34
 Najmaei, S.: GR+EM+NS+SS+TF-ThA3, 58
 Nakajima, A.: SS-TuP18, 28
 Nakajima, S.: SS-MoA8, 12
 Nakajima, T.: SS-TuP7, 26
 Nakamura, I.: SS-TuP29, 29; SS-TuP30, 30
 Nakamura, J.: GR+AS+EM+NS+SS-WeA12, 46; SS-TuP8, 26
 Nakatsuji, K.: GR+AS+NS+SS-ThM1, 51
 Nasse, M.: GR+AS+NS+SP+SS-TuA2, 20
 Nath, A.: GR+EM+NS+PS+SS+TF-MoM1, 3; GR+EM+NS+PS+SS+TF-MoM3, 4
 Nathanson, G.M.: SS-MoA1, 11
 N'Diaye, A.T.: GR+AS+EM+NS+SS-WeA10, 46
 Nedrygailov, I.: SS-MoM2, 5; SS-MoM3, 5; SS-TuP24, 29
 Nefedov, A.: OX+SS+TF+MI-MoA10, 10
 Negreiros, F.R.: SS+OX-WeM12, 39
 Nelin, C.J.: SS+OX-WeM9, 39
 Nelson, C.M.: EL+TF+BI+AS+EM+SS-MoA9, 9
 Nelson, F.J.: GR+AS+NS+SP+SS-TuA11, 21
 Netzer, F.P.: SS+OX-WeM12, 39
 Ney, A.: SS+OX-WeM5, 38
 Ney, V.: SS+OX-WeM5, 38
 Nguyen, H.M.: EL+TF+BI+AS+EM+SS-MoA2, 8
 Nienhaus, H.: SS-MoM5, 6
 Nishi, H.: SS-TuP32, 30
 Nishimoto, S.: SS-TuP17, 27
 Noei, H.: OX+SS+TF+MI-MoA10, 10
 Novikova, I.: TF+AS+SS-ThA8, 64
 Novoselov, K.: GR+AS+BI+PS+SS-WeM2, 34
 Ntwaeaborwa, O.M.: SS+OX-WeM11, 39
 Nyakiti, L.O.: GR+AS+BI+PS+SS-WeM9, 35; GR+AS+NS+SP+SS-TuA9, 21; GR+EM+NS+PS+SS+TF-MoM1, 3; GR+EM+NS+PS+SS+TF-MoM3, 4
 — O —
 O'Donnell, K.P.: AC+TF+SS+MI-MoA9, 8
 Oezkaya, B.: TF+AS+SS-ThA1, 63
 Offi, F.: AC+TF+SS+MI-MoA3, 7
 Ogaki, R.: BI+SS+NS-WeM1, 32
 Oh, D.-H.: SS+NS-ThA3, 60
 Ohkouchi, T.: GR+EM+NS+PS+SS+TF-MoM10, 5
 Ohno, S.: SS-MoA9, 12
 Ohta, T.: GR+AS+NS+SP+SS-TuA8, 20
 Ohtake, A.: SS-TuP8, 26
 Oleynik, I.I.: ET+SS+GR+SP-ThA4, 57; GR+AS+EM+NS+SS-WeA2, 45
 Ondeck, N.: SS-ThM2, 55
 Ondracek, M.: ET+SS+GR+SP-FrM4, 69
 Ondráček, M.: ET+SS+GR+SP-FrM5, 69
 Ong, S.W.: SS+EN+OX-ThM4, 53
 Ono, L.K.: SS-TuP27, 29
 Oppen, F.V.: SP+AS+BI+ET+MI+NM+NS+SS+TF-WeM4, 36
 Ortíz, V.: SS-TuP10, 26
 Osgood, R.M.: SS+NS-TuA4, 22; SS-TuP2, 24
 Oshima, M.: GR+AS+EM+NS+SS-WeA12, 46
 Ossowski, J.: TF+AS+SS-ThA2, 63
 Otani, T.: SS-ThM12, 56
 Outlaw, R.A.: GR+AS+NS+SS-ThM10, 52

— P —
 Pacholski, M.L.: AS+NS+SS+TF-WeA9, 45
 Page, S.J.: AS+NS+SS+TF-WeA8, 44
 Paiella, R.: EM+SS+AS+NS-ThM1, 50
 Palai, R.: AC+TF+SS+MI-MoA1, 7
 Palomino, R.: NS+AS+SS+SP-WeM12, 36
 Pan, H.B.: SS+NS-TuA11, 23
 Pan, M.H.: SS-WeM4, 40
 Pan, X.: SS+OX-WeM1, 38
 Pan, Y.H.: SS+NS-TuA11, 23
 Panaccione, G.: AC+TF+SS+MI-MoA3, 7
 Pande, K.: SS-TuP3, 24
 Paniagua, S.A.: SS-TuP14, 27
 Pantelides, S.T.: ET+SS+GR+SP-FrM1, 69
 Paolini, C.: VT+AS+SS-WeM3, 42
 Park, C.-Y.: GR+EM+NS+PS+SS+TF-MoM4, 4; SS+NS-ThA3, 60
 Park, H.: NS+AS+SS+SP-WeM12, 36
 Park, J.: SS-ThM1, 55; SS-TuP31, 30
 Park, J.H.: SS-ThM11, 56
 Park, J.-H.: GR+EM+NS+PS+SS+TF-MoM11, 5
 Park, J.Y.: SS-MoM1, 5
 Parkin, J.D.: SP+AS+BI+ET+MI+NM+NS+SS+TF-WeM9, 37
 Parsons, G.N.: EN+SS-FrM1, 68; EN+SS-FrM3, 68
 Pascual, J.I.: SP+AS+BI+ET+MI+NM+NS+SS+TF-WeM4, 36
 Peixoto, T.: SS+EM-WeA11, 47; SS-TuP21, 28; TF+AS+SS-ThA3, 63
 Peng, G.: SS-MoA7, 11; SS-TuP1, 24
 Peng, Q.: EN+SS-FrM3, 68
 Perea, D.E.: AS+NS+SS+TF-WeA3, 44; AS+NS+SS+TF-WeA4, 44
 Pereira, L.: AC+TF+SS+MI-MoA6, 7
 Perrine, K.A.: SS-ThA1, 61; SS-ThA2, 62; SS-WeM11, 41
 Perry, J.W.: SS-TuP14, 27
 Pertsin, A.J.: BI+SS+AS-TuM2, 14
 Petaccia, L.: AC+TF+SS+MI-MoA3, 7
 Petersen, E.: NS+AS+SS+SP-WeM2, 35
 Petrik, N.G.: SS+EN+OX-ThM3, 53; SS+EN+OX-ThM5, 53; SS-TuM5, 18; SS-TuM6, 18
 Petrosky, J.C.: AC+TF+SS+MI-MoA1, 7; AC+TF+SS+MI-MoA7, 8
 Phaneuf, R.J.: TF+EM+SS-ThA10, 67
 Phillipot, S.R.: EN+SS-FrM6, 69; OX+SS+TF+MI-MoA1, 9; SS+NS-ThA4, 60
 Pipe, K.P.: EM+SS+AS+NS-ThM13, 51
 Pitters, J.: SP+AS+BI+ET+MI+NM+NS+SS+TF-WeM2, 36
 Piva, P.: SP+AS+BI+ET+MI+NM+NS+SS+TF-WeM2, 36
 Podkolzin, S.: SS-WeA10, 49
 Podraza, N.J.: EL+TF+AS+EM+SS+PS+EN+NM-MoM1, 2; EL+TF+AS+EM+SS+PS+EN+NM-MoM4, 2
 Pohl, K.: SS-TuP4, 25
 Ponomarev, M.V.: EL+TF+AS+EM+SS+PS+EN+NM-MoM6, 2
 Pookpanratana, S.: TF+EM+SS-ThA6, 66
 Popovitz-Biro, R.: NS+AS+SS+SP-WeM4, 35
 Portoles, J.F.: SP+AS+BI+ET+MI+NM+NS+SS+TF-WeM10, 37
 Potapenko, D.V.: SS+NS-TuA4, 22
 Pradhan, P.: EL+TF+AS+EM+SS+PS+EN+NM-MoM1, 2
 Provo, J.L.: AC+TF+SS+MI-MoA4, 7
 Pu, H.: GR+AS+NS+SP+SS-TuA2, 20; SS-TuP3, 24
 — Q —
 Quardokus, R.C.: ET+SS+GR+SP-ThA3, 57
 Quinlan, R.A.: GR+AS+NS+SS-ThM10, 52
 Quinton, J.S.: SS+NS-ThA7, 60

— R —

Radja, A.: EL+TF+BI+AS+EM+SS-MoA2, 8
 Radue, E.: TF+AS+SS-ThA8, 64
 Rafik, A.: GR+AS+EM+NS+SS-WeA8, 45
 Rahinov, I.: SS-MoM4, 6
 Rahman, T.S.: SS+NS-ThA9, 61
 Ralsano, R.: ET+SS+GR+SP-FrM6, 70
 Raman, T.: SS-WeA1, 48
 Ramana, C.V.: TF+AS+SS-ThA11, 65;
 TF+AS+SS-ThA9, 64
 Rangan, S.: OX+SS+TF+MI-MoA6, 10
 Ranjan, V.: EL+TF+AS+EM+SS+PS+EN+NM-
 MoM1, 2
 Rao, M.V.: GR+EM+NS+PS+SS+TF-MoM1, 3
 Rappe, A.M.: SS+OX-WeM10, 39
 Rasmussen, A.M.H.: SS-ThM5, 55
 Raso, R.: AS+NS+SS+TF-WeA8, 44
 Reddemann, L.: TF+EM+SS-ThA9, 66
 Reid, D.: NS+AS+SS+SP-WeM2, 35
 Reihs, K.: TF+EM+SS-ThA9, 66
 Ren, T.: TF+EM+SS-ThA6, 66
 Resta, A.: GR+EM+NS+SS+TF-ThA6, 59
 Reznicek, A.: EL+TF+AS+EM+SS+PS+EN+NM-
 MoM9, 3
 Rhim, S.: GR+AS+NS+SP+SS-TuA2, 20
 Richardson, C.J.K.: TF+EM+SS-ThA10, 67
 Richter, C.A.: TF+EM+SS-ThA6, 66
 Richter, R.P.: BI+SS+NS-WeM10, 33
 Rigby-Singleton, S.: BI+SS+AS-TuM5, 14
 Rizzo, A.: AC+TF+SS+MI-MoA3, 7
 Roach, W.M.: VT+AS+SS-WeM10, 42;
 VT+AS+SS-WeM6, 42; VT+AS+SS-WeM9,
 42
 Roberts, A.J.: AS+NS+SS+TF-WeA8, 44
 Roberts, C.J.: BI+SS+AS-TuM5, 14; BI+SS+NS-
 WeM12, 33
 Robinson, J.T.: GR+AS+BI+PS+SS-WeM9, 35;
 GR+AS+NS+SP+SS-TuA8, 20;
 GR+AS+NS+SS-ThM3, 52
 Robinson, Z.R.: GR+AS+NS+SP+SS-TuA11, 21;
 GR+EM+NS+PS+SS+TF-MoM2, 4
 Roca i Cabarrocas, P.:
 EL+TF+AS+EM+SS+PS+EN+NM-MoM3, 2
 Rodenhausen, K.B.: EL+TF+BI+AS+EM+SS-
 MoA1, 8
 Rogalev, A.: SS+OX-WeM5, 38
 Rogers, B.R.: SS+OX-WeM4, 38; SS-TuP5, 25
 Rogers, J.A.: EM+SS+AS+NS-ThM5, 50
 Rojas, G.: NS+AS+SS+SP-WeM11, 36
 Roldan Cuenya, B.: SS+NS-ThA8, 61; SS+NS-
 TuA7, 22; SS-TuP25, 29; SS-TuP27, 29
 Roldan Cuenya, B.: SS-TuP28, 29
 Romriell, N.R.: TF+EM+SS-ThA8, 66
 Roodenko, K.: EL+TF+BI+AS+EM+SS-MoA2, 8;
 SS-TuP21, 28
 Ross, F.M.: GR+EM+NS+PS+SS+TF-MoM8, 4
 Rossi, F.: BI+SS+AS-TuM12, 15
 Rotello, V.: BI+SS+NS-WeM3, 32
 Rougemaille, N.: GR+AS+EM+NS+SS-WeA10,
 46
 Rousseau, R.: SS+EN+OX-ThM5, 53
 Rowe, J.E.: GR+AS+BI+PS+SS-WeM10, 35;
 GR+AS+NS+SP+SS-TuA11, 21
 Ruggieri, C.: OX+SS+TF+MI-MoA6, 10
 Ruocco, A.: AC+TF+SS+MI-MoA3, 7
 Ruoff, R.S.: GR+AS+NS+SP+SS-TuA11, 21;
 GR+AS+NS+SP+SS-TuA2, 20
 Ryadnov, M.G.: BI+SS+AS-TuM11, 15
 Rysz, J.: TF+AS+SS-ThA2, 63
 Ryzhkov, M.V.: AC+MI+SS+TF-MoM9, 1

— S —

Safron, N.: GR+AS+EM+NS+SS-WeA9, 45
 Sakai, M.: SS-TuP18, 28
 Sakalas, P.: GR+AS+NS+SS-ThM2, 52
 Sakurai, M.: GR+AS+EM+NS+SS-WeA12, 46
 Salib, D.: SP+AS+BI+ET+MI+NM+NS+SS+TF-
 WeM5, 36
 Samala, S.K.: TF+AS+SS-ThA9, 64

Sandin, A.A.: GR+AS+BI+PS+SS-WeM10, 35;
 GR+AS+NS+SP+SS-TuA11, 21
 Saraf, S.: SS-TuP12, 27
 Sarkar, A.: EL+TF+AS+EM+SS-TuP1, 24
 Scheele, M.: SS-MoM2, 5
 Schlaf, R.: ET+SS+GR+SP-ThA10, 58;
 ET+SS+GR+SP-ThA11, 58; TF+EM+SS-
 ThA11, 67
 Schlueter, J.A.: NS+AS+SS+SP-WeM11, 36
 Schmidt, A.K.: GR+AS+EM+NS+SS-WeA10, 46
 Schmidt, D.: EL+TF+BI+AS+EM+SS-MoA1, 8
 Schmidt, W.G.: SS-TuP21, 28
 Schnadt, J.: IS+AS+SS+EN-TuM12, 17
 Schofield, M.: GR+AS+NS+SP+SS-TuA2, 20; SS-
 TuP3, 24
 Schripf, R.D.: EM+SS+AS+NS-ThM11, 51
 Schröder, U.: GR+AS+NS+SP+SS-TuA7, 20
 Schroter, M.: GR+AS+NS+SS-ThM2, 52
 Schubert, E.: EL+TF+BI+AS+EM+SS-MoA1, 8
 Schubert, M.: EL+TF+BI+AS+EM+SS-MoA1, 8
 Schulte, K.: GR+AS+NS+SP+SS-TuA7, 20
 Scott, D.J.: BI+SS+AS-TuM5, 14
 Scott, T.B.: AC+TF+SS+MI-MoA6, 7
 Seal, S.S.: NS+AS+SS+SP-WeM2, 35; SS-TuP12,
 27
 Seebauer, E.G.: SS+EN+OX-ThM4, 53
 Seitz, O.: EL+TF+BI+AS+EM+SS-MoA2, 8
 Sekine, M.: GR+AS+NS+SS-ThM9, 52
 Sellers, J.R.V.: SS-TuM12, 19
 Sementa, L.: SS+OX-WeM12, 39
 Semidey-Flecha, L.: GR+AS+EM+NS+SS-
 WeA11, 46
 Seo, J.M.: SS-TuP9, 26
 Serov, A.: IS+AS+SS+EN-TuM6, 16
 Setvin, M.: ET+SS+GR+SP-ThA9, 57
 Seyller, Th.: GR+EM+NS+PS+SS+TF-MoM10, 5
 Shaat, S.K.: SS+OX-WeM11, 39
 Shafiq, N.: GR+AS+BI+PS+SS-WeM2, 34
 Shaifai, G.: SS+NS-ThA9, 61
 Shan, J.: SS-TuP19, 28
 Shao-Horn, Y.: IS+AS+SS+EN-TuM5, 16
 Sheehan, P.E.: GR+AS+BI+PS+SS-WeM9, 35;
 GR+AS+NS+SS-ThM3, 52
 Shen, M.: EN+SS-FrM2, 68
 Shikano, T.: GR+AS+EM+NS+SS-WeA12, 46
 Shimizu, H.: BI+SS+NS-WeM11, 33
 Shimizu, T.K.: SS-ThM12, 56
 Shin, B.G.: SS+NS-ThA3, 60
 Shin, H.: GR+EM+NS+PS+SS+TF-MoM4, 4
 Shin, H.-J.: GR+EM+NS+PS+SS+TF-MoM11, 5
 Sholl, D.: GR+AS+EM+NS+SS-WeA11, 46
 Shong, B.: SS+EM-WeA8, 47
 Shukla, N.: SS-ThM2, 55
 Shutthanandan, V.: AS+NS+SS+TF-WeA4, 44;
 SS+EN+OX-ThM11, 54
 Shyam, R.: SS+OX-WeM3, 38
 Silbaugh, T.L.: SS-WeM6, 40
 Siligardi, G.: BI+SS+AS-TuM12, 15
 Simchenko, S.V.: SS+EN+OX-ThM12, 54
 Simons, M.T.: TF+AS+SS-ThA8, 64
 Sinnott, S.B.: EN+SS-FrM6, 69; OX+SS+TF+MI-
 MoA1, 9; SS+NS-ThA4, 60
 Sivula, K.: IS+AS+SS+EN-TuM3, 15
 Skomski, D.: SS+NS-ThA11, 61
 Skuza, J.R.: VT+AS+SS-WeM6, 42
 Slattey, A.D.: SS+NS-ThA7, 60
 Smith, S.R.: SS-ThA3, 62
 Smolenski, K.W.: VT+AS+SS-WeM2, 42
 Song, E.B.: EM+SS+AS+NS-ThM11, 51
 Song, I.: GR+EM+NS+PS+SS+TF-MoM4, 4
 Song, Y.-B.: SS-TuP9, 26
 Sorescu, D.C.: SS-ThA8, 62
 Sorini, A.: EN+SS-FrM5, 68
 Sosolik, C.E.: SS+OX-WeM3, 38; SS-TuP36, 31
 Sotres, J.: BI+SS+AS-TuM3, 14
 Spies, M.: EL+TF+BI+AS+EM+SS-MoA9, 9
 Srinadhu, E.S.: SS+OX-WeM3, 38
 Srivastava, N.: GR+AS+NS+SP+SS-TuA10, 21
 Stair, P.C.: OX+SS+TF+MI-MoA3, 9

Stefani, G.: AC+TF+SS+MI-MoA3, 7
 Stevanovic, A.: SS+EN+OX-ThM6, 54
 Stine, R.: GR+AS+BI+PS+SS-WeM9, 35;
 GR+AS+NS+SS-ThM3, 52
 Stolbov, S.: EN+SS-FrM7, 69
 Styrov, V.: SS+EN+OX-ThM12, 54
 Su, D.: EN+SS-FrM4, 68
 Subramanian, V.: AS+NS+SS+TF-WeA4, 44
 Suemitsu, M.: GR+EM+NS+PS+SS+TF-MoM10,
 5
 Sumpter, B.G.: NS+AS+SS+SP-WeM11, 36; SS-
 WeM4, 40
 Sun, D.Z.: SP+AS+BI+ET+MI+NM+NS+SS+TF-
 WeM5, 36; SS-WeA1, 48
 Sun, G.F.: SS-WeM12, 41
 Sun, L.: TF+AS+SS-ThA10, 64
 Sundaram, G.: TF+EM+SS-ThA7, 66
 Sung, C.Y.: GR+AS+NS+SP+SS-TuA11, 21
 Surnev, S.: SS+OX-WeM12, 39
 Suto, S.: SS-MoA10, 12
 Sutter, E.: GR+EM+NS+SS+TF-ThA2, 58
 Sutter, P.W.: GR+AS+EM+NS+SS-WeA8, 45;
 GR+EM+NS+SS+TF-ThA2, 58
 Suzuki, T.: GR+AS+EM+NS+SS-WeA12, 46
 Suzuki, Y.: SS-TuP11, 26
 Švec, M.: ET+SS+GR+SP-FrM5, 69
 Swart, H.C.: SS+OX-WeM11, 39
 Sweeny, B.: EN+SS-FrM4, 68
 Sykes, C.H.: EM+SS+AS+NS-ThM9, 50; SS-
 MoA7, 11; SS-ThM3, 55; SS-TuP1, 24; SS-
 WeA2, 48; SS-WeM1, 39
 Synowicki, R.A.:
 EL+TF+AS+EM+SS+PS+EN+NM-MoM5, 2

— T —

Taing, J.: EN+SS-FrM5, 68; SS+NS-TuA3, 22
 Tait, S.L.: SS+NS-ThA11, 61; SS-MoA3, 11; SS-
 WeM3, 40
 Takagi, K.: GR+AS+NS+SS-ThM1, 51
 Takano, I.: SS-TuP11, 26; SS-TuP32, 30; SS-
 TuP6, 25; SS-TuP7, 26
 Tamanaha, C.R.: GR+AS+NS+SS-ThM3, 52
 Tan, X.: EL+TF+AS+EM+SS+PS+EN+NM-
 MoM4, 2
 Tanaka, S.: GR+AS+NS+SS-ThM1, 51
 Tang, J.-M.: SS-TuP4, 25
 Tantarini, G.F.: GR+AS+EM+NS+SS-WeA12,
 46
 Tao, F.: TF+AS+SS-ThA6, 64
 Tao, J.: SS-TuP15, 27
 Tatulian, S.A.: GR+AS+BI+PS+SS-WeM6, 34
 Taucer, M.:
 SP+AS+BI+ET+MI+NM+NS+SS+TF-WeM2,
 36
 ten Elshof, A.: EL+TF+BI+AS+EM+SS-MoA8, 9
 Teng, D.: GR+AS+EM+NS+SS-WeA11, 46
 Tenne, R.: NS+AS+SS+SP-WeM4, 35
 Teplyakov, A.V.: SS+EM-WeA12, 48; SS-TuP20,
 28
 ter Veen, H.R.J.: TF+AS+SS-ThA4, 63
 Terawaki, L.: SS-TuP31, 30
 Terfort, A.: SS+NS-ThA10, 61; TF+AS+SS-ThA2,
 63
 Terrones, H.: SS-WeM4, 40
 Thevuthasan, S.: AS+NS+SS+TF-WeA3, 44;
 AS+NS+SS+TF-WeA4, 44; SS-TuP26, 29;
 TF+AS+SS-ThA11, 65
 Thierley, M.: VT+AS+SS-WeM3, 42
 Thissen, P.: SS+EM-WeA11, 47; SS-TuP21, 28;
 TF+AS+SS-ThA3, 63
 Thomas, J.C.: SS+EM-WeA2, 47; SS-TuP34, 30
 Thomas, W.: BI+SS+AS-TuM6, 14
 Tian, F.Y.: SS-TuP20, 28
 Tiwald, T.E.: EL+TF+BI+AS+EM+SS-MoA1, 8
 Tkach, I.: AC+TF+SS+MI-MoA6, 7
 Tobin, J.G.: AC+MI+SS+TF-MoM9, 1
 Tompkins, H.G.:
 EL+TF+AS+EM+SS+PS+EN+NM-MoM8, 3
 Torun, B.: SS-ThA9, 62; TF+AS+SS-ThA1, 63
 Toyoda, A.: SS-TuP6, 25

- Trenary, M.: SS-WeM5, 40
Trioni, M.I.: AC+TF+SS+MI-MoA3, 7;
GR+AS+EM+NS+SS-WeA12, 46
Tromp, R.M.: GR+EM+NS+PS+SS+TF-MoM8, 4
Tronic, E.: BI+SS+AS-TuM6, 14
Tsverin, Y.: NS+AS+SS+SP-WeM4, 35
Turchanin, A.: GR+AS+BI+PS+SS-WeM11, 35
Tuscano, J.A.: TF+EM+SS-ThA8, 66
Tyagi, P.: GR+AS+NS+SP+SS-TuA11, 21;
GR+EM+NS+PS+SS+TF-MoM2, 4
Tyler, K.: SS-ThM11, 56
- **U** —
Ueba, T.: SS-TuP31, 30
Ueno, I.: SS-ThA10, 62
Ulijn, R.: BI+SS+AS-TuM9, 14
Urata, C.: SS-ThM1, 55
Urban, F.K.: EL+TF+AS+EM+SS+PS+EN+NM-
MoM10, 3
Ushigome, D.: GR+AS+EM+NS+SS-WeA12, 46
Utz, A.L.: SS-MoA4, 11
- **V** —
Valtiner, M.: BI+SS+NS-WeM5, 32
van de Loo, B.W.H.:
EL+TF+AS+EM+SS+PS+EN+NM-MoM6, 2
Van der Ven, A.: SS+EM-WeA2, 47; SS-TuP34,
30
Van Spyk, M.H.C.: SS-ThA1, 61; SS-WeM11, 41
VanDerslice, J.: EL+TF+BI+AS+EM+SS-MoA1,
8
Vega, A.: TF+AS+SS-ThA3, 63
Vemuri, R.S.: TF+AS+SS-ThA11, 65
Ventrice, Jr., C.A.: GR+AS+NS+SP+SS-TuA11,
21; GR+EM+NS+PS+SS+TF-MoM2, 4
Verdini, A.: SS+OX-WeM6, 38
Veyan, J.-F.: GR+AS+BI+PS+SS-WeM2, 34; SS-
WeA12, 49
Vilmercati, P.: AC+TF+SS+MI-MoA3, 7
Vlassioux, I.: ET+SS+GR+SP-ThA6, 57
Vogt, P.: GR+EM+NS+SS+TF-ThA6, 59
Vo-Van, C.: GR+AS+EM+NS+SS-WeA10, 46
- **W** —
Waerenbogh, J.-C.: AC+TF+SS+MI-MoA6, 7
Wagner, M.: SS+OX-WeM12, 39
Walker, G.: SS+OX-WeM4, 38; SS-TuP5, 25
Wallace, R.M.: GR+AS+EM+NS+SS-WeA1, 45
Walrath, J.C.: EM+SS+AS+NS-ThM13, 51
Walton, S.G.: GR+AS+BI+PS+SS-WeM9, 35;
GR+EM+NS+PS+SS+TF-MoM1, 3
Wang, C.: SS-WeM2, 40
Wang, H.: SS-TuP26, 29
Wang, J.: SS-TuP4, 25
Wang, K.L.: EM+SS+AS+NS-ThM11, 51
Wang, L.: AC+TF+SS+MI-MoA1, 7; TF+AS+SS-
ThA8, 64
Wang, Q.H.: GR+AS+BI+PS+SS-WeM1, 34
Wang, W.: ET+SS+GR+SP-ThA10, 58; SS-TuP26,
29
Wang, Y.: OX+SS+TF+MI-MoA10, 10
Wang, Z.-T.: SS+EN+OX-ThM5, 53; SS+EN+OX-
ThM9, 54; SS-TuM5, 18
Wasio, N.A.: ET+SS+GR+SP-ThA3, 57
Weaver, J.F.: SS+EN+OX-ThM10, 54; SS-TuP22,
28; SS-TuP23, 28
Weber, J.W.: EL+TF+AS+EM+SS+PS+EN+NM-
MoM6, 2
Wei, W.D.: EN+SS-FrM4, 68
Weinert, M.: GR+AS+NS+SP+SS-TuA2, 20; SS-
TuP3, 24
Wheeler, V.D.: GR+AS+NS+SP+SS-TuA9, 21;
GR+EM+NS+PS+SS+TF-MoM1, 3;
GR+EM+NS+PS+SS+TF-MoM3, 4
White, M.G.: NS+AS+SS+SP-WeM12, 36
Wiens, J.P.: SS-MoA1, 11
Wilde, M.: SS-MoA9, 12
Wilhelm, F.: SS+OX-WeM5, 38
William, C.T.: SS-ThM11, 56
Williams, P.M.: BI+SS+AS-TuM5, 14
Winkler, K.: GR+AS+NS+SP+SS-TuA1, 20
Winter, B.: SS-ThA1, 61; SS-ThA2, 62
Wodtke, A.M.: SS-MoM4, 6
Woicik, J.C.: OX+SS+TF+MI-MoA9, 10
Wolkow, R.A.:
SP+AS+BI+ET+MI+NM+NS+SS+TF-WeM2,
36
Wöll, Ch.: OX+SS+TF+MI-MoA10, 10
Wormeester, H.: EL+TF+BI+AS+EM+SS-MoA8,
9
Wu, J.: AC+TF+SS+MI-MoA1, 7
Wu, S.: GR+AS+NS+SP+SS-TuA12, 21
Wyrick, J.: SP+AS+BI+ET+MI+NM+NS+SS+TF-
WeM5, 36
- **X** —
Xia, Y.: SS-TuM10, 18
Xie, K.: SS-WeA3, 48
Xu, Y.: EL+TF+BI+AS+EM+SS-MoA9, 9;
GR+AS+EM+NS+SS-WeA11, 46
- **Y** —
Yakobson, GR+EM+NS+SS+TF-ThA8, 59
Yakou, F.: SS+OX-WeM5, 38
Yamada, T.: BI+SS+NS-WeM11, 33; SS-MoA10,
12; SS-TuP31, 30
Yan, H.: SS-WeA3, 48
Yang, K.: TF+AS+SS-ThA8, 64
Yang, P.: SS-TuP26, 29
Yang, X.: SS-WeA10, 49
Yang, Y.C.: VT+AS+SS-WeM1, 41
Yasumura, S.: SS-TuP8, 26
Yates, Jr., J.T.: SS+EN+OX-ThM6, 54; SS-TuM3,
17
Yazyev, O.V.: GR+AS+NS+SS-ThM5, 52
Ye, J.: SS-TuM10, 18
Ye, Y.F.: SS-TuP37, 31
Yeh, P.-C.: SS-TuP2, 24
Yellen, B.: BI+SS+NS-WeM9, 33
Yilmaz, D.E.: OX+SS+TF+MI-MoA1, 9
Yoda, S.: SS-ThA10, 62
Yoon, Y.: SS+EN+OX-ThM5, 53
Yoshimura, T.: GR+AS+NS+SS-ThM1, 51;
TF+EM+SS-ThA3, 65
Yu, J.: GR+AS+NS+SP+SS-TuA12, 21
Yu, S.W.: AC+MI+SS+TF-MoM9, 1
Yu, W.: SS-WeA9, 48
Yu, Z.: NS+AS+SS+SP-WeM4, 35; SS-TuP19, 28
- **Z** —
Zandvliet, H.J.W.: EL+TF+BI+AS+EM+SS-
MoA8, 9
Zang, F.: BI+SS+NS-WeM2, 32
Zarrouati, M.: GR+AS+BI+PS+SS-WeM1, 34
Zauscher, S.: BI+SS+NS-WeM9, 33
Zegenhagen, J.: GR+AS+NS+SP+SS-TuA9, 21
Zettl, A.: GR+AS+NS+SS-ThM5, 52
Zhan, Y.: GR+EM+NS+SS+TF-ThA3, 58
Zhang, B.: SS-TuM10, 18
Zhang, C.X.: EM+SS+AS+NS-ThM11, 51
Zhang, E.X.: EM+SS+AS+NS-ThM11, 51
Zhang, F.: SS+EN+OX-ThM10, 54
Zhang, L.: IS+AS+SS+EN-TuM3, 15
Zhang, S.: SS-TuP9, 26
Zhang, X.-G.: ET+SS+GR+SP-FrM1, 69;
ET+SS+GR+SP-ThA6, 57
Zhang, Z.: SS-TuM10, 18
Zhao, H.: IS+AS+SS+EN-TuM9, 16
Zhao, S.-G.: SS-TuP9, 26
Zhou, J.: SS+NS-TuA12, 23; SS-TuP13, 27
Zhou, Y.H.: SS+NS-TuA12, 23; SS-TuP13, 27
Zhu, J.F.: IS+AS+SS+EN-TuM3, 15; SS+NS-
TuA11, 23; SS-TuM9, 18; SS-TuP35, 30; SS-
TuP37, 31
Zhu, Y.: SP+AS+BI+ET+MI+NM+NS+SS+TF-
WeM5, 36
Zhu, Y.-Z.: SS-TuP9, 26
Zollner, S.: EL+TF+AS+EM+SS-TuP2, 24;
EL+TF+BI+AS+EM+SS-MoA9, 9
Zuilhof, H.: TF+EM+SS-ThA4, 65
Zuluaga, S.: EN+SS-FrM7, 69